Novel and Sustainable Production, Characterization, and Testing of Various Nanocarbons as Excellent Additives in Lubricants

A thesis submitted by

Nowduru Ravikiran

(Reg. No. 19ETPM07)

in the partial fulfilment of the requirement for the award of the degree of

Doctor of Philosophy

in

Materials Engineering

Under the supervision of

Prof. Dr.-Ing. V. V. S. S. Srikanth

School of Engineering Sciences and Technology University of Hyderabad Central University (P.O.) Hyderabad 500046 India



Dr. P. K. Jain

Associate Director ARCI, Hyderabad RCI Road, Balapur Hyderabad 500005 India



Declaration

I, Nowduru Ravikiran, declare that this thesis work entitled "Novel and Sustainable

Production, Characterization, and Testing of Various Nanocarbons as Excellent Additives

in Lubricants", submitted in partial fulfillment of the requirement for the award of Doctor of

Philosophy (in Materials Engineering) in the School of Engineering Sciences and Technology,

University of Hyderabad is completely my own work except for those referenced. This work was

done under the supervision of Prof. Dr.-Ing. V. V. S. S. Srikanth (University of Hyderabad)

and Dr. P. K. Jain (ARCI, Hyderabad). This report is a record of the bonafide research work

carried out by me and the results incorporated in it have not been reproduced/copied from any

source. This work has not been submitted to any other University or Institution for the award of

any other degree or equivalent.

Nowduru Ravikiran

Reg. No.: 19ETPM07 School of Engineering Sciences and Technology

University of Hyderabad



CERTIFICATE

This is to certify that the thesis entitled <u>Novel and Sustainable Production</u>, <u>Characterization</u>, and <u>Testagot Various Nanocarbons as Excellent Additives in Lubricants</u> Submitted by <u>Nowduru Ravikiran bearing</u> registration number <u>19ETPM07 (Ph.D. (Materials Engineering))</u> in partial fulfilment of the requirements for award of Doctor of Philosophy (Materials Engineering) in the <u>School of Engineering Sciences and Technology</u> is a bonafide work carried out by him under my supervision and guidance.

This thesis is free from plagiarism and has not been submitted previously in part or in full to this or any other University or Institution for award of any degree or diploma.

Parts of this thesis have been:

A. Published in the following publications:

- 1. Carbon Spheres and Carbon Soot for Tribological Applications in Advanced Nanomaterials 191-216 (2022) (ISBN: 978-3-031-11996-5) Chapter 2
- 2 Diamond and Related Materials 126, 109050 (2022) (ISSN: 1879-0062) Chapter 4
- 3 ACS Sustainable Chemistry & Engineering 11, 12045-12051 (2023) (ISSN: 2168-0485) Chapter 4
- 4. Diamond and Related Materials 141, 11063 (2024) (ISSN: 1879-0062) Chapter 4
- 5. Chem. Engineering and Processing-Process Intensification 199, 109747 (2024) (ISSN: 1873-3204) Chapter 4
- 6 Industrial & Engineering Chemistry Research, Accepted (2024) (ISSN: 1520-5045) Chapter 4

and

B. Presented in the following conferences:

- 1. International Conference on Global Conference for Decarbonization of Energy and Materials (GCDEM 2023) Singapore during 27–31 Dec 2023, organized by National University of Singapore, Solar Energy research Institute of Singapore and SunKonnect. Title of the oral presentation is "Sustainable kilogram-scale conversion of tire pyrolysis waste into nanosized onion-like carbons with extraordinary lubricant-additive properties".
- 2. Indian Conference on Carbon Materials (ICCM) 2023, BARC, Mumbai, India during 30 Nov-2 Dec 2023. organized by the Indian Carbon Society and BARC, Mumbai, Title of oral presentation is "A novel green process of making multi/few layers graphene and their application as lubricant additive".
- 3. International Conference, 244th ECS Meeting, Gothenburg, Sweden during 8–12 Oct 2023, organized by the Electrochemical Society, Title of the poster presented is "A novel and large-scale rapid green synthesis of few layer and multi-layer graphene".
- 4, 5th Asia-Oceania Sonochemical Society (AOSS) International Conference, 2023, NIT Warangal, India during 28– 30 Sep 2023, organized by NIT Warangal. Title of the oral presentation is "Ultrasonically dispersed 0-dimensional nano-carbons as tribo-additives in 15W40 motor oil".
- 5. International Conference on Diamond and Carbon Materials, Lisbon, Portugal during 4–8 Sep 2022, organized by Elsevier. The title of poster presented is "Novel few-layered graphene as an excellent additive in 15W40 engine oil for enhanced lubrication".
- 6. International conference on Reuse, Recycling, Upcycling, Sustainable Waste Management and Circular Economy (ICRSC 2022), during 9–11 Sept 2022, organized by Mahatma Gandhi University, Kerala. The title of oral presentation is "Modification and utilization of tyre pyrolysis waste carbon as friction/wear reducing additive in lubricant oil".

Further, the student has passed the following courses towards fulfilment of coursework requirement for Ph.D.

	Name	Credits	Pass/Fai
Course Code		1	Pass
PD801	Research Methodology	. 4	F 433
10001	Research and Publication Ethics	2	Pass
PD807		4	Pass
PD808	Problems in Surface Engineering		Dasa
PD809	Mechanical Behaviour At Various Length Scales	4	(3)

Supervisors V. V. S. S. Srikanth

Professor School of Engineering Sciences & Technology University of Hyderabad Hyderabad-500 046. िडीन /DEAN एस.ई.एस.टी / School of Engineering Sciences & Technology हैदराबाद विश्वविद्यालय UNIVERISTY OF HYDERABAD हैदराबाद / Hyderabad - 500046

Acknowledgments

I express my gratitude and respect to Prof. Dr.-Ing. V. V. S. S. Srikanth (School of Engineering Sciences and Technology (SEST), University of Hyderabad (UoH)) and Dr. P. K. Jain (International Advanced Research Centre for Powder Metallurgy and New Materials (ARCI), Hyderabad), my Ph.D. thesis supervisors, for their keen interest, invaluable guidance, strong motivation, and continuous encouragement throughout my work. Their support in professional and personal aspects will always be invaluable to me. Both are great mentors who gave timely guidance and complete freedom to explore new frontiers. Next, I express my gratitude to the Late Dr. G. Padmanabham and Dr. T. N. Rao of ARCI, Hyderabad, for encouraging and permitting me to register for Ph.D. at the UoH. Special thanks to Dr. T. N. Rao for extending his support in every possible way during my Ph.D. tenure. I would also like to thank Prof. P. Appa Rao, the former Vice Chancellor of UoH, and Prof. B. J. Rao, the current Vice Chancellor of UoH, for their support. I extend my special thanks to my Research Advisory Committee (RAC) members, Prof. Koteswararao V. Rajulapati and Dr. Venkata G. Kotnur, for their critical reviews during our meetings at UoH, and for providing constructive suggestions to make my work scientifically sound. Their insightful questions and discussions have helped me a lot in improving the quality of my work. I want to acknowledge the prestigious Prime Minister's Research Fellows (PMRF) scheme by the Ministry of Education for providing the fellowship and research grant, which helped me achieve excellence in various aspects. In this regard, I wish to thank Prof. Dr.-Ing. V. V. S. S. Srikanth (former PMRF scheme coordinator at UoH) for encouraging me and helping me secure the fellowship, and Prof. Jayprakash Gautam (Dean, SEST, UoH and Coordinator, PMRF scheme at UoH) for extending his support during my tenure as a PMRF fellow. I want to thank Dr. Balaji Padya, Dr. Ravi Kali, Dr. Sanjay Dhage, Mr. E. Konda, and Mr. Anjaiah (ARCI, Hyderabad) for their immense support. I am also thankful to all other employees and fellow UoH and ARCI, Hyderabad students who have helped directly or indirectly during my research work. Also, I would like to acknowledge my collaborators, D. Pavan K. Penumakala (BITS Hyderabad), Dr. Sai Rama Krishna Malladi (IIT Hyderabad), and Mr. S. Junaid (PhD scholar and fellow PMRF scheme, IIT Delhi) for their timely help. I acknowledge the DST SERB and the IoE directorate at UoH, for providing financial assistance to attend an international conference in Lisbon, Portugal, and an international conference in Singapore through their ITS grant (ITS/2022/001480) and travel grant (UoH-IoE/Travel/23/258), respectively. I want to express my heartfelt gratitude to my extended family, Mr. Akshay, Ms. Harita Pant, and Mrs. Swati Singh, who have supported me tirelessly through all the ups and downs. Their support, compassion, and shared fun have been critical in

keeping me balanced during the difficult stages of this journey. Each of them has uniquely impacted my personal and academic lives. Also, I would like to thank all my team members at the Surface Interface and Engineering Laboratory, SEST, for their direct and indirect support on this journey. Finally, I want to thank my parents for their constant support, encouragement, and sacrifices, which have served as the basis for my academic career. Their belief in me has been a constant source of inspiration, and I will be eternally grateful for their love and wisdom.

Nowduru Ravikiran

Table of Contents

Abstract	i
Chapter 1 Introduction	3
1.1 Tribology	3
1.2 Lubrication and Lubricants	3
1.3 Additives in Lubricants	7
1.4 Nanoadditives in Lubricants	10
1.5 Problem Statement	13
1.6 Objectives of the Thesis	15
1.7 Overview of the Thesis	15
References	15
Chapter 2 Literature Review	20
2.1 Lubricants, Additives and Nanoparticles	20
2.2 Nanocarbons as Lubricant Additives	27
2.2.1 0D Nanocarbons as Lubricant Additives	27
2.2.2 1D Nanocarbons as Lubricant Additives	33
2.2.3 2D Nanocarbons as Lubricant Additives	36
References	42
Chapter 3 Experimental Details	58
3.1 Processing of Materials	58
3.1.1 Processing of 0D Nanocarbons (RTS and OLC nanoparticles)	58
3.1.2 Processing of 1D MWCNTs	59
3.1.3 Processing of 2D MLG Nanoparticles	60
3.2 Materials Characterization	62
3.3 Preparation of Lubricants with Nanocarbons as Additives	62
3.4 Measurement of Rheological Properties of Lubricant Samples	64
3.5 Measurement of Tribological Properties using Lubricant Samples	66
References	68
Chapter 4 Results and Discussion	69
4.1 0D RTS Particles as Additives in Lubricants	69
4.2 0D TPW and OLC Particles as Additives in Lubricants	86

103
116
131
138
138
141

Abstract

This Ph.D. thesis addresses two crucial materials engineering aspects. They are: 1) nonavailability of kg scale production strategies for nanocarbons and 2) improving lubrication using nanocarbons (that are produced using sustainable methods) as additives. Nanocarbons are well-known for their unique and unsurpassed properties, making them potential materials in various applications, including lubrication. However, most of these envisaged applications are hindered by the non-availability of sustainable production strategies for these nanocarbons. These nanocarbons are primarily prepared on only a gram scale. On the other hand, it is wellknown that friction and wear losses in terms of energy savings, CO₂ emissions, and incurring costs are alarming. It is known that these undesired losses can be minimized through effective lubrication. One way of improving lubrication is to use efficient lubrication additives. This Ph.D. thesis reports the investigations on novel and sustainable production strategies of different nanocarbons (i.e., 0D, 1D, and 2D nanocarbons) and their use as additives in lubricants to improve lubrication. 0D nanocarbons, namely tyre pyrolysis waste (TPW) and onion-like carbon (OLC) particles, 1D multiwalled carbon nanotubes (MWCNTs), and 2D multi-layer graphene (MLG) particles, are produced on a large-scale using sustainable processes. These nanocarbons are then thoroughly characterized for general material characteristics and tested as lubricant additives in different lubricating oils following the specified ASTM standard. Ultrasonication was used to prepare the lubricant samples with additives. Comprehensive rheological and tribological tests are carried out to determine the effect of nanocarbon concentrations on the lubricating performance of the oils. Experimental studies have demonstrated and verified that employing carbon soot created by controlled burning of waste tyre tubes in lubricating oil (group-2 N500 de-waxed oil) can lower the coefficient of friction (CoF) and wear scar diameter (WSD) by 48.93% and 28.12%, respectively. TPW and OLC particles, as additives in low concentrations, can aid in reducing abrasive and WSD (12-20% by TPW and 17-30% by OLC). The dispersions of low concentrations (0.1wt.%) of 0D nanocarbons exhibited good stability (visually) for 30 days. As the concentrations increased, their sedimentation accelerated. Adding 0.1wt.% of the MWCNTs in a base oil (BO) improved the anti-friction property by 64%, and when dispersed in a commercial oil, the CoF was lowered by 48%. Due to the addition of 0.1wt.% of MWCNTs, the wear-preventive properties of the base and commercial oils were also improved by 60% and 30%, respectively. However, the dispersion stability of MWCNTs in the base and commercial oils is significantly lower than that of the considered 0D nanocarbons. MLG added

BO, reduced CoF by 25%, and reduced wear by 50%. Adding MLG to commercial oil increased CoF and wear resistance by 16% and 50%, respectively. The desired properties are effectively improved when these particles are used at low concentrations (0.1wt.% to 0.3wt.%), beyond which problems such as quicker agglomeration, related sedimentation, and property deterioration become more severe. The dispersion of nanocarbons in lubricating media (oils) caused abnormal changes in rheological properties. In most cases, a non-Einstein-like reduction in viscosity is found, which warrants further exploration through in-situ experiments that could shed light on particle-fluid interactions and aid in understanding fluid mechanics at the nanoscale. The underlying mechanism of wear-preventive behavior was also explained in each additive case. The produced nanocarbons in this work may be highly successful in other lubricating media, such as greases, where sedimentation and agglomeration are not significant concerns.

Chapter 1 Introduction

1.1 Tribology

Tribology is the scientific understanding and assessment of friction, lubrication, and wear. It aims to understand the underlying mechanisms and factors that influence friction, lubrication, and wear and to use this knowledge to design and develop materials, components, and systems with improved performance and reliability [1]. Tribology is an important area of research because friction, lubrication, and wear significantly impact the performance and efficiency of various engineering systems, such as internal combustion engines, gear systems, bearings, and tribo-electrochemical devices. In these systems, friction and wear can cause increased energy consumption, decreased efficiency, and reduced lifespan, while effective lubrication can improve performance and prolong the components' lifespan. Over the past few decades, there have been significant advancements in tribology, particularly in the exploration of new materials as additives for lubricants, as well as the application of novel methods for tribological testing and analysis. However, there is still much to be learned about the fundamental mechanisms and factors that influence tribological behavior, and opportunities for further research and innovation in this field are abundant. Tribology is of great significance for various industries, including transportation, manufacturing, and energy, where improved tribological performance can lead to significant improvements in efficiency, reliability, and sustainability.

1.2 Lubrication and Lubricants

Lubrication is a critical aspect of tribology, and its proper implementation can substantially remediate the performance and reliability of engineering systems. Lubrication refers to introducing a substance or substances between two surfaces subjected to contact and relative motion, with the primary objective of reducing friction and wear. Reduction in friction can improve energy efficiency, extend the lifespan of components, and reduce the risk of failure due to excessive wear. There are several mechanisms by which lubrication minimizes friction and wear [2]. The most important mechanisms are boundary, mixed, and hydrodynamic lubrication [3]. In boundary lubrication, the lubricant forms a thin film at the contacting interfaces, lowering friction by separating the surfaces and preventing direct contact. This type of lubrication is generally provided through the use of solid or liquid lubricants that form continuous films at the interfaces [4,5]. Mixed lubrication occurs when the tribo-film formed by the lubricant is not continuous, leading to direct contact of the surfaces in relative motion. In this situation, boundary lubrication mechanisms and boundary lubricants can still reduce

friction by providing a protective film between the surfaces [6]. Hydrodynamic lubrication is characterized by generating a pressure-driven fluid film at the contacting interfaces. In hydrodynamic lubrication, the lubricant is thrust into the interface between the two surfaces, generating a barrier of fluid that separates the surfaces, preventing direct contact [7]. Several factors, including the lubricant characteristics, the service conditions, and the design of the components in relative motion, can influence the effectiveness of lubrication.

The lubricant's viscosity plays a key role in determining its effectiveness, as it affects the flow properties of the lubricant to form a continuous protective layer at the interfaces. The load on the system can affect the lubricant film, as higher loads can lead to increased contact pressure and reduced lubricant film thickness. The speed of relative motion also influences lubrication, as higher speeds can reduce the effectiveness of the lubricant film. The system's temperature affects the viscosity and other properties of the lubricant, and high temperatures can reduce the effectiveness of lubrication. The surface finish of the components in relative motion can also impact the lubrication's effectiveness, as rough or damaged surfaces can do not allow the lubricant to build a continuous film. Selecting an appropriate lubricant is a critical factor in achieving effective lubrication. There are several factors to consider when selecting a lubricant, including compatibility with the materials of the components in relative motion, viscosity, and other properties relevant to the operating conditions, cost, availability, and environmental impact. The most commonly used lubricants are mineral oils, synthetic oils, and greases. The choice of lubricant is governed by the system's specific requirements like the operating conditions, materials of the components, and other factors.

Lubricants have been used for thousands of years to lower friction and associated wear [8]. Over time, the development of lubricants has evolved to meet the increasing demands of industrial and technological advancements. The use of lubricants dates back to ancient civilizations. Simple substances such as animal fats were applied over surfaces for lowering friction and wear. Lubrication was mentioned in the Vedas, i.e., as early as 1500 BCE and 1200 BCE. These texts describe how oils and fats can be used for lubrication purposes. Verbal sources describe use of sesame oil as a lubricant in the textile industry to prevent friction between the fibers during the spinning process. The Arthashastra, which is a treatise on economics and politics written by the philosopher Kautilya in the 3rd century BCE, contains detailed descriptions of the lubrication practices used in the metalworking industry. According to the text, various oils and fats were used to lubricate the tools used in metalworking, such as chisels and saws. The text also describes how oil could be used to prevent rust on metal objects [9]. In ancient Greece, olive oil was commonly used as a lubricant for machinery and vehicles.

In ancient Rome, olive oil was also used as a lubricant, and was widely recognized for its effect on tribological properties.

Modern lubricants' development began in the 19th century, with the advent of the industrial revolution [10]. The increased demand for improved lubricants for machinery and vehicles led to the developing of new and improved lubricant products. One of the first modern lubricants was petroleum jelly, which was developed in 1850 and quickly became popular for providing effective lubrication and safety against wear and corrosion. The development of the internal combustion engine (ICE) in the late 19th century also influenced lubricants' advance. ICE's high operating temperatures and extreme pressures required advancing lubricants with improved thermal stability and wear preventive properties. The development of synthetic lubricants began in the early 20th century with the advent of chemical synthesis. In the mid-20th century, the formulation of synthetic lubricants for automotive applications led to the widespread use of synthetic EOs [11,12]. Compared to traditional petroleum-based EOs, synthetic EOs offer improved performance, such as increased fuel efficiency and better wear protection. The increasing demand for improved fuel efficiency and reduction in emissions has led to the development of new low-viscosity lubricants, which offer improved fuel efficiency without sacrificing protection against wear. In addition, the development of bio-based lubricants, such as vegetable-based lubricants, has also gained popularity in recent years. These lubricants offer improved environmental performance compared to traditional lubricants and are widely used in agriculture and food processing applications [13]. The history of lubricants dates back to ancient civilizations and has evolved to meet the increasing demands of industrial and technological advancements. The development of modern lubricants, such as petroleum jelly, synthetic lubricants, and bio-based lubricants, has significantly impacted the performance and efficiency of machinery and vehicles. Today, lubricants are vital as they have a critical role in reducing parasitic friction and related wear in components and, thereby, improving the performance and durability of machinery and vehicles.

Engine oil (EO), a commonly used lubricant, is a critical component of ICE, and its proper selection and use can significantly impact engine's performance and longevity. EO serves several key functions in an engine, including lubrication, cooling, and cleaning. The primary function of EO is to provide lubrication between the engine's moving parts, reducing friction and wear. EO is designed to form continuous lubricanting film at interfaces, lowering friction and preventing direct contact between the surfaces. It is also engineered to guard against wear and corrosion, thereby prolonging the life of engine parts. In addition to lubrication, EO also plays a critical role in engine cooling. It absorbs heat generated by the engine, helping to

regulate engine temperature and prevent overheating. It has a high thermal capacity, allowing it to absorb and transfer heat efficiently. It also plays a role in cleaning the engine by removing contaminants and deposits that can accumulate over time. It is formulated with detergents and dispersants that help to keep the engine clean, removing deposits and preventing the formation of new ones. There are different types of EOs. They are are classified according to several key factors, including viscosity, performance level, and application. Some of the most common EOs based on viscosity are 5W-30, 10W-30, 10W-40, and 15W40. The choice of EO heavily relies on its viscosity, as it influences the oil's flow and lubricating properties under various operational conditions. EOs are also classified according to their performance level, with common classifications including American Petroleum Institute Service Categories and International Lubricant Standardization and Approval Committee ratings. Performance level classifications indicate the oil's ability to meet specific performance standards and requirements, such as fuel efficiency and emission control. EOs are also classified according to their intended application (passenger car, diesel, or high-performance engines). Oils tailored for specific applications are crafted to fulfill the unique needs of various engine types, encompassing performance and operational conditions. The selection of an appropriate EO is critical in ensuring engine performance and longevity. When selecting an EO, several factors should be considered. When choosing an EO, one should take into account the engine type and its specific needs, including performance, emission levels, and fuel economy. Also, the engine's working conditions, including factors like temperature, load, and speed, should be taken into account while picking an EO. The engine manufacturer may provide specific recommendations for the type and performance level of EO to use. Proper selection and use of EOs can significantly impact engine performance and longevity. Understanding the classification of EOs and the factors that influence selection is an important aspect of ensuring optimal engine performance. EOs are specially formulated lubricants designed to provide lubrication and protection for internal combustion engines. Base oils (BOs) are the foundation of lubricants and are used to create various lubricant formulations for different applications. They are derived from crude oil and are produced through various refining processes [14], including solvent extraction, hydrotreating [15], and hydrocracking [16]. BOs are classified based on their viscosity index, level of saturation, and molecular weight [17,18].

The most common types of BOs include:

- Mineral oils: These are the most widely used type of BOs and are produced by refining crude oil. They have a low viscosity index and are typically used in applications requiring a low-cost lubricant.

Introduction

- Synthetic oils: These are synthetically produced BOs, created through chemical procedures, and are engineered to exhibit enhanced performance traits compared to mineral oils. They possess a high index of viscosity, exceptional thermal stability, and minimal volatility, rendering them apt for utilization in applications demanding high temperatures and performance.
- Semi-synthetic oils: These are a blend of mineral and synthetic oils and are designed to provide a balance between performance and cost.
- Bio-based oils: These are BOs derived from renewable resources such as vegetable oils and animal fats. They are typically used in applications where an environmentally friendly lubricant is required.

The choice of BO for a specific application depends on several factors like operating temperature, load, and application requirements. Group 2 dewaxed oils are a type of mineral oil base stock that are commonly used as a BO in the formulation of lubricants. They are produced through a refining process that removes the wax from the crude oil, resulting in a high-quality BO with improved low-temperature properties. Group 2 dewaxed oils are characterized by their high viscosity index, low pour point, and good oxidative stability. This makes them suitable for use in various applications, including automotive lubricants, industrial gear oils, and hydraulic fluids. In comparison to Group 1 mineral oils, Group 2 dewaxed oils have a higher viscosity index and better low-temperature performance, making them suitable for use in regions with severe winter conditions. Their improved oxidative stability also provides better protection against corrosion and wear, making them ideal for use in high-load and high-temperature applications. The production of Group 2 dewaxed oils involves a combination of hydrotreating and solvent dewaxing processes. In the hydrotreating process, crude oil undergoes treatment with hydrogen under the influence of a catalyst to eliminate contaminants, wax included. The resulting product is then subjected to solvent dewaxing, where it is mixed with a solvent, such as hexane, to remove any remaining wax.

1.3 Additives in Lubricants

In addition to the BO, EOs contain various additives that enhance their performance and provide additional benefits [19]. The use of additives in EOs is an important aspect of EO technology and has been widely used for many decades to improve the performance of EOs. Several different EO additives are designed to provide specific benefits to EO performance [20]. Some of the most common types of EO additives include:

- Viscosity Improvers: Viscosity improvers are additives used to improve EO flow characteristics at low temperatures. This helps to prevent engine damage and wear during cold weather starting.
- Anti-wear (AW) Additives: These protect against metal/metal contact and reduce wear in high-stress engine components. These additives can include compounds such as zinc dialkyl dithiophosphate (ZDDP) and molybdenum compounds.
- Detergents: Detergents are additives that keep engine components clean and prevent deposits from forming. This helps to maintain engine performance and improve fuel efficiency.
- Dispersants: Dispersants are additives that help to keep EO clean by preventing the formation of sludge and varnish deposits.
- Antioxidants: Antioxidants are additives that help to prevent oxidative degradation of EOs and maintain their performance over time.
- Friction Modifiers: Friction modifiers are additives used to reduce friction between engine components, improving fuel efficiency and reducing emissions.
- Corrosion Inhibitors: Corrosion inhibitors are additives that help to prevent corrosion of engine components and protect against rust and other forms of corrosion.

The use of additives in EOs is carefully regulated to ensure that the additives do not adversely affect engine performance or emissions. Organizations such as API and ILSAC generally standardize and specify additive levels. The use of additives in EOs is an important aspect of EO technology and has been widely used for many decades to improve the performance of EOs. Additives provide a range of benefits, including improved viscosity, AW protection, cleaning, and corrosion protection.

Anti-friction (AF) and AW additives are key components of EOs [21]. These additives protect against metal/metal contact and reduce wear in high-stress engine components. Incorporation of AF and AW additives is crucial in EO technology. Their usage, which spans several decades, has been instrumental in enhancing the performance of these oils. There are several different types of AF and AW additives that are commonly used in EOs. ZDDP is one of the most widely used additive in EOs. ZDDP effectively reduces friction and wear in engine components and provides excellent AF/AW protection [22,23]. Molybdenum compounds, such as molybdenum disulfide (MoS₂), are also commonly used as AF and AW additives in EOs. These compounds provide excellent AF/AW protection and help to reduce friction between engine components. Boron compounds, such as boron nitride, are sometimes used as AF and AW additives in EOs [24]. These compounds provide excellent AF and AW protection and

help to reduce friction between engine components. Sulfur compounds, such as sulfurized fatty acids, are sometimes used as AF and AW additives in EOs. These compounds provide good AF and AW protection and help to reduce friction between engine components [25]. The use of AF and AW additives in EOs is carefully regulated to ensure that they do not adversely affect engine performance or emissions. Calcium sulfonate is a newer type of additive that is becoming increasingly popular in industrial lubricants [26]. It effectively reduces wear and has good resistance to high temperatures and water washouts. However, it can be expensive and not as effective as other additives in extreme pressure conditions. Using ZDDP can be problematic as it can degrade the effectiveness of the catalyst, leading to increased emissions [27]. MoS₂ is a solid lubricant that can be added to oils to reduce friction and wear. However, it can be difficult to disperse evenly in the oil and settle out over time, leading to uneven lubrication and potential damage to the equipment. Polytetrafluoroethylene (PTFE) is a solid lubricant that is commonly used in greases and other lubricants to reduce friction [28]. However, it can be difficult to incorporate into oils and can settle out over time, leading to inconsistent lubrication. Additionally, PTFE can react with some metals and cause increased wear and damage. Dimethylpolysiloxane (DMPS) is a silicone-based lubricant additive that is commonly used in industrial applications to reduce friction and wear [29]. However, it can be expensive and may not be effective in extreme high-temperature or high-pressure conditions. Additionally, DMPS may not be compatible with certain types of metals and can cause corrosion or other types of damage. These compounds provide good AW protection and help to reduce friction between engine components. The use of AW additives in EOs is carefully regulated to ensure that the additives do not adversely affect engine performance or emissions. AW additive levels are generally standardized and specified by industry organizations like the API and the ILSAC. Sulfur and phosphorus compounds are commonly found in AF and AW additives in EOs and other lubricants. These additives interact with metallic surfaces to create a protective layer that aids in warding off wear and tear. However, they can harm catalytic converters and cause increased emissions in some types of engines [30].

Many lubricant additives are derived from non-renewable resources, such as petroleum. This can lead to concerns about the sustainability of these resources and the impact of their extraction on the environment. Additionally, some lubricant additives contain substances that can harm the environment if they are not disposed of properly. Certain additives can be toxic to aquatic life if they enter waterways [31]. Lubricant additives are designed to work with specific types of oils and metals. If the wrong type of additive is used, or if the additive is not compatible with the oil or metal in the equipment being lubricated, it can result in decreased

performance or even damage to the equipment. While the current AF and AW lubricant additives can boost the efficiency of lubricants, their effectiveness in preventing wear and friction under extreme operating conditions is still limited. Some high-performance lubricant additives can be expensive, making them prohibitive for some applications. In some cases, the cost of the additive may be greater than the cost of the oil or equipment being lubricated. There are currently no industry-wide standards for lubricant additives, which makes it difficult for manufacturers and users to compare the performance of different products. This can result in confusion and uncertainty when selecting lubricants and additives. Certain additives in lubricants might include materials that are controlled or limited by regulatory bodies namely Environmental Protection Agency and Occupational Safety and Health Administration. This can result in additional compliance and reporting requirements for manufacturers and users, adding to the cost and complexity of using these additives.

1.4 Nanoadditives in Lubricants

In recent times, the incorporation of nanoparticles (NPs) as lubricant additives has garnered considerable interest owing to their capability to boost the lubricants' efficiency. NPs have structures (with dimensions of 1-100 nm) and properties on a nanoscale [32-34]. The distinctive characteristics of NPs render them appealing for incorporation as additives in lubricants. The following variety of NPs have been explored for their potential use as additives in lubricants:

- NPs: NPs, such as nanotubes, graphene, and metal NPs, have been used as lubricant additives. These particles have high specific surface areas and can form strong bonds with metal surfaces, reducing friction and wear.
- Nanocomposites, composed of a matrix material and a dispersion of NPs, have also been used as lubricant additives. These can enhance performance compared to conventional lubricants by virtue of their unique properties and larege specific surface area.
- Nanofluids: Nanofluids are suspensions of NPs in a liquid and have been used as lubricant additives. Nanofluids have been shown to have improved thermal stability and reduced friction compared to conventional lubricants.

The use of NPs as lubricant additives is still in the infant stage, and much research is still needed to understand their potential benefits and drawbacks fully. However, initial results have been promising, and there is significant potential for using NPs to enhance the performance of lubricants in various applications. Despite the potential benefits of using NPs as lubricant additives, several challenges and limitations must be addressed. These include:

Introduction

- Synthesis and Purification: Synthesis and purification of high-quality NPs can be challenging and expensive. This is an important factor to consider when developing NPs as lubricant additives.
- Stability: NPs can be unstable in certain environments, such as high temperatures and high pressure, which can limit their use as lubricant additives.
- Toxicity: The toxicity of NPs is a major concern, and their potential impact on human health and the environment must be carefully evaluated.

Nevertheless, the use of NPs as lubricant additives has significant potential and is an area that warrants further investigation. Adding NPs to EOs can affect their viscosity and viscositytemperature behavior. NPs are particles smaller than 100 nm, significantly smaller than the average size of conventional lubricant additives. The effect of NPs on viscosity is influenced by their size, shape, surface properties, and concentration [35]. NPs with a high aspect ratio, such as long and thin nanorods or nanotubes, can align with each other under shear and form ordered structures, known as NP chains, that can reduce the overall viscosity of the oil. On the other hand, NPs with a low aspect ratio, such as spherical NPs, tend to disperse randomly and increase their viscosity due to their Brownian motion and interparticle interactions. Another factor that affects the viscosity of EOs with NPs is their surface properties. Due to the reduced interaction with the oil molecules, NPs with hydrophobic surfaces tend to have a lower viscosity than NPs with hydrophilic surfaces. The surface modification of NPs with surfactants or stabilizers can also affect their viscosity by modifying the oil-NP interactions. The concentration of NPs in the EO also plays a role in determining the viscosity. At low concentrations, NPs tend to disperse randomly and have a limited effect on the viscosity. However, the NPs can form aggregates or clusters that significantly increase the viscosity at high concentrations. Nanocarbons (NCs) have been studied as potential lubricant additives. When added to lubricants, carbon NPs can form a protective layer on metal surfaces, lowering friction and preventing wear. NCs' functioning as additives in lubricants is based on their distinctive physical and chemical attributes. NCs, with their high aspect ratio, mechanical robustness, and extensive surface area, can establish potent interactions with surfaces at the interface. This enables them to serve as a shield, preventing direct contact between metal surfaces, consequently lowering friction and wear. Additionally, the high thermal conductivity and thermal stability of NCs allow them to effectively dissipate heat generated by friction, further reducing wear and improving the lubricant's overall performance. The high specific surface area of NCs also enables them to adsorb and trap contaminants and wear debris, further reducing friction and wear [36]. Numerous studies have investigated the potential benefits of using NCs as lubricant additives [37]. These studies have demonstrated improved friction and wear reduction, extended lubricant life, and energy efficiency in mechanical systems.

Furthermore, NCs can be used in combination with other lubricant additives to improve their effectiveness. Studies have shown that adding carbon nanotubes to lubricants containing traditional AW additives, such as ZDDP, can enhance their AW performance [38]. Despite these promising results, some challenges are associated with using NCs as lubricant additives. One of the main challenges is their tendency to agglomerate or form large structures, which can negatively impact their performance [39]. Additionally, the high cost of production and the difficulty of dispersing NCs evenly in the lubricant are barriers to their widespread use. The percentage of phosphorus, sulfur, and metals in lubricants can vary depending on the specific AW and AF additives used. These additives are typically used to enhance the lubricating properties of oils and reduce friction and wear in mechanical systems. Additives based on phosphorus, such as ZDDP, which are commonly used as AF and AW additives in lubricants, create a protective layer on metallic surfaces. This reduces friction and avoids direct contact between metals. Due to these additives, the phosphorus content in lubricants can range from 0.05% to 0.2% or higher, depending on the application and performance requirements. Sulfurcontaining compounds, such as organosulfur compounds or sulfurized fats, may be added to lubricants as extreme pressure (EP) additives. These additives provide additional protection under high loads and temperatures by forming a sacrificial layer on metal surfaces. The sulfur content in lubricants due to EP additives is typically in the 0.1% to 0.5% range. Lubricants may also contain certain metals (such as molybdenum, zinc, and calcium) as additives for their AW and AF properties. The concentration of these metals in lubricants is generally low, usually less than 0.1%. Some of the most widely studied NPs as lubricant additives are shown in Fig. 1 [40].

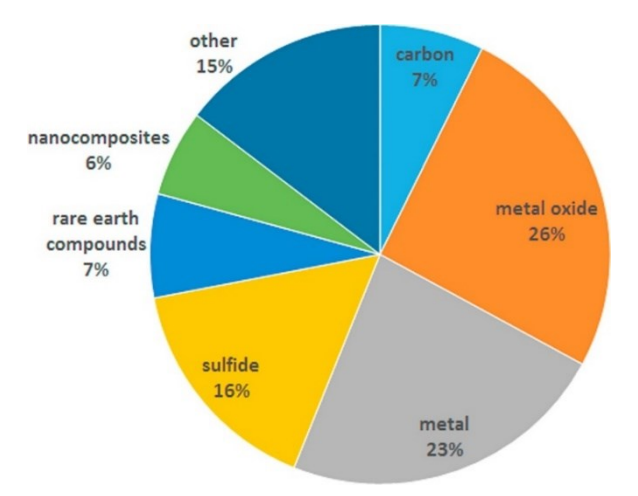


Figure 1. Various NPs used as lubricant additives (Reproduced with permission from [40]). Excessive phosphorus levels can lead to catalyst poisoning in specific emission control

systems, particularly in vehicles equipped with catalytic converters [41]. Phosphorus can coat the catalyst surface, reducing its effectiveness and potentially causing increased emissions. Phosphorus-containing lubricants can leave behind ash deposits when they burn or degrade. These ash deposits can accumulate in critical areas, such as piston rings or exhaust gas recirculation systems, leading to increased maintenance requirements and potential performance issues. Sulfur can contribute to the formation of corrosive by-products, such as sulfuric acid, during the combustion or oxidation of lubricants [21]. These by-products can damage engine components, including bearings, cylinder walls, and valve train components, leading to increased wear and reduced engine life. Similar to phosphorus, high levels of sulphur in lubricants can poison catalytic converters by coating the catalyst surface and inhibiting its ability to reduce harmful emissions. This is particularly relevant for vehicles equipped with advanced emission control systems. Metallic contaminants, such as copper, lead, or iron particles in lubricants, can act as abrasives and cause increased wear on engine components, reducing efficiency and potential damage. Certain metals can accelerate the oxidation process in lubricants, promoting the formation of sludge and deposits. These deposits can clog oil passages, reduce lubricant flow, and impair the overall lubrication performance.

1.5 Problem Statement

Minimizing friction and wear between contacting engineering surfaces is crucial for their sustainable functioning. Lubrication is a commonly used methodology in this context. It is well-known that lubricant additives enhance their rheological and lubrication properties, thereby minimizing tribological (mainly friction and wear) losses. Various (metal, metal oxide, metal sulfide, carbonaceous, graphenaceous, etc.) nanoparticles have emerged as excellent lubricant additives in the last decade. High specific surface area, enhanced specific strength, and other specialized functions make them excellent lubricant additives. Metal-based NPs have significant limitations restricting their usage as lubricant additives. These NPs are found to experience agglomeration issues, restricting their uniform dispersion and lowering their effectiveness in reducing friction and wear on the contacting surfaces. Compatibility issues with other lubricant constituents are found to cause phase separation or undesired reactions, lowering the overall performance. Some metal NPs pose even health and environmental hazards, necessitating careful handling and disposal. Costly production procedures, processing difficulties, and harsh operating environment restrictions contribute to their limited commercial viability. As a practical alternative, metal oxide (such as TiO₂, ZnO, etc.) and metal sulfide (such as MoS₂, WS₂, etc.) NPs are commonly used. However, the capacity of these NPs to

create stable, protective layers on contacting surfaces remains a considerable challenge because they tend to agglomerate. Some of these additives have abrasive qualities under high-pressure conditions. Concerns about their environmental impact and potential health concerns need even more careful handling and disposal. NPs with sulfur and phosphorus compounds are used as lubricant additives to decrease wear under high-pressure conditions. These elements, however, can harm vehicle catalytic converters by generating sulfates and phosphates that deposit on the catalyst surface, lowering efficiency and leading to catalyst deactivation. Lubricant formulations are constantly evolving to minimize or eliminate these components to decrease catalytic poisoning, particularly in formulas suited for use in automobiles equipped with contemporary emission control systems. Manufacturers are developing low-sulfur and lowphosphorus lubricants to provide adequate protection while lowering the risk of catalyst poisoning in modern engines equipped with catalytic converters. Recently, in the modifications made for motorcycle EOs (JASO T903:2023) by the Japanese Automotive Standards Organization, the upper limit of phosphorus has been lowered from 0.12% to 0.1% (limit 0.08%) -0.1%). The limit was not further lowered as it would require lower amounts of phosphorouscontaining additives, which could compromise the wear performance of the lubricant. However, the limits will narrow with time as more countries introduce newer norms similar to JASO T903:2023. In this direction, NCs could be vital in addressing the tribological issues and sustainably mitigating the sulfur/phosphorus/metal-free additives. NCs have been studied as potential lubricant additives. Numerous studies have investigated the potential benefits of using NCs as lubricant additives. These studies have demonstrated improved friction and wear reduction, extended lubricant life, and energy efficiency in mechanical systems. Furthermore, NCs can be used with other lubricant additives to improve their effectiveness. For example, adding carbon nanotubes to lubricants containing traditional AW additives, such as ZDDP, can enhance their AW performance. Despite these promising results, some challenges are associated with using NCs as lubricant additives. One of the main challenges is the potential for these NCs to agglomerate or form large structures, which can negatively impact their performance. Additionally, the high cost of production, lack of bulk-quantity production strategies, and the difficulty of dispersing these NCs uniformly in the lubricants are also barriers to their use as lubricant additives. This thesis explores the sustainable large-scale production of various NCs and their usability as lubricant additives. Considering all the challenges and issues associated with NCs as lubricant additives, this thesis's goals (in the following section) have been established.

1.6 Objectives of the Thesis

The following are the objectives of this thesis:

- ❖ To develop unique and sustainable techniques for producing various NCs such as carbon nanotubes, graphene, and carbon onions, with a focus on large-scale production.
- To reuse industrial by-products by converting them into value-added material and exploring their application as friction and wear preventive additives in lubricants.
- ❖ To conduct comprehensive characterization studies to elucidate the structural and morphological properties and thermal stability of the prepared NCs.
- To optimize the NCs concentration in the lubricants and optimize the dispersion parameters for preparing homogenous dispersions using probe sonication as the process intensifier.
- ❖ To study the rheological properties of the NCs added lubricants.
- ❖ To evaluate the lubrication performance of NC additions in different lubricants under the conditions specified by ASTM D 4172.
- ❖ To assess the sustainability aspects in material processing and the impact of the improvement in tribological properties of the lubricants on factors like energy loss.

1.7 Overview of the Thesis

Chapter 1 discusses tribology, friction, wear, lubrication, and additives and NPs as additives in lubricants for improving AF and AW properties. This chapter also presents the problem statement and objectives of this thesis. Chapter 2 presents a comprehensive literature review of relevant 0D, 1D, and 2D carbon materials to this thesis. Chapter 3 gives details of the experimental procedures in the large-scale production of various NCs, their characterization details, and testing of NCs added lubricants. Chapter 4 presents the results and discussion of this thesis work. This chapter is divided into three sections covering the results and discussion on 0D, 1D, and 2D NCs as lubricant additives. Chapter 5 contains the conclusions of this work and the immediate future scope of research. For convenience, the references are cited at the end of each chapter under the heading 'References'.

References

- [1] W. Jamison, Introduction to tribology, Journal of Vacuum Science and Technology 13(1) (1976) 76-81.
- [2] W.J. Bartz, Tribology, lubricants and lubrication engineering a review, Wear 49(1) (1978) 1-18.

- [3] M. Esfahanian, B. Hamrock, Fluid-film lubrication regimes revisited, Tribology Transactions 34(4) (1991) 628-632.
- [4] H. Spikes, Boundary lubrication and boundary films, Tribology Series 25 (1993) 331-346.
- [5] S.M. Hsu, R.S. Gates, Boundary lubricating films: formation and lubrication mechanism, Tribology International 38(3) (2005) 305-312.
- [6] H. Spikes, Mixed lubrication—an overview, Lubrication Science 9(3) (1997) 221-253.
- [7] R. Dai, Q. Dong, A. Szeri, Approximations in hydrodynamic lubrication, Journal of Tribology 114(1) (1992) 14-25.
- [8] K.J. Anderson, A history of lubricants, MRS Bulletin 16(10) (1991) 69-69.
- [9] Kautilya, The Arthashastra (Edited, rearranged, translated, and introduced by L. Rangarajan), Penguin Books India (1992). pp. 274-347. ISBN 10: 0140446036
- [10] D. Baderna, E. Boriani, F.D. Giovanna, E. Benfenati, Lubricants and additives: A point of view in Global Risk-Based Management of Chemical Additives I. The Handbook of Environmental Chemistry (18) (Eds. B. Bilitewski, R. Darbra, and D. Barceló) Springer (2011). pp. 109-132. DOI: 10.1007/698 2011 99
- [11] S.P. Srivastava, Lubricant additives-Present and future scenario (Chapter 1) in Advances in Lubricant Additives and Tribology (1st Edition), CRC Press (2009), pp. 1-9. ISBN-10: 8188305944
- [12] S.P. Srivastava, Introduction: Lubricant scenario (Chapter 1) in Developments in Lubricant Technology, John Wiley & Sons 2014), pp. 3-6. DOI: 10.1002/9781118907948.ch1
- [13] N. Zainal, N. Zulkifli, M. Gulzar, H. Masjuki, A review on the chemistry, production, and technological potential of bio-based lubricants, Renewable and Sustainable Energy Reviews 82 (2018) 80-102.
- [14] R.J. Prince, Base oils from petroleum (Chapter 1) in Chemistry and Technology of Lubricants (3rd Edition) (Eds. R.M. Mortier, M.F. Fox, and S.T. Orszulik), Springer (2010), pp. 3-33. DOI: 10.1023/b105569_1
- [15] J. Ancheyta, A. Alvarez-Majmutov, C. Leyva, Hydrotreating of oil fractions (Chapter 13) in Multiphase Catalytic Reactors: Theory, Design, Manufacturing, and Applications (Eds. Z.I. Önsan and A.K. Avci), Wiley (2016), pp. 295-329. DOI: 10.1002/9781119248491.ch13

- [16] S. Qader, G. Hill, Hydrocracking of petroleum and coal oils, Industrial & Engineering Chemistry Process Design and Development 8(4) (1969) 462-469.
- [17] T. Mang, G. Lingg, Base oils (Chapter 4) in Lubricants and Lubrication (Eds. W. Dresel and T. Mang), Wiley (2017), pp. 51-82. DOI: 10.1002/9783527645565.ch4
- [18] S.F. Brown, Base oil groups: manufacture, properties and performance, Tribology & Lubrication Technology 71(4) (2015) 32.
- [19] J. Braun, Additives (Chapter 6) in Lubricants and Lubrication (Eds. W. Dresel and T. Mang), Wiley (2017), pp. 117-152. DOI: 10.1002/9783527645565.ch6
- [20] I. Minami, Molecular science of lubricant additives, Applied Sciences 7(5) (2017) 445.
- [21] H. Li, Y. Zhang, C. Li, Z. Zhou, X. Nie, Y. Chen, H. Cao, B. Liu, N. Zhang, Z. Said, Extreme pressure and antiwear additives for lubricant: academic insights and perspectives, The International Journal of Advanced Manufacturing Technology 120(1-2) (2022) 1-27.
- [22] H. Spikes, The history and mechanisms of ZDDP, Tribology letters 17(3) (2004) 469-489.
- [23] J. Zhang, H. Spikes, On the mechanism of ZDDP antiwear film formation, Tribology Letters 63 (2016) 1-15.
- [24] P. Lin, G. Barber, Q. Zou, A.H. Anderson Jr, S. Tung, A. Quintana, Friction and wear of low-phosphorus engine oils with additional molybdenum and boron compounds, measured on a reciprocating lubricant tester, Tribology Transactions 51(5) (2008) 659-672.
- [25] H. Ding, X. Yang, L. Xu, M. Li, S. Li, S. Zhang, J. Xia, Analysis and comparison of tribological performance of fatty acid-based lubricant additives with phosphorus and sulfur, Journal of Bioresources and Bioproducts 5(2) (2020) 134-142.
- [26] N. Han, L. Shui, W. Liu, Q. Xue, Y. Sun, Study of the lubrication mechanism of overbased Ca sulfonate on additives containing S or P, Tribology Letters 14 (2003) 269-274.
- [27] S.J. Eaton, Accelerated Poisoning of Diesel Oxidation Catalysts by Zinc Dialkyldithiophosphate-Derived Phosphorus, Master's Thesis (2006), University of Tennessee. https://trace.tennessee.edu/utk_gradthes/1544
- [28] E.F. Rico, I. Minondo, D.G. Cuervo, The effectiveness of PTFE nanoparticle powder as an EP additive to mineral base oils, Wear 262(11-12) (2007) 1399-1406.

- [29] H. Schiefer, R. Awe, C. Whipple, Extending the Utility of Silicone Lubricants through Structural Modifications, Journal of Chemical and Engineering Data 6(1) (1961) 155-160.
- [30] H. Kaleli, The impact of crankcase oil containing phosphorus on catalytic converters and engine exhaust emissions, Industrial Lubrication and Tribology 53(6) (2001) 237-255.
- [31] I. Madanhire, C. Mbohwa, Lubricant additive impacts on human health and the environment in Mitigating Environmental Impact of Petroleum Lubricants, Springer (2016), pp. 17-34. DOI: 10.1007/978-3-319-31358-0
- [32] L. Duan, J. Li, H. Duan, Nanomaterials for lubricating oil application: A review, Friction 11(5) (2023) 647-684.
- [33] W. Zhai, K. Zhou, Nanomaterials in superlubricity, Advanced Functional Materials 29(28) (2019) 1806395.
- [34] F. Mariño, J.M.L. del Río, E.R. López, J. Fernández, Chemically modified nanomaterials as lubricant additive: time stability, friction, and wear, Journal of Molecular Liquids 382 (2023) 121913.
- [35] E.A. Taborda, C.A. Franco, M.A. Ruiz, V. Alvarado, F.B. Cortes, Experimental and theoretical study of viscosity reduction in heavy crude oils by addition of nanoparticles, Energy & Fuels 31(2) (2017) 1329-1338.
- [36] K.K. Gajrani, M.R. Sankar, Sustainable cutting fluids: thermal, rheological, biodegradation, anti-corrosion, storage stability studies and its machining performance, Encyclopedia of Renewable and Sustainable Materials 1 (2020) 839-852.
- [37] M.M. Rahman, M. Islam, R. Roy, H. Younis, M. AlNahyan, H. Younes, Carbon nanomaterial-based lubricants: review of recent developments, Lubricants 10(11) (2022) 281.
- [38] J. Kałużny, A. Kulczycki, W. Dzięgielewski, A. Piasecki, B. Gapiński, M. Mendak, T. Runka, D. Łukawski, O. Stepanenko, J. Merkisz, The indirect tribological role of carbon nanotubes stimulating zinc dithiophosphate anti-wear film formation, Nanomaterials 10(7) (2020) 1330.
- [39] R. Tonk, The challenges and benefits of using carbon nano-tubes as friction modifier lubricant additives, Materials Today: Proceedings 37 (2021) 3275-3278.

Introduction

[40] W. Dai, B. Kheireddin, H. Gao, H. Liang, Roles of nanoparticles in oil lubrication, Tribology International 102 (2016) 88-98.

[41] D. Puhan, Lubricant and lubricant additives (Chapter 9) in Tribology in Materials and Manufacturing - Wear, Friction and Lubrication (Eds. A. Patnaik, T. Singh and V. Kukshal), IntechOpen (2020). DOI: 10.5772/intechopen.93830

Chapter 2 Literature Review

2.1 Lubricants, Additives and Nanoparticles

The lubricants are blended using BOs, which are either derived from petroleum or synthetically formulated. The crude oils are processed using vacuum distillation, solvent extraction, dewaxing (slack removal), hydro-finishing, and some intermediate steps to remove vacuum residue and asphalt [1]. These processes are used to produce multi-grade oils with low sulphur content, low viscosity, and high energy efficiency. The lubricants are typically prepared to meet the standards of API, SAE, IPLSAC, and EAMA. The lubricants are characterized by studying the properties, namely viscosity, viscosity index (VI), pour-point and flash point, aniline content, acidity, sulfur content, carbon content, thermal stability, and volatility. Based on these properties and standards, API has categorized BOs into five groups (Group I to Group V). Group I BOs have a saturate of $\leq 90\%$, sulphur content > 0.03%, and a viscosity index of 80– 120. Group II and Group III BOs have a higher % of saturates (\geq 90) and a lower concentration of sulphur (≤ 0.03). While the Group II BOs have a viscosity index of 80–120, similar to that of Group I, the Group III BOs possess a higher viscosity index of \geq 120, making them superior in viscosity retention at higher temperatures. Group I to Group III BOs are mineral-based oils produced from different refining techniques. Group IV and Group V BOs are primarily synthetic and prepared by chemically modifying petroleum products. The synthetic oils can be tuned as per the requirement by controlling the processing methods to show superior lubrication, viscosity index, and reduced sulphur content [1].

Various BOs are used in different proportions to prepare an oil formulation for a specific application. The BOs impart the properties like volatility, flash point, aniline point, carbon residue, etc., to the final product depending on the molecular structure of their inherent constituents. However, specific properties like viscosity and viscosity index w.r.t temperatures, AF characteristics, AW behaviour, oxidation stability, etc., are modified using additives. The lubricating oils perform various functions simultaneously, requiring multiple additives to be dispersed in them. Lubricating oils commonly consist of dispersants, detergents, anti-oxidants, AW agents, friction modifiers, corrosion inhibitors, extreme pressure agents, viscosity index improvers, pour-point dispersants, etc. AW agents reduce rapid wear on metals like steel by forming a compound on the surfaces that distributes the load more effectively. ZDDP, phosphines, di-thiocarbonates, and sulphates are some common AW agents [1].

Oil-based lubricants have been playing a vital role in the automobile industry for many years. A wide range of products is utilized in different applications to maintain the life and performance of the equipment. On average, the additives in these blends comprise 10–20% of the total volume. Some commonly used automotive and transmission oils are gasoline EOs, transmission fluids, diesel EOs, two-stroke EOs, rail EOs, and marine EOs. The type and number of additives to be used are dependent on the application. In diesel EOs, high contents of detergents, dispersants, anti-wear, and viscosity index improvers are used as additives to counter the high degree of wear, resulting in incomplete fuel combustion and the diesel engine's poor performance.

On the other hand, dispersants, detergents, anti-oxidants, anti-wear, and rust inhibitors are blended in large volumes in the marine EOs to function in the saline environment effectively. A similar composition is found in rail EOs as well. The gasoline oils, two-stroke EOs, and transmission oils have a lower content of additives than the additives mentioned above, but additives like friction modifiers, VI modifiers, and pour-point depressants will increase in content. Industrial applications use complex machinery having moving parts like gear, hydraulics, compressors, turbines, and cutting oils. Such components require lubrication to prevent breakdowns. In this context, hypoid gear, hydraulic oils (heavy-duty/general purpose), compressor, turbine, and metalworking oils are used. Industrial oils do not require dispersant and detergent additives. However, high amounts of anti-wear and extreme pressure additives and nominal quantities of secondary additives like anti-foam, anti-oxidant, and pour-point depressants are used.

AF and AW lubricant additives have long been utilized in various sectors to improve the performance and durability of equipment and mechanical systems. These additives include a variety of chemicals meant to minimize friction, reduce wear, and increase overall lubrication efficacy. ZDDP is one of the most often utilized AW additives in engine lubricants. It forms a safeguarding coating on metallic surfaces that minimizes friction and inhibits direct contact between surfaces [2]. However, it can cause phosphorus and zinc accumulation, which can cause problems in contemporary catalytic converters and influence pollution control systems. MoS₂ as an AF additive creates a shielding layer between surfaces, diminishing friction and associated wear [3-5]. However, its effectiveness can diminish under extreme pressure and high temperatures. Graphite is another solid lubricant known for its AF properties [6]. Challenges associated with conventional lubricant additives are multifaceted. One major concern is the balance between improving performance and addressing environmental impact. Certain additives containing elements like phosphorus, sulfur, or metals can adversely affect emission

control systems, catalytic converters, and the environment. Moreover, under severe operating conditions like high temperatures and pressures, some additives might show reduced efficiency, which in turn lessens their overall dependability. Dispersibility and stability issues often arise with solid lubricant additives like MoS₂, graphite, and hexagonal boron nitride (h-BN), impacting their uniform distribution within lubricants and compromising their efficiency. Furthermore, the need for continual and sustainable innovation to meet evolving industry demands and stringent regulations while maintaining cost-effectiveness poses a perpetual challenge in the realm of conventional lubricant additives. Finding a balance between performance enhancement, environmental sustainability, regulatory compliance, and cost-efficiency remains an ongoing challenge for the development and application of these additives in lubrication technology.

The utilization of NPs as additives in lubricants presents a host of advantages over traditional additives due to their unique properties and behaviours at the nanoscale. One of the most significant advantages lies in their ability to form robust and durable boundary films between moving surfaces [7]. The diminutive size and extensive specific surface area of the nanoparticles allow them to infiltrate surface inconsistencies and bind firmly to metallic surfaces, thereby boosting their ability to bear loads, reducing the occurrence of direct contact between metals. This attribute enhances resistance to wear, prolonging the durability of mechanical elements like engine components, gears, bearings, and other machines that are exposed to forces of friction. Moreover, NPs offer a level of customization not typically found in conventional additives. Engineers can tailor NPs' size, shape, surface chemistry, and composition to achieve specific application lubrication requirements. NPs with 0D, 1D, or 2D possess exceptional thermal conductivity, aiding in effective heat dissipation within the lubricant. This property not only contributes to maintaining the lubricant's stability at high temperatures but also helps in reducing the risk of thermal breakdown or degradation.

Another critical advantage is the compatibility of NPs with various BOs and commercial additive packages, ensuring stability within the lubricant formulation. NPs can be engineered to have a high affinity for the BO, preventing their agglomeration or settling, which might otherwise compromise the lubricant's efficacy. Furthermore, some NPs possess improved oxidative stability, prolonging the lubricant's lifespan by reducing its susceptibility to degradation caused by oxidation, thereby maintaining its performance over more extended periods [8]. Additionally, the multifunctionality of NPs stands out as a promising aspect. These materials often possess multiple beneficial properties simultaneously, such as lubrication enhancement, reinforcement, improved thermal conductivity, and more. This characteristic

allows us to develop lubricants with tailored functionalities to address specific challenges in various industries, such as automotive, aerospace, manufacturing, and more. Despite these advantages, challenges such as scalability for mass production, cost-effectiveness, and a comprehensive understanding of their long-term environmental impact remain significant considerations. Nonetheless, ongoing research and technological advancements in nanomaterial synthesis, dispersion, and application continue to push the boundaries of nanotechnology, indicating a potential paradigm shift in lubrication technology toward adopting nanomaterial-based additives for improved performance and efficiency in diverse industrial applications. Various classes of NPs that have shown potential as lubricant additives are shown in Fig. 2 [9].

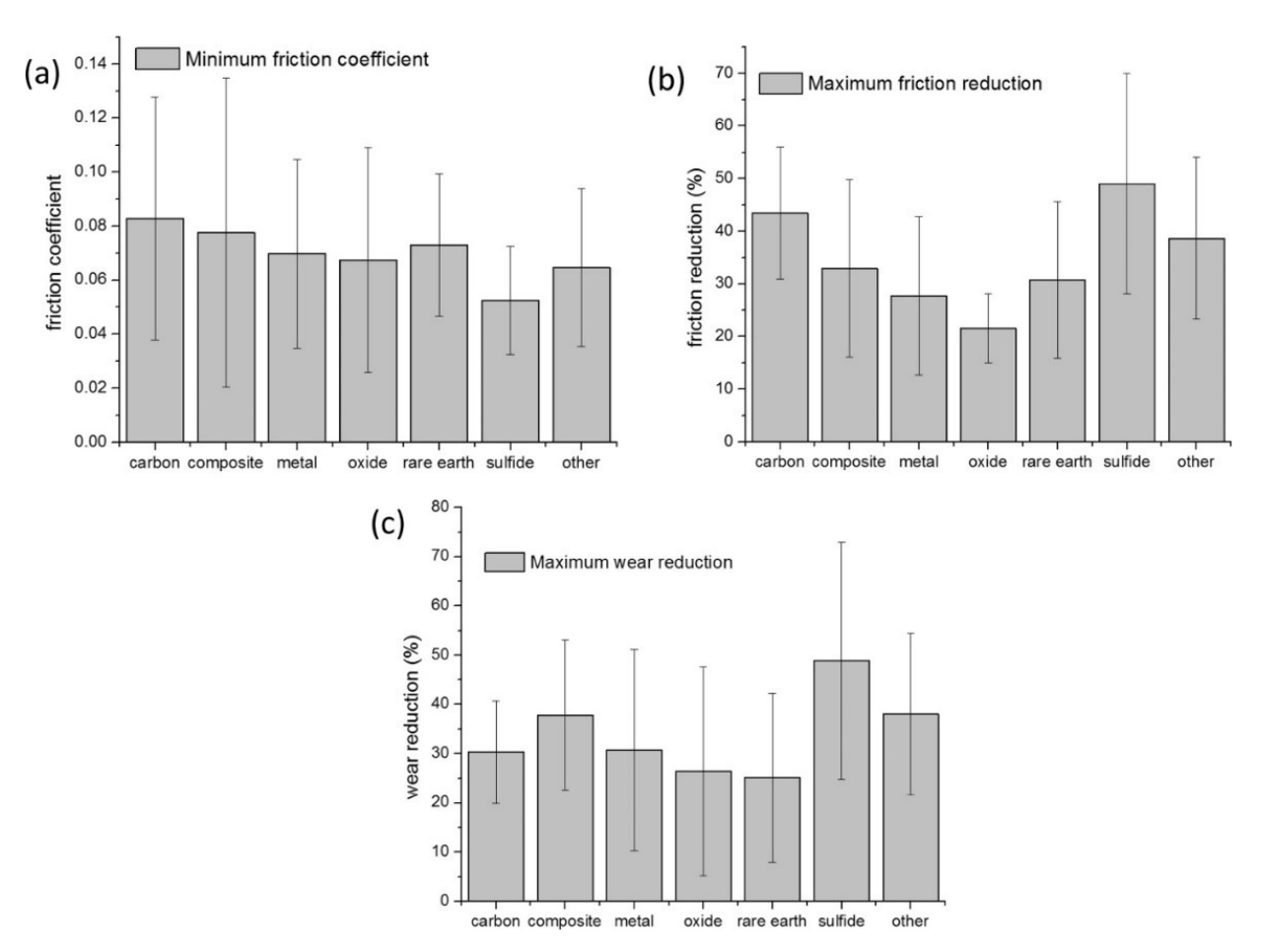


Figure 2. Tribological performance comparison of various NPs based on different chemical compositions (Reproduced with permission form [9]).

NPs with varying morphologies form robust boundary films that reduce friction between moving surfaces, significantly mitigating wear and tear [10]. Because of their increased surface area, NPs' shape substantially impacts friction and wear reduction, allowing for higher atomic-

level interactions and decreased real contact areas between surfaces. Certain NPs have unique mechanical qualities, such as high hardness and strength, which help to reinforce surfaces and resist wear. Furthermore, some NPs function as lubricants, generating protective layers and reducing direct surface contact. Furthermore, NPs with self-healing capabilities and nanostructured surfaces can reduce wear by rearranging or trapping lubricants. Overall, the morphology of NPs determines their surface features, lubricating abilities, and mechanical strength, all of which contribute considerably to friction and wear reduction in various applications. Different morphologies of NPs and their respective tribological performance as lubricant additives are shown in Fig. 3 [10].

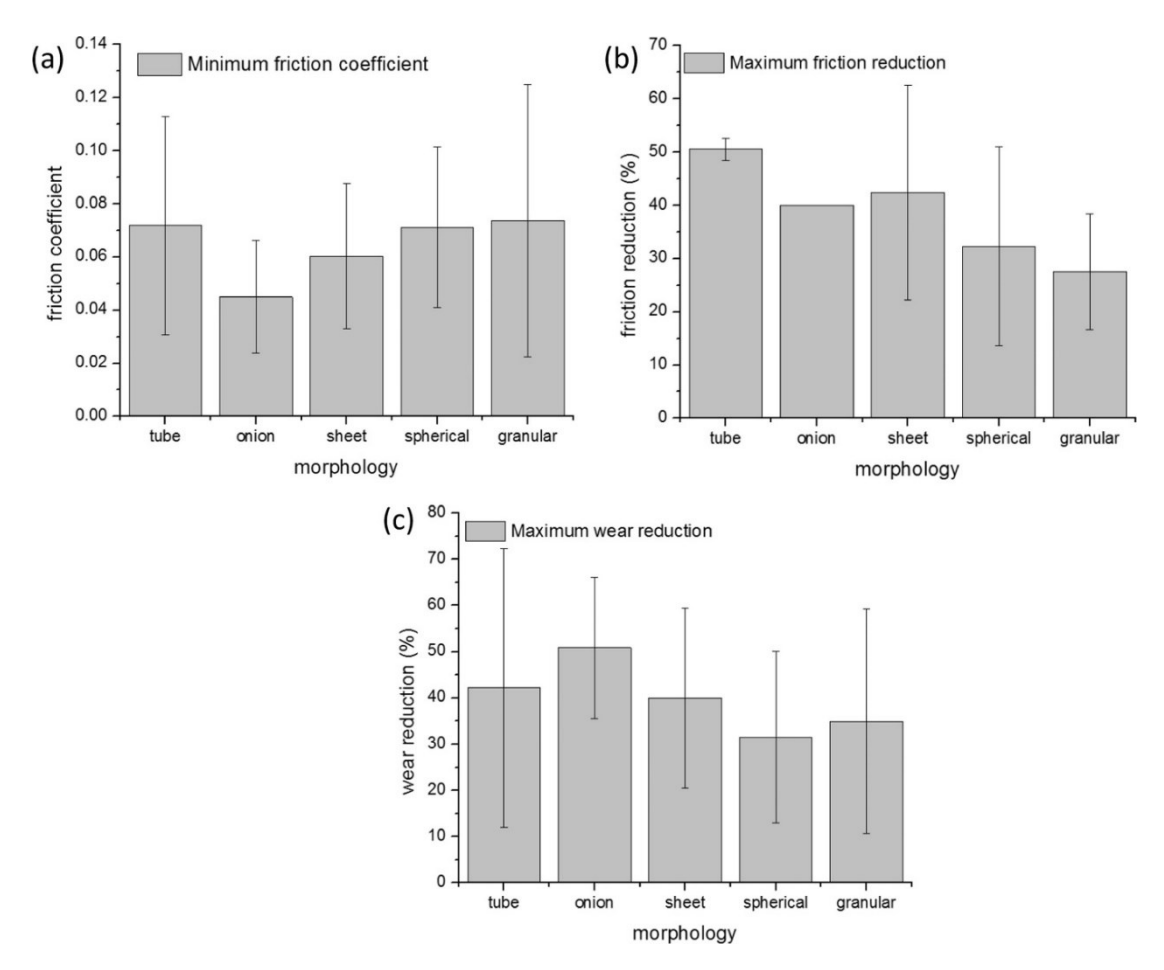


Figure 3. Tribological performances of nanoparticles with different morphology (Reproduced with permission form [9]).

Certain lubricant additives reduce friction dramatically while simultaneously having excellent AW properties. Functional polymers, oil-soluble organic compounds, organic friction modifiers and NPs, which have recently been explored for this role, are examples of such additives. NPs are a diverse class of materials that have shown promising potential in the field

of tribology, showcasing exceptional enhancements in properties when used as additives in lubricants. Despite a vast number of research completed over the previous several decades, the number of reports exploring NPs as lubricating oil additives has increased steeply [11]. From Fig. 2 it can be noted that metals, oxides and carbon NPs are highly effective as lubricant additives and could potentially improve tribological properties of the lubricating media in which they are used. Metal NPs as lubricant oil additives have exceptional physico-chemical characteristics [12-15]. Therefore, their excellent AF, AW, and self-healing ability have been well professed. Metallic NPs (mainly in the form of oxides and sulphides) have been studied extensively for their lubricating properties. Cu NPs have garnered special attention due to their extraordinary features [16-18], and they can greatly enhance the tribological properties of lubricating oil. Cu NPs, when used as lubricant additives potentially decrease energy wastage in comparison to Co and Fe NPs [19] and were more effective for friction and wear reduction when added separately [20]. However, the type of oil is worth noting. Cu NPs performed exceptionally well as AF and AW agents in nonpolar oil, owing to their deposition on rubbing surfaces. Nonetheless, Cu NPs might potentially harm the lubricating layer of polar oil on the surface where metal/metal contact occurs [21]. Cu NPs with adequate mechanical properties have been examined as friction modifiers, and they are effective friction-reducing and wearpreventive agents with self-healing capabilities [22,23]. Surface-modified Cu particles that disperse well in oils significantly improved the oil's tribological qualities. As demonstrated experimentally, cu particles produced a protective coating on the wear track with a slippery texture. It was argued that the protective layer works as a sacrificial shear layer, mitigating wear loss on the rubbing surfaces [24-26]. Similarly, Ce, Ni, Pd, Ag, and Zn NPs with outstanding dispersibility in lubricants have been reported to minimize friction when dispersed in BOs and properly mixed EOs [27]. Keen interest has been in using Ni NPs as additives [12]. Chen et al. [28] showed the use of Ni NPs in polyalphaolefin (PAO) tweaked into having varied sizes with good dispersion stability led to improved friction and anti-wear behaviour. Their study showcased preparation of oil-soluble metal NPs with excellent dispersion stability in oil. Apart from Cu and Ni NPs, various metal NPs like Ag [29], Sn [30], Fe [30], Co [20], Pb [31], Au [32], Bi [33], Mo [34], W [34], and Ga [35] have been explored as lubricant additives. The AW mechanism of soft metallic NPs, is dominated by the superlative hardness and shear modulus, however, this phenomenon has little effect on the AF properties. Both AW and AF mechanisms are due to metallic tribo-films forming over the worn-out surfaces. In the case of harder metallic NPs, the NPs form a protective film or act as rollers. Tribological behaviours depend on which effect is dominant [33]. Although the metal NPs seem effective, they

negatively affect the oxidation stability of the lubricating media. Presence of metals is one of the most prime causes of the degradation of lubricating oil in engines. Many studies have been carried out to examine the effect of various metals on the deterioration of lubricating oils. Elements like Fe, Cu, and Pb are well-known catalysts for the degradation of oils. Cu salts, as well as Cu in bulk form, are efficient catalysts. Furthermore, increasingly metal-based catalysts that might successfully catalyse the oxidative breakdown of oil have been found. It is thus important that apart from the tribological qualities, the impact of adding metal NPs on the oxidation stability of the lubricants must also be focused on [36]. Metal oxides have also proven effective in reducing friction and wear when added into lubricating blends. PAO6 oil loaded with spherical CuO, ZrO2, and ZnO NPs as additives helped reduce the friction and wear through a third body and tribo-sinterization mechanism [37]. Similarly, spherical CuO, TiO₂, and diamond NPs used as additives resulted in a good reduction in friction and wear, with CuO being the best [38,39]. The friction reduction was due to viscosity effect at low temperature and rolling effect at high temperature. The wear reduction mechanism was attributed to the formation of a layer-like deposit of CuO particles on the wear track to reduce the shearing stress on the surface asperities, eventually enhancing the tribological properties. It was claimed that nano-rod-like CuO particles dispersed and stabilized in ionic liquids resulted in a friction reduction of 15–43% and wear reduction by 26-43% compared to polyethylene glycol 200 and 10W-40 EO [40]. Likewise, Cu/CeO₂, Al₂O₃/SiO₂, and ZrO₂/SiO₂ hybrid/composite NPs were studied as efficient and effective additives in lubricants [41-43].

It was reported that adding MoS₂ NPs (the inorganic fullerenes) to PAO oil resulted in substantial reductions in the friction and wear values due to their crystalline order and particle size [44]. Apart from MoS₂ and WS₂, other metal-based sulfides such as CuS and ZnS particles as lubricant additives have been proven to give excellent friction modification and wear prevention [45-48]. Metal borate particles have exceptional load-bearing ability, thermal stability, and anti-wear characteristics and have been studied as additives in lubricant media [49-51]. It was reported that adding calcium-borate particles to lubricant oils reduced friction and wear [52,53]. After observing the remarkable solid lubricating capabilities of hexagonal boron nitride (h-BN), NPs of h-BN were dispersed in lubricants. Improvements in the coefficient of friction and wear resistance on using h-BN NPs as additives in oil/water/greases were observed, which was assumed to result from the intermediate tribo-film formed over the wear tracks by deposition followed by recurring exfoliation mechanism of h-BN [54,55]. Si₃N₄/DLC thin films revealed super lubricity behaviors with PAO6 oil dispersed with 1.0 wt.% of h-BN as lubricant filler [56]. The super lubricity attained could be explained as a reduction

in the direct contact area. The h-BN particles act as a buffer layer with weak van der Waals forces between its layers that function like nano ball bearings between point-like contact surfaces. CaCO₃ NPs were used to improve the load-bearing ability, wear resistance, and frictional properties of PAO. The presence of a boundary tribo-film of CaCO₃, CaO, iron oxides, and some organic compounds on the worn surfaces was confirmed [57]. Another choice was the use of CaF₂ nanocrystals as friction modifiers. Here too, tribo-layers composed of CaF₂, CaO, iron oxides, and some organic compounds were formed on the rubbed wear tracks, and the thickness of boundary film was about 12 nm [58].

2.2 Nanocarbons as Lubricant Additives

2.2.1 0D Nanocarbons as Lubricant Additives

Materials with spherical morphology that exhibit a rolling mechanism (instead of or in addition to a sliding mechanism) for lubrication are helpful for tribological applications. Micron-sized silica spheres [59] and fullerene (C₆₀) [60] are two classic examples. However, few experimental works are available in this context due to shortcomings in synthesizing the materials adequately and controlling the properties, repeatability, economics, and environmental viability [61]. Nonetheless, several published reports have inspired advanced research [59-76]. Adding 0.01 wt.% diesel soot to PAO helped the lubricant reduce friction and improve the anti-wear characteristics [62]. Carbon nano-onions (CNOs) are excellent additives to the lubricant [63] and excellent solid lubricants [64]. The absence of dangling bonds on the surface of CNOs facilitated their easy sliding and rolling-off on friction surfaces when used as lubricant additives [63]. The size (< 100 nm) of CNOs and their pseudo-spherical morphology enabled them to behave like ball-bearings at the nano-scale when used as solid lubricants [64]. Additionally, the closed structure (graphitic layers arranged in an onion ring-like form) of CNOs renders their thermodynamic stability and high mechanical strength. However, the defects induced in the outer-most layer of the CNOs may increase the chances of bonding CNOs with the rubbing surfaces' material, thereby resulting in detrimental friction and wear characteristics. On the other hand, to support the use of CNOs in tribological applications, novel CNOs preparation from bio-diesel-soot has also been elucidated. The graphene fragments [65,66] of high contortion in the bio-diesel-soot facilitated onion-like morphology [67]. Carbon black and carbon soot (CS) (derived from wasted bio-mass) have also been used to study the tribological effects when dispersed in various lubricating media [68-75]. Many efforts have been put into synthesizing and characterizing carbon spheres (CSPs) by chemical vapor deposition (CVD), pyrolysis techniques [77-80], and hydrothermal processes for

tribological applications [81-87]. The most common method to synthesize CSPs is the hydrothermal method [80,81], in which glucose is typically carbonized. In this method, a specific molar (0.5–1M) glucose solution is first prepared and then held isothermally (above the melting temperature and close to the decomposition temperature of 180 °C) in an autoclave aided with stirring for 6–10 h. Subsequently, after natural cooling to ambient temperature, the sediment is washed with DI water and alcohol. After washing, the material is vacuum-dried at 60-80 °C for 4-6 h to obtain CSPs. CSPs can also be prepared by ultrasonication-assisted copolymerizing resorcinol and formaldehyde solutions [83]. In the hydrothermal method, CSPs form saccharide precursors through the typical steps, namely dehydration and fragmentation of sugars, polymerization or condensation of the dehydrated and fragmented species, aromatization of the polymers, and finally, the nucleation and growth in the solution. The final step is diffusion and linkage of species from the solution to the nuclei surfaces. Another interesting method is the non-catalytic atmospheric pressure chemical vapor deposition method, in which C₂H₂-H₂-Ar gas mixture is reacted at 950 °C to form CSPs in the gas phase [84]. CSPs are typically made of 98–99% carbon; the rest, metallic impurities, depend on the impurities in the starting precursors. The diameter of the CSP particles is typically in the submicron range. The CSPs (with spherical shape and a smooth peripheral surface) are anticipated to act as third body particles that can occupy the spaces between the asperities of contacting surfaces and minimize the contact pressure, ultimately diminishing friction and wear losses. Xray diffractogram of CSPs, when seen, shows a broad (002) graphitic primary Bragg's peak typically in the 2θ range of $24-26^{\circ}$. This indicates that CSPs typically possess only a low degree of graphitization [84]. However, suitable post-synthesis, complimenting well with X-ray diffraction studies. Transmission electron microscopy can also be used to complement the Xray diffraction and Raman scattering analyses. heat treatment can improve the crystallinity of CSPs while minimizing the amorphous content in CSPs [61]. Complimentary Raman scattering analysis confirms the low degree of graphitization in CSPs. The Raman spectrum of CSPs shows the typical D peak at 1340 cm⁻¹ and G band at 1575 cm⁻¹, corresponding to structural defects and graphitic content present in CSPs. The high ratio of the intensity of the D band and intensity of the G band shows a low degree of graphitization [84,85]. Due to the smooth outer graphitic layers, non-hollow structure, and the presence of C–O, C=C, and C–H bonds [84,85], the CSPs are supposed to exhibit high elastic modulus and hardness values favorable for their use in tribological applications (especially as additives in lubricants). In this context, nanoindentation studies have shown that, indeed, CSPs can have elastic modulus and hardness values of 16.5 GPa (with a standard deviation (SD) of 4.8 GPa) and 1.2 GPa (with an SD of 0.6 GPa) [83]. Apart from the mechanical properties, it has been suggested that if CSPs are very small in size (say only few nms.), they fail to contribute to the rolling mechanism. Instead, CSPs may get trapped in rough asperities on the surfaces, hindering the shearing process at the contact surfaces [85]. Therefore, CSPs with dimensions larger than the roughness of the shearing surfaces have been recommended for the role of rolling friction. Several works reported improved tribological properties using CSPs additives in lubricants by considering the above recommendations. In one recent work, 0.5 wt.% of CSPs were dispersed in Castrol 5W-40 EO [82]. The CSPs dispersed lubricant was then used to improve the tribological performance of polyetheretherketone (PEEK). It may be noted that PEEK is now a popularly used material in engineered sliding components. CSPs prepared using hydrothermal carbonization have enough functional groups attached to their surfaces, leading to the strong interactions of CSPs and lubricating oil, resulting in excellent stability of the dispersions. With the increase in temperature from 10 to 65 °C, adding 0.5 wt.% CSPs had a marginal influence on the viscosity. Tribological tests were performed on a ring-on-disk (tungsten steel upper ring block and lower stationary PEEK disk) apparatus at ambient temperature and relative humidity of 36%. Extreme operating conditions were applied to the CSPs added lubricant during the tribological tests conducted under a load of 1500 N (contact pressure of 187 MPa), sliding velocity of 150 rpm for 15 min. Tribological test results showed a reduction in friction coefficient (23.5–33.2%) and wear rate (24.2%) with CSP dispersed oil compared to the BO. The observed improvement was attributed to the homogenous blending of BO and the CSPs. It is understood that during the sliding of friction pairs, surfaces slide against each other, and the CSPs added lubricant fills the asperities and voids, forming a tribo-film to take the load and minimize the friction. In the above-discussed study, CSPs have spherical morphology resulting in rolling movement, thus elevating the tribological performance. Coefficient of friction (CoF) values recorded using different wt.% of CSPs in Castrol 20W-40 oil [84] showed a maximum reduction in the CoF, and any other concentration above 0.3 wt.% of CSPs increased CoF values. It was observed that for lower concentrations below 0.3 wt.% of CSPs, CoF values were close to that contributed by the neat oil. The CoF values surpassed the neat oil case at very low concentrations of 0.05 and 0.01 wt.% of CSPs. When the CSPs are added in very low concentrations, they fail to form a uniform film by adhering to the moving surfaces and create resistance to the asperities under an applied force. However, at the optimal concentration of CSPs, a uniform layer of protecting material and the spherical morphology act parallelly and create a rolling effect called a 'nano-bearing' effect. This effect allows the surfaces to slide smoothly over the CSPs' tribo-layer, thus reducing the direct surface-to-surface contact, which

minimizes wear. At higher concentrations (higher than the optimal concentration) of CSPs, agglomeration takes place, causing sedimentation. The sedimented or lump-like CSPs fail to act as an efficient lubricant additive and, on the contrary, act as barriers to the sliding surfaces. It was also found that the CoF values fall rapidly during the initial stage of the testing and then stabilize, attaining a fixed value with time. This characteristic is due to the unstable contact between the sliding surfaces in the initial stage of the test. In another interesting work, CSPs dispersed BO showed a similar tribological behaviour as that of the virgin BO, but lower and consistent CoF values were measured, indicating the enhanced lubricating performance of CSPs in the BO [87]. Tribological tests were performed using ball-on-disk (52100 chromium steel ball and 304 stainless steel disks with an RMS surface roughness of 0.1 µm). Over 50% of wear volume reduction was observed when CSPs dispersed BO was used. The wear track dimensions on the ball and disk decreased by using the CSPs dispersed BO. Interestingly, posttesting formed tribo-films (between the sliding friction pairs) were highly graphitic, inferring that the CSPs were present on the sliding contact area and improved the tribological properties. CSPs were also used as grease-lubricating additives [86], and excellent results have been observed. CSPs were dispersed in lithium lubricating grease, and it was experimentally found that 1 wt.% CSPs in lithium grease delivered the optimal anti-wear and AF properties. CoF was reduced by 20.43%, and wear volume was decreased by 49.30% when CSPs dispersed grease was used. The worn surface was relatively smooth with few shadow furrows. This work indicated that the concentration of the additives is an important aspect, and it is always recommended to perform percolative studies to determine the optimal concentration. In this work, when using the CSPs as the additive particles, enhanced lubrication is observed only up to a threshold value of CSPs concentration and above which CSPs started to show a negative impact. Here too 'micro-roller' effects, repairing and forming the protective film are the reasons for enhanced tribological properties of CSPs dispersed grease lubricant.

Combustion of standard candles has been the most popular method to prepare CS. Candles are highly rich in hydrocarbons (paraffin waxes with carbons in the range of C16–C30) derived from crude petroleum oil. The CS particles collected from burning standard candles have graphitic layers with an onion-like core [88]. CS particles collected from the exterior flame of the candle are fully oxidized NPs of homogenous shape and size. The combustion flame's outer zone has a sufficient oxygen supply compared to the following intermediate and core zones. The combustion smoke from the bio-diesel soot dried at 120 °C for 3 h and subsequently grounded results in the granular CS particles [89]. However, the yield in the combustion of bio-diesel soot is meager. 1 kg bio-diesel yields only 13–18 g of CS. It is important to note that

various factors may render the combustion incomplete, leading to inhomogeneous (in size and shape) CS particles. Therefore, many attempts have been made to alter and tailor CS particles to enhance their properties. Several techniques were proposed to prepare oxygen-containing functional groups by oxidizing the surface of carbon blacks and other carbon nanostructures [90]. One such technique is to use an organic base and surfactant [91]. By doing so, CS particles decorated with hydroxyl groups can be prepared on a large scale. These functionalized CS particles have enhanced dispersion and performance when added to water. Primary (diesel) soot particles directly collected from a diesel engine's exhaust pipe with four cylinders of a typical passenger car exhaust pipe are either spherical or nearly spherical with sizes in the range of 30–50 nm [92]. The surface morphology of these CS particles is extremely irregular, and agglomeration of these CS NPs was noticed in the form of long chains due to adhesive interaction between them [93]. An interesting study showed that hydrophobic CS particles can be prepared by controlling the atmosphere near the combusting candle [93]. The combustion was carried out in a perforated chamber that enhanced the air availability by creating a laminar flow and ultimately facilitating lean combustion. Converting wasted materials into CS particles has also been taken up by researchers. For example, rubber waste (bicycle's rubber tube) was converted into highly homogenous CS particles with sizes of 50–100 nm [94]. The wasted rubber tube was burnt using the flame of a typical burner in a fume hood, and the combustion soot was collected on a glass surface. The soot was then ground and annealed in a tubular furnace at 900 °C for 5 h in an inert (Ar gas) atmosphere to obtain graphitized CS particles finally. Even though CS and CSPs synthesis processes are divergent, their morphology and structural characteristics are strikingly similar. The diameter of the CSPs is typically a few tens of nm to few hundreds of nm. The high-resolution transmission electron microscopy indicates that the CSPs particles are formed by layer-by-layer deposition and graphitized post-annealing. A similar morphology is also reported for CS particles synthesized by different methods [64,95]. Diffraction and spectroscopic studies showed that CS particles have similar crystalline and bonding/phase characteristics as CSPs [94]. The graphitization level can be controlled during combustion or by an appropriate heat treatment post-combustion. It is evident from the spectroscopic studies that the CS particles mainly consisted of carbon and oxygen. The diffraction studies have established that CS particles are nanosized and are quasi-crystalline. The studies reveal that concentric graphitic layers constitute CS particles with poor graphitization. in relative motion slide over each other, reducing the wear and friction. Similar to CSPs, the spherical morphology can give the nano-bearing effect when deployed in lubricants used at interfaces of sliding surfaces. The soot formation mechanism involves the formation of radicals from hydrocarbon molecules, and eventually, the radicals grow into soot particles on a suitable substrate [95-97]. The CS particles obtained from bio-diesel soot were dispersed in water and used as a lubricating medium [89]. Due to the addition of CS particles, the tribological performance of rubbing surfaces improved at low to high loads, indicating that the CS particles came in-between the rubbing surfaces and acted as nano-bearings, even under a high load. This was attributed to the onion-like structure of the soot, causing the reduced friction coefficient and wear rates. CS particles acted as a spacing agent between the rubbing surfaces and gave a rolling effect between the moving pairs. At high loads, exfoliated graphitic layers formed from the CS particles during the sliding. CS particles were also functionalized by treating them with nitric acid. The functionalization yielded better tribological properties compared to the as-synthesized CS particles. The additional functional groups helped the CS to adhere better on the surfaces. The CoF and wear volume for steel-steel contacts lubricated by neat perfluoropolyether and mixtures with varying mass concentrations of CS NPs were observed. Polyether performed with meagre AF properties, the CoF being around 0.185. The AF behaviour of polyether was enhanced by adding CS particles. The mixtures comprise CS particles and polyether outrun the neat polyether for lubricating properties for steel-steel contacts under varying test conditions (high temperature, step-loading). The enhanced properties were attributed to the spherical shape of CS particles, consisting of layered graphene internal structure. The soot particles act as roller bearing between the surfaces, decreasing the wear. It has been experimentally observed that for the same concentration of CS particle addition, the CoF increases with an increase in the CS particle size. During the sliding action of the contact surfaces, the larger particles are pushed out of the contact area. Also, larger particles occupy more area (while being less in number), resulting in smaller contact areas with other particles and higher contact areas with the sliding surfaces, causing an increase in the CoF [61]. However, it has also been observed that increasing the concentration of CS-sodium dodecyl sulphate mixture in the lubricant can help to lower the CoF, but much-increased concentrations will restrict the rolling movement of particles and cause a rise in CoF.

CS particles were also tried as additives in greases. For example, the average CoF of lithium grease was lowest (0.1076) for a soot content of 1.0 wt.%, reduced by 21.35% as compared to (0.1368) lithium grease [86]. This indicated that the lithium grease with appropriate soot has superior tribological properties. As the percentage of soot rises from 0 to 1.0 wt.%, the wear volume reduces from 0.012734 to 0.006456 mm³, and the reduction rate is 49.28%. However, the wear volume increased as the soot content surpassed 1.0 wt.%. The improved performance was also attributed to the 'micro-roller' effect when the surfaces slide. High carbon content

was detected on the wear tracks, indicating that soot can adhere to the surfaces, promoting rolling friction among the surfaces and eventually reducing the friction and wear by forming a suitable tribo-film. A unique study involving textured surfaces and diesel-based CS particles reported lower friction and wear [92]. The PAO oil with CS particles showed a CoF of 0.1 without any texturing on the surface. Even with textured surfaces, there was no significant reduction compared to the CS-dispersed sample. The PAO without CS (here diesel soot) samples are seen to have higher wear scar width values. The untextured sample shows the biggest scar of 1150 μm, which reduces with increased texturing density. However, the addition of CS into the PAO oil and the texturing effect drastically reduces the scar width, keeping it in a low range of 280–300 μm. This reduction is due to the prevention of contact by the CS particles. The CS particles act as nano-bearings between the two surfaces, eventually forming a tribo-film on the surface. Such films have been confirmed in several reports [72,74,92,95].

2.2.2 1D Nanocarbons as Lubricant Additives

This section summarises the scientific development of 1D NCs production and application as lubricant oil additives. Carbon nanotubes (CNTs) are the most widely known 1D NCs. CNTs drew much attention by virue of their unique properties and applications in nanotechnology. The structure of CNTs is cylindrical, with diameters ranging from a few nm to hundreds of nm. [98]. Several synthesis methods and structural alterations are currently being developed for suitable uses. These synthesis processes lack focus on a sustainable and continuous production of CNTs. CNTs are divided into two types based on the inner wall present in them. Singlewalled carbon nanotubes (SWNTs), which are essentially single-layer graphene sheets with diameters between 1-2 nm, were first utilized in 1993. The synthesis of CNTs necessitates the use of a catalyst, and the properties of the CNTs can vary based on the processing parameters. Double-walled carbon nanotubes (DWNTs) are composed of two separate carbon nanotubes, where the larger one envelops the smaller one. The diameter of the larger tube ranges from 2-4 nm, while the smaller tube has a diameter between 1-3 nm. On the other hand, multi-walled carbon nanotubes (MWCNTs) have diameters varying from 2 to 50 nm, and they are constructed from several layers of coiled graphene. The Russian doll model is a very common model of MWCNTs, which involves graphene layers organized in concentric circles, and the parchment model, where a lone graphene layer is coiled around itself numerous times, giving it the appearance of a rolled-up piece of paper. Various methods have been used to synthesize CNTs, but the yield, purity, and structure of the resulting CNTs often fall short of expectations. Therefore, there is a need for researchers to innovate new techniques for synthesizing CNTs with enhanced features. Various factors, such as the size of the catalyst, can influence the structure, diameter, purity, and other properties of CNTs. The cost-effectiveness of the carbon source used in CVD procedures is a critical consideration. The carbon source is used to produce CNTs, so the cost of the carbon source largely determines the cost of the CNTs. Therefore, efforts should be directed towards finding new carbon sources, and placed on designing and developing a continuous synthesis process [99].

CNTs, particularly MWCNTs, have been extensively studied for their superior frictionreducing properties. MWCNTs, with their unique structure properties of coaxial cylindrical multi-layer graphene, have demonstrated potential as AF and AW additives [100]. Predictive theoretical models have suggested that the interfacial shear forces between layers of MWCNTs are quite low. However, structural defects in non-concentric layers can significantly increase the shear force, which tends to increase progressively with the length of the CNT. On the other hand, the chemical inertness of unmodified CNTs results in minimal adsorption on the surfaces in question. There have been significant advancements in the field of CNTs in recent years. To counteract the chemical inertness of CNTs, substantial surface functionalization was accomplished using stearic acid [101], Cobalt [102], carboxyl [103], and many more [104], and the friction behaviors are influenced by the density of the modifier on the surface [101,105]. MWCNTs with 0.08 wt.% polymeric aryl phosphates (PAPs) improved friction reduction by approximately 60% and anti-wear performance by about 95% [106]. The mechanism and rheological behavior of MWCNTs in the lubricating media were also investigated [105-107]. Notably, CNT additives were evaluated in the EO [108]. The research showed that incorporating CNTs into EO lowered the motoring torque by 7%. It was observed that during normal operation, the oil's shear force effectively dispersed the CNTs in the engine, and the oil filter system successfully removed CNT clusters. Ball on disc tests conducted on COOHfunctionalized MWCNTs dispersed in PAO4 and PAO6 oils in different concentrations (0.025 - 0.15 wt.%) showed significant reduction in the CoF by around 27% and the wear volume by approximately 88% at 0.05 wt.% and 0.025 wt.% of CNTs in PAO, respectively. In PAO6, the best CoF and wear volume were achieved with additive concentrations of 0.075 and 0.05 wt.%, respectively. The results suggested that nano lubricants based on PAO6 had the most effective frictional properties, while those based on PAO4 showed excellent AW performance. To better understand the lubrication process of MWCNTs, the worn surfaces were examined using various analytical techniques [103]. Fly-ash derived from oil was identified as a promising source to produce CNTs as lubricant additives in BOs (Saudi Aramco 100SN, 500SN, and 150BS), which exhibited superior tribological performance even at very low concentrations.

These CNTs were more effective in reducing the CoF between two metal surfaces compared to other NCs. A 20% reduction in CoF at CNTs concentration of 0.1 wt.% was recorded. A rheological analysis revealed that the viscosity of the 500SN oil impregnated with 0.1 wt.% CNTs is effectively like the pure oil. It can be recommended that CNTs derived from fly-ash could be an efficient additive for AF and AW lubrication [104]. An experiment was conducted where a BO mixed with MWCNTs was used as a lubricant on nodular cast iron surfaces in contact with steel to evaluate its tribological performance. The study, which utilized a pin-ondisc method, found that the BO enriched with MWCNTs surpassed the performance of the BO alone in terms of tribological properties. Furthermore, incorporating MWCNTs into the BO improved its ability to bear load and its stability as a lubricant. The processes that led to the enhanced performance of the lubricating oil with MWCNTs on nodular cast iron were also explored, scrutinized, and recorded [109]. Experimental trials were carried out on Mobil gear 627 and paraffinic mineral oils, both infused with different quantities of MWCNTs as additives, to assess their AW, load-bearing ability, and CoF. The outcomes from these trials suggest that incorporating MWCNTs into BOs aids in friction reduction and enhances AW characteristics. Wear trials demonstrate that mineral oil with MWCNTs decreases wear by 68% and 39% in comparison to the base Mobil gear 627 and paraffinic mineral oils, respectively. Moreover, measurements of friction reduction reveal that mineral oil with MWCNTs reduces friction by about 57% and 49% compared to the base Mobil gear 627 and paraffinic mineral oils, respectively. The formation of a tribo-layer composed of elements from the nanoparticles was confirmed through SEM micrographs and EDX chemical analysis [110]. MWCNTs were dispersed in SAE 10W40 oil using ultrasonic waves and used as additives. The tribological properties were evaluated using reciprocating wear tests. The experimental setup replicated the interaction between the piston ring and cylinder liner under a variety of scenarios, including diverse contact pressures and sliding speeds. The flow properties of the MWCNTnanolubricant samples displayed non-Newtonian traits (shear-thinning), while the SAE 10W-40 oil showed behavior similar to a Newtonian fluid. The CoF reduced by 4%-34% and 26%-32% under varying loads and velocities. Furthermore, after a sliding distance of 22.57 km at a load of 240 N and a speed of 0.33 m/s, the specific wear rate of the surfaces reduced by 29% and 40%, respectively. These findings imply that MWCNTs could be effective additives in lubricants. [111]. To address the poor dispersion of MWCNTs they were subjected to ball milling to reduce the length of the MWCNT and stabilized with surfactant prior to dispersing in the test oil. Electromagnetic and Raman studies were conducted to determine the effect of the ball milling. 0.5wt.% of the long and short-lived MWCNT are dispersed in the test oil (EP

140 gear oil). Light scattering techniques are utilised to determine the stability of scattered MWCNTs. The AW, AF, and extreme pressure qualities of test oils are evaluated using a 4ball wear tester. Ball milling of MWCNTs has a substantial effect on lubricant stability and tribological properties. Raman spectroscopy demonstrates that up to 10-hour ball milling did not generate any flaws on the MWCNT surface. The dispersion of shorter MWCNTs considerably increased the lubricant's stability and AF performance. Long-term ball milling lowers the advantage [112]. Single-walled carbon nanotubes (SWCNTs) and MWCNTs were incorporated into SAE 10W40 motor oil to evaluate their tribological characteristics. In comparison to standard EO without SWCNT and MWCNT, the introduction of MWCNTs into the oil resulted in a 67% reduction in the Wear Scar Diameter (WSD), while the addition of SWCNTs led to a 38% decrease in the WSD. The average CoF dropped by 56% with MWCNTs and 48% with SWCNTs, a phenomenon that could be linked to changes in viscosity The experimental results show that lubricating oil with MWCNTs performs better as an AW and AF additive than SWCNTs [113]. MWCNTs, employed as nano-additives in varying amounts together with a surfactant, were experimentally evaluated for their tribological properties using a conformal block on a disc testing arrangement. The experimental parameters and the sizes of the block and disc were established based on the Sommerfeld number (0.0025), which suggests a mixed lubrication regime. The performance of the lubricant was assessed by monitoring the frictional force and the rise in temperature throughout the experiment [114].

2.2.3 2D Nanocarbons as Lubricant Additives

Based on its physicochemical characteristics, graphene stands out as one of the most robust, ultra-thin, and lightweight materials [115]. While this description is accurate at the atomic level, graphene's behavior varies at the micro level. Graphene is a two-dimensional material, composed of a single layer of carbon atoms, less than 10 nm thick, arranged in a sp²-bonded honeycomb lattice. The symmetric arrangement of carbon-carbon bonds in 2D graphene results in high specific surface area (~2600 m²/g), making it an ideal material for numerous applications [116]. Major commercial graphene manufacturing remains difficult due to the various complexities in the processes employed, which vary depending on the application. The top-down and bottom-up processes are the two routes through which graphene could be synthesized [117]. For the majority of applications that necessitate the large-scale creation of graphene, the top-down approach is typically preferred. This strategy encompasses methods such as peeling, electrochemical procedures, and laser erosion. Conversely, bottom-up techniques like chemical gas deposition, electric arc discharge, thermal decomposition, and

plasma formation can yield graphene of superior quality with appealing electrical characteristics, but the production rates are not feasibly scalable. In the field of tribology, graphene exhibits unique AF and AW properties that distinguish it from other materials. In addition to its renowned thermal, electrical, optical, and mechanical attributes, graphene can also serve as a lubricant in both solid and colloidal liquid forms. The primary advantages of its outstanding tribological behavior include its robust chemical stability, remarkable mechanical durability, and the simplicity with which it can slide on its tightly packed and atomically level surface. The exceptional mechanical robustness of graphene aids in reducing wear on interacting surfaces. Furthermore, due to its atomically sleek features and low surface energy, graphene can replace solid layers that are commonly employed to reduce the adhesion and friction of interacting pairs [118].

Graphene acts as a component in liquid lubricants such as oil and water, and it is also employed independently as a solid lubricant [118,119]. The first mechanical peeling of graphene from large graphite crystals using clear tape has been well-documented [120] and despite being just a few atoms in thickness, it exhibits remarkable stability and unique properties. Later, it was shown that AFM cantilever can be used to peel off graphene layers from graphite crystals on the microscale [121]. Single-layer graphene nanosheets range in size from nanometres to several tens of micrometers. Ball milling is a less expensive method of preparing graphene than AFM cantilevers. On a macro scale, Jeon et al. exfoliated graphene using dry ice and ball milling [122], where edge-selective carboxylated graphite was created. The graphite was dispersed in various solvents during the ball milling process and selfexfoliated into single- and few-layer structures. Experiments were done to determine the inherent properties of mechanically exfoliated graphene. Jeon et al. also developed graphene nanoplatelets with functionalized edges [123]. Providing enough kinetic energy to graphitic frameworks in this process broke the C-C bonds, resulting in active (free radicals) carbon species and graphene nanoplatelets with functionalized edges. Suvarna et al. performed jaggery-assisted ball milling to synthesize graphene [124]. Arao et al. explored salt-assisted ball milling to prepare exfoliated graphene [125]. The study discovered that salts, such as potassium carbonate or sodium acetate, when attached to the active carbon at the graphite's edge, assist in creating a stable colloid that reduces the electrical repulsion resulting from ionic separation. This enables graphene to be evenly distributed in solvents with a low boiling point, like water. The strong mechanical characteristics, large specific surface area, and chemical stability of graphene make it an attractive substance for lubrication applications. Although previous methods produce high-quality graphene with minimal defects, they are restricted in

terms of complexity and yield. Graphene, being a flat, single-atom-thick sheet of carbon, can easily penetrate friction barriers, preventing direct contact between sliding surfaces [126]. Due to its nano-sized effect, graphene exhibits high surface activity, enabling it to adsorb onto the rubbing surface and form a shielding film throughout the lubrication process [127,128]. This adsorption phenomenon is primarily composed of physical and chemical adsorption. Graphene lubricating supplements with minimal chemical reactivity can mend and fill in damaged surfaces by establishing a protective layer of physical adsorption, dependent on their loadbearing ability. Moreover, graphene can chemically adsorb onto steel surfaces, facilitated by reactive free bonds. It attaches securely to original iron surfaces, significantly diminishing their surface energy. Metal surfaces coated with graphene become almost inactive, exhibiting extremely low adhesion and shear force during friction [129]. The application of high pressure and heat during contact can lead to the disintegration of tribofilms and the formation of a new structural state. Direct examination of the tribo layers formed on the friction contacts, even at the nanoscale, showed an evolution in their arrangement [130,131]. Graphene that has been exfoliated, typically achieved through thermal and/or chemical exfoliation methods, usually possesses a substantial specific surface area, elevated interlayer spacing, and minimal structural defects. Numerous studies have been carried out on graphene nanosheets with different levels of exfoliation used as lubricant additives and their nanostructural changes during friction. Highly exfoliated graphene tends to stack and arrange under pressures and shearing forces, forming a stable and layered adsorption coating aligned with the sliding direction on the contact surfaces, markedly improving the tribological characteristics [132]. As a result, the structural alteration of graphene induced by friction is broadly acknowledged, with the advancement of structuring and even the process of becoming graphite playing a pivotal role in graphene's lubrication. The innate self-lubricating characteristics of graphene are ascribed to its feeble interlayer contact intensity. When graphene nano-sheets or nano-spheres slide across a graphene surface, the inherent ultra-low friction of graphene can be realized through interlayer sliding at non-aligned junctions [133,134]. The frictional forces among graphene layers are not consistent, and the interlayers can readily shift from a state of minimal friction (incommensurate) to a state of significant friction (commensurate). The distance between layers largely influences the interlayer van der Waals force and the sliding obstacle in graphene. Comprehensive computations using molecular force field statics were performed to examine the effect of interlayer spacing on the tribological attributes of graphene. Increasing the gap between layers diminishes the frictional forces between graphene sheets (the inherent layer spacing of graphene is 0.334 nm). As mentioned earlier, the chemical reduction of SRGO

results in a larger interlayer spacing of 4.25 Å. Due to the ease of interlayer sliding among SRGO graphene layers, nanosheets with extremely high exfoliation exhibit superior tribological performance compared to those with low exfoliation [132]. The findings illuminate the possibility of managing friction between graphene sheets and their potential applications. Since its discovery [120], graphene has demonstrated enormous potential to revolutionize various applications [135]. However, each application necessitates a distinct sort of graphenaceous material. Applications such as electronics and sensors require the use of carefully controlled mono or bi-layered graphene with minimal surface and edge defects. In contrast, applications like structural composites, lubricants, and electrode materials necessitate the use of few-layered graphene (FLG, consisting of 4-10 layers) or multi-layered graphene (MLG, more than 10 layers). These applications can tolerate a significant number of defects, as long as the physicochemical properties remain consistent. However, to cater to the needs of these applications, it's crucial to produce graphenaceous materials on a large scale, ideally on a kilogram scale [136]. In this context, liquid phase exfoliation (LPE) has been recommended as a method for producing substantial quantities of graphenaceous materials [137]. Liquid Phase Exfoliation (LPE) entails spreading the material to be exfoliated in an appropriate solvent (or a mixture of solvents) and then applying intense shear forces, leading to exfoliation in a liquid medium. The process is influenced by several parameters, including surface tension, Hansen solubility parameters, the types of solvents used, the design of the processing equipment, and the application of sonication [138-143], help to tailor the exfoliation. As per fundamental research, elements like surfactants, functionalization, among others, play a significant role in the successful Liquid Phase Exfoliation (LPE) of graphite into graphene [144]. Many experiments have described the synthesis of various graphenaceous forms employing LPE or a combination of LPE and sonication in polar, organic, and polar-clean [143,145,146] solvents with detailed discussions on dispersion and exfoliation mechanisms [147,148] and on the compatibility with solvents [149], different methodologies [138] and the associated challenges [140]. Table 1 lists relevant details from LPE-related works that report on processing various graphenaceous forms. Even though the papers in Table 1 are hailed as having the possibility for scaling up, there are no particular reports on the kg-scale sustainable production of graphenaceous materials. One of the significant hurdles in commercializing MLG is scaling up its production process from the lab-scale to the pilot-scale and finally to the industrial-scale. At the same time, the production process should be efficient, cost-effective, and sustainable. 2D materials (such as MLG, FLG, MoS₂, WS₂, and h-BN) are held by weak van der Waals forces along the normal to their basal planes, rendering low shear strength along

the basal planes. This facilitates consecutive layers to slide over each other easily when shear forces are applied, creating a self-lubricating effect. The in-plane covalent bonding among atoms in the basal planes gives these 2D materials high modulus and strength.

Table 1. Reports on LPE leading to the formation of various graphenaceous forms.

Starting material	End material	Solvent	Surfactant	Yield	Application
Purified natural graphite flakes	FLG	DI water	Sodium cholate	g scale [150]	Conductive thin films
Graphite flakes	GO nanosheets	DI water	-	g scale [151]	Medical applications
Natural graphite flakes	FLG	N-Methyl pyrrolidone (NMP)	-	g scale [152]	High electrical conducting films
Natural graphite flakes	FLG	N-Methyl pyrrolidone (NMP)	-	g scale [153]	Flexible electronics
Pristine expanded graphite powder	FLG	Water and N, N-dimethylformam ide	-	g scale [154]	Applications requiring high-quality graphene
Graphite flakes	MLG	Water and Dimethyl sulfoxide	-	g scale [155]	Engineering applications

By virtue of their aspect ratio, 2D materials can cover multiple surface asperities on the contacting surfaces, which eventually reduces the actual contact area of the contacting surfaces, substantially minimizing the coefficient of friction (CoF) and wear. Graphene, in particular, has attracted enormous attention as a lubricating material with the ability to deliver very low CoF and reduce wear between contacting surfaces [156,157]. The concentration of the graphene, the number of layers of graphene nanosheets, the dispersion stability, and the lubrication conditions are the most critical elements that determine the lubricating

characteristics of graphene-based nano lubricants [156-160]. Graphene derived from top-down processes is more viable for application as lubricant additives, considering the aspects of yield and sustainability. A unique approach based on concentrated solar radiation was utilized to exfoliate graphite oxide, yielding ultrathin graphene (UG). The frictional characteristics, antiwear (AW), and extreme pressure (EP) qualities of graphene-based EO nanofluids have been studied. Compared to BO, nanofluids enhance their frictional characteristics, AW, and EP qualities by 80%, 33%, and 40%, respectively. The improvement was ascribed to graphene's nano-bearing mechanism in EO and graphene's ultimate mechanical strength [161]. However, the approach used to produce graphene in this study appears exotic but practically unsustainable. Electrochemically exfoliated graphene diffused consistently in polyethylene glycol 200 (PEG200) enhanced tribological properties, particularly thinner and smaller modified-graphene with decreased friction and wear (reduced by 16% and 25.9%, respectively). The modified-graphene and as-formed protective layer on the mating contacts provide this important lubricating function. Furthermore, the interfacial contact changed the additive into an overlapping and ordered-sheet structure [162]. Experimental studies with 3dimensional graphene nanosheets produced in an arc-discharge CVD as a lubricant additive showed tribological improvements. Under low and high loads (4.2 mm/s sliding speed and roughly 1.0 GPa contact pressure), the reduction in friction and wear were 29.1% and 55%, respectively, compared to the BO. However, the material failed to lubricate effectively at higher loads owing to deteriorated structure [163]. Thermally reduced graphite oxide (Gr-O) was explored as a lubricant additive in a BO. The BO's varying CoF between 0.15 to 0.20 was significantly reduced by using 0.5wt.% Gr-O in the oil. At larger concentrations (1.0 wt.%), the Gr-O particles were suspected to aggregate and block the sliding motion, resulting in a higher friction coefficient. Also, it was concluded that the structural flaws of fold and wrinkling in Gr-O nanosheets can reduce their lubricating properties [164]. In a study using commercially procured graphene nano additives in a 5W30 oil, CoF was reduced by 15%, and wear scar was reduced by 33%. The worn surfaces were characterized to understand the tribofilm formation of graphene nano additives [165]. The tribological behaviour of lubricants (Pongamia oil and 15W40 EO) with and without the addition of commercial graphene nanoplatelets (GNPs) was studied. Worn surface analysis revealed the polishing impact of GNPs on the surfaces. The inclusion of 0.05 wt.% GNPs in lubricants reduced friction and wear by 17.5% and 12.24% (Pongamia oil), respectively, and by 11.96% and 5.14% (15W40 EO), respectively [166].

However, challenges in the sustainable synthesis, dispersibility, and stability of NCs within lubricant formulations hinder their widespread adoption. Although numerous studies have

shown that NCs improve lubricity when used as additives in lubricants, little emphasis has been placed on the sustainable synthesis of carbon-based nanostructures. The synthesis of graphene, carbon nanotubes (CNTs), and 0D NCs like onion-like carbon holds enormous promise as lubricant additives, but it faces significant obstacles in terms of scalability, energy consumption, and environmental impact. Environmental issues are exacerbated by resource-intensive procedures. Sustainable efforts attempt to decrease energy consumption and waste output by utilising alternate precursors and optimised synthesis conditions. Controlling material purity and consistency for scale production is a difficulty in NCs synthesis faces several hurdles which involves costly precursors and complicated multi-step procedures. To solve these issues, it is clear from the literature that renewable precursor materials and energy-efficient synthesis techniques must be investigated. Ultimately, ensuring the sustainable and eco-friendly production of these NCs and further exploring them as lubricant additives to improve the wear preventive and AF properties requires innovative approaches to minimise energy usage, waste production, and reliance on hazardous materials.

References

- [1] S.P. Srivastava, Advances In Lubricant Additives and Tribology (1st Edition), CRC Press (2009), ISBN-10: 8188305944.
- [2] J. Zhang, H. Spikes, On the mechanism of ZDDP antiwear film formation, Tribology Letters 63 (2016) 1-15.
- [3] J. Guo, R. Peng, H. Du, Y. Shen, Y. Li, J. Li, G. Dong, The application of nano-MoS₂ quantum dots as liquid lubricant additive for tribological behavior improvement, Nanomaterials 10(2) (2020) 200.
- [4] N. Rajendhran, S. Palanisamy, P. Periyasamy, R. Venkatachalam, Enhancing of the tribological characteristics of the lubricant oils using Ni-promoted MoS₂ nanosheets as nanoadditives, Tribology International 118 (2018) 314-328.
- [5] M. Kalin, J. Kogovšek, M. Remškar, Mechanisms and improvements in the friction and wear behavior using MoS₂ nanotubes as potential oil additives, Wear 280 (2012) 36-45.
- [6] C.-G. Lee, Y.-J. Hwang, Y.-M. Choi, J.-K. Lee, C. Choi, J.-M. Oh, A study on the tribological characteristics of graphite nano lubricants, International Journal of Precision Engineering and Manufacturing 10 (2009) 85-90.

- [7] Deepika, Nanotechnology implications for high performance lubricants, SN Applied Sciences 2 (2020) 1-12.
- [8] R. Andrievski, Review of thermal stability of nanomaterials, Journal of Materials Science 49 (2014) 1449-1460.
- [9] W. Dai, B. Kheireddin, H. Gao, H. Liang, Roles of nanoparticles in oil lubrication, Tribology International 102 (2016) 88-98.
- [10] M.M. Rahman, M. Islam, R. Roy, H. Younis, M. AlNahyan, H. Younes, Carbon nanomaterial-based lubricants: Review of recent developments, Lubricants 10(11) (2022) 281.
- [11] L. Duan, J. Li, H. Duan, Nanomaterials for lubricating oil application: A review, Friction 11(5) (2023) 647-684.
- [12] R. Chou, A.H. Battez, J. Cabello, J. Viesca, A. Osorio, A. Sagastume, Tribological behavior of polyalphaolefin with the addition of nickel nanoparticles, Tribology International 43(12) (2010) 2327-2332.
- [13] M. Sarno, W.A.A. Mustafa, A. Senatore, D. Scarpa, One-step "green" synthesis of dispersable carbon quantum dots/poly (methyl methacrylate) nanocomposites for tribological applications, Tribology International 148 (2020) 106311.
- [14] J. Wang, W. Zhuang, W. Liang, T. Yan, T. Li, L. Zhang, S. Li, Inorganic nanomaterial lubricant additives for base fluids, to improve tribological performance: Recent developments, Friction 10(5) (2022) 645-676.
- [15] I.E. Uflyand, V.A. Zhinzhilo, V.E. Burlakova, Metal-containing nanomaterials as lubricant additives: State-of-the-art and future development, Friction 7 (2019) 93-116.
- [16] M.K.A. Ali, X. Hou, M.A. Abdelkareem, Anti-wear properties evaluation of frictional sliding interfaces in automobile engines lubricated by copper/graphene nanolubricants, Friction 8 (2020) 905-916.
- [17] H. Yu, Y. Xu, P. Shi, B. Xu, X. Wang, Q. Liu, H. Wang, Characterization and nanomechanical properties of tribofilms using Cu nanoparticles as additives, Surface and Coatings Technology 203(1-2) (2008) 28-34.
- [18] B. Li, X. Wang, W. Liu, Q. Xue, Tribochemistry and antiwear mechanism of organic—inorganic nanoparticles as lubricant additives, Tribology Letters 22 (2006) 79-84.

- [19] Y. Choi, C. Lee, Y. Hwang, M. Park, J. Lee, C. Choi, M. Jung, Tribological behavior of copper nanoparticles as additives in oil, Current Applied Physics 9(2) (2009) e124-e127.
- [20] J. Padgurskas, R. Rukuiza, I. Prosyčevas, R. Kreivaitis, Tribological properties of lubricant additives of Fe, Cu and Co nanoparticles, Tribology International 60 (2013) 224-232.
- [21] F.L.G. Borda, S.J.R. de Oliveira, L.M.S.M. Lazaro, A.J.K. Leiróz, Experimental investigation of the tribological behavior of lubricants with additive containing copper nanoparticles, Tribology International 117 (2018) 52-58.
- [22] J. Zhou, Z. Wu, Z. Zhang, W. Liu, Q. Xue, Tribological behavior and lubricating mechanism of Cu nanoparticles in oil, Tribology Letters 8 (2000) 213-218.
- [23] S. Tarasov, A. Kolubaev, S. Belyaev, M. Lerner, F. Tepper, Study of friction reduction by nanocopper additives to motor oil, Wear 252(1-2) (2002) 63-69.
- [24] M. Zhang, X. Wang, W. Liu, X. Fu, Performance and anti-wear mechanism of Cu nanoparticles as lubricating oil additives, Industrial Lubrication and Tribology 61(6) (2009) 311-318.
- [25] Q. Pan, X. Zhang, Synthesis and tribological behavior of oil-soluble Cu nanoparticles as additive in SF15W/40 lubricating oil, Rare Metal Materials and Engineering 39(10) (2010) 1711-1714.
- [26] X. Xiong, Y. Kang, G. Yang, S. Zhang, L. Yu, P. Zhang, Preparation and evaluation of tribological properties of Cu nanoparticles surface modified by tetradecyl hydroxamic acid, Tribology Letters 46 (2012) 211-220.
- [27] Z. Tang, S. Li, A review of recent developments of friction modifiers for liquid lubricants (2007–present), Current Opinion in Solid State and Materials Science 18(3) (2014) 119-139.
- [28] Y. Chen, Y. Zhang, S. Zhang, L. Yu, P. Zhang, Z. Zhang, Preparation of nickel-based nanolubricants via a facile in situ one-step route and investigation of their tribological properties, Tribology Letters 51 (2013) 73-83.
- [29] C. Kumara, H. Luo, D.N. Leonard, H.M. Meyer, J. Qu, Organic-modified silver nanoparticles as lubricant additives, ACS Applied Materials & Interfaces 9(42) (2017) 37227-37237.

- [30] S. Zhang, L. Hu, D. Feng, H. Wang, Anti-wear and friction-reduction mechanism of Sn and Fe nanoparticles as additives of multialkylated cyclopentanes under vacuum condition, Vacuum 87 (2013) 75-80.
- [31] M. Abad, J. Sánchez-López, Tribological properties of surface-modified Pd nanoparticles for electrical contacts, Wear 297(1-2) (2013) 943-951.
- [32] S. Beckford, J. Cai, J. Chen, M. Zou, Use of Au nanoparticle-filled PTFE films to produce low-friction and low-wear surface coatings, Tribology Letters 56 (2014) 223-230.
- [33] M. Flores-Castañeda, E. Camps, M. Camacho-López, S. Muhl, E. García, M. Figueroa, Bismuth nanoparticles synthesized by laser ablation in lubricant oils for tribological tests, Journal of Alloys and Compounds 643 (2015) S67-S70.
- [34] S. Zhang, Y. Li, L. Hu, D. Feng, H. Wang, AntiWear effect of Mo and W nanoparticles as additives for multialkylated cyclopentanes oil in vacuum, Journal of Tribology 139(2) (2017) 021607.
- [35] B. He, S. Liu, X. Zhao, J. Liu, Q. Ye, S. Liu, W. Liu, Dialkyl dithiophosphate-functionalized gallium-based liquid-metal nanodroplets as lubricant additives for antiwear and friction reduction, ACS Applied Nano Materials 3(10) (2020) 10115-10122.
- [36] G. Denison Jr, Oxidation of lubricating oils, Industrial & Engineering Chemistry 36(5) (1944) 477-482.
- [37] A.H. Battez, R. González, J. Viesca, J. Fernández, J.D. Fernández, A. Machado, R. Chou, J. Riba, CuO, ZrO₂ and ZnO nanoparticles as antiwear additive in oil lubricants, Wear 265(3-4) (2008) 422-428.
- [38] Y. Wu, W. Tsui, T. Liu, Experimental analysis of tribological properties of lubricating oils with nanoparticle additives, Wear 262(7-8) (2007) 819-825.
- [39] S. Ingole, A. Charanpahari, A. Kakade, S.S. Umare, D.V. Bhatt, J. Menghani, Tribological behavior of nano TiO₂ as an additive in base oil, Wear 301(1-2) (2013) 776-785.
- [40] R. Gusain, O.P. Khatri, Ultrasound assisted shape regulation of CuO nanorods in ionic liquids and their use as energy efficient lubricant additives, Journal of Materials Chemistry A 1(18) (2013) 5612-5619.

- [41] S.Y. Ma, S.H. Zheng, H.Y. Ding, W. Li, Anti-wear and reduce-friction ability of ZrO₂/SiO₂ self-lubricating composites, Advanced Materials Research 79 (2009) 1863-1866.
- [42] V. Mangam, S. Bhattacharya, K. Das, S. Das, Friction and wear behavior of Cu–CeO₂ nanocomposite coatings synthesized by pulsed electrodeposition, Surface and Coatings Technology 205(3) (2010) 801-805.
- [43] D. Jiao, S. Zheng, Y. Wang, R. Guan, B. Cao, The tribology properties of alumina/silica composite nanoparticles as lubricant additives, Applied Surface Science 257(13) (2011) 5720-5725.
- [44] R. Rosentsveig, A. Gorodnev, N. Feuerstein, H. Friedman, A. Zak, N. Fleischer, J. Tannous, F. Dassenoy, R. Tenne, Fullerene-like MoS₂ nanoparticles and their tribological behavior, Tribology Letters 36 (2009) 175-182.
- [45] L. Zhang, J. Tu, H. Wu, Y. Yang, WS₂ nanorods prepared by self-transformation process and their tribological properties as additive in base oil, Materials Science and Engineering A 454 (2007) 487-491.
- [46] X. Kang, B. Wang, L. Zhu, H. Zhu, Synthesis and tribological property study of oleic acid-modified copper sulfide nanoparticles, Wear 265(1-2) (2008) 150-154.
- [47] Y. Min, M. Akbulut, R.K. Prud'homme, Y. Golan, J. Israelachvili, Frictional properties of surfactant-coated rod-shaped nanoparticles in dry and humid dodecane, The Journal of Physical Chemistry B 112(46) (2008) 14395-14401.
- [48] J. Yang, H. Yao, Y. Liu, Y. Zhang, Synthesis and tribological properties of WSe₂ nanorods, Nanoscale Research Letters 3 (2008) 481-485.
- [49] V. Normand, J. Martin, L. Ponsonnet, K. Inoue, Micellar calcium borate as an antiwear additive, Tribology Letters 5 (1998) 235-242.
- [50] K. Varlot, J. Martin, C. Grossiord, R. Vargiolu, B. Vacher, K. Inoue, A dual-analysis approach in tribochemistry: application to ZDDP/calcium borate additive interactions, Tribology Letters 6 (1999) 181-189.
- [51] G. Zhao, Q. Zhao, W. Li, X. Wang, W. Liu, Tribological properties of nano-calcium borate as lithium grease additive, Lubrication Science 26(1) (2014) 43-53.

- [52] L. Hao, J. Li, X. Xu, T. Ren, Preparation and tribological properties of a kind of lubricant containing calcium borate nanoparticles as additives, Industrial Lubrication and Tribology 64(1) (2012) 16-22.
- [53] J. Li, L. Hao, X. Xu, T. Ren, Tribological synergism of surface-modified calcium borate nanoparticles and sulfurized olefin, Industrial Lubrication and Tribology 64(4) (2012) 217-223.
- [54] O. Çelik, N. Ay, Y. Göncü, Effect of nano hexagonal boron nitride lubricant additives on the friction and wear properties of AISI 4140 steel, Particulate Science and Technology 31(5) (2013) 501-506.
- [55] D.-H. Cho, J.-S. Kim, S.-H. Kwon, C. Lee, Y.-Z. Lee, Evaluation of hexagonal boron nitride nano-sheets as a lubricant additive in water, Wear 302(1-2) (2013) 981-986.
- [56] Q. Zeng, F. Yu, G. Dong, Superlubricity behaviors of Si₃N₄/DLC Films under PAO oil with nano boron nitride additive lubrication, Surface and Interface Analysis 45(8) (2013) 1283-1290.
- [57] M. Zhang, X. Wang, X. Fu, Y. Xia, Performance and anti-wear mechanism of CaCO₃ nanoparticles as a green additive in poly-alpha-olefin, Tribology International 42(7) (2009) 1029-1039.
- [58] L. Wang, B. Wang, X. Wang, W. Liu, Tribological investigation of CaF₂ nanocrystals as grease additives, Tribology International 40(7) (2007) 1179-1185.
- [59] S.G. Vilt, N. Martin, C. McCabe, G.K. Jennings, Frictional performance of silica microspheres, Tribology International 44(2) (2011) 180-186.
- [60] Y.-R. Jeng, Y.-H. Huang, P.-C. Tsai, G.-L. Hwang, Tribological properties of carbon nanocapsule particles as lubricant additive, Journal of Tribology 136(4) (2014) 041801.
- [61] G. Cheng, L. Dong, L. Kamboj, T. Khosla, X. Wang, Z. Zhang, L. Guo, N. Pesika, J. Ding, Hydrothermal synthesis of monodisperse hard carbon spheres and their water-based lubrication, Tribology Letters 65 (2017) 1-9.
- [62] M.-f. Guo, Z.-b. Cai, Z.-c. Zhang, M.-h. Zhu, Characterization and lubrication performance of diesel soot nanoparticles as oil lubricant additives, RSC Advances 5(123) (2015) 101965-101974.

- [63] L. Joly-Pottuz, B. Vacher, N. Ohmae, J. Martin, T. Epicier, Anti-wear and friction reducing mechanisms of carbon nano-onions as lubricant additives, Tribology Letters 30 (2008) 69-80.
- [64] A. Hirata, M. Igarashi, T. Kaito, Study on solid lubricant properties of carbon onions produced by heat treatment of diamond clusters or particles, Tribology International 37(11-12) (2004) 899-905.
- [65] Y. Jung, J. Hwang, C. Bae, Assessment of particulate matter in exhaust gas for biodiesel and diesel under conventional and low temperature combustion in a compression ignition engine, Fuel 165 (2016) 413-424.
- [66] N. Savic, M.M. Rahman, B. Miljevic, H. Saathoff, K.-H. Naumann, T. Leisner, J. Riches, B. Gupta, N. Motta, Z. Ristovski, Influence of biodiesel fuel composition on the morphology and microstructure of particles emitted from diesel engines, Carbon 104 (2016) 179-189.
- [67] D.J. Growney, O.O. Mykhaylyk, L. Middlemiss, L.A. Fielding, M.J. Derry, N. Aragrag, G.D. Lamb, S.P. Armes, Is carbon black a suitable model colloidal substrate for diesel soot?, Langmuir 31(38) (2015) 10358-10369.
- [68] A. Kontou, M. Southby, H. Spikes, Effect of steel hardness on soot wear, Wear 390 (2017) 236-245.
- [69] E. Hu, K. Dearn, B. Yang, R. Song, Y. Xu, X. Hu, Tribofilm formation and characterization of lubricating oils with biofuel soot and inorganic fluorides, Tribology International 107 (2017) 163-172.
- [70] A. Clague, J. Donnet, T. Wang, J. Peng, A comparison of diesel engine soot with carbon black, Carbon 37(10) (1999) 1553-1565.
- [71] G. Ferraro, E. Fratini, R. Rausa, P. Fiaschi, P. Baglioni, Multiscale characterization of some commercial carbon blacks and diesel engine soot, Energy & Fuels 30(11) (2016) 9859-9866.
- [72] C.L.X. Hu, Novel approach for improved tribological behavior of biodiesel soot in liquid paraffin, China Petroleum Processing & Petrochemical Technology 21(1) (2019) 101.
- [73] E. Hu, X. Hu, T. Liu, Y. Liu, R. Song, Y. Chen, Investigation of morphology, structure and composition of biomass-oil soot particles, Applied Surface Science 270 (2013) 596-603.

- [74] C.L.D.Z.X. Hu, Effect of biodiesel soot on the tribological behavior of liquid paraffin, China Petroleum Processing & Petrochemical Technology 20(3) (2018) 106.
- [75] A.L. Boehman, J. Song, M. Alam, Impact of biodiesel blending on diesel soot and the regeneration of particulate filters, Energy & Fuels 19(5) (2005) 1857-1864.
- [76] J.W. Robinson, Y. Zhou, P. Bhattacharya, R. Erck, J. Qu, J.T. Bays, L. Cosimbescu, Probing the molecular design of hyper-branched aryl polyesters towards lubricant applications, Scientific Reports 6(1) (2016) 18624.
- [77] P. Wang, J. Wei, B. Huang, X. Qin, S. Yao, Q. Zhang, Z. Wang, G. Xu, X. Jing, Synthesis and characterization of carbon spheres prepared by chemical vapour deposition, Materials Letters 61(26) (2007) 4854-4856.
- [78] P.K. Tripathi, S. Durbach, N.J. Coville, CVD Synthesis of solid, hollow, and nitrogen-doped hollow carbon spheres from polypropylene waste materials, Applied Sciences 9(12) (2019) 2451.
- [79] Y.Z. Jin, C. Gao, W.K. Hsu, Y. Zhu, A. Huczko, M. Bystrzejewski, M. Roe, C.Y. Lee, S. Acquah, H. Kroto, Large-scale synthesis and characterization of carbon spheres prepared by direct pyrolysis of hydrocarbons, Carbon 43(9) (2005) 1944-1953.
- [80] J. Du, L. Liu, Y. Yu, H. Lv, Y. Zhang, A. Chen, Confined pyrolysis for direct conversion of solid resin spheres into yolk–shell carbon spheres for supercapacitor, Journal of Materials Chemistry A 7(3) (2019) 1038-1044.
- [81] C. Chen, X. Sun, X. Jiang, D. Niu, A. Yu, Z. Liu, J. Li, A two-step hydrothermal synthesis approach to monodispersed colloidal carbon spheres, Nanoscale Research Letters 4 (2009) 971-976.
- [82] C. Wu, C. Wei, X. Jin, R. Akhtar, W. Zhang, Carbon spheres as lubricant additives for improving tribological performance of polyetheretherketone, Journal of Materials Science 54(6) (2019) 5127-5135.
- [83] A.A. Alazemi, A.D. Dysart, V.G. Pol, Experimental investigation of the mechanical and surface properties of sub-micron carbon spheres, Lubricants 8(7) (2020) 77.
- [84] R. Panickar, C. Sobhan, S. Chakravorti, Investigations on tribological properties of non-catalytic CVD synthesized carbon spheres in lubricant, Diamond and Related Materials 106 (2020) 107834.

- [85] J. Fei, Y. Qi, L. Luo, Y. Gu, J. Huang, Synergistic effect of talc/carbon spheres composite as oil-based additive enhancing the lubricating properties for steel-steel contact, Lubrication Science 32(2) (2020) 80-89.
- [86] T. Li, B. Pan, C. Wang, S. Zhang, S. Huang, Effect of eco-friendly carbon microspheres on the tribological behavior of lithium lubricating grease, UPB Scientific Bulletin Series B 81 (2019) 57-68.
- [87] X. Lv, L. Cao, T. Yang, Y. Wan, J. Gao, Lubricating behavior of submicrometer carbon spheres as lubricant additives, Particulate Science and Technology 38(5) (2020) 568-572.
- [88] S. Menon, J. Hansen, L. Nazarenko, Y. Luo, Climate effects of black carbon aerosols in China and India, Science 297(5590) (2002) 2250-2253.
- [89] C. Li, M. Li, X. Wang, W. Feng, Q. Zhang, B. Wu, X. Hu, Novel carbon nanoparticles derived from biodiesel soot as lubricant additives, Nanomaterials 9(8) (2019) 1115.
- [90] H. Boehm, Some aspects of the surface chemistry of carbon blacks and other carbons, Carbon 32(5) (1994) 759-769.
- [91] A. Khanam, S. Tripathi, D. Roy, M. Nasim, A facile and novel synthetic method for the preparation of hydroxyl capped fluorescent carbon nanoparticles, Colloids and Surfaces B: Biointerfaces 102 (2013) 63-69.
- [92] J.-F. Peng, M.-X. Shen, Z.-B. Cai, Nano diesel soot particles reduce wear and friction performance using an oil additive on a laser textured surface, Coatings 8(3) (2018) 89.
- [93] B.N. Sahoo, B. Kandasubramanian, An experimental design for the investigation of water repellent property of candle soot particles, Materials Chemistry and Physics 148(1-2) (2014) 134-142.
- [94] R. Kali, B. Padya, T. Rao, P. Jain, Solid waste-derived carbon as anode for high performance lithium-ion batteries, Diamond and Related Materials 98 (2019) 107517.
- [95] G. Huang, Q. Yu, Z. Ma, M. Cai, F. Zhou, W. Liu, Fluorinated candle soot as the lubricant additive of perfluoropolyether, Tribology Letters 65 (2017) 1-11.
- [96] R. Berkowitz, Soot formation: a new mechanism for an old problem, Physics Today 71(11) (2018) 18-20.

- [97] I.M. Kennedy, Models of soot formation and oxidation, Progress in Energy and Combustion Science 23(2) (1997) 95-132.
- [98] S. Iijima, T. Ichihashi, Single-shell carbon nanotubes of 1-nm diameter, Nature 363(6430) (1993) 603-605.
- [99] S. Rathinavel, K. Priyadharshini, D. Panda, A review on carbon nanotube: An overview of synthesis, properties, functionalization, characterization, and the application, Materials Science and Engineering B 268 (2021) 115095.
- [100] W. Zhai, K. Zhou, Nanomaterials in superlubricity, Advanced Functional Materials 29(28) (2019) 1806395.
- [101] C. Chen, X. Chen, L. Xu, Z. Yang, W. Li, Modification of multi-walled carbon nanotubes with fatty acid and their tribological properties as lubricant additive, Carbon 43(8) (2005) 1660-1666.
- [102] D.-L. Cursaru, C. Andronescu, C. Pirvu, R. Ripeanu, The efficiency of Co-based single-wall carbon nanotubes (SWNTs) as an AW/EP additive for mineral base oils, Wear 290 (2012) 133-139.
- [103] H. Kumar, A. Harsha, Enhanced lubrication ability of polyalphaolefin and polypropylene glycol by COOH-functionalized multiwalled carbon nanotubes as an additive, Journal of Materials Engineering and Performance 30 (2021) 1075-1089.
- [104] N. Salah, M.S. Abdel-Wahab, A. Alshahrie, N.D. Alharbi, Z.H. Khan, Carbon nanotubes of oil fly ash as lubricant additives for different base oils and their tribology performance, RSC Advances 7(64) (2017) 40295-40302.
- [105] E. Dardan, M. Afrand, A.M. Isfahani, Effect of suspending hybrid nano-additives on rheological behavior of engine oil and pumping power, Applied Thermal Engineering 109 (2016) 524-534.
- [106] K. Gong, X. Wu, G. Zhao, X. Wang, Tribological properties of polymeric aryl phosphates grafted onto multi-walled carbon nanotubes as high-performances lubricant additive, Tribology International 116 (2017) 172-179.
- [107] V. Chauveau, D. Mazuyer, F. Dassenoy, J. Cayer-Barrioz, In situ film-forming and friction-reduction mechanisms for carbon-nanotube dispersions in lubrication, Tribology Letters 47 (2012) 467-480.

- [108] J. Kałużny, A. Merkisz-Guranowska, M. Giersig, K. Kempa, Lubricating performance of carbon nanotubes in internal combustion engines—engine test results for cnt enriched oil, International Journal of Automotive Technology 18 (2017) 1047-1059.
- [109] N. Jeyaprakash, S. Sivasankaran, G. Prabu, C.-H. Yang, A.S. Alaboodi, Enhancing the tribological properties of nodular cast iron using multi wall carbon nano-tubes (MWCNTs) as lubricant additives, Materials Research Express 6(4) (2019) 045038.
- [110] W. Khalil, A. Mohamed, M. Bayoumi, T. Osman, Tribological properties of dispersed carbon nanotubes in lubricant, Fullerenes, Nanotubes and Carbon Nanostructures 24(7) (2016) 479-485.
- [111] A. Elagouz, M.K.A. Ali, H. Xianjun, M.A. Abdelkareem, Thermophysical and tribological behaviors of multiwalled carbon nanotubes used as nanolubricant additives, Surface Topography: Metrology and Properties 9(4) (2021) 045002.
- [112] K.R.R. Chebattina, V. Srinivas, N.M. Rao, Effect of Size of multiwalled carbon nanotubes dispersed in gear oils for improvement of tribological properties, Advances in Tribology 2018 (2018).
- [113] N. Kumar, P. Goyal, Experimental study of carbon nanotubes to enhance tribological characteristics of lubricating engine oil SAE10W40, IOP Conference Series: Materials Science and Engineering 1225 (2022) 012052.
- [114] K. Lijesh, D. Kumar, S. Muzakkir, H. Hirani, Thermal and frictional performance evaluation of nano lubricant with multi wall carbon nano tubes (MWCNTs) as nano-additive, AIP Conference Proceedings 1953 (2018) 100032.
- [115] A. Dhanola, K.K. Gajrani, Novel insights into graphene-based sustainable liquid lubricant additives: A comprehensive review, Journal of Molecular Liquids (2023) 122523.
- [116] K.K. Gajrani, M.R. Sankar, Past and current status of eco-friendly vegetable oil based metal cutting fluids, Materials Today: Proceedings 4(2) (2017) 3786-3795.
- [117] K.K. Gajrani, M.R. Sankar, Sustainable cutting fluids: Thermal, rheological, biodegradation, anti-corrosion, storage stability studies and its machining performance, Encyclopedia of Renewable and Sustainable Materials 1 (2020) 839-852.

- [118] L. Arvizu-Rodriguez, U. Paramo-García, F. Caballero-Briones, Low resistance, high mobility reduced graphene oxide films prepared with commercial antioxidant supplements, Materials Letters 276 (2020) 128176.
- [119] S. Liang, Z. Shen, M. Yi, L. Liu, X. Zhang, S. Ma, In-situ exfoliated graphene for high-performance water-based lubricants, Carbon 96 (2016) 1181-1190.
- [120] K.S. Novoselov, A.K. Geim, S.V. Morozov, D.-e. Jiang, Y. Zhang, S.V. Dubonos, I.V. Grigorieva, A.A. Firsov, Electric field effect in atomically thin carbon films, Science 306(5696) (2004) 666-669.
- [121] Y. Zhang, J.P. Small, W.V. Pontius, P. Kim, Fabrication and electric-field-dependent transport measurements of mesoscopic graphite devices, Applied Physics Letters 86(7) (2005).
- [122] I.-Y. Jeon, Y.-R. Shin, G.-J. Sohn, H.-J. Choi, S.-Y. Bae, J. Mahmood, S.-M. Jung, J.-M. Seo, M.-J. Kim, D. Wook Chang, Edge-carboxylated graphene nanosheets via ball milling, Proceedings of the National Academy of Sciences 109(15) (2012) 5588-5593.
- [123] I.Y. Jeon, S.Y. Bae, J.M. Seo, J.B. Baek, Scalable production of edge-functionalized graphene nanoplatelets via mechanochemical ball-milling, Advanced Functional Materials 25(45) (2015) 6961-6975.
- [124] K. Suvarna, N. Binitha, Graphene preparation by jaggery assisted ball-milling of graphite for the adsorption of Cr (VI), Materials Today: Proceedings 25 (2020) 236-240.
- [125] Y. Arao, R. Kuwahara, K. Ohno, J. Tanks, K. Aida, M. Kubouchi, S.-i. Takeda, Mass production of low-boiling point solvent-and water-soluble graphene by simple salt-assisted ball milling, Nanoscale Advances 1(12) (2019) 4955-4964.
- [126] B. Gupta, N. Kumar, K. Panda, S. Dash, A. Tyagi, Energy efficient reduced graphene oxide additives: Mechanism of effective lubrication and antiwear properties, Scientific Reports 6(1) (2016) 18372.
- [127] Z. Li, C. Xu, G. Xiao, J. Zhang, Z. Chen, M. Yi, Lubrication performance of graphene as lubricant additive in 4-n-pentyl-4'-cyanobiphyl liquid crystal (5CB) for steel/steel contacts, Materials 11(11) (2018) 2110.
- [128] S.T. Pham, S. Wan, K.A. Tieu, M. Ma, H. Zhu, H.H. Nguyen, D.R. Mitchell, M.J. Nancarrow, Unusual competitive and synergistic effects of graphite nanoplates in engine oil on the tribofilm formation, Advanced Materials Interfaces 6(19) (2019) 1901081.

- [129] H. Xie, B. Jiang, J. Dai, C. Peng, C. Li, Q. Li, F. Pan, Tribological behaviors of graphene and graphene oxide as water-based lubricant additives for magnesium alloy/steel contacts, Materials 11(2) (2018) 206.
- [130] T. Filleter, J.L. McChesney, A. Bostwick, E. Rotenberg, K.V. Emtsev, T. Seyller, K. Horn, R. Bennewitz, Friction and dissipation in epitaxial graphene films, Physical Review Letters 102(8) (2009) 086102.
- [131] Y.J. Shin, Y. Wang, H. Huang, G. Kalon, A.T.S. Wee, Z. Shen, C.S. Bhatia, H. Yang, Surface-energy engineering of graphene, Langmuir 26(6) (2010) 3798-3802.
- [132] J. Zhao, Y. Huang, Y. Li, T. Gao, Z. Dou, J. Mao, H. Wang, Y. He, S. Li, J. Luo, Superhigh-exfoliation graphene with a unique two-dimensional (2D) microstructure for lubrication application, Applied Surface Science 513 (2020) 145608.
- [133] J. Luo, J. Kim, J. Huang, Material processing of chemically modified graphene: some challenges and solutions, Accounts of Chemical Research 46(10) (2013) 2225-2234.
- [134] J. Luo, H.D. Jang, J. Huang, Effect of sheet morphology on the scalability of graphene-based ultracapacitors, ACS Nano 7(2) (2013) 1464-1471.
- [135] V.B. Mbayachi, E. Ndayiragije, T. Sammani, S. Taj, E.R. Mbuta, Graphene synthesis, characterization and its applications: A review, Results in Chemistry 3 (2021) 100163.
- [136] K.M. Wyss, D.X. Luong, J.M. Tour, Large-scale syntheses of 2D materials: Flash joule heating and other methods, Advanced Materials 34(8) (2022) 2106970.
- [137] A. Gutiérrez-Cruz, A.R. Ruiz-Hernández, J.F. Vega-Clemente, D.G. Luna-Gazcón, J. Campos-Delgado, A review of top-down and bottom-up synthesis methods for the production of graphene, graphene oxide and reduced graphene oxide, Journal of Materials Science 57(31) (2022) 14543-14578.
- [138] M.I. Kairi, S. Dayou, N.I. Kairi, S.A. Bakar, B. Vigolo, A.R. Mohamed, Toward high production of graphene flakes—a review on recent developments in their synthesis methods and scalability, Journal of Materials Chemistry A 6(31) (2018) 15010-15026.
- [139] J. Shen, Y. He, J. Wu, C. Gao, K. Keyshar, X. Zhang, Y. Yang, M. Ye, R. Vajtai, J. Lou, Liquid phase exfoliation of two-dimensional materials by directly probing and matching surface tension components, Nano Letters 15(8) (2015) 5449-5454.

- [140] C. Huo, Z. Yan, X. Song, H. Zeng, 2D materials via liquid exfoliation: A review on fabrication and applications, Science Bulletin 60(23) (2015) 1994-2008.
- [141] F. Goni, A. Chemelli, F. Uhlig, High-Yield Production of Selected 2D Materials by Understanding Their Sonication-Assisted Liquid-Phase Exfoliation, Nanomaterials 11(12) (2021) 3253.
- [142] M. Wang, X. Xu, Y. Ge, P. Dong, R. Baines, P.M. Ajayan, M. Ye, J. Shen, Surface tension components ratio: an efficient parameter for direct liquid phase exfoliation, ACS Applied Materials & Interfaces 9(10) (2017) 9168-9175.
- [143] V. Paolucci, G. D'Olimpio, L. Lozzi, A.M. Mio, L. Ottaviano, M. Nardone, G. Nicotra, P. Le-Cornec, C. Cantalini, A. Politano, Sustainable liquid-phase exfoliation of layered materials with nontoxic polarclean solvent, ACS Sustainable Chemistry & Engineering 8(51) (2020) 18830-18840.
- [144] M. Monajjemi, Liquid-phase exfoliation (LPE) of graphite towards graphene: An ab initio study, Journal of Molecular Liquids 230 (2017) 461-472.
- [145] C.V. Gomez, M. Guevara, T. Tene, L. Villamagua, G.T. Usca, F. Maldonado, C. Tapia, A. Cataldo, S. Bellucci, L.S. Caputi, The liquid exfoliation of graphene in polar solvents, Applied Surface Science 546 (2021) 149046.
- [146] Y. Hernandez, V. Nicolosi, M. Lotya, F.M. Blighe, Z. Sun, S. De, I.T. McGovern, B. Holland, M. Byrne, Y.K. Gun'Ko, High-yield production of graphene by liquid-phase exfoliation of graphite, Nature Nanotechnology 3(9) (2008) 563-568.
- [147] L. Li, M. Zhou, L. Jin, L. Liu, Y. Mo, X. Li, Z. Mo, Z. Liu, S. You, H. Zhu, Research progress of the liquid-phase exfoliation and stable dispersion mechanism and method of graphene, Frontiers in Materials 6 (2019) 325.
- [148] Z. Li, R.J. Young, C. Backes, W. Zhao, X. Zhang, A.A. Zhukov, E. Tillotson, A.P. Conlan, F. Ding, S.J. Haigh, Mechanisms of liquid-phase exfoliation for the production of graphene, ACS Nano 14(9) (2020) 10976-10985.
- [149] W. Du, X. Jiang, L. Zhu, From graphite to graphene: direct liquid-phase exfoliation of graphite to produce single-and few-layered pristine graphene, Journal of Materials Chemistry A 1(36) (2013) 10592-10606.

- [150] S. Lund, J. Kauppila, S. Sirkiä, J. Palosaari, O. Eklund, R.-M. Latonen, J.-H. Smått, J. Peltonen, T. Lindfors, Fast high-shear exfoliation of natural flake graphite with temperature control and high yield, Carbon 174 (2021) 123-131.
- [151] C. Cai, N. Sang, Z. Shen, X. Zhao, Facile and size-controllable preparation of graphene oxide nanosheets using high shear method and ultrasonic method, Journal of Experimental Nanoscience 12(1) (2017) 247-262.
- [152] M. Zhou, T. Tian, X. Li, X. Sun, J. Zhang, P. Cui, J. Tang, L.-C. Qin, Production of graphene by liquid-phase exfoliation of intercalated graphite, International Journal of Electrochemical Science 9(2) (2014) 810-820.
- [153] W. Gu, W. Zhang, X. Li, H. Zhu, J. Wei, Z. Li, Q. Shu, C. Wang, K. Wang, W. Shen, Graphene sheets from worm-like exfoliated graphite, Journal of Materials Chemistry 19(21) (2009) 3367-3369.
- [154] L. Zhu, X. Zhao, Y. Li, X. Yu, C. Li, Q. Zhang, High-quality production of graphene by liquid-phase exfoliation of expanded graphite, Materials Chemistry and Physics 137(3) (2013) 984-990.
- [155] B. Padya, N. Narasaiah, P. Jain, T. Rao, A facile co-solvent strategy for preparation of graphene nanoplatelet powder: An industrially viable innovative approach, Ceramics International 45(10) (2019) 13409-13413.
- [156] K. Suresh, P. Selvakumar, G. Kumaresan, M. Vijayakumar, M. Ravikumar, N.R. Jenita, A critical review on the effect of morphology, stability, and thermophysical properties of graphene nanoparticles in nanolubricants and nanofluids, Journal of Thermal Analysis and Calorimetry 148(2) (2023) 451-472.
- [157] H.P. Mungse, K. Gupta, R. Singh, O.P. Sharma, H. Sugimura, O.P. Khatri, Alkylated graphene oxide and reduced graphene oxide: Grafting density, dispersion stability to enhancement of lubrication properties, Journal of Colloid and Interface Science 541 (2019) 150-162.
- [158] G. Paul, H. Hirani, T. Kuila, N. Murmu, Nanolubricants dispersed with graphene and its derivatives: An assessment and review of the tribological performance, Nanoscale 11(8) (2019) 3458-3483.

- [159] L. Liu, M. Zhou, X. Li, L. Jin, G. Su, Y. Mo, L. Li, H. Zhu, Y. Tian, Research progress in application of 2D materials in liquid-phase lubrication system, Materials 11(8) (2018) 1314.
- [160] H. Zaharin, M. Ghazali, N. Thachnatharen, F. Ezzah, R. Walvekar, M. Khalid, Progress in 2D materials based nanolubricants: A review, FlatChem 38 (2023) 100485.
- [161] V. Eswaraiah, V. Sankaranarayanan, S. Ramaprabhu, Graphene-based engine oil nanofluids for tribological applications, ACS Applied Materials & Interfaces 3(11) (2011) 4221-4227.
- [162] Z. Han, C. Gan, X. Li, P. Feng, X. Ma, X. Fan, M. Zhu, Electrochemical preparation of modified-graphene additive towards lubrication requirement, Tribology International 161 (2021) 107057.
- [163] T. Ouyang, Y. Shen, W. Lei, X. Xu, L. Liang, H.S. Waqar, B. Lin, Z.Q. Tian, P.K. Shen, Reduced friction and wear enabled by arc-discharge method-prepared 3D graphene as oil additive under variable loads and speeds, Wear 462 (2020) 203495.
- [164] J. Zhao, Y. Li, J. Mao, Y. He, J. Luo, Synthesis of thermally reduced graphite oxide in sulfuric acid and its application as an efficient lubrication additive, Tribology International 116 (2017) 303-309.
- [165] B. Alqahtani, W. Hoziefa, H.M. Abdel Moneam, M. Hamoud, S. Salunkhe, A.B. Elshalakany, M. Abdel-Mottaleb, J.P. Davim, Tribological Performance and Rheological Properties of Engine Oil with Graphene Nano-Additives, Lubricants 10(7) (2022) 137.
- [166] Y.J.J. Jason, H.G. How, Y.H. Teoh, F. Sher, H.G. Chuah, J.S. Teh, Tribological behaviour of graphene nanoplatelets as additive in pongamia oil, Coatings 11(6) (2021) 732.

Chapter 3 Experimental Details

3.1 Processing of Materials

3.1.1 Processing of 0D Nanocarbons (RTS and OLC nanoparticles)

The 0D NCs in this work were derived from waste tyre and tubes. Waste cycle rubber tubes [1] were used to produce spherical soot-like carbon NPs with a diameter of 100-150 nm. The rubber tubes were first shredded into smaller pieces, washed in hot water, and dried to remove impurities like mud, oil, etc., which could be present on the tubes. The dried rubber pieces are then directly subjected to thermal decomposition under atmospheric pressure, and the fumes produced are allowed to condense on a borosilicate surface uniformly. The condensate was collected and isothermally annealed at 900 °C in the Ar atmosphere for 120 min to obtain carbon soot (as revealed by different characterization techniques). The annealing process helps remove unwanted elements like sulfur, oxygen, or other impurities in the collected condensate. The entire process was carried out under a fume hood to prevent the burning fumes from contaminating the room (Fig. 4). A gas filter was used at the exhaust of the thermal decomposition set-up to trap any particulates and reduce the hazard of exhaust gases, if any. The prepared CS NPs are named Rubber-Tube Derived Soot (RTS) NPs and were further characterized and studied for the desired application.

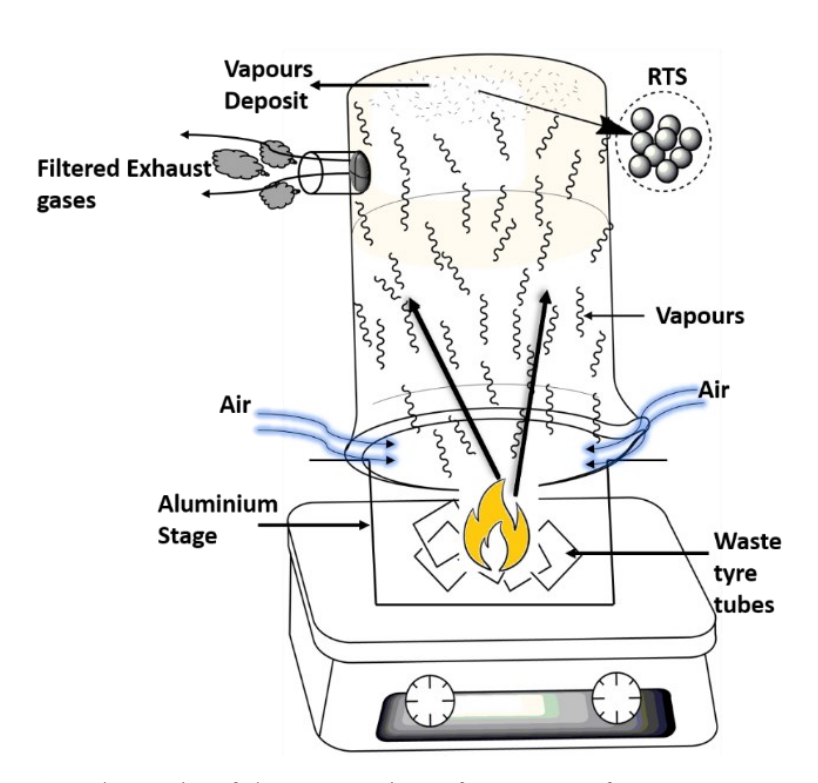


Figure 4. Schematic of the processing of RTS NPs from waste tyre tubes.

Other 0D nanocarbons considered in this study are tyre pyrolysis waste (TPW) particles and onion-like carbon (OLC) particles derived from TPW. Approximately 30-35% of carbon is obtained after waste tyres are pyrolyzed. This carbon is reused as filler materials in the rubber industry. However, it has not been utilized as lubricant additives or processed into high-value material. TPW was procured from a local tyre pyrolysis plant at ₹3 per kg. 800 g of as-procured TPW was then filled in a custom-made graphite boat (250 mm ×10 mm× 30 mm) with a lid and placed in a furnace for heating. The material in the furnace was heated in an argon atmosphere at 10 °C/min (10 cpm) to a temperature of 2200 °C and maintained for 1 h. Then, the furnace was naturally cooled to room temperature, after which the resultant powder (subsequently characterized as OLC) was collected. The as-procured TPW and the as-prepared OLC were characterized using various characterization techniques to understand its microstructure, crystallinity, bonding structure, and degradation behavior. The conversion of TPW into OLC has been performed at 2200 °C for 1 h after understanding the structural changes in amorphous carbon as a function of temperature [2-4]. The conversion efficiency of the TPW conversion to OLC was calculated as 90-93% by weight after several repetitions.

3.1.2 Processing of 1D MWCNTs

A customized fluidized bed reactor (Fig. 5) is used for processing the MWCNTs. The fluidized bed can be assumed of like an assortment of particles that behave like a fluid when a fluidizing agent (a gas or a liquid) is purged through it from below. As the velocity of the purged fluid increases, the friction leads to a drop in the pressure across the bed. The drag force on the particles due to the purged fluid acting upwards escalates until it equals the perceived weight of the particles on the bed. This results in the commencement of fluidization at a certain minimum fluidization speed. This fluidization regime typically exhibits the highest heat and mass transfer rates. Although the typical heat transfer coefficient from gas to particle is small (between 5-20 W/m²K) and could possibly be a hinderance for any fluid-solid system, the high surface area of the fine particles on the bed mitigates this issue. Therefore, the heat transfer between fluid-to-particle is hardly ever the limiting factor in fluidized-bed arrangements. This implies that the bed is maintained at a consistent and regulated temperature, allowing for a more accurate understanding of temperature dependent growth of MWCNTs in fluidized bed arrangements. Efficient blending in properly engineered fluidized beds results in a consistent system. As a result, all catalyst particles encounter the feed gases and partake in the reaction, offering a superior gauge of output per unit mass of catalyst compared to stationary bed reactors. In the majority of heterogeneous reaction systems, an expanded catalyst contact

surface is advantageous for the chemical reaction; this is also true during the production of MWCNTs and will boost the total reaction effectiveness.

The reaction zone in the fluidized bed reactor (Fig. 5) is a stainless steel (SS) tube (107 mm in inner diameter and 530 mm in height). An SS mesh is used as a gas distributor, while an electrical furnace equipped with a thermocouple located at the center of the SS tube allows the fluidized bed temperature to be monitored. The furnace is heated to 750 °C, and then the Ar gas (at 7.6 SLM) is introduced to maintain an inert atmosphere in the furnace, followed by the simultaneous introduction of C₂H₂ gas (at 2.5 LPM) and Ni catalysts into the furnace. The reaction is allowed for 3 min, after which the C₂H₂ gas flow is stopped. MWCNTs (in g scale) are formed on the SS gas distributor, which is cooled to room temperature under the Ar gas flow to avoid the oxidation of MWCNTs.



Figure 5. The vertical fluidized bed reactor used for the production of MWCNTs.

3.1.3 Processing of 2D MLG Nanoparticles

Natural Graphite Flakes (NGF, mesh size +40) were first intercalated using a mixture of analytical grade H₂SO₄ and HNO₃ in the ratio 3:1 by volume. The intercalation was done under constant stirring to ensure homogeneity of the entry of the intercalant ions into the van der Waals gaps of graphite layers of NGF followed by diluting the mixture with water to attain a pH of 7. The intercalated graphite (IG) was dried using bloating paper to remove the residual water. After drying, the IG was subjected to thermal shock at 1000 °C in a furnace to obtain expanded graphite (EG). The optical images of NGF, IG, and EG are shown in Fig. 6. The NGF is flaky and shiny, while distorted flakes constitute the IG. EG has an accordion-like morphology, and the graphitic layers held along the c-axis of graphite could exfoliate off easily under the slightest applied shear force.

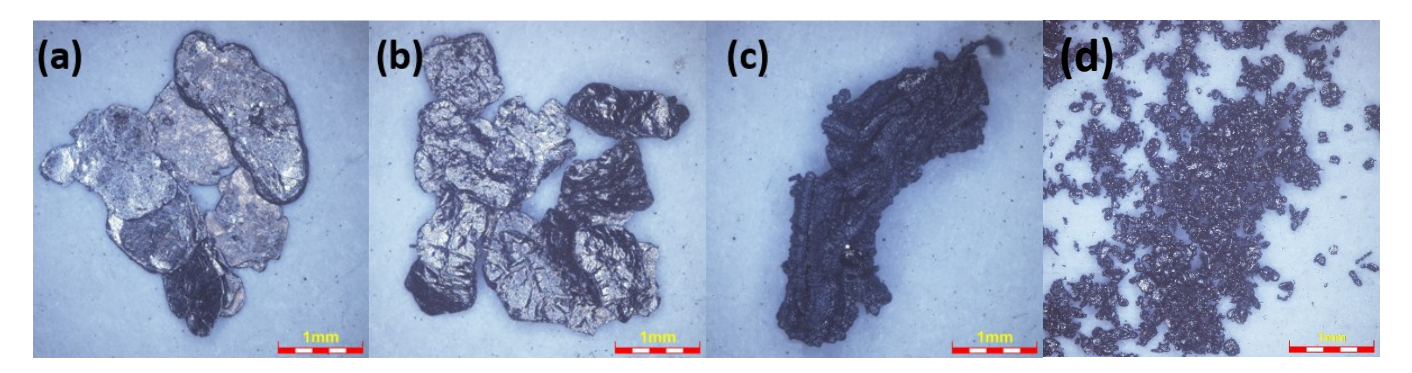


Figure 6. Optical microscopy images of (a) NGF, (b) IG, (c) EG and (d) MLG.

1 kg of EG was mixed in a mixture of water and isopropanol in an optimized ratio and then subjected to shear forces in a high rpm stator-rotor-based shear mixer in anticipation of the exfoliation of EG. The resultant slurry was sonicated (SONICS Vibra Cell probe sonicator) in on/off mode for further exfoliation. The sonicated slurry was washed using deionized water to remove any solvent, filtered, and dried at 100 °C, resulting in 0.96 kg of MLG powder, as revealed by various characterization techniques. For clarity purposes, the schematic of the preparation process of MLG nanoparticles is shown in Figure 7.

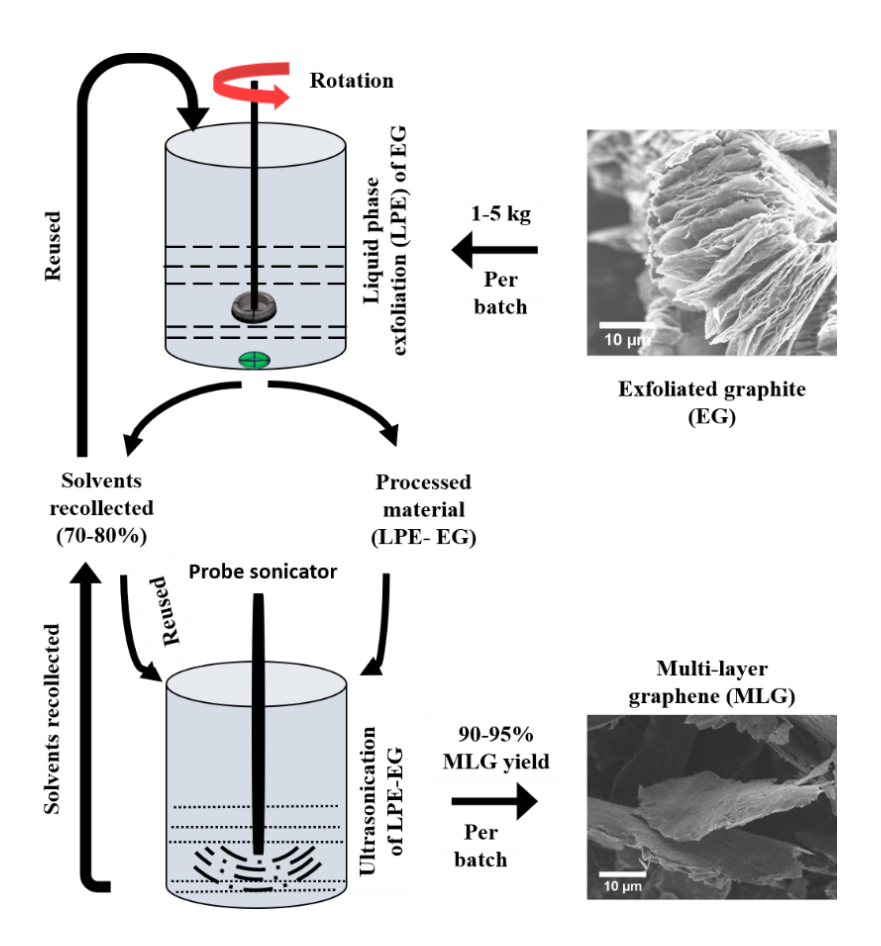


Figure 7. Schematic showing the processing of MLG from NGF.

3.2 Materials Characterization

The morphology of the nanocarbons produced in this work was recorded using a field emission scanning electron microscope (FESEM, Carl-Geiss Gemini 500) and a high-resolution transmission electron microscope (HRTEM, FEI TecnaiTF20) operated at 2 kV and 200 kV, respectively. Energy dispersive x-ray analysis (EDXA) was carried out for two samples (TPW and OLC) using FESEM (operated at 18 kV) to know the elemental compositions. For high-resolution TEM imaging, the samples were prepared by uniformly dispersing different nanocarbons in ethanol and carefully dropping the dispersion over holy-carbon grids. The RTS particles were subjected to high-resolution transmission electron microscopy using the JEM F200 JEOL from Japan. The TPW and OLC loaded grids were observed using the FEI Tecnai TF20 microscope with a maximum accelerating voltage of 200 KV. The MLG and MWCNT samples were imaged using FEI Technai G² S-Twin microscope.

The x-ray diffraction (XRD) technique was used to characterize the prepared nanocarbons for crystallinity and phase information. Bruker D8 Advance equipped with Cu K α (λ = 1.54 Å) was used to record the diffractograms in the 2 θ range of 10–100° by using a step size of 0.02°/min. Raman spectrum of the RTS nanoparticles was recorded with a confocal micro-Raman spectrometer (Alpha 300 WITec, Germany) using a near-field scanning optical microscope equipped with a 514 nm laser and a spectral resolution of 1 cm⁻¹. The Raman spectra of TPW and OLCs were recorded using a confocal micro-Raman spectrometer (WITec UHTS 600) equipped with a 532 nm laser. A Labram HR spectrometer (HORIBA Jobin–Yvon, Japan) using 532 nm laser excitation was used to record the Raman spectra of the produced MWCNTs, NGF, and MLG. The prepared nanocarbons were studied for their thermal stability in air using the thermogravimetry technique on Simultaneous Thermal Analyzer (STA 449 Jupiter). Approximately 10-12 mg of the prepared nanocarbons were loaded into Al₂O₃ crucibles with a lid to cover the crucible during the heating. The samples were heated to a temperature of 1000 °C at a heating rate of 10 °C/min (10 cpm). Air was purged during the entire process at a flow rate of 150 sccm.

3.3 Preparation of Lubricants with Nanocarbons as Additives

In this work, probe sonication was used to disperse the nanocarbons in lubricants. Ultrasonication plays an important role in the proper dispersion of nano additives in lubricants. Ultrasonication generates cavitation bubbles in the lubricant. When these bubbles implode, high shear forces and microjets are locally generated. These help in contravention of nano additive

agglomerates, ensuring even dispersion of nano additive particles throughout the lubricant. Furthermore, ultrasonication speeds up the mixing process, lowering the time required to achieve a homogenous dispersion compared to other mixing approaches. Practically, ultrasonication is energy-efficient and scalable. It facilitates easy and precise process control to optimize the nano lubricant preparation. Even the undesirable hot spots (which can be detrimental in the case of lubricants) can be easily circumvented by the choice of process parameters. The additive-free Group-2 dewaxed N500 oil obtained from Hindustan Petroleum Corporation Ltd., India, was used as the BO in this work. The BO without any additives was considered to understand the AW and anti-friction properties of the developed nanocarbons as additives in lubricants. Three test samples of each nanocarbon developed were prepared by dispersing 0.1wt. %, 0.3 wt.%, and 0.5wt.% of the materials in the BO. The probe sonicator (SONICS Vibra Cell probe sonicator) was operated at 40% amplitude in on/off mode (15 s each). A water bath was used to mitigate the heat generated during the process because heating can impact the rheological properties. All the samples were sonicated for 3 h to ensure homogenous dispersion of the nanocarbons. The samples are visually observed for any sedimentation after being left undisturbed for 90 days. Higher concentrations (> 0.5 wt.%) weren't prepared due to observable sedimentation in 0.5 wt.% sample. The nanocarbons were also dispersed in a commercial oil (CO). The CO used is ENI Tristar 15W40, which is an API CF-4 multigrade diesel engine oil having good AW and anti-corrosion properties. 15W-40 engine oil is a multi-viscosity oil that is extensively used in automobiles, trucks, and certain heavy machines. The numbers "15W" and "40" in the oil's name refer to its viscosity ratings, which characterize its flow properties at various temperatures. The digits and the "W" stand for the following: "W" in this grade stands for "winter," and the number before it (15 in this example) represents the viscosity of the oil at low temperatures. In chilly conditions, lower numbers suggest better flow. In practice, this implies that the oil will flow more smoothly in cold circumstances, giving better protection during cold engine starter. The number after the "W" (40 in this example) reflects the viscosity of the oil at operating or high temperatures. Higher numbers imply thicker oil that is more suitable for high-temperature situations. When the engine is heated, this helps to maintain optimum lubrication and protection. The advantage of 15W-40 engine oil is that it is designed to function well in a wide temperature range, making it suited for a variety of climates and applications. It provides exceptional cold-start protection and keeps the engine lubricated at high temperatures, which is critical for engine durability and efficiency. Older petrol and diesel engines, as well as certain current diesel engines, agricultural equipment and heavy-duty trucks, all utilize 15W-40 engine oil. It strikes a compromise

between cold-weather performance and high-temperature resistance, making it an adaptable choice for a wide range of vehicles and machines. The TPW and OLC were dispersed in an additive-free group-II dewaxed N500 BO. Group-II BO is used in formulating commonly used EOs; hence, studying its characteristic changes in wear and coefficient of friction (CoF) will help understand the feasibility of the materials as lubricant additives. The additive-free BO will ensure no synergism or antagonism between other additive compounds and the carbonaceous materials used as fillers.

3.4 Measurement of Rheological Properties of Lubricant Samples

The rheological properties (i.e., viscosity and shear stress) of the nanocarbons-dispersed lubricants were evaluated on a Brookfield rheometer R/S-CPS+ working on Searles's principle using a co-axial cylindrical spindle CC3 45 DIN by applying a shear rate of 0-1000 sec⁻¹. In the field of tribology, viscosity is used to describe the flow properties of lubricants and is an important factor in determining the performance of lubricated systems. Viscosity is expressed in units of centipoise (cP) or poise (P), and is dependent on temperature, pressure, and the chemical composition of the lubricant. For example, increasing temperature generally leads to a decrease in viscosity, while increasing pressure often leads to an increase in viscosity. In lubricants, viscosity is an important factor in determining the load-carrying capacity, film strength, and friction reduction properties of the fluid. High-viscosity lubricants are typically better at carrying heavy loads, providing better film strength, and reducing friction. On the other hand, low-viscosity lubricants are easier to pump and flow through small orifices, making them more suitable for applications where high fluid flow is required. A viscometer, which gauges the duration required for a specific volume of fluid to pass through a capillary at a set shear rate, can be used to ascertain the viscosity of a lubricant. The most used viscometers in tribology are the Brookfield viscometer and the rotational viscometer. In addition to its importance in tribology, viscosity is also used in other scientific and industrial fields, including rheology, fluid mechanics, and chemical engineering. For instance, in rheology research, viscosity serves as a metric for the mechanical characteristics of intricate fluids like polymer solutions, suspensions, and emulsions. To sum up, viscosity is a crucial attribute of fluids that signifies its opposition to flow.

Viscosity measurement of lubricants is an important aspect in tribology and plays a crucial role in the selection of appropriate lubricants for different applications. A rotational rheometer is one of the commonly used instruments to measure the viscosity of lubricants. In a rotational rheometer, the lubricant sample is placed between two parallel plates and subjected to shear

stress by rotating one of the plates while the other plate remains stationary. The applied shear rate and the resulting shear stress are used to determine the lubricant's viscosity. A key benefit of employing a rotational rheometer to measure viscosity is its ability to assess viscosity across a broad spectrum of shear rates. This is crucial for understanding how the lubricant's flow characteristics vary under diverse conditions. One of the benefits of rotational rheometers is their ability to measure viscosity at elevated temperatures, which is crucial for analyzing the performance of lubricants under high-temperature conditions. Additionally, rotational rheometers can evaluate the viscosity of non-Newtonian fluids, which are fluids whose behavior deviates from Newton's law of viscosity. Such fluids, including polymers, display a stress response that varies with time and have a viscosity that is dependent on the shear rate. By assessing the viscosity of these fluids at various shear rates, rotational rheometers can yield valuable insights into their flow characteristics. In summary, due to their capacity to measure viscosity across a broad range of shear rates and at high temperatures, as well as their ability to evaluate the viscosity of non-Newtonian fluids, rotational rheometers are extensively employed for viscosity measurements of lubricants. This is vital for comprehending the flow properties of these substances.

Rheological tests were conducted using a rotational rheometer, which operates based on Searle's principle, utilizing the shear rate sweep method. This technique is widely used in rheology to ascertain the viscosity and flow characteristics of materials. The process involves subjecting a sample to varying shear rates while recording the resultant stress or torque. To execute a shear rate sweep, a small quantity of the sample is positioned in the measurement gap of the rheometer's measuring geometry, typically comprising two concentric cylinders or a parallel plate setup. The sample is then exposed to a sequence of rotational speeds, or shear rates, and the corresponding stress or torque is measured. The shear rate is determined by dividing the velocity of the measuring geometry by the gap between the cylinders or plates. As the shear rate escalates, the material undergoes increasing degrees of deformation, leading to alterations in its viscosity and flow behavior. The collected data is usually represented as a curve plotting viscosity against shear rate. This graph can reveal crucial information about the material's flow behavior, such as whether it exhibits shear thinning, shear thickening, or yield stress behavior. Such insights are valuable for predicting how the material will respond under various processing or handling scenarios. Shear rate sweep is a widely used method for measuring the rheological properties of materials in rotational rheometers. Some of the advantages of using shear rate sweep include: Broad Range of Shear Rates: Shear rate sweep allows for the viscosity measurements to be done over a broad range of applied shear rates,

from very low to very high. This is important because the viscosity of many materials can vary significantly over different shear rates. Accurate Measurement of Viscosity: By measuring the stress or torque as a function of applied shear rate, shear rate sweep provides a direct measurement of the material's viscosity. This allows for accurate characterization of the material's rheological properties. Easy to Perform: Shear rate sweep is a relatively simple and straightforward method that can be easily performed on most rotational rheometers. It does not require specialized equipment or complex sample preparation. Useful for Quality Control: Shear rate sweep is often used for quality control in manufacturing processes, as it can quickly and easily detect changes in the rheological properties of materials. Provides Information on Material Behavior: Shear rate sweep can provide important information on the flow behavior of materials, including shear thinning, shear thickening, and yield stress. This information can be useful for understanding how materials will behave under different processing or handling conditions.

3.5 Measurement of Tribological Properties using Lubricant Samples

The Four ball wear test is a commonly used method for evaluating the wear and friction properties of lubricants. The test is performed using a specialized tribometer, which is designed to simulate conditions similar to those encountered in typical industrial and automotive applications. The four-ball wear test consists of four steel balls that are placed in contact with one another, with a lubricant between them. The balls are then subjected to a controlled load, which is typically in the range of 40-60 kg, and rotated against each other. The test is performed for a specified period of time, typically 10-60 min, and the resulting wear scar on the balls is measured to determine the wear preventive characteristics of the lubricant. The coefficient of friction between the balls is also measured during the test, and is used to evaluate the friction preventive performance of the lubricating media. The four-ball wear test is used to evaluate the performance of lubricants in a wide range of industrial and automotive applications. It is commonly used to evaluate EOs, gear oils, and other types of lubricants that are used in highload and high-temperature environments. The test is useful for assessing the ability of lubricants to reduce friction and wear, and to protect metal surfaces from corrosion and damage. The four-ball wear test has several advantages, including its ability to provide a rapid and accurate assessment of the wear and friction properties of lubricants. The four - ball wear test is an important tool for lubricant developers, manufacturers, and users, and continues to be widely used in the industry.

ASTM D4172 is a standard test method for determining the wear characteristics of lubricants. The test is commonly referred to as the "Four Ball Wear Test" and is used to evaluate the performance of lubricants in high-load, high-temperature applications. The same has been used in this work. The test is performed using a specialized tribometer that consists of four steel balls that are placed in contact with one another, with a lubricant between them. The balls are then subjected to a controlled load, which is typically in the range of 40 kg (392N \pm 5N), and rotated against each other. The tribological test is conducted over a set duration of 1 h, and the ensuing wear mark on the balls is evaluated to gauge the wear resistance of the lubricant. The friction coefficient between the balls is also recorded during the test, serving as a measure of the lubricant's friction preventive performance. The measurements of the wear scar diameters formed on the 4-ball wear test specimens is done using an optical microscope with 10X magnification. The test sample should be cleaned and polished before conducting the test to ensure that the surface is smooth and free from any contaminants. The sample is then placed in the 4-ball wear test apparatus and the test is conducted. After the test is completed, the sample is removed from the test apparatus and cleaned to remove any debris or residual lubricant. The fixed balls along with the die is then mounted onto the microscope. Care should be taken to ensure that the sample is mounted in a way that allows the wear scar to be viewed clearly under the microscope. The sample is then imaged using the 10X magnification objective lens. The microscope should be focused on the wear scar to obtain a clear image. The diameter of the wear scar can be measured using the in-built image analysis software (TC capture). The measured wear scar diameter is recorded as per the test conditions such as load, speed, and duration of the test. In summary, the wear scar diameter measurement of 4-ball wear test samples using an optical microscope with 10X magnification involves preparing the sample, mounting it onto a microscope and analyzing the wear scar image to determine the diameter. This technique provides a reliable and accurate method for evaluating the wear resistance of materials under sliding or rolling contact. The wear scar depth, h (in mm) was calculated using Equation 1 [5], where $K_1 = 48.22 \times 10^{-3} \text{ mm}^{-1}$, $K_2 = 3.35 \times 10^{-6} \text{ mm}^2 \text{ N}^{-1}$, and $K_3 = 1.63 \times 10^{-4}$ mm $N^{-2/3}$ for the steel balls, L is load applied in N and d is the WSD in mm.

$$h = K_1 d^2 + \left(\frac{K_2 L}{d}\right) - K_3 L^{2/3}$$
 (Equation 1)

The average wear volume loss (V) values on the rubbing surfaces (here, surfaces of the steel balls used for wear testing) in mm³ were calculated using Equation 2 [6], where d is the WSD in mm, W is the load in N, $C_1 = 1.55 \times 10^{-2} \text{ mm}^{-1}$ and $C_2 = 1.09 \times 10^{-6} \text{ mm}^2 \text{ N}^{-1}$.

$$V = C_1 d^4 - C_2 Wd (Equation 2)$$

References

- [1] R. Kali, B. Padya, T. Rao, P. Jain, Solid waste-derived carbon as anode for high performance lithium-ion batteries, Diamond and Related Materials 98 (2019) 107517.
- [2] K. Bogdanov, A. Fedorov, V. Osipov, T. Enoki, K. Takai, T. Hayashi, V. Ermakov, S. Moshkalev, A. Baranov, Annealing-induced structural changes of carbon onions: high-resolution transmission electron microscopy and Raman studies, Carbon 73 (2014) 78-86.
- [3] F. Zhang, K. Fan, J. Yu, F. Saba, J. Sun, Pulsed direct current field-induced thermal stability and phase transformation of nanodiamonds to carbon onions, RSC Advances 9(25) (2019) 14360-14371.
- [4] C. He, N. Zhao, C. Shi, X. Du, J. Li, Effect of annealing on the structure of carbon onions and the annealed carbon coated Ni nanoparticles fabricated by chemical vapor deposition, Journal of Alloys and Compounds 472(1-2) (2009) 230-233.
- [5] A. Bos, The temperature at the wear scars of the four-ball apparatus, Wear 31(1) (1975) 17-27.
- [6] I. Feng, A new approach in interpreting the four-ball wear results, Wear 5(4) (1962) 275-288.

Chapter 4 Results and Discussion

4.1 0D RTS Particles as Additives in Lubricants

Figures 8 and 9 show the morphological images of RTS nanoparticles as observed using SEM and TEM. The images (Figs. 8 and 9) reveal that RTS nanoparticles are spherical with 50-100 nm sizes. The sample's HRTEM image (Fig. 9 (b)) reveals a heliocentric-like arrangement of graphene layers in each RTS nanoparticle. At the same time, a closer observation reveals a great degree of disorderedness in the arrangement of the graphitic layers. In the XRD pattern (Fig. 10) of RTS nanoparticles, the broad peak at 2θ equals 23.7° is indexed to the (002) plane in graphite. The (002) diffraction peak in bulk graphite is typically recorded at 2θ equals 26.6° . Another broad diffraction peak at 43.6° is indexed to the (101) plane in graphite. The broadness of the recorded diffraction peaks indicates a low degree of graphitization (in other words, a high degree of disorderedness). The interlayer spacing in RTS nanoparticles is calculated to be 0.375 nm, which is higher than that in crystalline graphitic carbon.

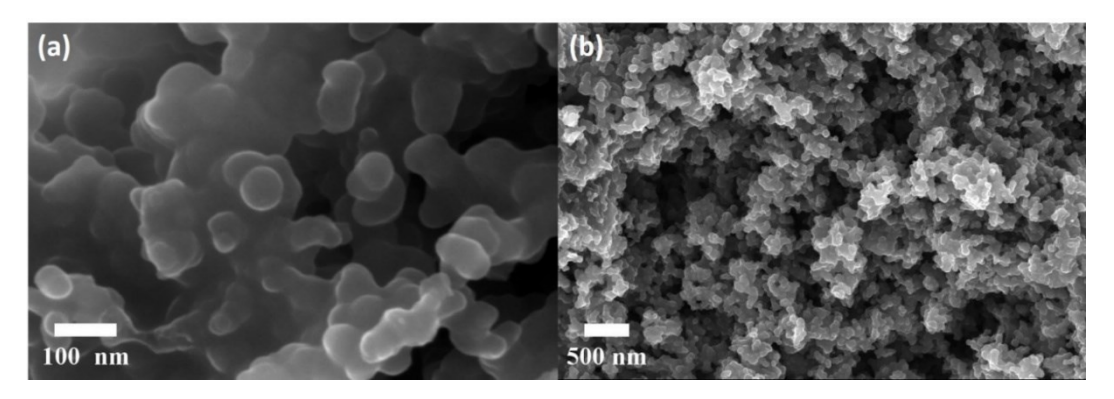


Figure 8. SEM images of RTS nanoparticles at (a) higher and (b) lower magnifications.

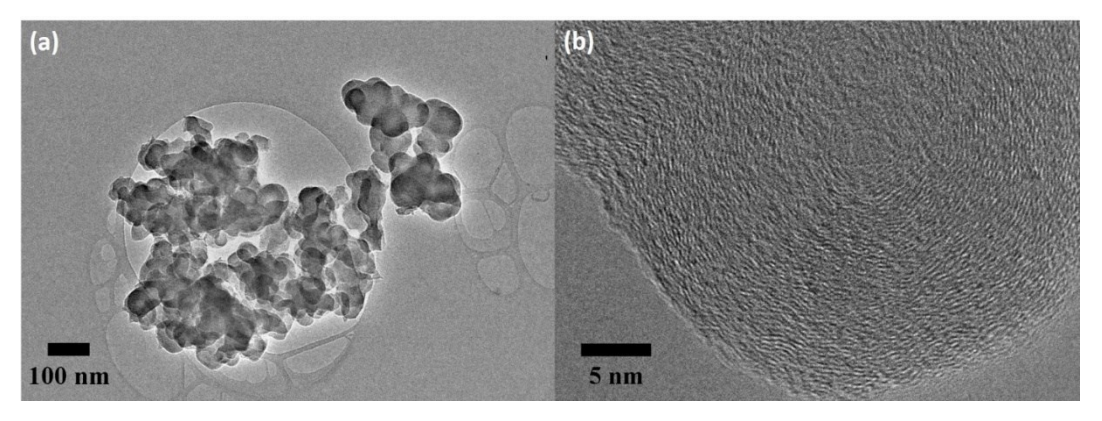


Figure 9. (a) Low magnification TEM image of RTS nanoparticles and (b) HRTEM image of a single RTS nanoparticle.

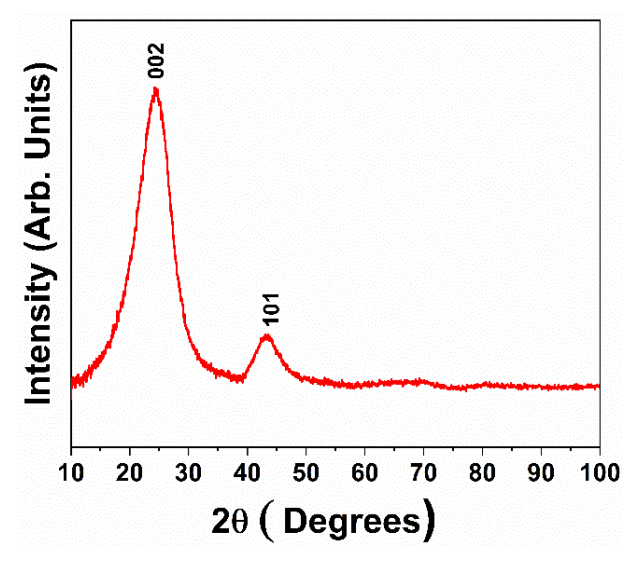


Figure 10. XRD pattern of RTS nanoparticles.

Figure 11 shows the Raman spectrum of RTS nanoparticles. The spectrum exhibits peaks at 1343, 1583, and 2887 cm⁻¹ corresponding to the typical disordered (D), graphitic (G), and 2D bands. The appearance of these bands confirms that sp² hybridized graphitic carbons constitute RTS nanoparticles. The high intensity of the D band confirms the high degree of disorderedness complementing well with the XRD and electron microscopic analyses. The appearance of the blue-shifted 2D peak confirms the multilayer stacking of concentric graphitic layers in RTS nanoparticles. The multilayer stacking is complementing well with the HRTEM analysis. The observations made here correlate well with corresponding electron microscopy [1], X-ray diffraction [2-7] and Raman observations [8] made earlier on carbon soot particles prepared by various methods.

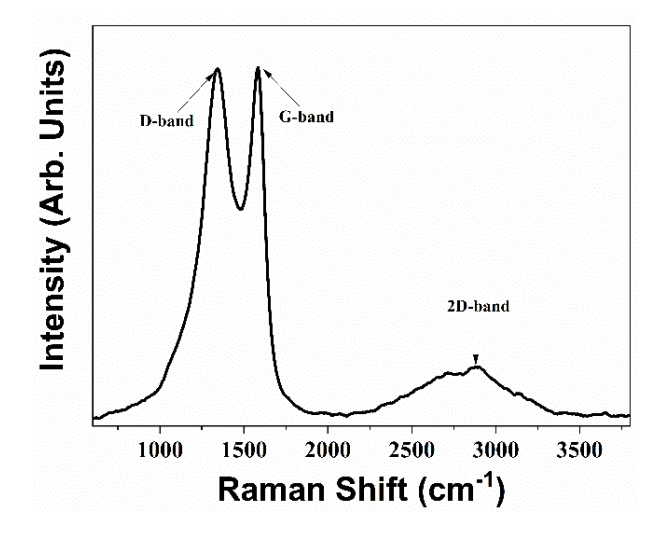


Figure 11. Raman spectrum of RTS nanoparticles.

Amorphous carbon forms degrade around 300 °C while graphitic materials start degrading around 700 °C. The RTS nanoparticles exhibited an on-set thermal degradation above 460 °C (Fig. 12), implying a low degree of graphitization. Above 460 °C, the mass loss occurs in a linear pattern, directly proportional to the increasing temperature. 94% of the total mass of RTS is degraded from the initial decomposition temperature of 460 °C to the final decomposition temperature of 828 °C. The thermogravimetric analysis (TGA) curve of RTS consists of no secondary degradation peaks during the decomposition process, which affirms the absence of any other elements as significant constituents. The smooth degradation curve also indicates the absence of any volatile material in the sample, with no residual mass being the direct indication of the absence of ash in the sample. The absence of any sharp minor peaks is conclusive to claim that no oxidation reaction occurred until the on-set temperature was reached. The delayed thermal degradation of the RTS nanoparticles with a low degree of graphitization is attributed to the heliocentric arrangement of the graphitic layers because the outer layers slow down the heat transfer to the inner layers. Simultaneously, any amorphous constituents (for example, organic impurities, sulfur compounds, etc.) in RTS nanoparticles will start decomposing through oxidative degradation (under air) at a much lower temperature than crystalline graphite. For convenience and a better understanding of the thermal degradation of RTS nanoparticles, differential scanning calorimetry (DSC) and difference thermogravimetry (DTG) curves are also shown along with the TGA curve in Fig. 12.

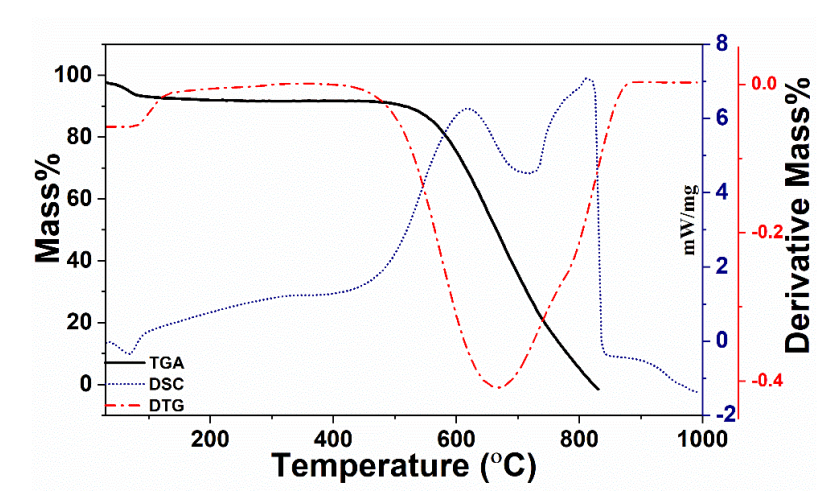


Figure 12. Thermal decomposition profiles of RTS nanoparticles.

Fig. 13 shows the viscosity values as a function of the temperature of different RTS-added lubricant samples. The BO's viscosity (Fig. 13 (a)) is reduced with increasing temperature. The BO with an initial viscosity of 153 cP at room temperature (RT) exhibited a drastic reduction

of 64.05% in viscosity at 40 °C. It is a well-known fact that oils tend to lose their viscosity as temperature increases. The oil molecules exert attractive forces on each other across flowing layers, resulting in viscosity (viscous force). As temperature rises, viscosity decreases due to high thermal energy in the liquid molecules, which easily overcomes these attractive forces prevailing in the oil. At higher temperatures, the additives in oil are expected to help retain the rheological properties.

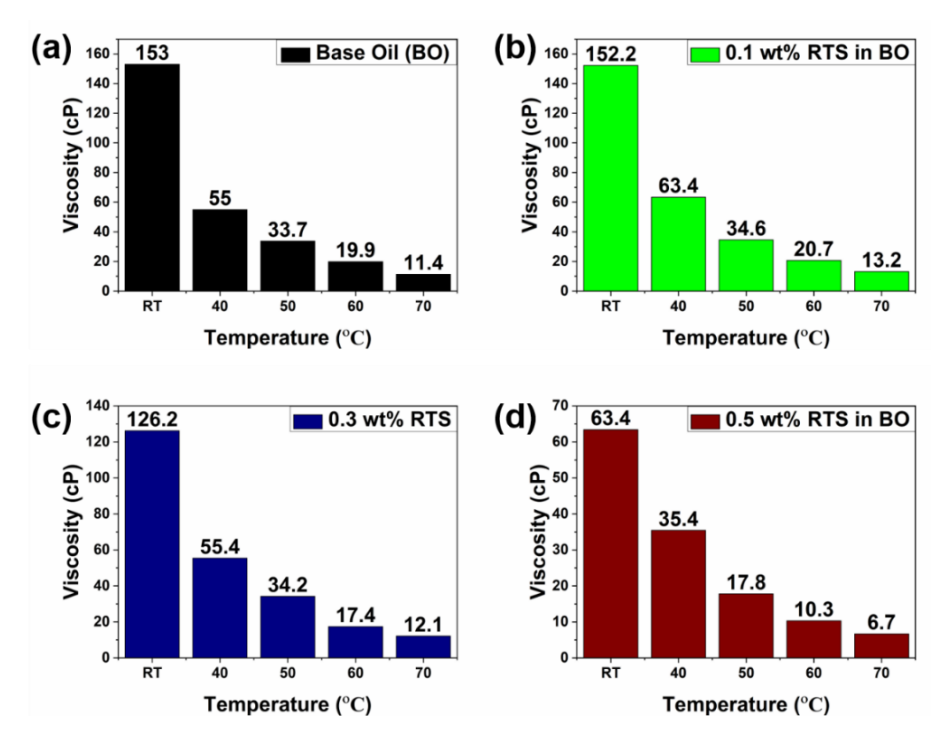


Figure 13. Viscosity values of (a) BO, (b) 0.1 wt.% RTS in BO, (c) 0.3% RTS in BO, and (d) 0.5% RTS in BO at different temperatures ranging from RT to 70 °C.

Fig. 13 (b) shows the viscosity of BO dispersed with 0.1 wt.% of RTS at different temperatures. At RT, the viscosity value was almost the same as that of the BO, implying negligible impact of dispersion of RTS nanoparticles on the viscous forces of BO. As the concentration of RTS is increased to 0.3 wt.%, a moderate reduction in viscosity value is observed as the initial viscosity value falls to 126.2 cP at RT. Further reduction in viscosity was observed with an increase in the concentration of the RTS nanoparticles, as shown in Fig. 13 (d). The viscosity is drastically lowered to 63.4 cP at RT for 0.5 wt.% dispersion of RTS in the BO, implying that 0.5 wt.% of RTS is undesirable for lubrication because it resulted in the reduction of the viscosity value by 53.56%. This means that the RTS has to be used cautiously in optimized concentrations to maintain the viscosity values in the required range.

The reduction in viscosity with the addition of RTS nanoparticles is attributed to the smooth surfaces of these nanoparticles, which may lead to reduced cohesive forces among the fluid layers upon dispersion. The fluid layers experience lower internal resistance to flow due to the addition of the nanoparticles. When the shear rate is applied, the soot particles mollify the internal friction (reducing the viscous force between fluid layers), reducing viscosity values. It was reported in the literature [9], that adding 0.3 wt.% of carbon spheres to a neat oil resulted in a reduction of 3% in viscosity. Reduction in crude oil viscosities was recorded experimentally and theoretically by using different concentrations of SiO₂, Fe₃O₄, and Al₂O₃ nanoparticles as additives. This behavior was attributed to increased packing factor, interactions, and aggregation between nanoparticles and hampered interactions between the nanoparticles and the asphaltene aggregates of crude oil [10]. The RTS dispersion improved the viscosity values of the lubricant at high temperatures, irrespective of the concentration added. This implies that the RTS nanoparticles acted as poor conductors of heat, mitigating the effect of heat on the oil molecules, which eventually prevents the breakdown of the oil molecules' bonds and helps retain the viscosity.

Improvement in the viscosity retention (Table 2) is observed as the RTS concentration increased from 0.1 wt.% to 0.5 wt.%. The improved viscosity retention at higher temperatures reduces lubricant thinning, eventually leading to better tribo-film formation at the interface of rubbing surfaces. Lubricant thinning at higher temperatures results in poor tribological behavior of the moving contact surfaces. The RTS nanoparticles alleviate the effect of temperature on the BO, preventing drastic viscosity loss at elevated temperatures.

Table 2. Percentage of viscosity retained compared to the initial viscosity of different lubricant samples

Sample	Temperature				
	RT	40 °C	50 °C	60 °C	70 °C
ВО	100%	35.95%	22.03%	13.01%	7.45%
0.1 wt.% RTS in BO	100%	41.66%	22.73	13.6 %	8.67%
0.3 wt.% RTS in BO	100%	43.9%	27.1%	13.79%	9.59%
0.5 wt.% RTS in BO	100%	55.84%	28.08%	16.25 %	10.57 %

The behavior of different samples was compared to the applied shear rate at various temperatures to comprehend the shear stress profiles and correlate the reduced viscosity after RTS addition to the BO. From Fig. 14 (a), it is observed that there is a linear increase in the

shear stress as the shear rate increases. At RT, the shear stress value at 50 sec⁻¹ is below 10 Pa, while its value is 149 Pa at 1000 sec⁻¹. When the temperature is raised to 40 °C, the shear stress is reduced to 64.28 Pa and eventually reduced to 20.85 Pa at 70 °C. This observation is attributed to the broken intermolecular bonds and increased energy of oil molecules, which makes them overcome the resistance to flow and cause them to thin out.

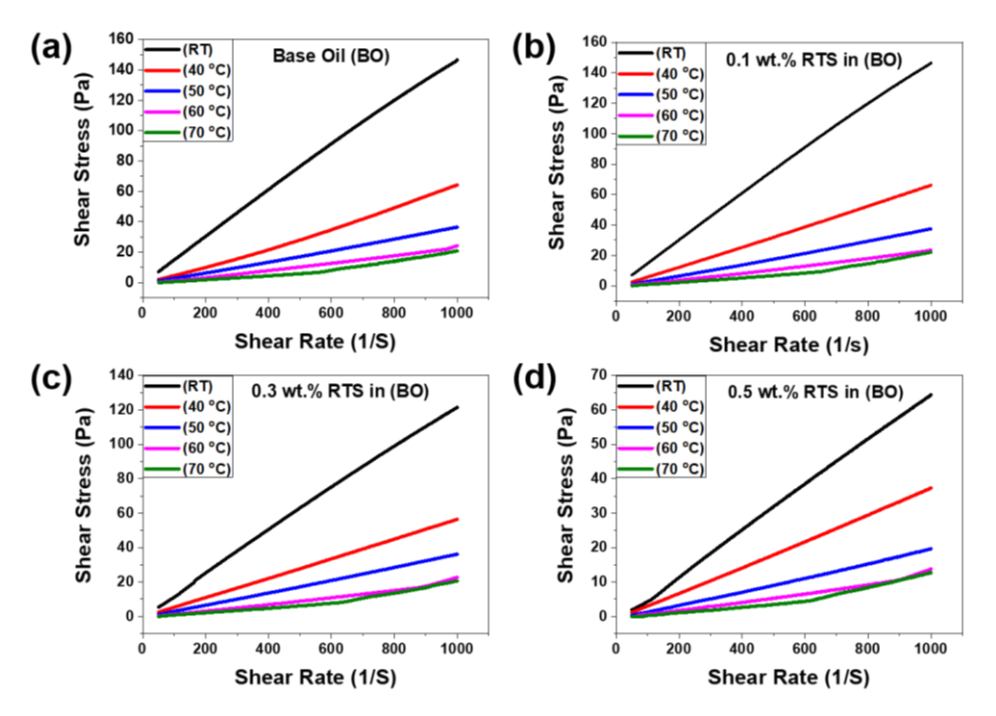


Figure 14. Shear stress versus shear rate as a function of the temperature of (a) BO, (b) 0.1 wt.% RTS in BO, (c) 0.3 wt.% RTS in BO, and (d) 0.5 wt.% RTS in BO.

The reduced shear stress in the lubricant samples is definitely due to RTS dispersion in the BO. The sphere-like soot particles with the graphitic layers lessen the resistance to flow between the layers of oil under the shear rate applied. Nanoparticles possess a high specific surface area. Due to their small particle size (100 nm), the RTS particles increase the apparent surface area of the BO fluid layers on which the applied shear rate acts since shear stress is dependent on the area over which the force acts, the value of shear stress reduces with the addition of RTS. The 0.1 wt. % concentration (Fig. 14 (b)) doesn't exhibit much reduction in shear stress values (146 Pa at RT and 22.07 Pa). However, as the concentration increases to 0.3 wt.%, the count of RTS nanoparticles in the oil increases, facilitating the easy and efficient flow of the fluid layers and preventing boundary layer formation in the oil sample, contributing to low shear stress. Fig. 14 (c) shows the shear stress values in the 0.3 wt.% sample, 121.45 Pa at RT and 20.54 Pa at 70 °C. A low shear stress of 63.468 Pa is generated in the 0.5 wt.%

sample at RT and 12.789 Pa at 70 °C. The shear stress results correlate well with the viscosity trend (Fig. 13). The addition of RTS nanoparticles reduces the viscosity and shear stress in the BO, which affirms the assumption that the nanoparticles facilitate the easy flow of layers of oil over each other, reducing the inter-layer friction, which is the cause of shear stress in fluids.

The reduced shear stress in the nanoparticles' dispersed samples and the reduced viscosity qualitatively indicate that the fluid layers under the applied shear rate are experiencing lower resistance to flow. Even though the viscosity reduction trend observed here is an apparent deviation from many rheological models predicting viscosity changes with the dispersion of solid particles, the data recorded closely resembles relevant rheological models [11,12]. Nanoparticles defy the hydrodynamic effect on the viscosity as predicted by the Einstein model. Instead, they induce a change in the dispersing medium's conformation and free volume, resulting in a non-Einstein-like decrease of viscosity [13]. The interaction between the oil molecules and the RTS nanoparticles can plausibly reduce the cohesive attraction forces between fluid layers, causing less resistance to flow when the shear rate is applied.

Further, if the fluid's viscosity is higher, the thickness of the boundary layer in proximity to the surface of the dispersed nanoparticle is higher, and vice versa. The addition of RTS nanoparticles, specifically 0.3wt.%, and higher concentrations in BO resulted in the modification of BO's rheological properties in such a way that its viscosity and shear stress were reduced drastically attributed to the local (within the boundary layer) convective heat transfer enhancement and thinning of the laminar sublayer [14]. However, further experimentation (which is beyond the scope of this thesis work) is needed to confirm this sort of empirical understanding in the case of RTS nanoparticles [14].

Sedimentation of the particles was visually observed over 90 days. On the 90th day, the sample had a dispersion of 0.5 wt.% RTS was found to have the highest sedimentation, while the samples havinf a dispersion of 0.1 wt.% RTS and 0.3 wt.% RTS exhibited moderate sedimentation during this period. The more significant sedimentation in the case of the sample with 0.5 wt.% RTS dispersion is due to increased collisions and aggregation between the RTS particles, resulting from a high concentration in the BO.

The tribological tests are carried out at room temperature (RT) and 70 °C to understand the effect of temperature on the lubricating properties of the RTS dispersed oils. Notably, at 70 °C, the BO lost almost 93% of its viscosity. Fig. 15 and 16 depict the variation of frictional torque (FT) values as a function of the RTS concentration at RT and 70 °C, respectively. The BO sample showed an initial FT value of 1.35 Kg-m (during 250 - 470 sec), which eventually

reduced to 1.04 Kg-m towards the end of the test. The 0.1 wt.% of RTS dispersed oil exhibited a higher FT than the BO. 0.1 wt.% of RTS dispersed oil exhibited an initial FT value of 1.65 Kg-m (after 150 sec), which reduced to 0.82 Kg-m at 3600 sec. A further increase in the RTS concentration increased the FT values. 0.3 wt.% of RTS dispersed oil exhibited an initial FT value of 1.75 Kg-m (after 190 sec), which gradually reduced and stabilized to 1.14 Kg-m towards the end of the test. Adding 0.5 wt.% of RTS to the oil resulted in an initial FT value of 1.42 Kg-m, which remained almost constant throughout the test, and an FT value of 1.26 Kg-m was observed at 3600 sec.

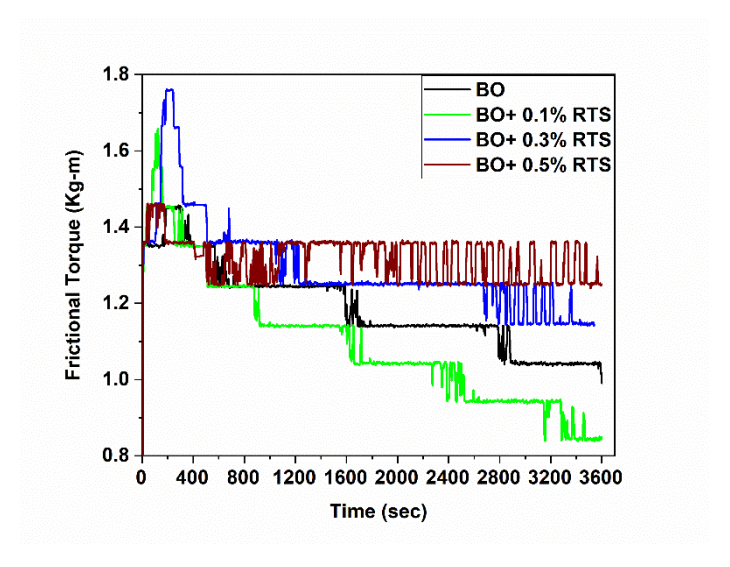


Figure 15. Representative frictional torque behavior of test specimens lubricated at RT with BO, 0.1 wt.% RTS in BO, 0.3 wt.% RTS in BO, and 0.5 wt.% RTS in BO.

When keenly observed, the FT profiles in Fig. 15 show that the BO and 0.1wt.% of RTS in BO could consistently reduce the FT during the test process at RT. In contrast, the higher concentration (i.e., 0.3 wt.% and 0.5 wt.% of RTS in BO) samples showed a lesser reduction in their respective FT profiles. Out of all tested samples, the 0.1 wt.% RTS in the BO sample took the least time (163 sec) to form a protective lubricating film, lowering the FT compared to BO (562 sec), 0.3 wt.% RTS in BO (442 sec) and 0.5 wt.% RTS in BO (404 sec). This is attributed to the RTS nanoparticles in the BO entering between the sliding surfaces, forming a tribo-layer quickly and giving a continuously reducing FT profile.

From Fig. 13, it is well understood that the BO retained a mere 7.45% of its initial viscosity as the temperature increased to 70 °C. It is essential that a material intended to reduce friction and wear functions effectively at high temperatures, too. Therefore, the RTS dispersed lubricant samples and the BO are subjected to wear tests at 70 °C, with other conditions remaining the same. At 70 °C, the BO sample showed an initial FT of 1.26 Kg-m (at 228 sec),

which increased to 1.74 Kg-m (after 980 sec) and then remained nearly constant till the end of the test. The initial low FT value is due to the easy flowability of the BO in between the ball-to-ball interface due to low viscosity. However, the low viscous fluid fails to form a uniform and sustainable tribo-film, causing a haphazard increase in FT. BO with 0.1wt.% of RTS nanoparticles displayed a continuously decreasing FT profile (Fig. 16), with an initial and final FT of 1.43 Kg-m and 0.54 Kg-m, respectively. A similar trend in the FT profile is observed in the case of 0.3 wt.% RTS in BO. The FT profile of 0.5 wt.% RTS dispersed sample resembled the FT profile of the 0.3 wt.% RTS dispersed sample from 600 sec but with slightly higher FT values. In this case, an initial FT value of 1.46 Kg-m was measured.

The FT value was reduced to 1.27 Kg-m before 500 sec and relatively remained stable till 3600 sec with an end FT of 1.04 Kg-m. The increase in FT values for higher concentrations of RTS in BO (0.3 wt.% and 0.5 wt.%) is attributed to the agglomeration of the RTS nanoparticles. The RTS nanoparticles in lubricant are intended to form a tribo-layer and reduce friction. Instead, they might have started agglomerating at higher concentrations, creating lumps that resisted the unresisted sliding of the ball surfaces over each other. However, further investigation is needed to confirm the agglomeration and formation of lumps.

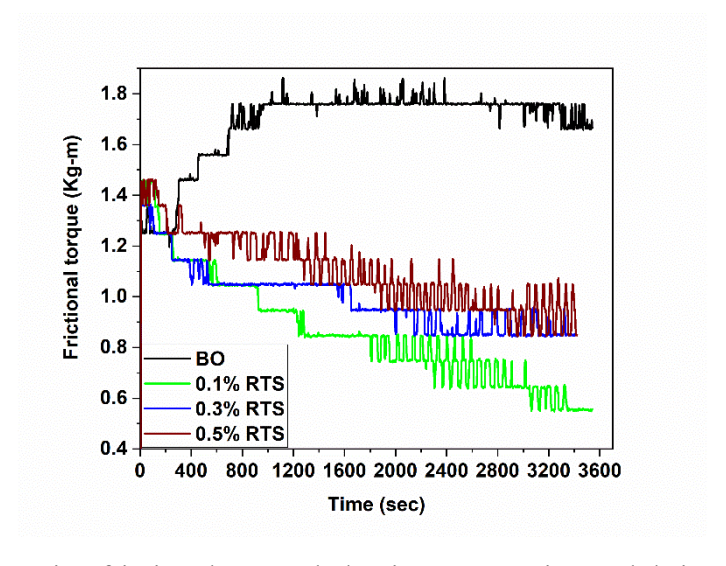


Figure 16. Representative frictional torque behavior test specimens lubricated at 70 °C of BO, 0.1 wt.% RTS in BO, 0.3 wt.% RTS in BO, and 0.5 wt.% RTS in BO.

The avg. FT values recorded for different lubricant samples at RT and 70 °C are shown in Table 3. At RT and 70 °C, FT was reduced by adding 0.1wt.% of RTS nanoparticles in BO. At RT, the avg. FT value was 1.185 Kg-m for BO, which was reduced to 1.092 Kg-m (~9% reduction) by adding 0.1 wt.% of RTS nanoparticles in BO. With a further increase in the RTS concentration in BO, the avg. FT value could be increased to higher values than the avg. FT in

the case of BO. At 70 °C, the avg. FT value was reduced to 0.862 Kg-m from 1.66 Kg-m (48.75% reduction). A trend of increase in the FT values with increasing concentration of the RTS particles was seen at 70 °C as well. The lowering of the FT values is attributed to the well-dispersed RTS particles at 0.1wt.% RTS addition. The higher concentrations of RTS particles in BO lowered the viscosity, which caused the oil to fail to lubricate the rubbing surfaces effectively. The increase in FT is plausibly the combined effect of reduced viscosity and agglomerated RTS nanoparticles creating higher friction at the sliding interface.

Table 3. Calcul	lated avg. FT	values from	the 4-ball	wear tests.
1				

	At RT		At 70 °C	
Sample	Avg. FT	Std. Dev.	Avg. FT	Std. Dev.
	(Kg-m)		(Kg-m)	
Base Oil (BO)	1.185	0.00948	1.665	0.00878
0.1 wt.% RTS in BO	1.092	0.00964	0.862	0.01208
0.3 wt.% RTS in BO	1.288	0.00696	0.991	0.00576
0.5 wt.% RTS in BO	1.317	0.00355	1.100	0.00699

From Fig. 15 and Fig. 16, it is evident that the 0.1 wt.% RTS dispersed BO gives a consistently reducing FT profile with the lowest FT values. From the FT profile observations, it is plausible that the BO at RT can form an intermediate film, which it fails to do at 70 °C. In the case of 0.3 wt.% and 0.5 wt.% RTS addition to BO, the uniform barrier could not be formed between the surfaces. Instead, additional resistance to the surfaces' smooth motion is generated at RT and 70 °C. However, with 0.1 wt.%, a stable barrier seems to have formed repetitively after every ~500 - 600 sec at RT and 70 °C, reducing the FT value. 0.1 wt.% RTS addition formed the most effective tribo-film at both RT and 70 °C, reflected in the smooth and consistently lowering FT profiles along with the lowest FT values. 0.3 wt.% and 0.5 wt.% RTS addition might have resulted in agglomeration of the particles at both RT and 70 °C.

Fig. 17 shows the avg. wear scar diameter (WSD) values recorded on the wear-testing balls (three stationary balls and the top ball) after the testing at RT. In the case of BO, an avg. WSD of 1288.66 μm was recorded on the test specimens, as shown in Fig. 17 (sample A), and the lowest avg. WSD of 1075.33 μm was recorded in the case of 0.1 wt.% RTS dispersed BO. The WSD values are lower and consistent in the case of specimens lubricated using 0.1 wt.% RTS dispersed BO, indicating that 0.1 wt.% RTS addition is optimal. In the case of 0.3 wt.% and 0.5 wt.% of RTS additions in BO, an excess number of RTS nanoparticles in the dispersion

might have resulted in agglomeration, poor lubrication, increased wear, and higher WSD values. Even more, than adequate nanoparticles in the dispersion agglomeration and formation of third body wear-causing particles could result in higher WSD values.

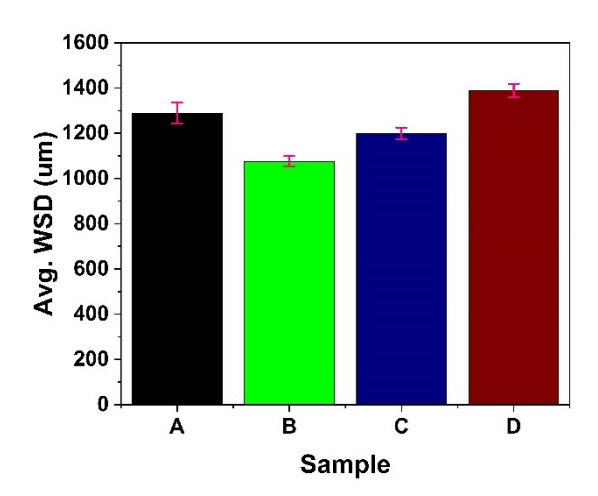


Figure 17. Avg. WSD values at RT. A, B, C, and D represent samples tested using BO, 0.1 wt.%, 0.3 wt.%, and 0.5 wt.% of RTS in BO, respectively.

The wear debris formed after the surface asperities plastically deformed and broke off, leading to abrasive wear on the surface. The extensive wear scars observed on the worn surfaces are shown in Fig. 18 (a) implies that the BO at RT could not prevent the surfaces from wearing as it fails to form a protective tribological film to keep them apart. The addition of the 0.1 wt.% RTS to the BO reduces the wear scar and the wear intensity, which is affirmed by the wear scar images shown in Fig. 18 (b). Detailed observation of the wear scars reveals that a distinct reduction of the wear track size is visible after adding 0.1 wt.% of RTS in the BO. When the concentration of RTS is increased to 0.3 wt.% and 0.5 wt.%, it is found that the wear scar starts increasing, which implies that the agglomerated RTS nanoparticles at higher concentrations can act like abrasive bodies and hence are undesirable, which can be seen from Figs. 18 (c) and (d). The avg. WSD values are reduced by 16.55% and 6.93% with 0.1 wt.% and 0.3 wt.% of RTS in BO, respectively, while the addition of 0.5 wt.% RTS in BO led to an increase of 7.70% in the WSD. This confirms the excellent ability of the RTS nanoparticles to reduce wear and friction when added to a lubricating oil in optimized quantity.

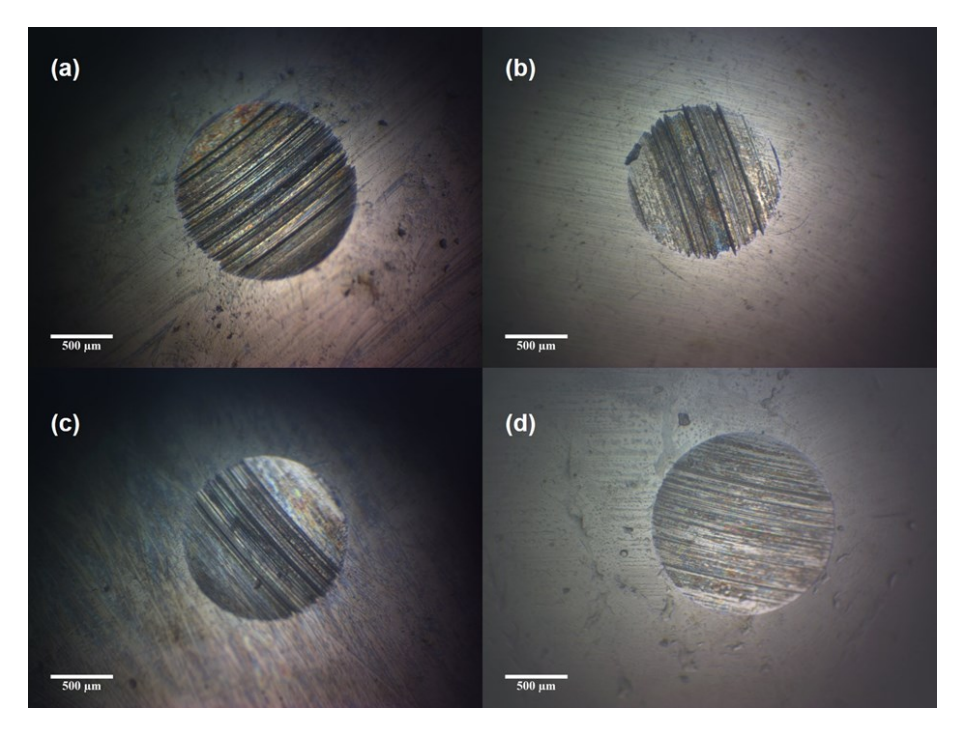


Figure 18. Wear scar images on the ball specimens tested at RT with (a) BO (b) 0.1 wt.% RTS added BO (c) 0.3 wt.% RTS added BO, and (d) 0.5 wt.% RTS added BO. The length of the scale bar in all images is 500 µm.

In the case of RTS dispersed oil samples, it is observed that the area of abrasive wear is reduced (Figs. 18 (b), (c), and (d)), implying a reduced contact area between the ball-to-ball surfaces. The lower concentration, i.e., 0.1 wt.% RTS addition minimizes the intensity of wear, but the higher concentrations, i.e., 0.3 wt. % and 0.5 wt.% RTS additions in BO show an increase in the WSD and the intensity of wear (Figs. 18 (c) and (d)). Similar wear tracks were reported on adding carbon soot (CS) in Castrol 20W40 motor oil [9], while it was observed that adding 1 wt.% CS caused an increase in wear [15]. Lower wear rate and coefficient of friction (CoF) were found when polyetheretherketone was lubricated using hybrid oil containing CS [16]. In another work, wear volume and wear scar reduction were reported, and adsorption of CS on weak tracks was also confirmed [17]. Superior reductions in WSD values were obtained on laser-textured surfaces using PAO4 oil loaded with CS particles derived from diesel compared to reductions only due to texturing [18], which emphasizes that lubricant additives play an essential role in wear resistance irrespective of the surface enhancements. Like in other reported works, mild traces of oxidative wear (Fig. 18) were also observed in the present study. During the rubbing of metals over each other, high contact stresses are generated at the interface, causing a rapid rise in local temperature, possibly leading to oxidation of the contact surfaces.

Fig. 19 shows the WSD values recorded on the wear-testing balls (three stationary and the top balls) after the testing at 70 (C). An avg. WSD value of 1668 μm was observed on the ball specimens tested with BO at 70 °C), which is higher than the avg. WSD at RT, indicating BO's inefficiency in effectively lubricating the sliding surfaces at a higher temperature. The lowest avg. WSD is recorded for the ball specimens tested using 0.1 wt.% RTS in BO followed by the values recorded in the case of 0.3 wt.% and 0.5 wt.% of RTS in BO. An avg. reduction of 28.12% was achieved with the 0.1 wt.% of RTS in BO, followed by a reduction of 23.65% and 20.49% using the concentrations of 0.3 wt.% and 0.5 wt.% RTS in BO, respectively. At RT, the 0.5 wt.% RTS added BO sample performed worse than the BO w.r.t wear resistance. Even though at 70 °C 0.3 wt.% and 0.5 wt.% RTS in BO samples showed higher WSD than 0.1 wt.% RTS in BO still outperforms the BO, which is attributed to the presence of RTS nanoparticles in the lubricant. The increase in avg. WSD and avg. FT in the case of these samples is plausibly due to the combined effect of lower viscosity and agglomeration of RTS nanoparticles. However, this poor performance has to be further explored.

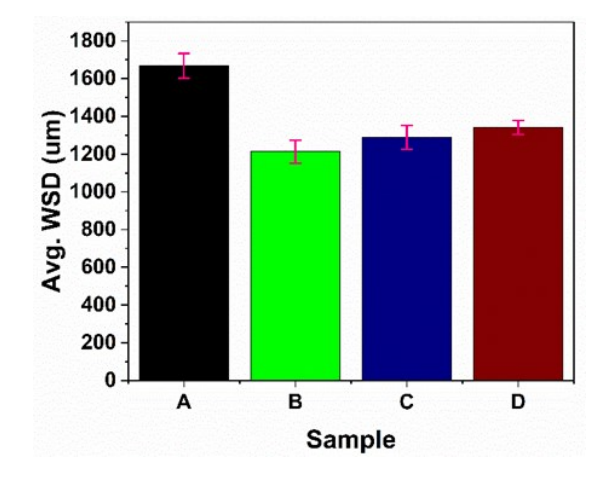


Figure 19. Avg. WSD values at 70 °C. A, B, C, and D represent BO, 0.1 wt.%, 0.3 wt.%, and 0.5 wt.% of RTS in BO, respectively.

From the above observations, it can be stated with high confidence that 0.1 wt.% of RTS is the threshold limit for RTS dispersion in the considered BO. This value will change as the lubricating medium changes. Adding the RTS nanoparticles above this concentration will lead to unwanted agglomeration, causing lump formation and faster sedimentation of the additives. Also, as discussed w.r.t. Figs. 13 and 14, excess particles make the BO lose its viscosity, making it unsuitable for applications.

The wear scar images of the surfaces of the balls tested with the lubricant samples at 70 °C are shown in Fig. 20. On careful observation, the wear pattern and WSD in the case of samples

lubricated using BO and 0.1 wt.% RTS added BO (Figs. 20 (a) and (b)) indicate extreme abrasive wear in the former case while minimal damage due to wear in the latter case. The wear scar on the specimens in the case of 0.1 wt.% RTS in BO is representative of significantly less abrasive wear than the mildly worn-out scars in the case of 0.3 wt.% and 0.5 wt.% RTS in BO (Figs. 20 (c) and (d)). From the observations, it can be stated that the optimized concentrations of the RTS enabled the particles to get adsorbed on the contacting surfaces and formed a protective layer preventing direct metal-to-metal contact for the majority of the time during the test. These wear tracks are similar to those shown in Fig. 18. This establishes the hypothesis that the RTS nanoparticles reduce wear when added in adequate concentration to the BO.

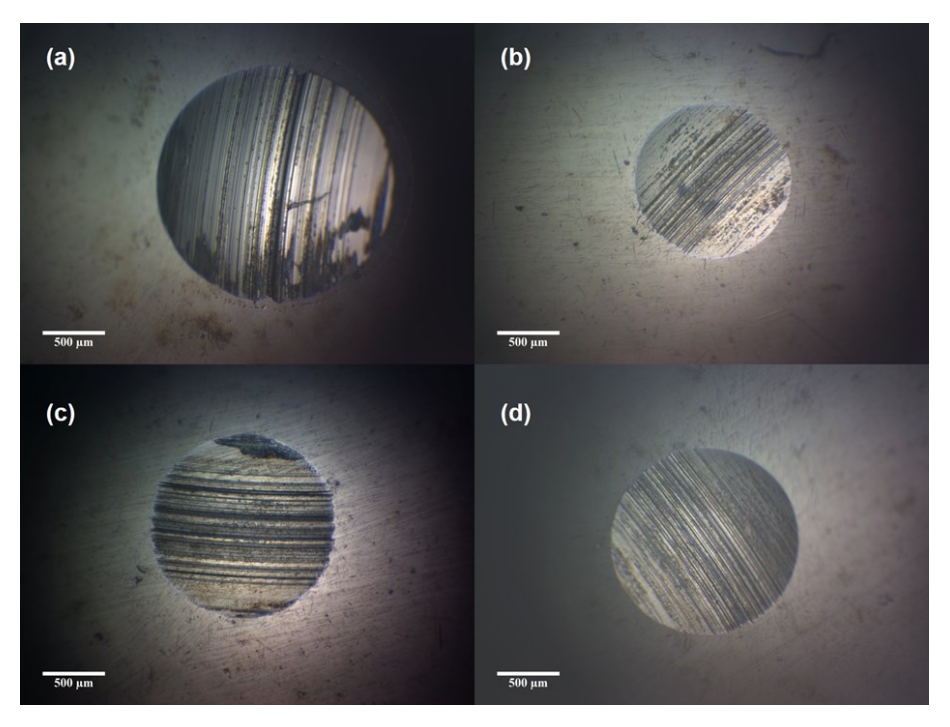


Figure 20. Wear scar images on the ball specimens tested at 70 °C with (a) BO, (b) 0.1 wt.% RTS added BO (c) 0.3 wt.% RTS added BO, and (d) 0.5 wt.% RTS added BO. The length of the scale bar in all images is 500 μm.

Fig. 21 shows all lubrication cases' calculated avg. CoF values at RT and 70 °C. At RT, for the 0.1 wt. % RTS addition case, the CoF value is the lowest. This observation again shows that 0.1 wt.% RTS addition is optimal. At this concentration, the viscosity and the shear stress are not lowered too much, facilitating the formation of a uniform tribo-layer between the rubbing surfaces lowering CoF, FT, and wear. At the higher concentrations (i.e., 0.3 wt.% and 0.5 wt.% RTS additions in BO), the BO's rheological properties (viscosity and shear stress) are drastically changed. A uniform tribo-layer is not formed between the rubbing surfaces,

increasing the resistance between the rotating ball surfaces during the test leading to a higher CoF value. Drastically, reduction in viscosity increases the flowability of the lubricant in between the rubbing surfaces and does not allow the formation of a uniform tribo-layer as the lubricant quickly shears off. However, the presence of RTS nanoparticles at optimal concentration helps maintain a lower CoF value. At the same time, in this case, the agglomeration of the RTS nanoparticles resulted in poor tribological characteristics. The CoF values recorded at 70 °C displayed a similar trend to those recorded at RT. However, at 70 °C, as the lubricants undergo thinning due to the increased temperature, slightly higher CoF values are observed for the lubricant samples. Similar trends in tribological performance were reported in the case of adding 0.3 wt.% and 0.5 wt.% of CS nanoparticles in Castrol 20W-40 oil [9] and 5W30 multigrade oil [17], respectively. At RT, CoF was reduced by ~9% for samples subjected to tribological test using 0.1 wt.% of RTS in BO, and at 70 °C, a fall in CoF by 48.93% was observed for the same concentration of the RTS nanoparticles. Further increase in RTS concentration in BO led to the rise in the CoF, which is attributed to the drastically lowered viscosity and agglomeration of the nanoparticles (due to high concentration) between the rubbing surfaces.

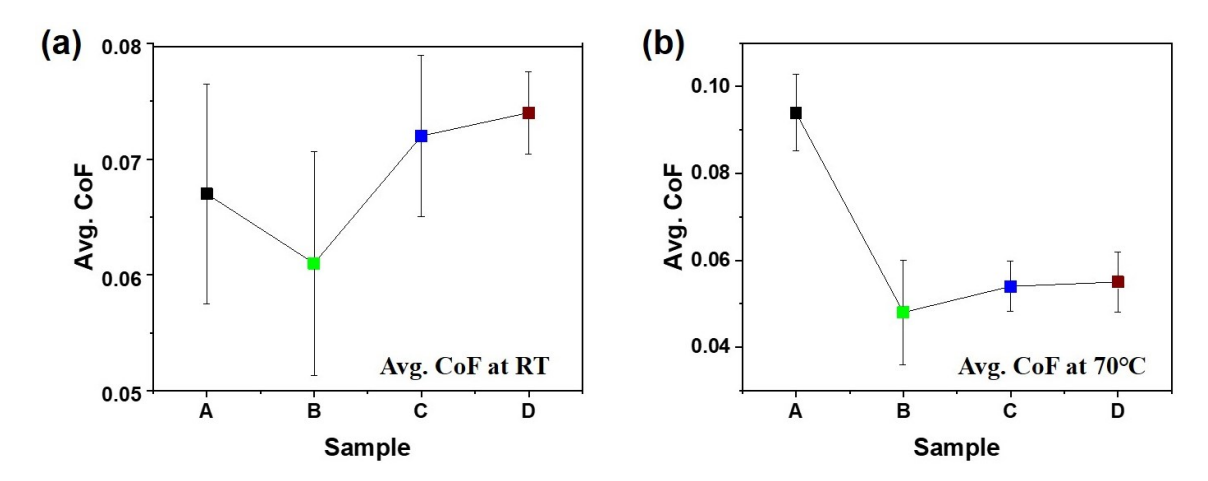


Figure 21. Avg. CoF values (a) at RT and (b) at 70 °C.

Each CS particle has concentric spherical graphene sheets. This arrangement gives rise to weak interaction with the materials CS adheres to because only π electrons exist on the surface, causing weak intermolecular bonding [19]. Also, the CS nanoparticles have a high elastic modulus of 16.5 GPa and hardness of 1.2 GPa [20]. It has been observed that the structure of CS nanoparticles wasn't destroyed during the running-in of friction tests, along with the presence of lamellar structures of carbon after the test confirming the breaking of CS nanoparticles [5]. The spherical CS nanoparticles provide a roller effect at the interface of the

contacting surfaces where the particles support the surfaces, converting sliding friction into rolling friction during the test, which lowers the CoF. Also, the small sizes of the CS nanoparticles ease their entry into the surface asperities of contacting surfaces, creating a filling and repairing action under applied load [15]. In the present study, spheroidal RTS nanoparticles have characteristics similar to typical CS nanoparticles reported earlier. When present in an adequate concentration, the nanoparticles act like nano-bearings, giving a rolling effect on the two rubbing surfaces. This mechanism (schematically shown in Fig. 22) helps to reduce the direct contact of the asperities. It prevents debris particles from entering the contact area, minimizing the surfaces' abrasive wears.

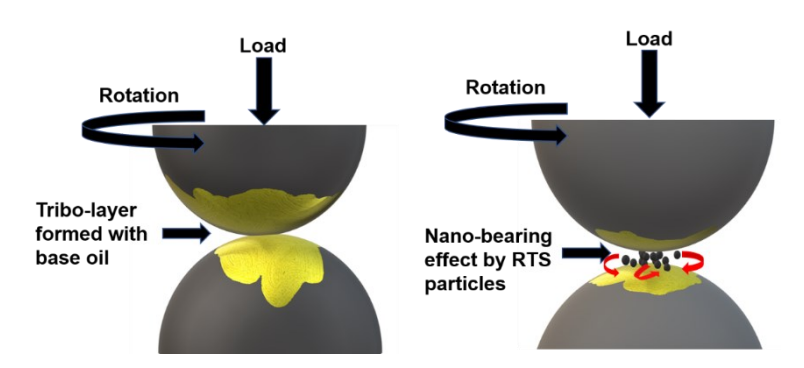


Figure 22. Schematic of nano-ball bearing lubricating mechanism by RTS particles.

Also, the spheroidal RTS particles get adsorbed on the surfaces and act as soft additives unless agglomerated because of the graphitic layers' presence and amorphous nature. The RTS nanoparticles absorb the load. Therefore, the high stresses generated at the point of contact between the balls are quickly dissipated from the surface, delaying wear initiation on the surfaces. The BO forms a tribo-layer at the interface of rubbing surfaces but fails to minimize the contact between the surfaces, resulting in higher WSD. However, RTS nanoparticles added to BO become more effective as a lubricant additive because the spheroidal nanoparticles can reduce the contact area between the two rubbing surfaces, leading to lower WSD values. Herein, this rolling effect is more prominent at 0.1 wt.% RTS addition in BO. To understand the impact of RTS particles on the wear scars, detailed SEM imaging of the wounds (in the case of 0.1 wt.% RTS in BO and BO) was performed, as shown in Fig. 23. Upon careful observation, Fig. 23 shows an intensely worn-out surface with abrasive wear characteristics. Numerous abrasion lines can be seen on the scar of the ball tested with BO, indicating BO's inefficiency as an AW lubricant. The wear scars on the balls tested with 0.1 wt.% RTS in BO show reduced intensity of the abrasive wear, as seen in Fig. 20 (b). The frequency of the abrasion lines is lower, which affirms that the RTS particles in optimized concentrations reduce the direct surface-to-surface contact and lower the friction by assisting in the easy sliding of surfaces in relative motion. The wear scars are studied for the surface's protective layer (tribolayer) formation after the test. It is hypothesized that the RTS nanoparticles that are adsorbed on the balls' surfaces, act like nano-bearings, and produce a rolling effect, eventually reducing friction and wear. To confirm this, Raman spectroscopy was carried out on the wear scars. The Raman spectrum in Fig. 24 corresponds to the use of 0.1 wt.% RTS in BO as the lubricant. It shows distinct D and G bands, indicating the presence of RTS nanoparticles on the scar. Also, the Raman spectrum resembles that of RTS nanoparticles as shown in Fig. 11. The distinct D and G bands are not observed in the BO case. The Raman observations confirm the presence of the RTS nanoparticles on the wear scars of the balls tested using the RTS in BO lubricant, supporting the hypothesis related to the rolling effect mechanism and that the RTS nanoparticles in optimized concentrations act as AW and AF additives in a lubricating medium.

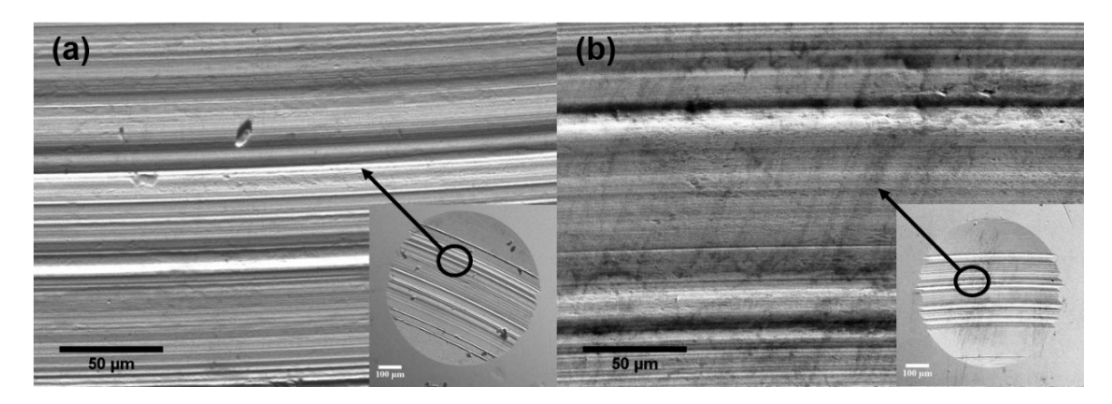


Figure 23. SEM micrographs of wear scars on the balls tested with (a) BO and (b) 0.1 wt.% RTS in BO. Insets in (a) and (b) are the corresponding lower magnification (length of scale $bar = 100 \mu m$) images of wear scars.

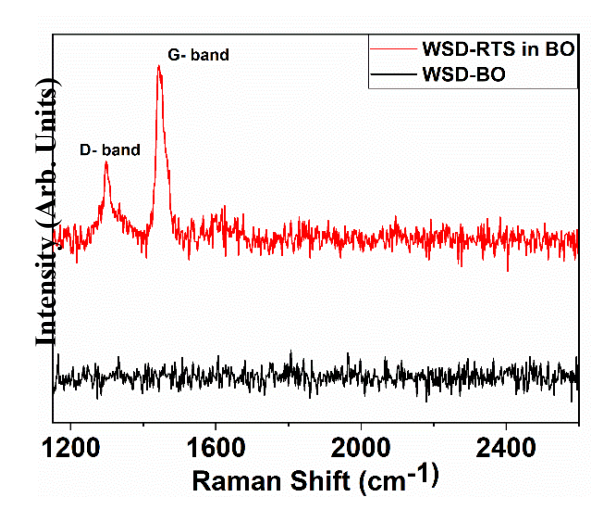


Figure 24. Raman spectra were recorded on the wear scars on the balls, which were tested with BO and 0.1 wt.% RTS in BO.

4.2 0D TPW and OLC Particles as Additives in Lubricants

FESEM images of TPW (Fig. 25 (a)) and OLC (Fig. 25 (b)) indicated similar morphologies, while the respective HRTEM images (Fig. 25 (c) and 25 (d)) indicated distinct morphologies. HRTEM images of TPW (Fig. 25 (c)) and OLC (Fig. 25 (d)) showed they are nanosized. However, the TPW particles are slightly bigger than those of OLC. Further, TPW particles have a highly disordered structure; therefore, no lattice planes are discernible in Fig. 25 (c). It is well known that at temperatures above 2000 °C, carbon atoms from the inside of the amorphous spherical particles (here TPW particles) vaporize, diffuse, and rearrange themselves into graphene-like fragments (having non-six-fold rings) within the structure, leading to the formation of concentric ring-like arrangement of graphene layers [21-24] as in OLC shown in Fig. 25 (d). The interplanar spacing measured in Fig. 25 (d) is ~0.34 nm, indicating that graphene-like layers constituted OLC. The XRD patterns of TPW and OLC are shown in Fig. 26 (a), which distinctly shows the effect of the heat treatment process. Heat treatment of TPW at 2200 °C has resulted in the appearance of a prominent (002) graphitic peak and a broad (004) graphitic peak [25] in the case of OLC. Also, the emergence of (101) hexagonal graphitic peaks in the case of OLC indicates excellent graphitization [25]. The heat treatment also helped remove the impurities (except Ca) while TPW was converted into OLC.

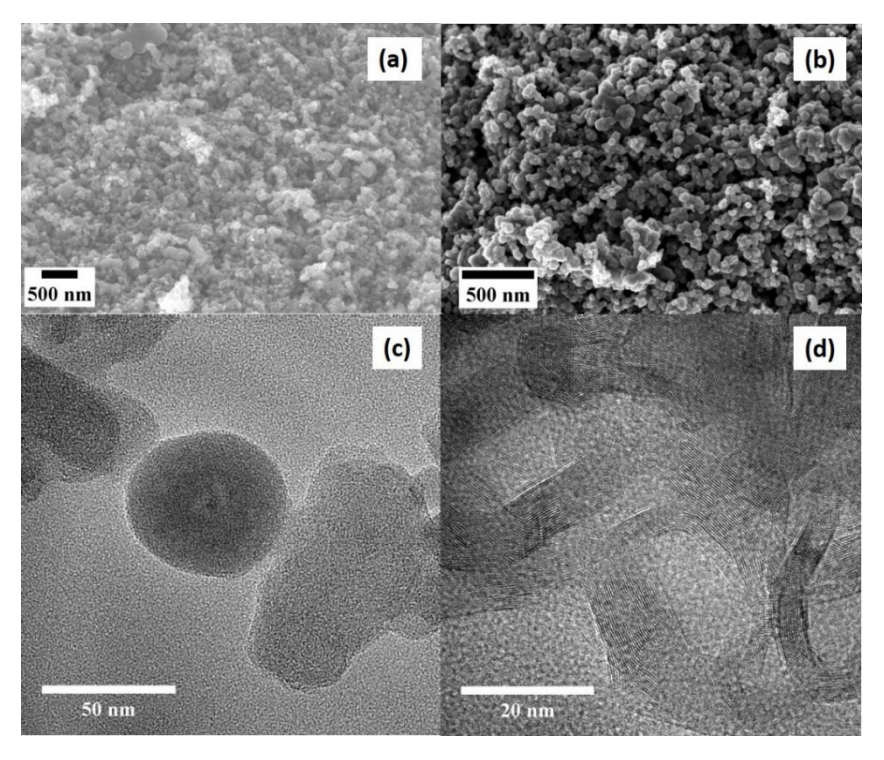


Figure 25. (a) and (b) FESEM images of TPW and OLC particles, respectively; (c) and (d) HRTEM images of TPW and OLC particles, respectively.

Apart from the improved degree of graphitization, the heat treatment also helped remove the impurities (except Ca) while TPW was converted into OLC. The presence of different impurities in TPW is shown in Fig. 26 (a). No distinct (002) graphitic peak or other relevant carbon diffraction peaks are seen in TPW's diffraction pattern (Fig. 26 (a)), indicating that the carbon in TPW is highly disordered. In OLC's case, the diffraction peaks are indexed to (100), (103), (014), and (110) crystallographic planes in graphitic carbon (Fig. 26 (a)). The interplanar spacing (d-spacing) in OLC calculated by considering the (002) graphitic peak is ~0.349 nm, which correlates very well with the HRTEM observation in this context. The broadening of (002) and (004) graphitic peaks in the case of OLC is attributed to the combination of local distortion in graphitic planes and small particle size (here, in the range of 30-70 nm) [26].

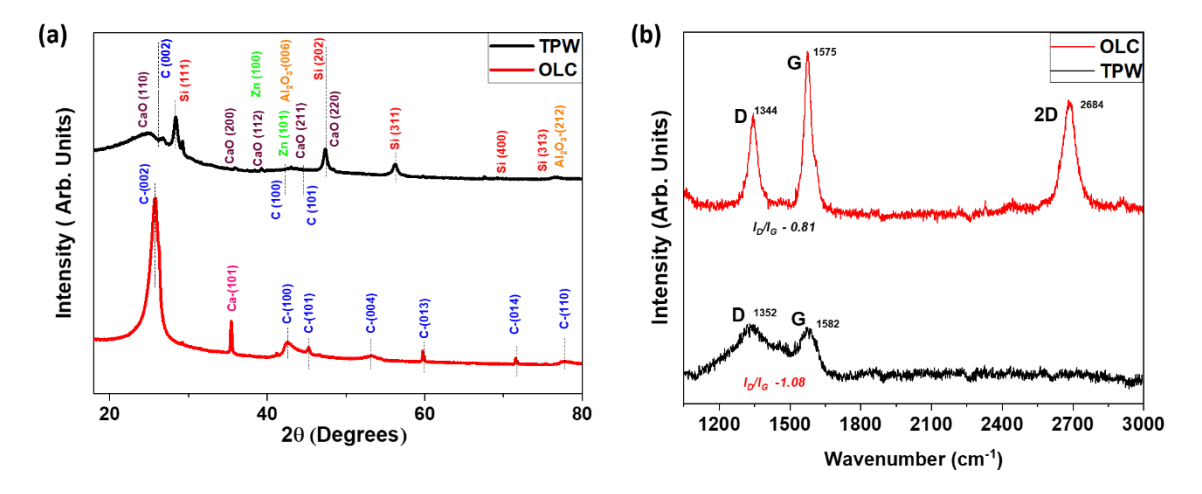


Figure 26. (a) XRD patterns and (b) Raman spectra of TPW and OLC samples.

From EDXA, the elemental compositions (atomic %) of TPW and OLC are found to be 93.4% C, 5.3% O₂, 0.1% Al, 0.4% Si, 0.4% S, 0.1% Ca, and 0.3% Zn and 99.9% C and 0.1% Ca, respectively. All impurities (except trace amounts of Ca) were removed during the heat treatment of TPW at 2200 °C because at this temperature, S, Al, Al₂O₃, Zn, and Si vaporize and escape. Calcium oxide may also have evaporated if TPW was heat treated above 2500 °C. Observations made through EDXA were well complemented by the XRD observations. The Raman spectra of TPW and OLC are shown in Fig. 26 (b). In the case of TPW, the signature Raman bands, namely, the disordered (D) carbon band at ~1352 cm⁻¹ and the graphitic (G) band at ~1582 cm⁻¹, are observed. The D band's intensity ratio to that of the G band was measured as 1.08, indicating the poor graphitic nature of TPW [8,25,27]. On the other hand, in the case of OLC, in addition to the D band at 1344 cm⁻¹ and the G band at 1575 cm⁻¹, another prominent band, namely the 2D band (overtone of D band) at 2684 cm⁻¹, is observed. The 2D band's appearance indicates the presence of graphene layers in OLC particles [8, 27, 28]. The

slight asymmetry of the 2D band suggests that the OLC particles are constituted by multiple graphene layers, complementing well with the HRTEM observations (Fig. 25 (d)). In the case of OLC, the D band's intensity ratio to that of the G band was measured as 0.81, indicating enhanced graphitization [8,25,27,28] attributed to the heat treatment.

The thermal degradation of TPW and OLC are shown in Fig. 27. The TPW showed a mass loss of 17.56%, while the OLC showed a mass loss of 4.22%. OLC's higher and better thermal stability is attributed to its enhanced crystallinity and graphitic nature [29], as revealed by HRTEM, XRD, and Raman scattering studies. In the case of TPW, the low on-set degradation temperature is due to its oxidation, which is attributed to its high structural disorder [29], as revealed by HRTEM, XRD, and Raman scattering studies. On the other hand, the improved degree of graphitization helps (because it requires higher temperatures to react with oxygen) delay the thermal degradation of OLC [29].

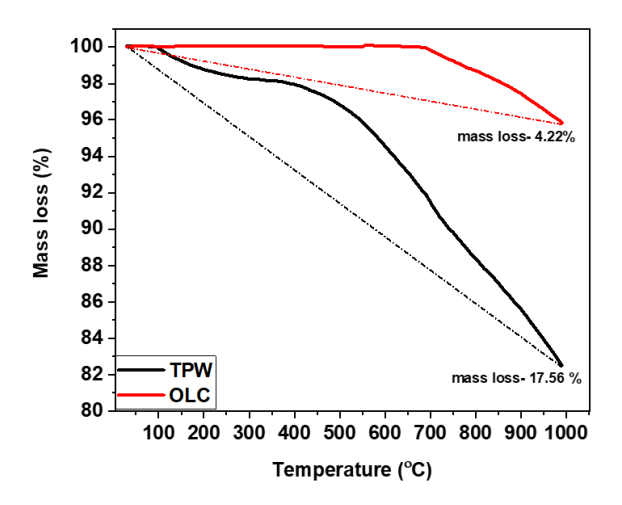


Figure 27. Thermal degradation profiles of TPW and OLC.

BO's rheological properties (viscosity and shear stress) and the dispersions of TPW and OLC in BO are shown in Fig. 28 and 29, respectively. The viscosity (Fig. 28 (a)) and shear stress (τ) (Fig. 28 (b)) profiles of the TPW dispersed BO samples are compared with that of the BO. The BO's viscosity increases to 150 cP at a shear rate of 53 sec⁻¹ and remains almost constant throughout the test period, with the shear rate increasing to 1000 sec⁻¹. The 0.1 wt.% TPW dispersed BO shows a viscosity of 74.16 cP at a shear rate of 107 sec⁻¹ and further increases to 94.02 cP (at a shear rate of 338.15 sec⁻¹) and then stabilizes at this value till the end of the test. The 0.3 wt.% TPW dispersed BO shows a slight increase in the viscosity (101.6 cP) compared to the preceding concentration with a similar viscosity curve. The 0.5 wt.% TPW dispersed BO was found to have the lowest viscosity of 80.97 cP. All in all, it is observed that BO's viscosity is reduced due to the dispersion of TPW particles.

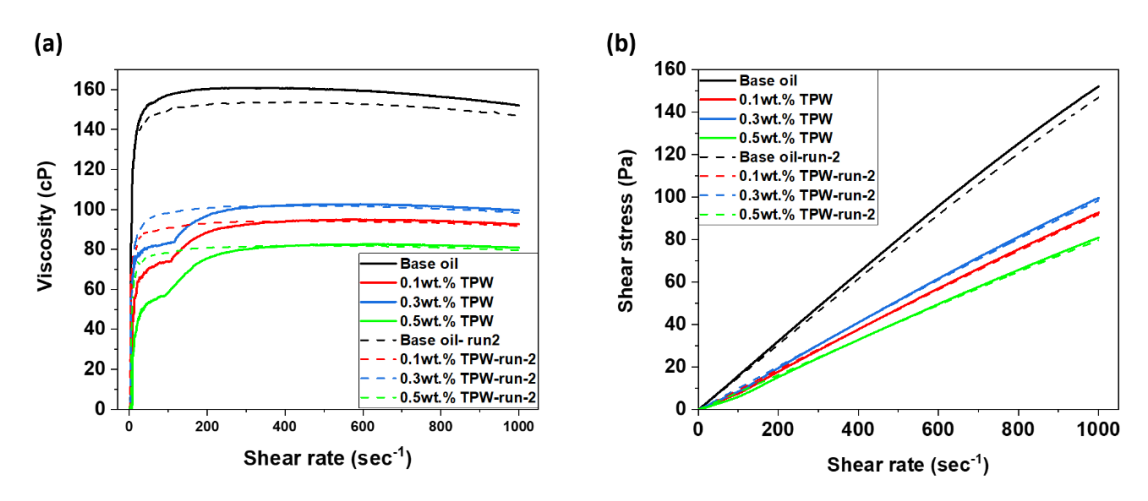


Figure 28. Effect of TPW dispersion on BO's (a) viscosity and (b) shear stress.

The shear stress (τ) profiles of the BO and the TPW dispersed BO shown in Fig. 28 (b) indicate that all the samples exhibit Newtonian behavior. The BO has a τ of 152.065 Pa at 1000 sec⁻¹ while the 0.1 wt.% TPW dispersed BO has a lower τ of 92.658 Pa, while 0.5 wt.% TPW dispersed BO has the lowest τ of 79.678 Pa. The dispersion of TPW particles in BO lowers the τ drastically, resulting in lower internal resistance between the fluid layers under the applied shear rate and thus correlates well with the reduced viscosity due to the dispersion of TPW, as shown in Fig. 28 (a). The viscosity (Fig. 29 (a)) and shear stress (τ) (Fig. 29 (b)) profiles of the OLC dispersed BO samples are compared with that of the BO. Similar to the effect of TPW dispersion in BO on the reduction in viscosity, a general trend of viscosity reduction was also observed in the case of OLC dispersion in BO. However, the decrease was drastic (> 50%) in the case of 0.3 wt.% and 0.5 wt.% OLC dispersions in BO. The slight increase in viscosity (however, still much lower than BO's) during the second run of these samples is attributed to slight sedimentation, which signifies the role of the dispersion of OLC in BO in reducing the viscosity. The OLC dispersions' τ values are lower than that of BO. However, the reduction was drastic (> 50%) in the case of 0.3 wt.% and 0.5 wt.% OLC dispersions in BO.

Although the viscosity data deviate from the standard rheological models, which predict the viscosity behaviour of fluids with the dispersion of solid particles, similar trends were reported in other studies in which various nanoparticles were dispersed in oils [10-12, 30]. Such a deviation is attributed to nanoscale effects, which lead to defiance of the hydrodynamic effect on the viscosity as predicted by the Einstein model; on the contrary, the nanoscale effects induce a change in the dispersing medium's conformation and free volume, resulting in a non-Einstein-like decrease of viscosity [13]. The nanoparticles (the nanosized TPW and OLC particles) interact with the oil molecules and reasonably decrease the cohesive attraction forces between fluid layers of BO, resulting in lowered resistance to flow under the applied shear rate.

Further understanding and explaining the peculiar trend of BO's viscosity reduction with the dispersion of TPW and OLC in different concentrations requires in-depth studies aided by simulations and analytical tools.

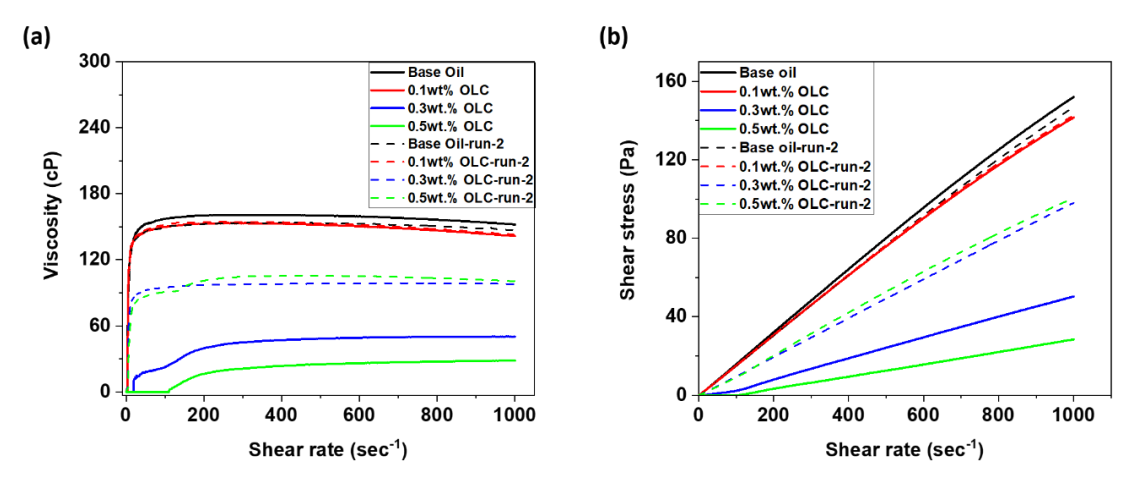


Figure 29. Effect of OLC dispersion on BO's (a) viscosity and (b) shear stress.

The CoF values versus testing time recorded at room temperature are shown in Fig. 30 for BO and the dispersions of TPW and OLC in BO. The initial CoF at the interface of specimens lubricated using BO and TPW dispersed BO samples at 50 sec is ~0.75. However, BO showed a reduced CoF value of ~0.055 at the end of the test (i.e., at 3600 sec). Approximately similar values were recorded when TPW-dispersed BO samples were used in the test. A similar reducing trend of CoF values was recorded when OLC-dispersed BO samples were used in the test. However, 0.3 wt.% of OLC in BO helped reduce CoF at room temperature (Fig. 30 (b)). In contrast, the highest concentration, i.e., 0.5 wt.% of OLC in BO, resulted in a substantial rise in the CoF values falling in the range 0.08-0.09 attributed to the agglomeration of the OLC particles in the dispersion, which is also reflected in the rheological properties shown in Fig. 29. The avg. CoF values at room temperature are shown in Fig. 31 for BO and the dispersions of TPW and OLC in BO. Fig. 31 shows only nominal changes in the avg. CoF values in the case of different dispersions of TPW and OLC in BO.

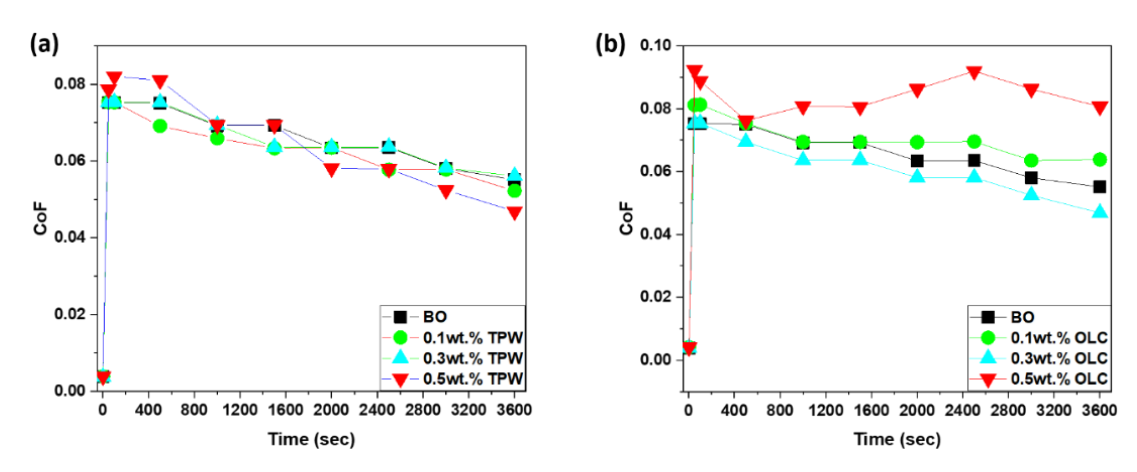


Figure 30. CoF versus time when (a) BO and TPW dispersed BO samples and (b) BO and OLC dispersed BO samples are used in the test at room temperature.

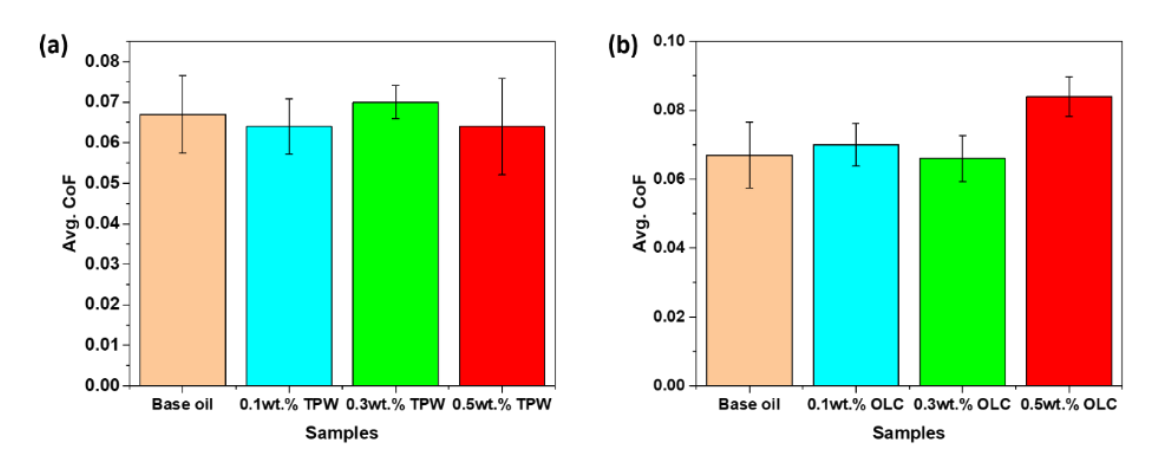


Figure 31. Avg. CoF values when (a) BO and TPW dispersed BO samples and (b) BO and OLC dispersed BO samples are used in the test at room temperature.

Further, the CoF values versus testing time recorded at 75 °C is shown in Fig. 32. At 75 °C when BO was used in the testing, it resulted in a CoF value of 0.07, which eventually increased to 0.10 close to 1200 sec and remained close to 0.09 towards the end of the test. There was a reduction in the CoF values when the TPW dispersed BO samples (except for 0.5 wt.% TPW dispersed BO sample) were used in the testing. On the contrary, all the OLC dispersed BO samples resulted in considerably reduced CoF values with testing time compared to the CoF values recorded when BO was used for testing at 75 °C (Fig. 32 (b)). The avg. CoF values at 75 °C is shown in Fig. 33 for BO and the dispersions of TPW and OLC in BO. The avg. CoF values at 75 °C clearly show that TPW and OLC dispersed BO samples help achieve significant AF properties compared to BO, affirming that TPW and OLC play a significant role as AF additives in lubricants.

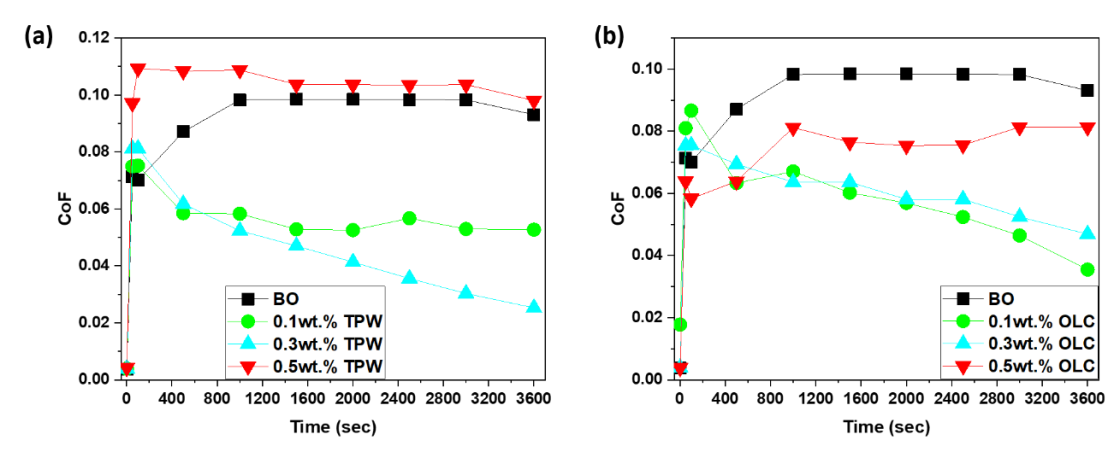


Figure 32. CoF versus time when (a) BO and TPW dispersed BO samples and (b) BO and OLC dispersed BO samples are used in the test at 75 °C.

The measured CoF values show that TPW, when used in excess concentration (above 0.3 wt.% in Group 2 N500), significantly increases the CoF. However, OLC at an equivalent concentration maintains the CoF at a lower value than that of samples lubricated with BO. The reduced CoF values recorded when TPW-dispersed BO samples are used in testing are attributed to the uniform dispersion of TPW in the BO, facilitating smooth sliding of the surfaces even after a reduction in the viscosity of BO after TPW dispersions. However, when used in high concentration (above 0.3 wt.%), the dispersed BO shows further reduction in viscosity, and the TPW particles start to agglomerate, causing friction between the rubbing surfaces and failing to help better the lubrication. Similarly, the OLC dispersed BO samples helped reduce the CoF values substantially, and even at a higher concentration (0.5 wt.% of OLC), low CoF values were recorded, unlike in the case of 0.5 wt.% TPW dispersed BO attributed to the heliocentric graphene-like layers in OLC particles facilitating enhanced smooth sliding of the surfaces.

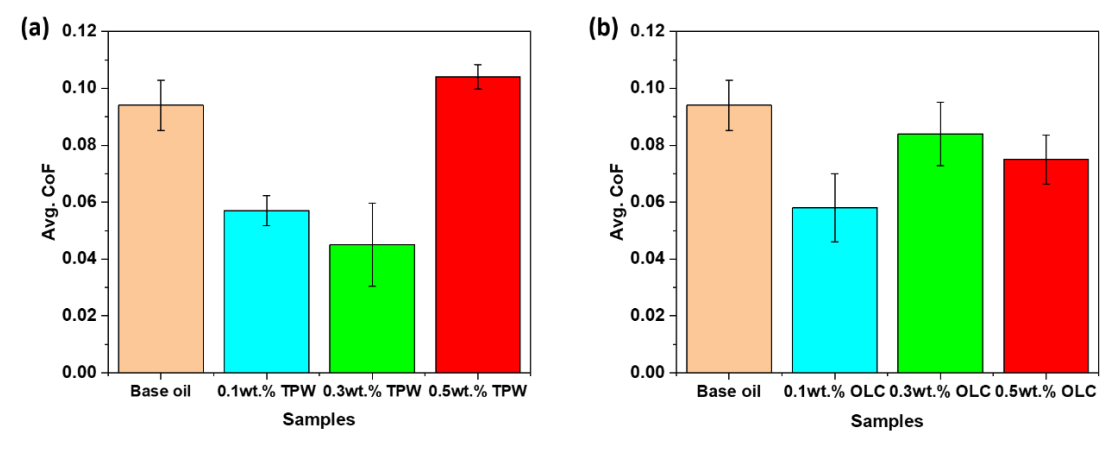


Figure. 33. Avg. CoF values when (a) BO and TPW dispersed BO samples and (b) BO and OLC dispersed BO samples are used in the test at 75 °C.

Table 4 compares the lowest CoF values reported using OLC and carbon soot as additives in lubricating oils. Computer simulations and experiments on OLC as lubricant additives revealed a synergistic rolling-sliding of these nanoparticles as the leading cause of adequate lubrication [31]. Using OLC and carbon soot as additives in lubricating oils has also reduced wear, a discussion on which is presented in the following paragraphs.

Source of carbon soot or OLC	Medium	CoF
Nanodiamonds	PAO	0.08 [32], 0.06 [31] and 0.03 [33]
CH_4+O_2	SN150	0.03 [34]
Commercial carbon black	CD SAE 15W40	0.05 [35]
Candle soot	H ₂ O	0.2 [2]
Tyre-tube soot	G2 N500	0.04 [30]
TPW	G2 N500	0.035 (This study)

Table 4. CoF values result from using carbon soot and OLC as additives in lubricants.

TPW and OLC dispersed BO and BO samples were used as lubricants to test the wear resistance properties. The avg. WSD and avg. vertical displacement (h) [36] in mm of the tested ball specimens at room temperature and 75 °C are shown in Fig. 34 and 35, respectively. The avg. WSD and h values recorded when TPW and OLC dispersed BO and BO samples are used as lubricants during the wear tests at room temperature, and 75 °C are shown in Fig. 34 and 35, respectively. The use of 0.1 wt.% and 0.3 wt.% TPW dispersed BO samples as lubricants resulted in WSD reduction of 9.95% and 13.03%, respectively, while 0.1 wt.% and 0.3 wt.% OLC dispersed BO samples resulted in a WSD reduction of 8.08% and 4%, respectively. On the contrary, 0.5 wt.% TPW and OLC dispersed BO samples resulted in an 18.52% and 19.47% increase in WSD values (significantly high) attributed to the agglomeration of the additives in BO. In all lubricant cases, h values showed a similar trend to WSD values.

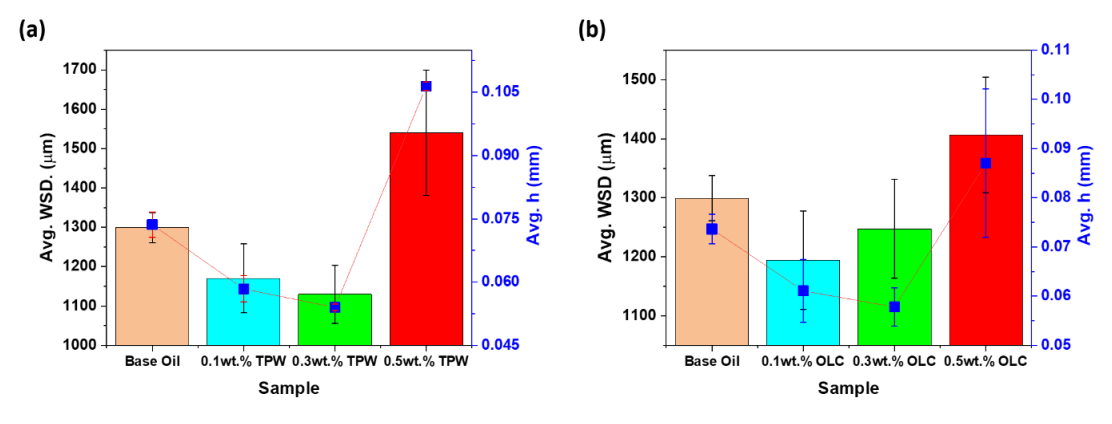


Figure 34. Avg. WSD and h values when (a) BO and TPW dispersed BO samples and (b) BO and OLC dispersed BO samples are used as lubricants in the wear test at room temperature.

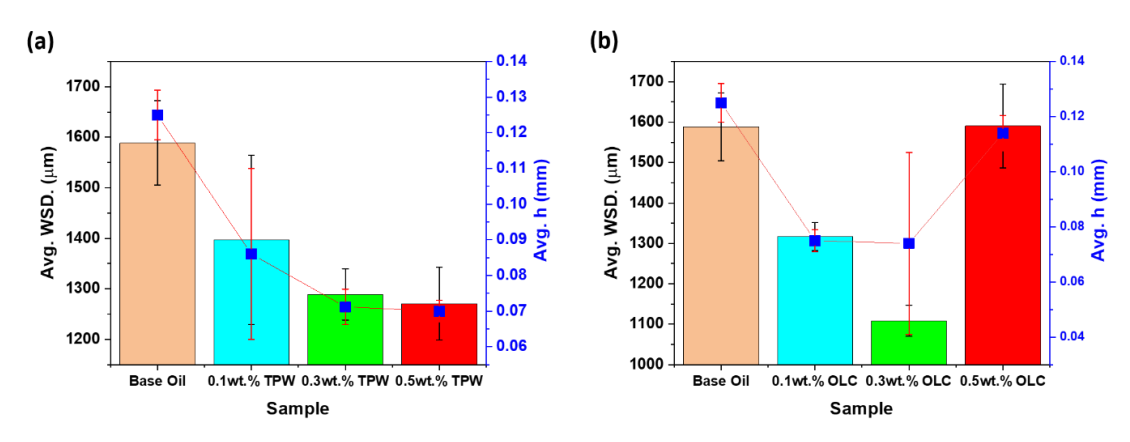


Figure 35. Avg. WSD and h values when (a) BO and TPW dispersed BO samples and (b) BO and OLC dispersed BO samples are used as lubricants in the wear test at 75 °C.

At 75 °C, TPW and OLC dispersed BO samples, when used as lubricants, helped lower the avg. WSD and h values except for 0.5 wt.% OLC dispersed BO sample (Fig. 35), which gave an aberrant result. With these observations, it can be inferred that the spherical and nanosized TPW and OLC particles, when used in optimized quantity (here 0.1 wt.% and 0.3 wt.% of additives), act like nano-bearings reducing the direct surface-surface contact between the test specimens resulting in low WSD values. A higher 'h' value indicates a higher worn-out material from the wear scar. When used in optimized concentrations, nanosized TPW and OLC particles prevent severe elastic deformation of the steel ball surface at the point of contact under the applied load and sliding conditions, resulting in reduced wear depth concavity. However, at a higher concentration (i.e., 0.5 wt.%) of OLC in BO, an abrupt increase in WSD and h is attributed to the agglomeration of the particles in BO. The agglomerates act as third-body particles and participate in the material wear. The avg. wear volume loss (V) [37] values on the rubbing surfaces (here, surfaces of the steel balls used for wear testing) are shown in Fig. 36.

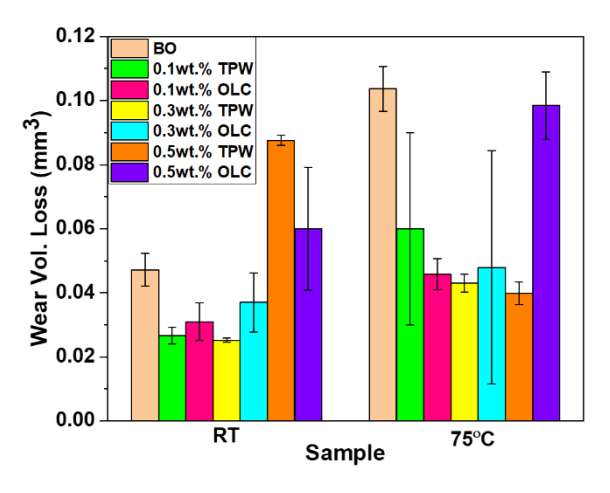


Figure 36. Avg. wear volume loss in test specimens when TPW and OLC dispersed BO samples, and BO are used as lubricants at RT and 75 °C.

When used as lubricants at room temperature, the TPW and OLC dispersed BO samples reduced V values except for 0.5 wt.% TPW and OLC dispersed BO samples, which gave aberrant results. 0.1 wt.% and 0.3 wt.% TPW dispersed BO samples abated wear volume losses by 43.64% and 46.61%, respectively. When used as lubricants at 75 °C, the TPW and OLC dispersed BO samples reduced V values substantially. At 75 °C, 0.1 wt.%, 0.3 wt.% and 0.5 wt.% TPW dispersed BO samples helped reduce wear volume losses by 42.1%, 58.53%, and 61.62%, respectively, while 0.1 wt.%, 0.3 wt.% and 0.5 wt.% OLC dispersed BO samples helped reduce wear volume losses by 55.83%, 53.80%, and a nominal 5.014%, respectively. The observations on wear volume losses indicate the ability of the TPW and OLC to act as AW additives in lubricating media. However, the concentration of the additives has to be cautiously chosen according to the dispersing medium to achieve improved lubricating properties. The experimental results show that 0.3 wt.% of TPW and OLC is optimal for the additive-free group-II N500 BO. Fig. 37 shows the optical micrographs of the minor wear scars on the steel balls tested using TPW and OLC dispersed BO and BO samples at room temperature and 75 °C. The wear scars in the case of TPW (Fig. 37 (b) and (e)) and OLC (Fig. 37 (c) and (f)) dispersed BO displayed a reduced WSD and lowered the intensity of the abrasive wear in the steel balls.

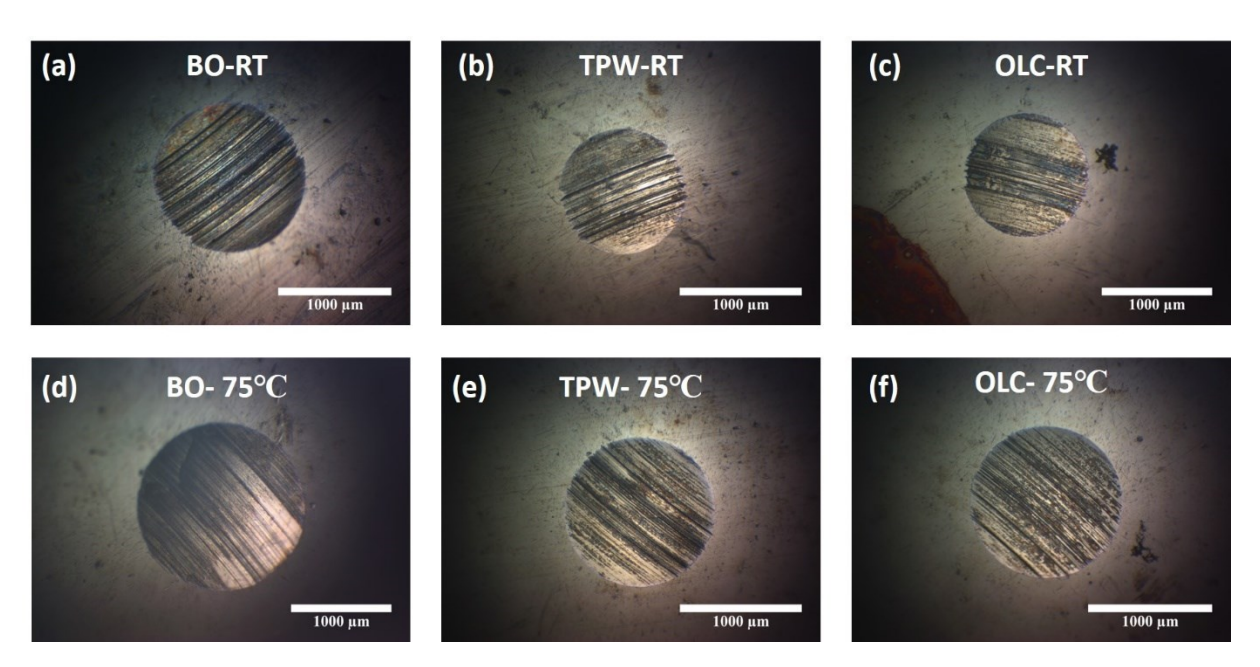


Figure 37. Optical micrographs of the wear scars on the steel balls tested using TPW and OLC dispersed BO and BO samples at room temperature and 75 °C. RT in the figure is the abbreviation of room temperature.

The wear scar recorded by using BO at RT and 75 °C had a larger diameter and excessive abrasive wear within the wear scar. In contrast, specimens tested with TPW and OLC dispersed BO samples at room temperature had reduced abraded area within a smaller wear scar. Even at 75 °C, the use of TPW and OLC dispersed BO samples resulted in a lower wear intensity along with lower WSD. These observations indicate that TPW and OLC dispersed BO samples with optimal concentrations of TPW and OLC can reduce friction, wear, and related losses. Similar observations have been reported w.r.t reduction in WSD in the case of cycle tyre tube-derived C-soot as an additive in dewaxed N500 base oil [30], nano diamond-derived C-onions as an additive in PAO oil [31,32], detonation mixture-derived C-onions as an additive in SN150 [34], and fullerene soot as an additive in mineral oil (MC-20) [38]. The importance of optimal concentration of additives for securing better wear characteristics has also been reported [38]. C-soot samples derived from bio-diesel and diesel vehicle exhausts have also helped reduce wear when used as an additive in lubricating media [18,39]. The load applied during the tribological tests falls in the low load regime, implying the predominance of rolling and sliding mechanisms (i.e., the additives act like nano-ball bearings) of TPW and OLC to enhance the lubrication and consequently improve the tribological properties [2,40].

Nano additives change the viscosity of lubricants, i.e., their flow properties change, limiting or enhancing their capacity to adequately lubricate interfaces. Therefore, the influence of the concentration of nano additives and the uniformity of their dispersion in the lubricant on its viscosity must be carefully considered to negate any adverse impact on performance. Here, ultrasonication-aided dispersion of TPW and OLC particles in CO helped achieve optimal viscosity. Fig. 38(a) shows a non-Einstein-like reduction in CO viscosity after the dispersion of the TPW particles. CO's viscosity was reduced by 19, 29.2, and 22.9% when 0.1, 0.3, and 0.5 wt.% of TPW particles were dispersed in CO.

Fig. 38 (b) shows a reduced viscosity of CO after the dispersion of OLC particles in it. CO's viscosity was decreased by ~35.94% when 0.1 and 0.3 wt.% of OLC particles were dispersed in CO. When the OLC particles' concentration in CO was increased to 0.5wt%, the viscosity was reduced by ~29.5%. Theoretically, the reduced viscosity of a lubricant is undesirable in improving its ability to enhance AF and AW behavior. Less viscous lubricants generate thinner tribo-layers between the contacting components, resulting in higher surface contacts and, thereby, higher interface friction.

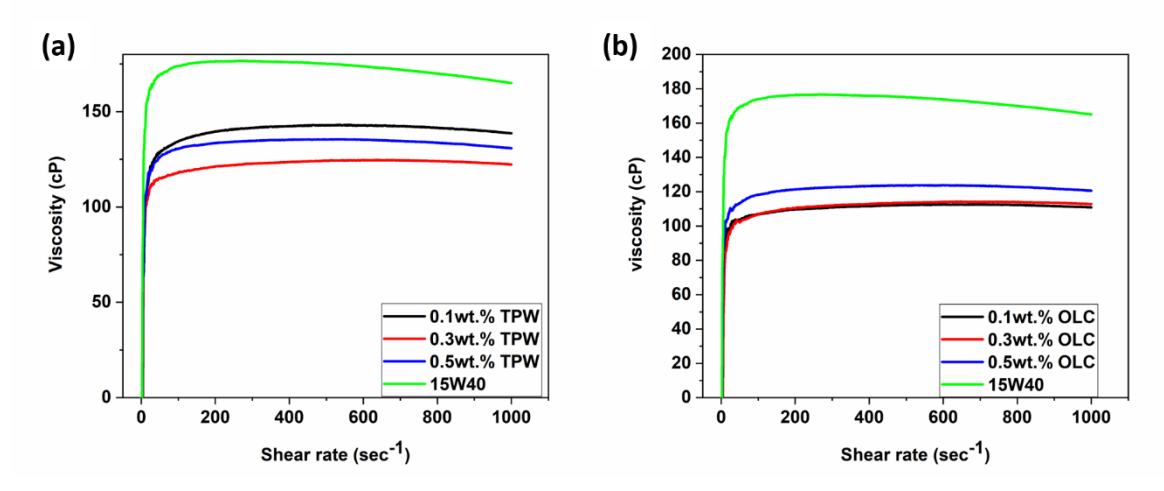


Figure 38. Viscosity versus shear rate profiles of (a) TPW and (b) OLC particles' added CO in comparison to that of CO.

Furthermore, low-viscosity lubricants may lack the load-bearing capacity to support components under high pressures, increasing wear. When the lubricant film breaks down under high loads and speed, the ability to provide boundary lubrication decreases, leaving the surfaces prone to wear. The flow curves of all the lubricant samples in Fig. 39 indicate a linear variation (Newtonian nature) in shear stress with the shear rate. It can be noted that the dispersion of TPW and OLC particles in CO does not change the rheological behavior of the CO. However, the internal shear stress in response to the applied shear rate generated in the lubricant samples containing TPW and OLC particles is lower than that of CO. This correlates well with the reduced viscosity values of TPW and OLC particles dispersed CO samples as per the well-known Newton's law of viscosity.

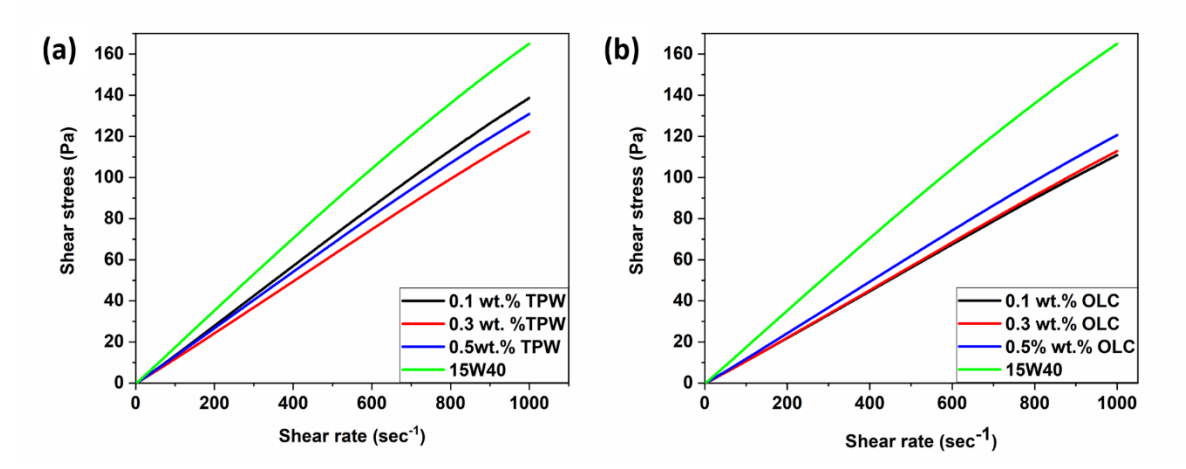


Figure 39. Shear stress versus shear rate profiles of (a) TPW and (b) OLC particles' added CO in comparison to that of CO.

The law significantly establishes that the higher the fluid's viscosity, the greater its resistance to deformation or flow under a given shear stress. Lubricants with low viscosity have lesser resistance to flow, allowing them to move more readily between the contacting surfaces. This characteristic helps to reduce shear stress by implying more effortless movement between contacting surfaces, which reduces friction and wear. However, extremely low viscous lubricants may not provide appropriate protection under high loads or harsh circumstances. However, the exact role of dispersion of nano additives in lubricants and associated rheological changes is still uncertain. Several studies report increased viscosity when nano additives are dispersed in the lubricants. In contrast, other reports claim a reduction in the lubricant's viscosity upon adding the nano additives. Nonetheless, it is apparent from Fig. 38 and 39 that when TPW and OLC particles are dispersed in CO, the rheological properties of CO are altered. Further, during the tribological tests, the avg. CoF was recorded as a function of time (Fig. 40). The CoF of CO was observed to be 0.069 at 100 sec, which reduced to 0.063 at 1000 sec and remained stable at 0.058 from 2000 sec till 3000 sec and ends at 0.052 at 3600 sec (end of the test). The CoF was found to be reducing linearly with time. 0.1wt% TPW added CO exhibited the same initial (i.e., at 100 sec) CoF as CO, which remained constant until 2000 sec. However, the CoF lowered to 0.051 at 3000 sec and 0.041 at 3600 sec.

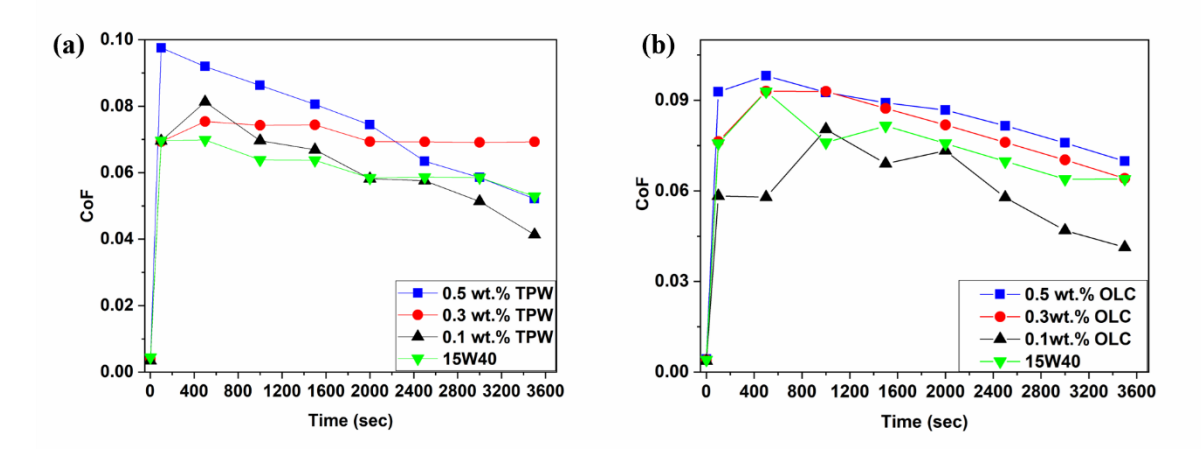


Figure 40. CoF profiles of when (a) TPW and (b) OLC particles' added CO and CO samples are used as lubricants in the tribological tests.

It is observed that a further increase in the TPW concentration in the CO does not positively impact the tribological properties. From Fig. 40 (a), it can be seen that 0.3wt% and 0.5wt% additions of TPW are detrimental to improving the anti-friction ability of the lubricant. In the case of 0.3wt% of TPW addition, the CoF increased from 0.069 (at 100 sec) to 0.074 (at 1000 sec), which remained nearly the same throughout the test duration. In the case of 0.5wt% of

TPW addition, the initial (i.e., at 100 sec) CoF was 0.097, which linearly reduced to 0.052 at 3600 sec, similar to the behavior of CO. Typically, CO reduces the CoF by forming an effective barrier that separates the surfaces and prevents direct contact. The barrier is a thin tribo-layer that uses additives to minimize surface resistance. The tribo-layer lowers friction and wear. This layer might comprise lubricant molecules that attach to the surface or additives intended to stick to metal surfaces. As the CoF reduces with time, the CO may flow more easily between the surfaces, resulting in a profuse tribo-layer. The dispersion obtained using TPW in low concentration (0.1wt%) in CO is more homogenous and stable, with almost no noticeable sedimentation for seven days. This allowed the TPW spherical nanosized particles to enter the contact interfaces effectively. The TPW particles potentially serve as nano-ball bearings, facilitating low-resistance sliding of the surfaces. The tribo-layer formed by the CO gets reinforced with the TPW nanoparticles, so the CoF is further lowered.

The 0.1wt% TPW-infused CO becomes more effective after 2000 sec. This could be inferred as the incubation time for the TPW nanospheres to enter the interface and instate themselves in the tribo-layer, after which they contribute as lubricant additives. However, using higher concentrations of the TPW does not result in homogenous and stable lubricant samples. Visible sedimentation is noted in both samples (i.e., 0.3wt% and 0.5wt% TPW addition cases) after 24 h, potentially due to agglomeration of the TPW nanoparticles. The agglomerated TPW nanoparticles could hinder their uniform dispersion, restrict entry into the sliding interfaces, and act like third-body abrasive particles that elevate CoF and wear on the contact surfaces.

Also, from Fig. 38, it can be seen that the TPW-dispersed CO lubricant samples have lower viscosity values compared to CO. Theoretically, reduced viscosity could lead to discontinuous and unsuitably thinner tribo-layer formation, eventually leading to an increase in CoF and wear. However, even with lower viscosity, CO with 0.1wt% of TPW shows excellent behavior in this context, attributed to the nano-ball bearing effect mentioned above. Therefore, it is inferred that low concentrations of TPW nanoparticles in CO could prove effective as anti-friction (AF) additives. OLC particles' dispersed CO samples exhibited similar behaviour. It can be seen from Fig. 40 (b) that OLC nanoparticles as additives in CO amplified its friction resistance properties, especially when dispersed in low concentration. The CO had an initial CoF of 0.075 at 100 sec, which raked up to 0.09 at 500 sec, after which it stabilized at 0.07 and remained ~0.063 towards the end of the test. Adding 0.1wt% of OLC into CO maintains a low initial CoF of 0.058 at 100 sec and ends at 0.04 at 3600 sec. Higher OLC concentrations (0.3wt% and 0.5wt%) show a higher CoF profile throughout the test duration.

CO results in an avg. CoF of 0.075, which is reduced to 0.063 upon adding 0.1wt% TPW (Fig. 41 (a)). However, a further increase in the concentration of TPW causes a rise in the CoF. The avg. CoF values for 0.3wt% and 0.5wt% TPW additions are 0.076 and 0.097, respectively. A similar trend in the avg. CoF values is observed upon adding OLC particles in varying concentrations. Dispersion of 0.1wt% of OLC in CO lowered the avg. CoF to 0.062, while it increased to 0.076 when the concentration was raised to 0.3wt%. A further increase in avg. CoF to 0.086 can be noticed in Fig. 41(b) when the concentration of OLC was 0.5wt%. In high concentrations, TPW and OLC particles tend to agglomerate and sediment rapidly, giving rise to resistance at the contacting surfaces, thus compromising their intended lubricating effect. Furthermore, an excess of these 0D nanocarbons can exceed the lubricant's dispersing capacity, resulting in abrasive clusters or deposits that increase friction. Further analysis was made on wear scars to establish improved wear characteristics, if any.

Figure 42 shows the avg. WSD and wear scar depth (h) values. A \sim 9% reduction in the WSD and h values was noticed in the specimen tested using a 0.1wt% TPW-loaded CO sample. Higher concentrations of TPW in CO caused an unwanted increase in the WSD, shown in Fig. 42 (a). CO modified by dispersing OLC particles showed inferior AW characteristics with an increase of 12% and 7 % in WSD and h values, respectively. Further, optical images of the wear scars and the avg. wear volume loss (WVL) of test specimens tested using the lubricant samples are shown in Fig. 43.

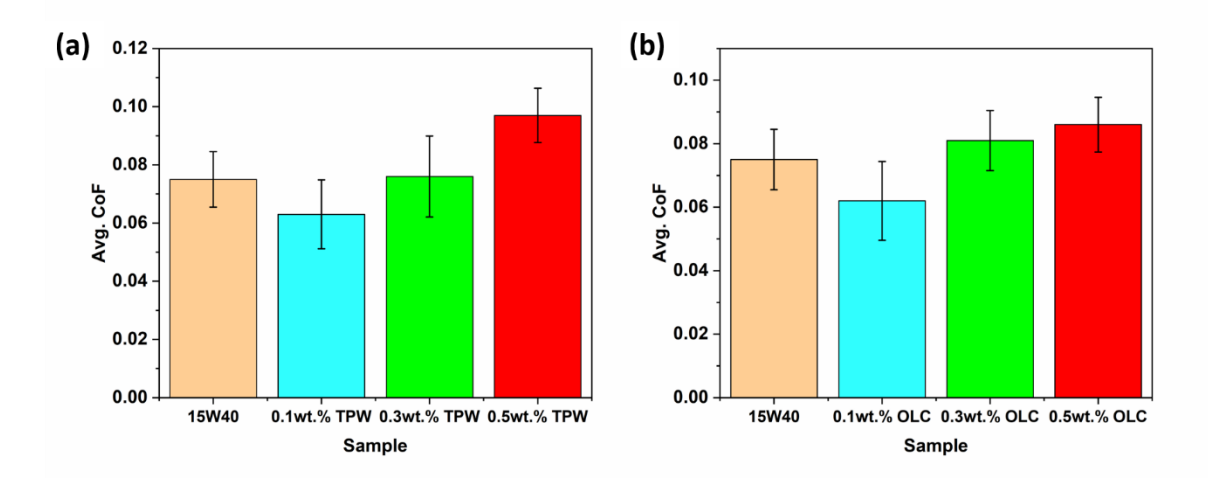


Figure 41. Avg. CoF values when (a) TPW and (b) OLC particles' added CO and CO samples are used as lubricants in the tribological tests.

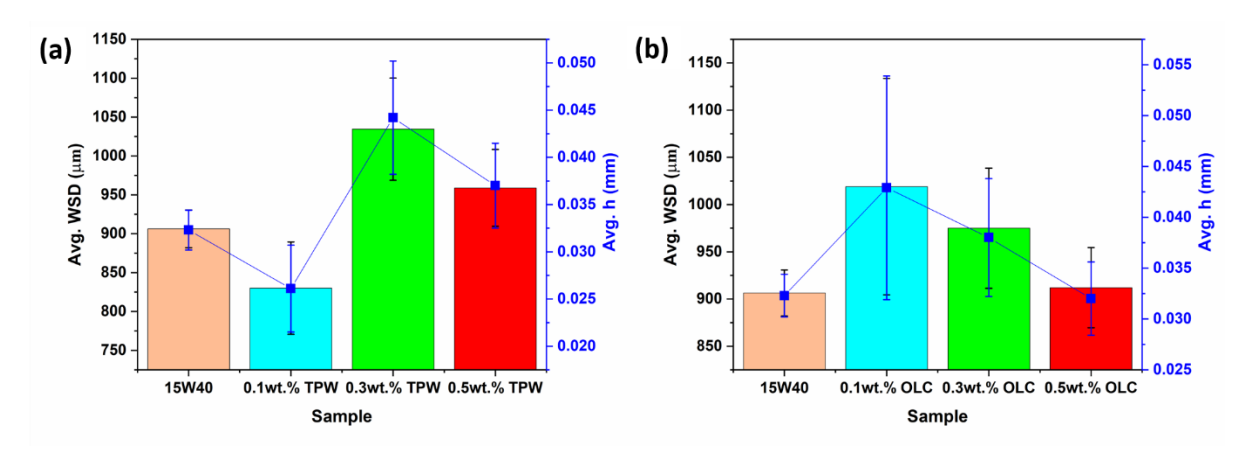


Figure 42. Avg. WSD and h values when (a) TPW and (b) OLC particles' added CO and CO samples are used as lubricants in the tribological tests.

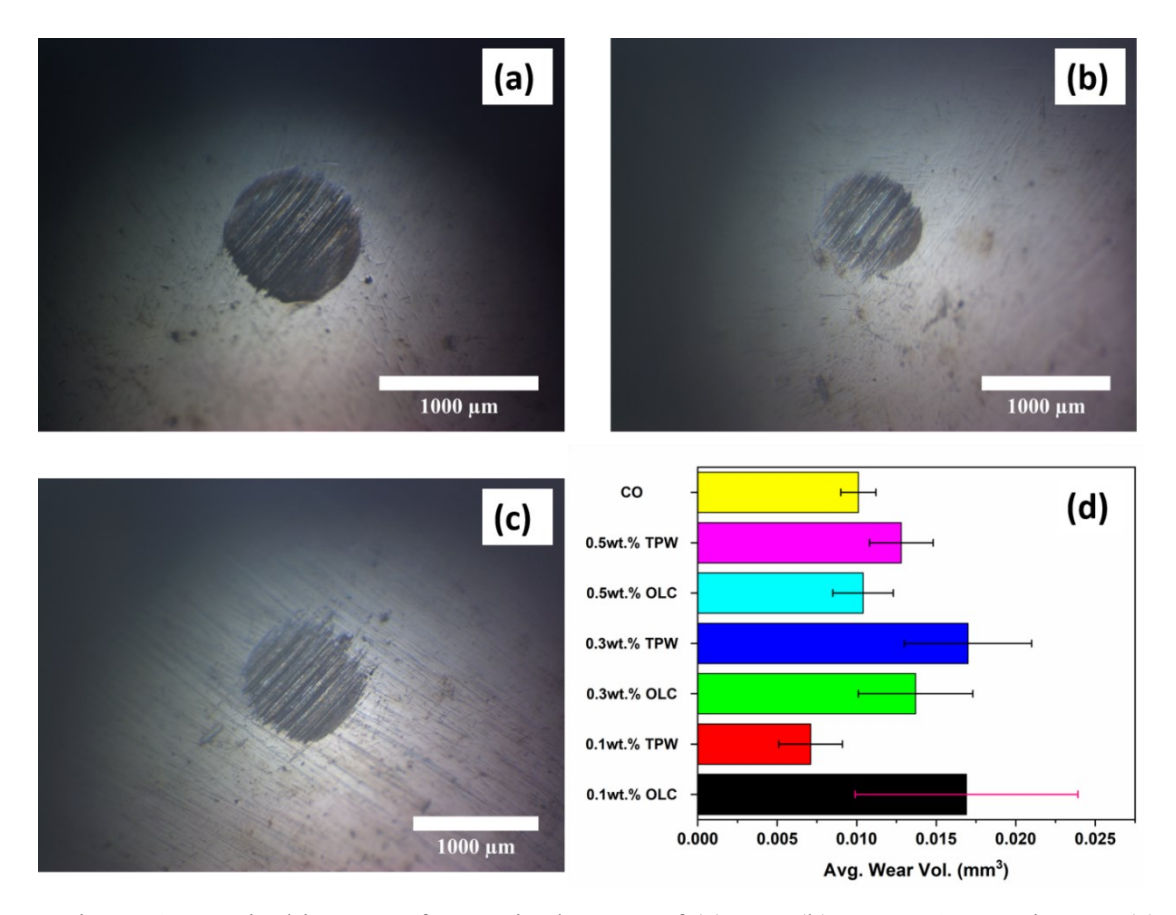


Figure 43. Optical images of WSD in the case of (a) CO, (b) 0.1wt.% TPW in CO, (c) 0.5wt.% OLC in CO as lubricants; (d) avg. wear volume loss (mm3) on specimens tested.

The optical micrograph of the WSD shown in Fig. 43 (a) is of the specimen tested with CO. The WSD in the case of wear tests using 0.1wt% TPW in CO and 0.5wt% OLC in CO are shown in Fig. 43 (b) and 43 (c), respectively. The WSD is reduced for the lubricant samples consisting of TPW and OLC particles. The intensity of wear within the scar is also reduced

substantially when the nanocarbons are added to the CO. Specifically, the TPW proves highly efficient in elevating the wear resistance ability of CO. TPW particles tend to produce a protective tribo-film that limits direct surface-to-surface contact and minimizes frictioninduced wear. The spherical nanoparticles of TPW could possess great load-bearing capacity, owing to which they could evenly distribute stresses at the interface, reducing localized pressure and eventual wear. Along with these, the TPW particles could potentially create a ballbearing effect at the nanoscale, which enables smoother sliding of the surfaces, cumulatively improving the AF and AW improving ability of CO. Out of all the concentrations of TPW in CO, the lowest, i.e., 0.1wt.% proves to be most effective in reducing wear. It effectively lowers WVL by 29%. Although the OLC nanoparticles substantially improve the AF ability of the CO, they fail to simultaneously elevate the wear-resistant ability of CO. Dispersion of OLC particles in different concentrations in CO doesn't show any reductions in the wear. Instead, the wear increases in a detrimental way. From Fig. 43 (d), an increase in the WVL by 65% (for 0.1wt% OLC addition) and 35% (for 0.3wt% OLC addition) was observed, which is undesired. However, the increase in wear associated with using OLC nanoparticles as additives could be due to their higher hardness and the possibility for enhanced agglomeration or clustering. While these nanoparticles might minimize friction, their hardness can also create abrasive wear on uniformly dispersed surfaces.

In a previous study [31], OLC-added polyalphaolefin oil was tested as a lubricant. It has been argued that the OLC particles facilitated sliding and rolling-off between surfaces in relative motion. OLC particles' closed structure (graphitic layers arranged in an onion ring-like form) rendered thermodynamic stability and high mechanical strength. However, the defects induced in the outer-most layer of these particles may increase the chances of their bonding with the rubbing surfaces' material, resulting in detrimental friction and wear characteristics. On the other hand, novel nanocarbons prepared from bio-diesel-soot were also thoroughly tested to support using OLC-like additives in lubricants. The graphene fragments [41,42] of high contortion in the bio-diesel-soot facilitated onion-like morphology [43]. Other novel carbons have also been studied [6,7,44-48]. Diesel-extracted soot particles as lubricant additives resulted in low friction and wear on textured surfaces [18]. Soot particles act as nanobearings between the two surfaces, forming a tribo-film on the surface. Several reports have proven the existence of such films. [5,7,18,45].

4.3 1D MWCNTs as Additives in Lubricants

From the FESEM images (Figs. 44 (a) and (b)), the cylindrical morphology and high aspect ratio of MWCNTs are evident. The TEM images (Figs. 44 (c) and (d)) further confirm the cylindrical morphology and high aspect ratio. TEM images also confirm the typical hollow, nano-tubular, and multi-walled (i.e., concentric cylinders made of graphene layers) nature of the MWCNTs. The low-magnification FESEM image (Fig. 44 (a)) shows that the MWCNTs are entangled. The X-ray diffractogram (Fig. 45 (a)) shows that the MWCNTs are highly crystalline. The diffraction peaks at 20 equals 26°, 44° and 53° are indexed to (002), (100), and (004) crystallographic planes in graphite. (100) and (004) planes are perpendicular to the tube axis [49]. The appearance of the diffraction peaks corresponding to (100) and (004) planes implies that the graphene layers constituting the concentric cylinders are along the tube axis. The d-spacing calculated from the (002) peak is 0.34 nm, the typical interplanar spacing between the graphene layers in MWCNTs [49].

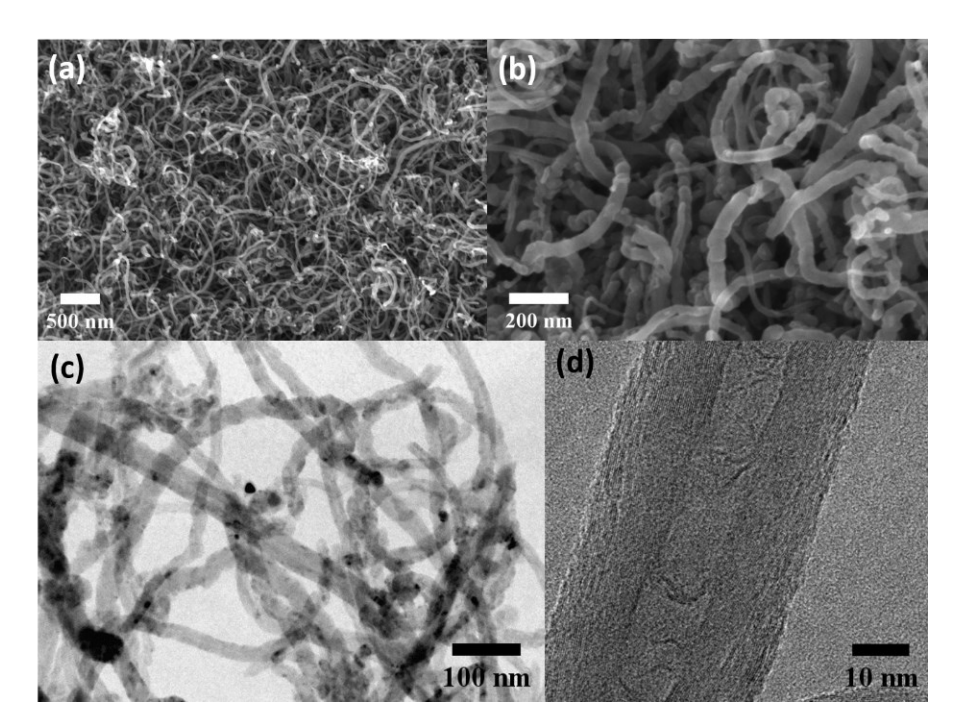


Figure 44. (a) and (b) FESEM images of MWCNTs recorded at different magnifications; (c) and (d) TEM images of MWCNTs recorded at different magnifications.

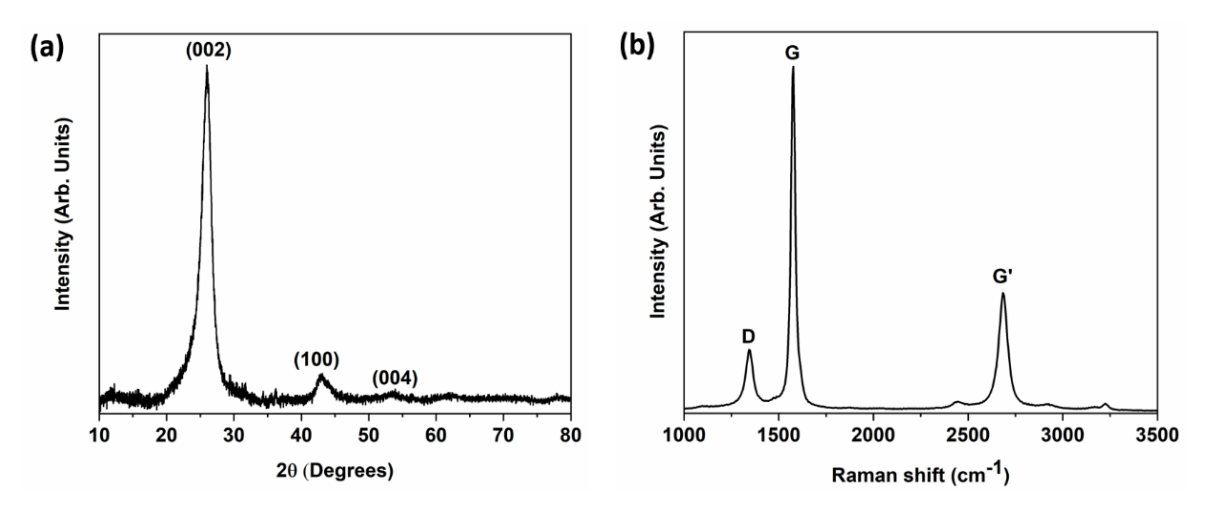


Figure 45. (a) X-ray diffractogram and (b) Raman spectrum of the as-prepared MWCNTs.

The Raman spectrum (Fig. 45(b)) doesn't show the radial breathing mode below 500 cm⁻¹, implying the multi-walled nature of the as-prepared MWCNTs. ¹⁴ The sample shows fingerprint vibrational bands around 1344 cm⁻¹, 1577 cm⁻¹, and 2684 cm⁻¹, which are attributed to the typical D-bank (Disordered band), G-band (Graphitic band), and 2D or G'-peak (overtone of D-band) in MWCNTs prepared by other techniques [49]. The ratio of the integrated areas under the D and G-bands (I_D/I_G) is the measure of the graphitization index of MWCNTs. A low I_D/I_G ratio implies fewer defects in MWCNTs. Similarly, higher values of I_{2D}/I_G and I_{2D}/I_D indicate long-range ordering and good crystallinity of the graphitic network in the sample, respectively. I_D/I_G, I_{2D}/I_G, and I_{2D}/I_D ratios for the MWCNTs in this work are calculated to be 0.285, 0.632, and 2.214, respectively, implying that the as-prepared MWCNTs are highly graphitic, with fewer defects and good crystallinity.

Figure 46(a) shows the rheograms of BO and the MWCNTs dispersed BO samples. Figure 46 (b) shows the flow curves of BO and the MWCNTs dispersed BO samples. Three different samples of MWCNTs added BO, namely BO + NT1 (0.1wt.%), BO + NT2 (0.3wt.%), and BO + NT3 (0.5wt.%) are tested. Figure 4a shows that the viscosity remains the same over the applied shear rate ($>50~\text{sec}^{-1}$) for all the samples, indicating the absence of any shear thinning or shear thickening.

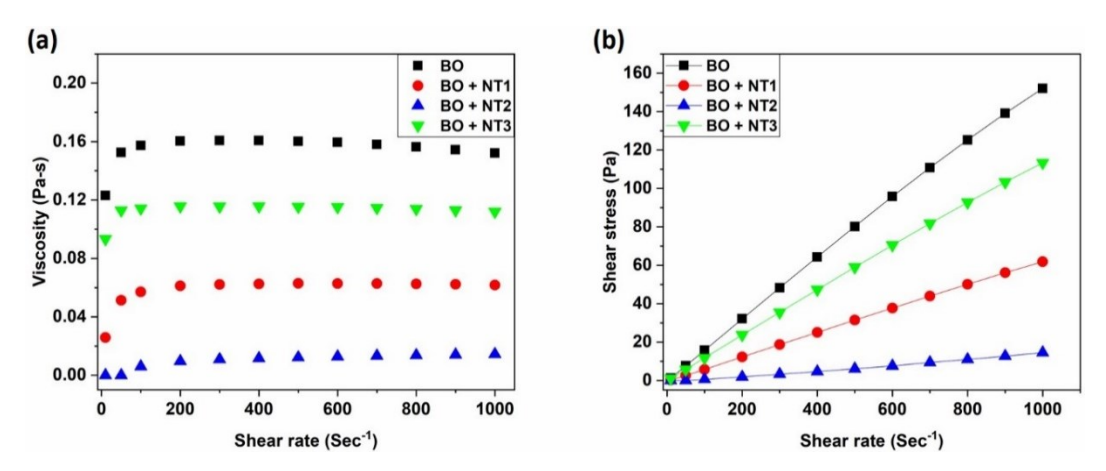


Figure 46. Rheological properties of BO and MWCNT dispersed BO samples: (a) Viscosity as a function of shear rate and (b) Shear stress as a function of shear rate.

A slight shear thickening is observed in all the MWCNTs dispersed samples for shear rates up to 50 sec⁻¹. It can be noted that adding the MWCNTs to BO lowers the viscosity. The viscosity of BO + NT1 is 59% lower than that of BO, while that of BO + NT2 is 90% lower than that of BO. However, a higher concentration of the MWCNTs in BO (BO + NT3) shows a viscosity reduction of only 26%. The flow curves (Fig. 46 (b)) also indicate a reduced internal shear stress in the MWCNTs dispersed BO samples. The reduction in lubricant viscosity following the dispersion of MWCNTs can be attributed to various factors. The size and distribution of MWCNTs inside the lubricant are important because a more uniform dispersion with smaller agglomerates reduces viscosity. MWCNTs' surface modification and their concentration in the lubricant could influence molecular interactions and lead to changes in viscosity. The degree of aggregation or dispersibility of MWCNTs is critical, as effective dispersion reduces agglomeration while increasing lubricant flow. A similar reduction trend in viscosity was noticed in the case of MWCNTs dispersed CO samples (Fig. 47 (a)). Three different samples of MWCNTs added CO, namely CO + NT1 (0.1wt.%), CO + NT2 (0.3wt.%), and CO + NT3 (0.5wt.%) are tested. The CO + NT1 sample shows 37% lower viscosity than the CO. CO + NT2 and CO + NT3 samples show viscosity values that are 27% and 24% less than that of CO. The overall viscosity of the CO and the MWCNTs dispersed CO samples remains the same throughout the range of applied shear rate (> 50 sec⁻¹). The flow curves of the CO and MWCNTs dispersed CO samples (Fig. 47 (b)) exhibit linearity, indicating the samples follow Newton's law of viscosity (i.e., the shear stress is directly proportional to the shear rate) of the lubricant samples.

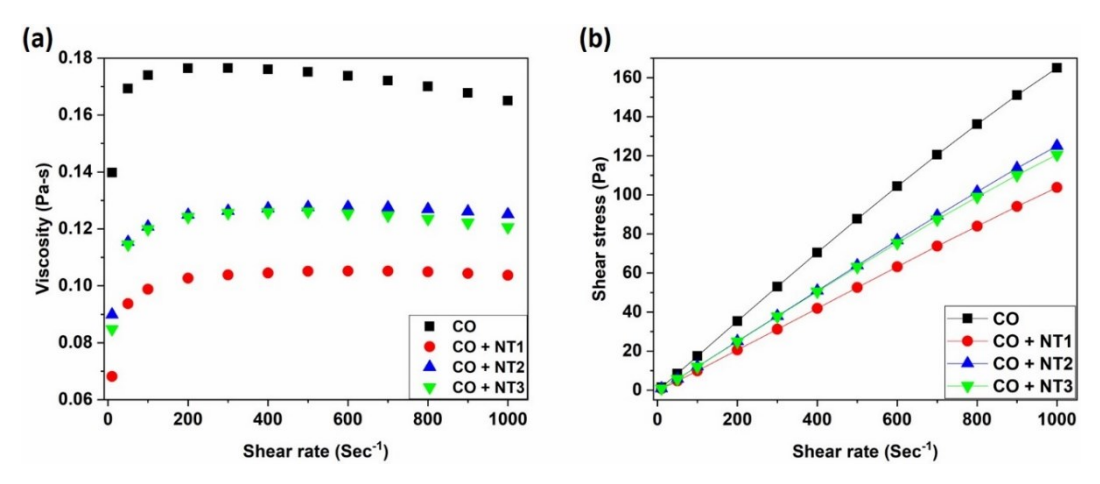


Figure 47. Rheological properties of CO and MWCNT dispersed CO samples: (a) Viscosity as a function of shear rate and (b) Shear stress as a function of shear rate.

MWCNTs dispersed lubricating media have often helped significantly reduce the coefficient of friction (CoF) [50-53]. The presence of MWCNTs in lubricating media creates a lubricating system in such a way that the MWCNTs form a protective layer between contacting surfaces. As a result, they facilitate smoother movement of the contacting surfaces by minimizing direct metal-to-metal contact and reducing frictional forces. This reduction in CoF can enhance the efficiency of machinery, lower wear and tear on components, and contribute to improved overall performance in various industrial applications where lubrication is essential. In this work, as shown in Fig. 48 (a), it can be observed that at room temperature (RT), there is no significant improvement in the anti-friction characteristics of BO even after adding MWCNTs in varying concentrations. However, when the same lubricant samples are tested as per the ASTM standard, i.e., at 75 °C Fig. 48 (b), substantial improvement in anti-friction characteristics can be observed. The BO results in a CoF of 0.04 at 400 sec, after which the friction can be seen increasing to a peak value of 0.09 at 1600 sec, which lowers to 0.07 towards the end of the test (3600 sec). From Figure 6b, the BO + NT1 sample clearly does a splendid job of reducing the CoF. It can be observed that the CoF of 0.047 at 400 sec keeps lowering to the end value of 0.008 at 3600 sec, which is clearly close to the super-lubrication regime. The BO + NT2 and BO + NT3 result in a CoF of 0.05 at 400 sec, while at 3600 sec, BO + NT2 and BO + NT3 result in CoF values of 0.04 and 0.03, respectively. The average CoF values at RT (Fig. 48 (c)) indicate minimal impact of the MWCNTs addition to BO. However, the average CoF values at 75 °C (Fig. 48 (d)) show that MWCNTs are critical in reducing the average CoF. It may be noted that at 75 °C, BO loses more than 90% of its viscosity, thereby reiterating the importance of additives (here, MWCNTs) in improving anti-friction properties at the operating temperatures.

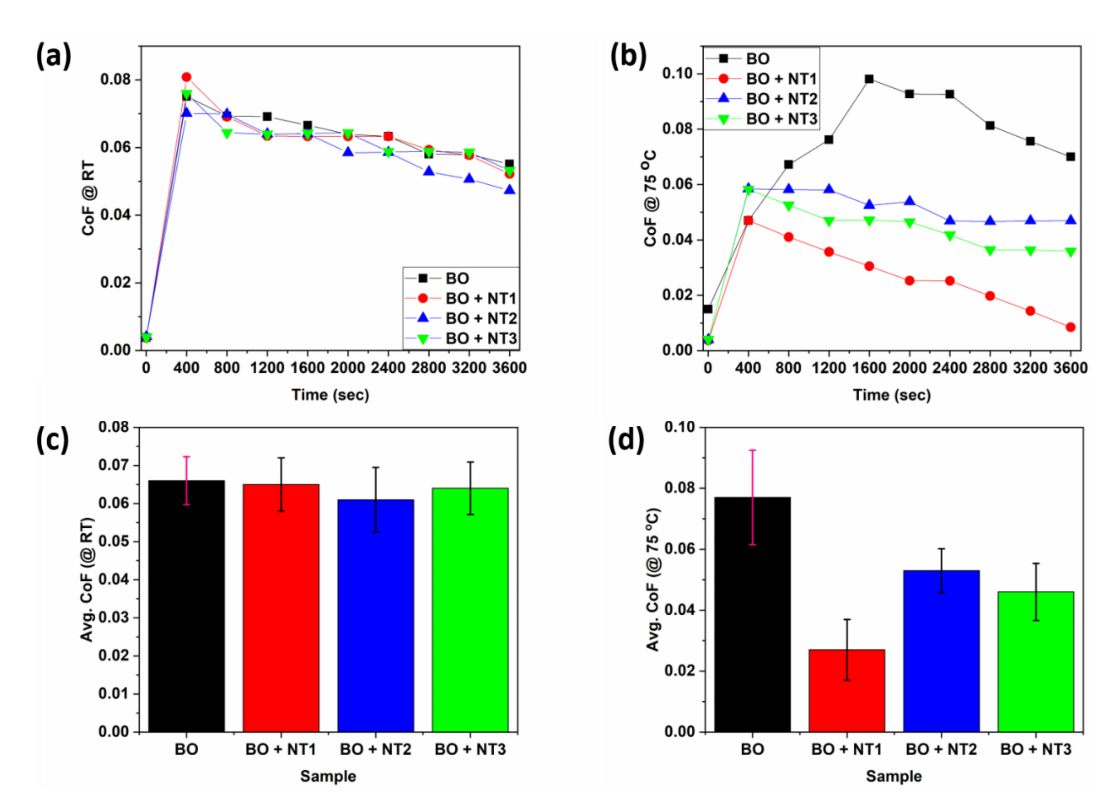


Figure 48. CoF data when BO and MWCNT dispersed BO samples are tested as lubricants: CoF versus time at (a) RT, (b) 75 °C, and Avg. CoF at (c) RT and (d) 75 °C.

Figure 49 shows the CoF data when CO and MWCNT dispersed CO samples are tested as lubricants. The CoF profiles in Figs. 49 (a) and (b) distinctly show the efficient reduction in friction when MWCNTs are dispersed in CO. It can be observed that when CO is tested as a lubricant at RT, the CoF profile increases with time. The initial CoF remains at 0.075 till 800 sec, after which it shoots up to 0.1 and remains nearly the same throughout the remaining test duration. The initial CoF values in the case of the MWCNTs dispersed CO samples are almost the same (~ 0.06) from the beginning of the test until 1600 sec. However, the CO + NT1 and CO + NT2 samples increased CoF from 2000 sec onwards. In the case of the CO + NT1 sample, the CoF increases to 0.075, while in the case of CO + NT2, the CoF goes up to 0.086 towards the end of the test. The CoF in the CO + NT3 sample case remains almost unchanged throughout the test. At RT, the reduction in average CoF in the case of CO (Fig. 49 (c)) is nearly the same for all the different concentrations of MWCNTs in it. The low and high concentrations of MWCNTs in the CO do not show striking changes in the anti-friction behavior. At 75 °C, the MWCNT concentrations become crucial in tailoring the anti-friction property of the CO. The CoF profiles improved in the case of low concentrations of MWCNTs in CO. The CO resulted in a CoF of 0.09 at 400 sec, which lowers to 0.06 towards the end of the test. The CO + NT1 sample results in an initial CoF of 0.05 at 400 sec, which reduces to a

very low value of 0.024 towards the end of the test. The CO + NT2 sample results in slightly higher CoF values of 0.057 and 0.03 at 400 sec and 3600 sec, respectively. Further increase in MWCNTs concentration, i.e., CO + NT3 sample, did not effectively lower the friction. It resulted in an initial CoF of 0.057 at 400 sec and 3600 sec. It can be observed from Fig. 49 (b) that the CO + NT3 sample shows a surge in CoF values from 400 sec to 1600 sec. It can be stated that the CO + NT1 sample is the best in terms of reducing friction. The percentage (%) of average CoF reductions obtained using the BO, CO, and the MWCNTs dispersed BO and CO samples are shown in Table 5 and Table 6, respectively.

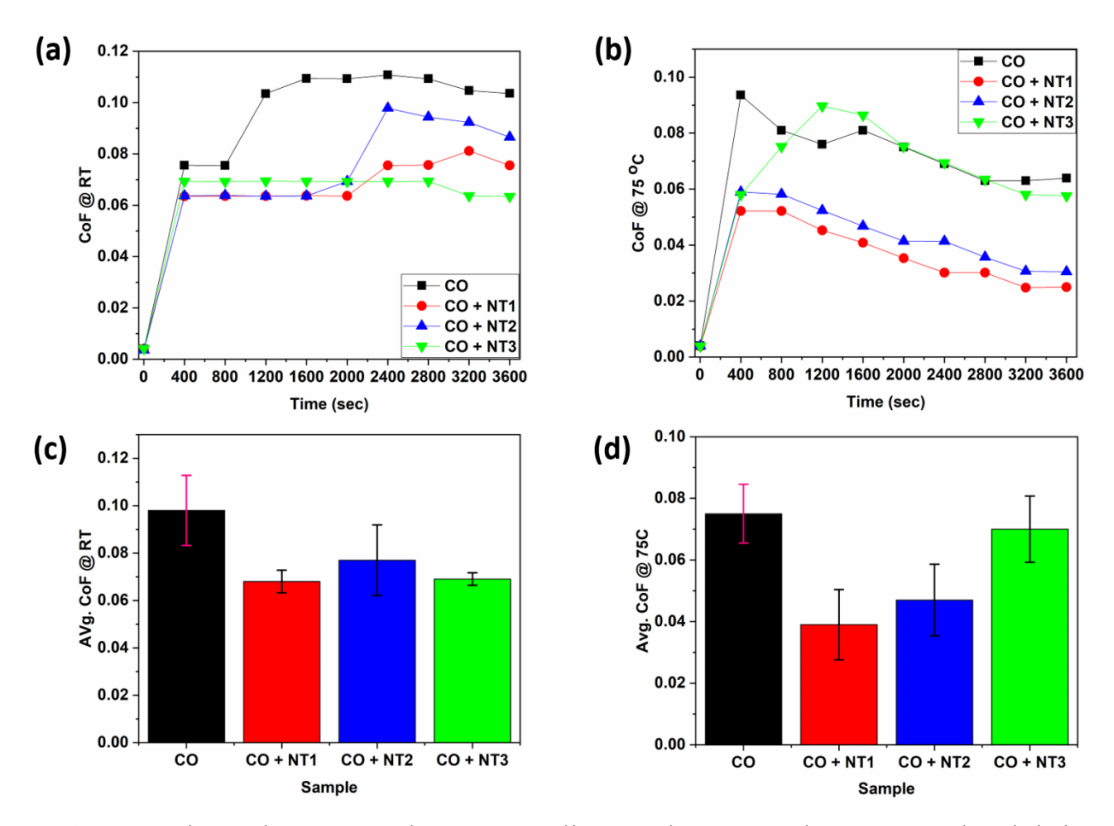


Figure 49. CoF data when CO and MWCNT dispersed CO samples are tested as lubricants: CoF versus time at (a) RT, (b) 75 °C, and Avg. CoF at (c) RT and (d) 75 °C.

Table 5. Avgerage CoF values and percentage reduction in CoF when BO, CO, and MWCNTs dispersed BO and CO samples are tested as lubricants at RT and 75 °C.

Lubricant	Average	% reduction	Average	% reduction
Sample	CoF at RT	in Average	CoF at 75 °C	in Average
		CoF		CoF
ВО	0.066	-	0.077	-
BO + NT1	0.065	1.51%	0.027	64.93%
BO + NT2	0.061	7.57%	0.053	31.16%
BO + NT3	0.064	3.03%	0.046	40.25%
CO	0.098	-	0.075	-
CO + NT1	0.068	30.61%	0.039	48%
CO + NT2	0.077	21.42%	0.047	37.33%
CO + NT3	0.069	29.59%	0.07	6.66%

Table 6. Maximum and minimum CoF values when BO, CO, and MWCNTs dispersed BO and CO samples are tested as lubricants at RT and 75 °C.

Lubricant	Maximum	Maximum	Minimum	Minimum
Sample	CoF at RT	CoF at 75 °C	CoF at RT	CoF at 75 °C
ВО	0.0759	0.0981	0.0551	0.07
BO + NT1	0.080	0.0638	0.0532	0.0037
BO + NT2	0.0759	0.0760	0.0472	0.0039
BO + NT3	0.070	0.0758	0.0532	0.0040
CO	0.1108	0.0936	0.0756	0.0639
CO + NT1	0.0812	0.0522	0.0636	0.0249
CO + NT2	0.0978	0.0579	0.0636	0.0304
CO + NT3	0.0692	0.0896	0.0634	0.0575

MWCNTs added BO and CO samples' wear-preventive nature is assessed by measuring the wear scar diameter (WSD), wear volume loss (WVL), and wear scar depth (h). Figure 50 shows the average WSD values measured on the test specimens subjected to wear test using BO and the MWCNTs dispersed BO samples. At RT, the average WSD reduction improvement is

nominal in the case of MWCNTs dispersed BO (Fig. 50 (a)). 0.1wt.% MWCNTs dispersed BO results in ~ 9% average WSD reduction. The wear-preventive properties deteriorated in the case of samples with higher concentrations of the MWCNTs. 0.3wt.% MWCNTs dispersed BO sample did not improve the average WSD reduction. In the case of 0.5wt.% MWCNTs dispersed BO sample, the average WSD increased by 3%. At 75 °C, the wear-preventive characteristic of BO is significantly improved due to the addition of the MWCNTs (Fig. 50 (b)). The average WSD was reduced substantially by 30% when BO was loaded with MWCNTs. As the concentration of the MWCNTs increased to 0.3wt.%, the average WSD reduction was found to be ~26.5%, which further deteriorated to 17% when the concentration of MWCNTs was increased to 0.5wt.%.

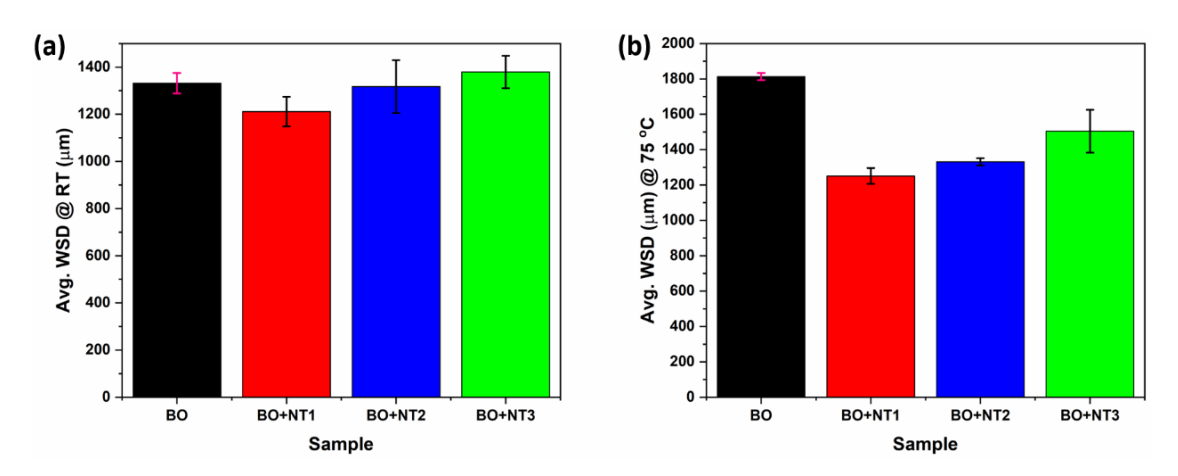


Figure 50. Average WSD values at (a) RT and (b) 75 °C in the case of BO and MWCNTs dispersed BO samples.

Figure 51 shows the improved wear-preventive characteristics (WVL and h) of MWCNTs dispersed BO samples at 75 °C. Figure 51 (a) shows a 36% improvement in the average WVL on the test specimens when 0.1wt.% MWCNTs dispersed BO was used as the lubricant. 0.3wt.% and 0.5wt.% MWCNTs dispersed BO samples were detrimental. 0.5wt.% MWCNTs dispersed BO sample resulted in a 16% increase in the wear. At 75 °C, a similar trend was observed (Fig. 51 (b)). The test specimens lubricated using low concentrations of MWCNTs in BO show reduced wear. Adding 0.1wt.% and 0.3wt.% of MWCNTs to BO helped improve the wear-preventive properties by 54% and 64%, respectively. However, 0.5wt.% MWCNTs dispersed BO sample improved the wear-preventive properties by only 23%.

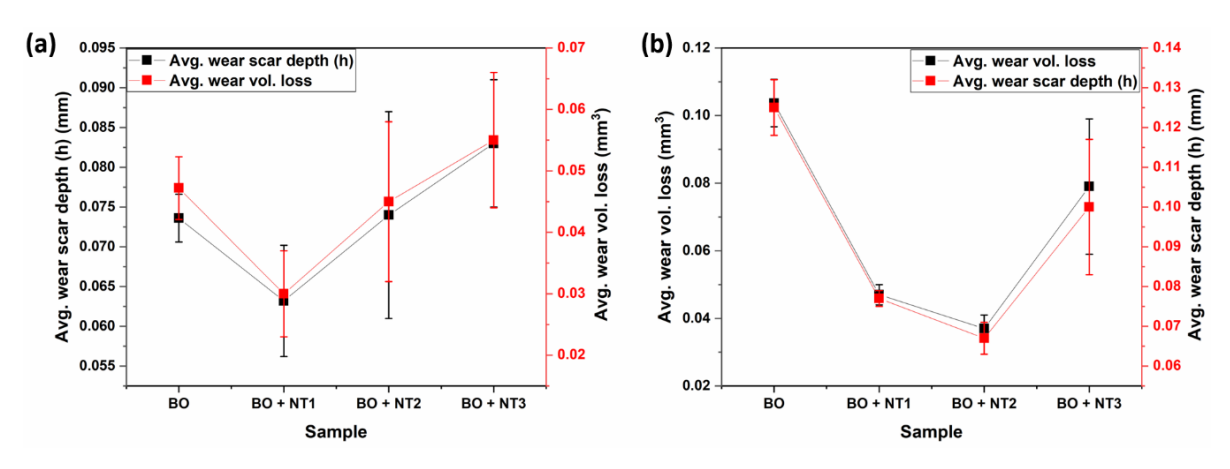


Figure 51. Average WVL and h at (a) RT and (b) 75 °C in the case of BO and MWCNTs dispersed BO samples.

Figure 52 shows the wear-preventive properties when CO and MWCNTs dispersed CO samples are tested as lubricants at RT and 75 °C. At RT (Fig. 52 (a)), the average WSD was 17% lesser in the case of 0.1wt.% of MWCNTs dispersed CO sample. 0.3wt.% of MWCNTs dispersed CO sample resulted in a nominal improvement of 2% in wear-preventive properties. However, the average WSD was 21% lesser in the case of 0.3wt.% MWCNTs dispersed CO sample. At 75 °C, MWCNTs added CO samples do not have the desirable effect on the wear-preventive properties. Figure 52 clearly shows no improvements in the average WSD values. These values rather increase when the MWCNTs-infused CO samples are used as lubricants. 0.1wt.% MWCNTs dispersed CO sample resulted in a nominal reduction by 7%, while 0.3wt.% and 0.5wt.% MWCNTs dispersed CO samples resulted in a 32% higher average WSD as compared to the case of CO.

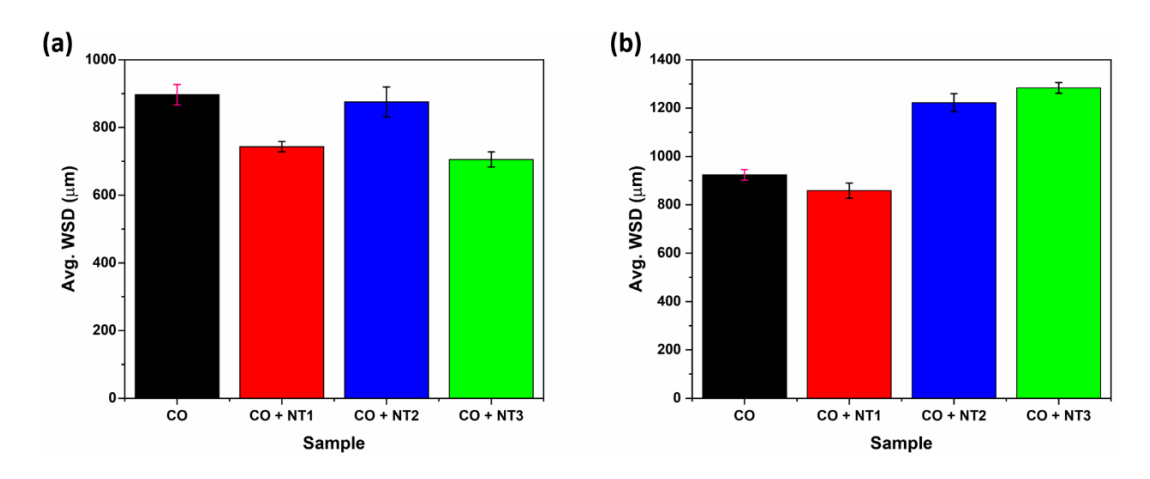


Figure 52. Average WSD values at (a) RT and (b) 75 °C in the case of CO and MWCNTs dispersed CO samples.

Figure 53 shows the wear-preventive properties of CO and MWCNTs dispersed CO samples at RT and 75 °C. At RT (Fig. 53 (a)), the reduction in WVL and h are anomalous. 0.1wt.% MWCNTs dispersed CO resulted in a 32% reduction in the average WVL and h, while 0.3wt.% MWCNTs dispersed CO caused an abrupt increase in wear, making the lubricant sample undesirable for use. On the contrary, 0.5wt.% MWCNTs dispersed CO results in a ~ 39% improvement in the wear-preventive characteristics. At 75 °C (Fig. 53 (b)), the use of 0.1wt.% MWCNTs dispersed CO lowered the average WVL and h by ~30%. However, 0.3wt.% and 0.5wt.% MWCNTs dispersed CO samples drastically increased the average WVL and h values, indicating to abstain from adding MWCNTs in high concentrations in CO. The wear scar images obtained on the test specimens are shown in Figures 54 and 55. Wear-preventive characteristics are measured from these images.

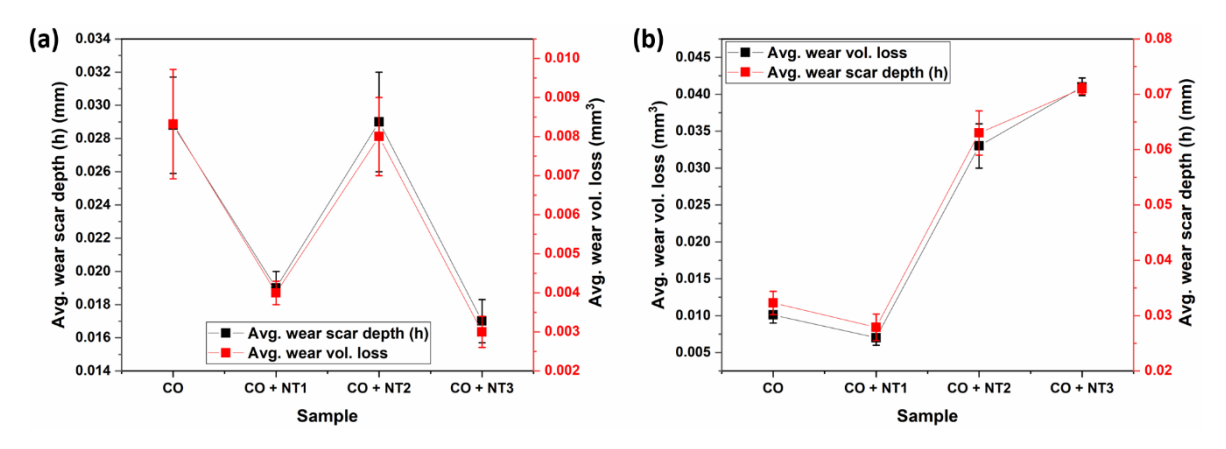


Figure 53. Average WVL and h at (a) RT and (b) 75 °C in the case of CO and MWCNTs dispersed CO samples.

The lubrication mechanism of MWCNTs was speculated as penetration into surface asperities and rolling between contacting surfaces, similar to a roller bearing action, with small and short MWCNTs demonstrating superior performance than thick and lengthy ones due to lower agglomeration and interlocking [50]. MWCNTs from carbon-rich fly ash were evaluated as lubricant additives for 150SN BO. The CoF was lowered by approximately 25% at a concentration of 0.1wt.% MWCNTs. The rheological behavior was also investigated, and it was discovered that the viscosity of the BO impregnated with 0.1wt.% MWCNTs differed little from that of pure oil [51]. MWCNTs generated from fly ash, when combined with sunflower BO in various concentrations (0.005wt.% to 0.5wt.%), showed that even at a low concentration of 0.1wt.% MWCNTs, the CoF was reduced by roughly 58%. This behavior was linked to creating a protective graphitic carbon layer between the surfaces in contact [52]. The nanolubricant made with SAE 5W-30 at a concentration of 0.06 wt.% improved thermal

conductivity the most, which can be ascribed to the surface characteristics of MWCNTs. When 0-0.06wt.% MWCNTs added SAE 5W-30 was used as the lubricant, and the WSD and CoF values were reduced due to the creation of a stable hydrodynamic lubricant coating. A concentration of MWCNTs >0.06wt.% caused more significant agglomeration and inhomogeneity of MWCNTs in the lubricant, leading to higher WSD and CoF values. Overall, these nano lubricants have the potential to reduce friction and wear, increase lubricity and machine component longevity, and save fuel consumption [53]. The as-prepared MWCNTs in this work performed extraordinarily as lubricant additives. Because of factors like their high aspect ratio and structure, MWCNTs operate as nano-scaled spacers and rollers between sliding surfaces, reducing direct contact and load-bearing. MWCNTs adhere to surface imperfections, producing a protective interface that drastically reduces friction. The MWCNTs align and form durable tribofilms on the surfaces under sliding conditions, decreasing direct contact and resulting in low friction between the contacting surfaces. When MWCNTs are utilized as lubricant additives, the combination of load-bearing capabilities, tribofilm production, and temperature management significantly reduces friction. The lubricating mechanism of MWCNTs as lubricant additives is shown in Figure 56.

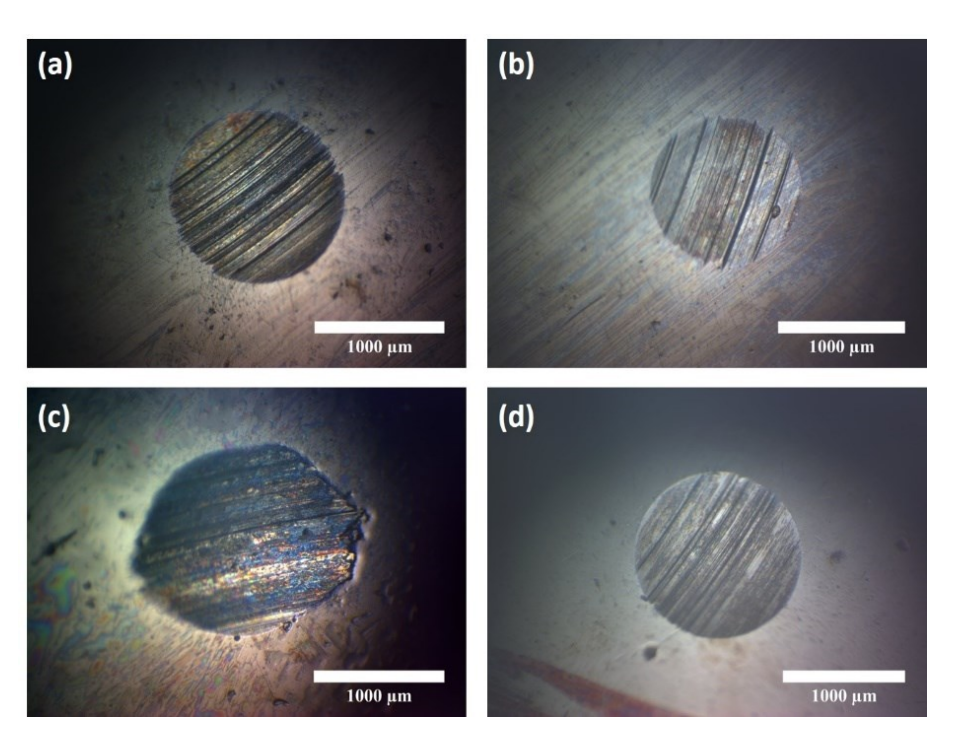


Figure 54. Wear scars obtained on test specimens using (a) BO at RT, (b) 0.1wt.% MWCNTs in BO at RT, (c) BO at 75 °C, and (d) 0.11wt.% MWCNTs in BO at 75 °C.

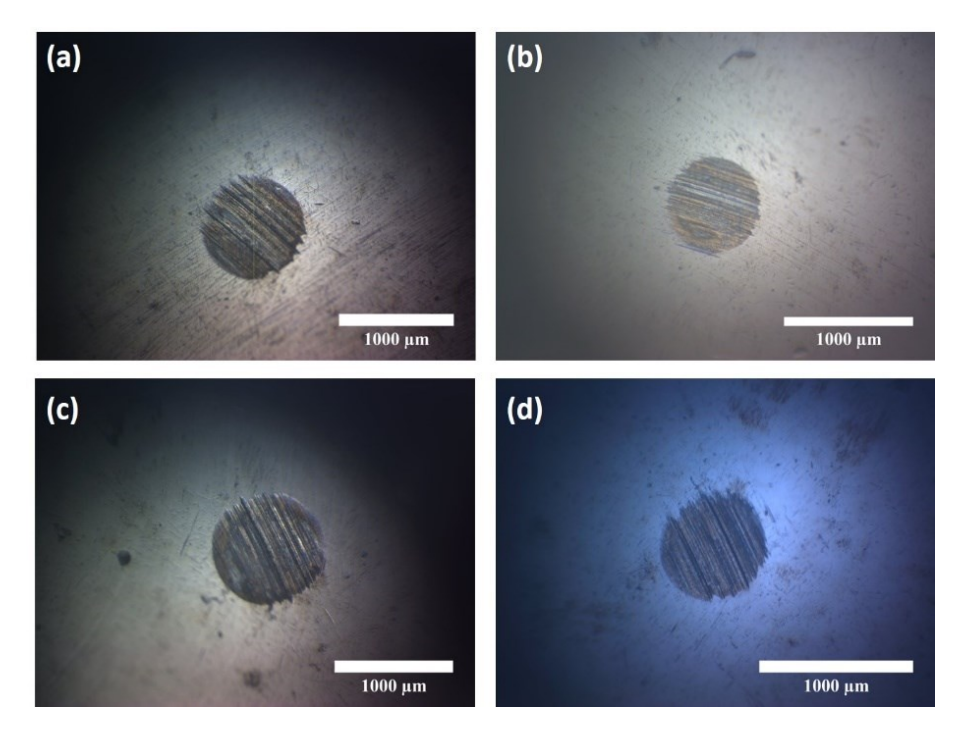


Figure 55. Wear scars obtained on test specimens using (a) CO at RT, (b) 0.1wt.% MWCNTs in CO at RT, (c) CO at 75 °C, and (d) 0.11wt.% MWCNTs in CO at 75 °C.

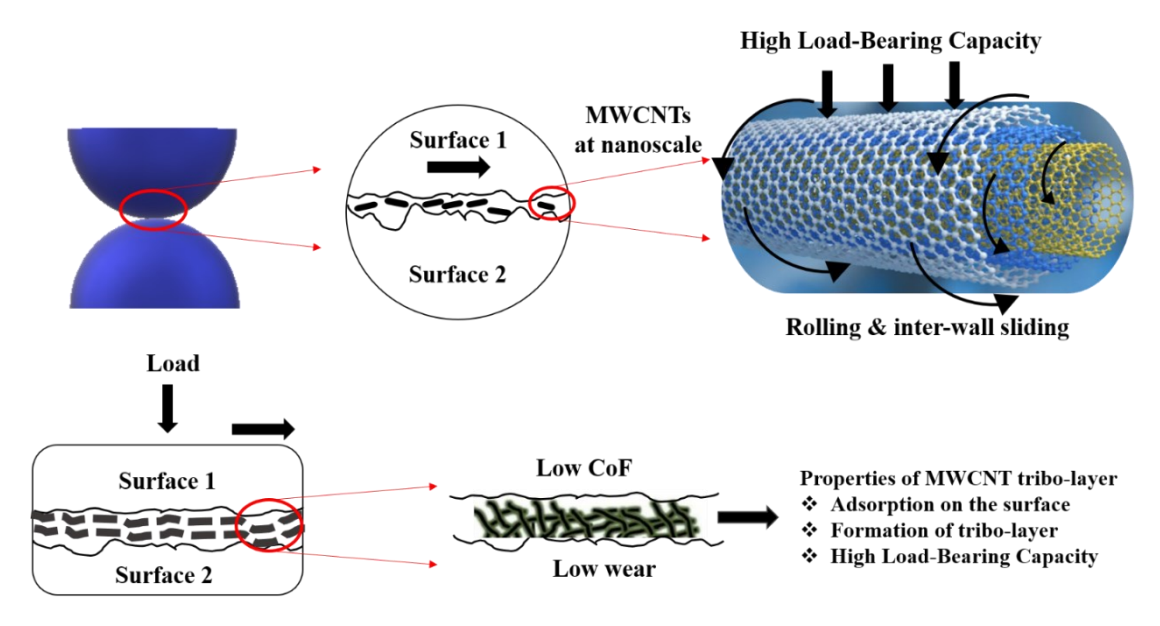


Figure 56. Lubricating mechanism of MWCNTs at nanoscale and macroscale.

MWCNTs have an extremely high aspect ratio and specific surface area because their structure consists of many concentric graphene layers that are smoothly rolled into a cylindrical shape. MWCNTs' tubular form allows for rolling and sliding motions at the nanoscale. When used as lubricant additives, MWCNTs can align themselves between sliding surfaces, reducing direct contact between them. As MWCNTs roll and slide, they act as barriers against surface-

to-surface contact, resulting in a considerable decrease in molecular friction. MWCNTs can modify the lubricant's rheological properties at the nanoscale. Because of their unusual shape, MWCNTs added lubricants can display shear-thinning behavior, which means their viscosity decreases under shear stress. This feature allows the lubricant to flow more freely between moving parts, lowering viscous drag and increasing lubrication efficiency. Additionally, the graphitic structure of MWCNTs creates a solid lubricating mechanism. The sp² hybridized carbon atoms in graphene layers have low shear resistance, allowing MWCNTs to function as solid lubricants. This lowers friction and wear between contacting surfaces, extending the total life of the lubricated system. While nanoscale processes concentrate on molecule interactions, macroscale mechanisms involve the collective behavior of MWCNTs within the lubricant, which influences overall lubrication performance. MWCNTs have a great load-bearing capacity thanks to their strong carbon-carbon bonding. MWCNTs, when added to lubricants, can endure large loads while equally distributing pressure across surfaces. This load-bearing capacity keeps surface asperities from coming into direct contact, decreasing wear [54]. MWCNTs aid in producing a tribofilm, a protective coating that forms on sliding surfaces during lubrication. MWCNTs combine with other additives and surfaces to generate a tribofilm, which works as a wear and corrosion barrier. This improves the lubricant's anti-wear qualities and provides consistent performance over time. The lubricating mechanism of MWCNTs as additives is a complex combination of nanoscale and macroscale events, as shown in Figure 56.

At the macro scale MWCNTs enhance the stiffness of the lubricant film, improving load-bearing capacity of microscopic surface irregularities (asperities), leading to better load distribution. Dynamic behaviour studies show that MWCNTs reduce vibration in roller bearings lubricated with grease [30]. However, maintaining an optimal concentration of MWCNTs (typically below 0.5 wt.%) is crucial to avoid agglomeration and precipitation. Beyond that threshold concentration, strong Van der Waals interactions can hinder their effectiveness in reducing friction and wear [55]. In a study with SAE 10W40 engine oil, using MWCNTs as additives reduced the CoF by 56% and the WSD by 67% showing better tribological properties than SWCNTs [56]. MWCNTs with 0.08 wt.% polymeric aryl phosphates (PAPs) improved friction reduction by approximately 60% and anti-wear performance by about 95% [57]. Ball on disc tests (using SRV 5 tribometer) conducted on COOH-functionalized MWCNTs dispersed in polyalphaolefin (PAO 4 and PAO 6) in different concentrations (0.025 - 0.15 wt.%) showed significant reduction in the CoF by around 27% and the wear volume by approximately 88% at 0.05 wt.% and 0.025 wt.% of CNTs in PAO,

respectively [58]. Fly-ash derived (OFA) CNTs as lubricant additives in base oils (Saudi Aramco 100SN, 500SN, and 150BS) exhibited superior tribological performance even at very low concentrations. These CNTs were more effective in reducing the CoF. A 20% reduction in the CoF at a CNT concentration of 0.1 wt.% was noticed [51]. A base oil mixed with MWCNTs was used as a lubricant on nodular cast iron surfaces in contact with steel to evaluate its tribological performance using a pin-on-disc method. Incorporating MWCNTs into the base oil improved its ability to bear load and its stability as a lubricant. The processes that led to the enhanced performance of the lubricating oil with MWCNTs on nodular cast iron were also explored, scrutinized, and recorded [59]. Experimental trials were carried out on Mobil gear 627 and paraffinic mineral oils, both infused with different quantities of MWCNTs as additives, to assess their AW, load-bearing ability, and CoF. The outcomes from these trials suggest that incorporating MWCNTs into base oils aids in friction reduction and enhances AW characteristics. Wear trials demonstrate that mineral oil with MWCNTs decreases wear by 68% and 39% in comparison to the base Mobil gear 627 and paraffinic mineral oils, respectively. Moreover, measurements of friction reduction reveal that mineral oil with MWCNTs reduces friction by about 57% and 49% compared to the base Mobil gear 627 and paraffinic mineral oils, respectively [60]. MWCNTs were dispersed in SAE 10W40 oil using ultrasonic waves and used as additives. The flow properties of the MWCNT nanolubricant samples displayed non-Newtonian traits (shear-thinning), while the SAE 10W-40 oil showed behaviour like a Newtonian fluid. The CoF reduced by 4%-34% and 26%-32% under varying loads and velocities. Furthermore, after a sliding distance of 22.57 km at a load of 240 N and a speed of 0.33 m/s, the specific wear rate of the surfaces reduced by 29% and 40%, respectively. These findings imply that MWCNTs could be effective additives in lubricants [61].

4.4 2D MLG Particles as Additives in Lubricants

Figure 57 shows the FESEM images of NGF and EG. It can be observed from Fig. 57 (a) that the NGF is constituted by ~500-700 µm sized flakes-like morphology, which changes into an accordion-like shape after exfoliation. It can be observed from Fig. 57 (b) that EG has a puffy worm-like morphology. When these puffy worms were subjected to rapid liquid phase shearing and followed by cavitation-induced intense local shock-wave energy release during probesonication, they were fragmented into particles with fewer graphene sheets named MLG particles, which had sheet-like morphology with a lateral size of few microns and thickness in nanometres as shown in Figs. 58 (a) and (b), respectively. When used as a lubricant additive, the large lateral dimensions of the MLG particles are expected to reduce the direct contact area

between the surfaces sliding over each other, minimizing the friction during sliding. The high-resolution TEM image (Fig. 58 (b)) shows the layered structure of one representative MLG particle, each constituted by 8-12 graphene layers. This layered structure of MLG is expected to enhance the lubrication properties when MLG is used as a lubricant additive because these layers are held by weak Van der Waals bonding and can easily slide under shearing forces.

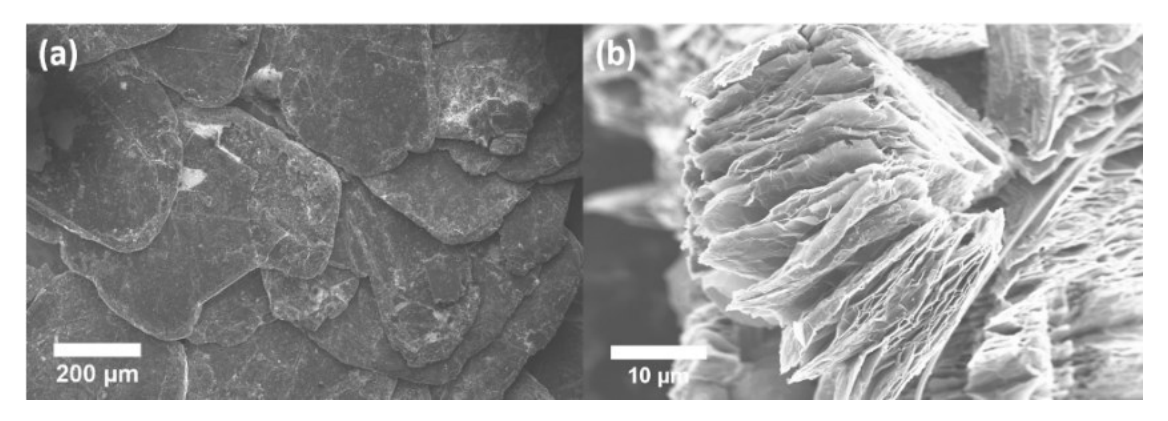


Figure 57. FESEM images of (a) NGF and (b) EG.

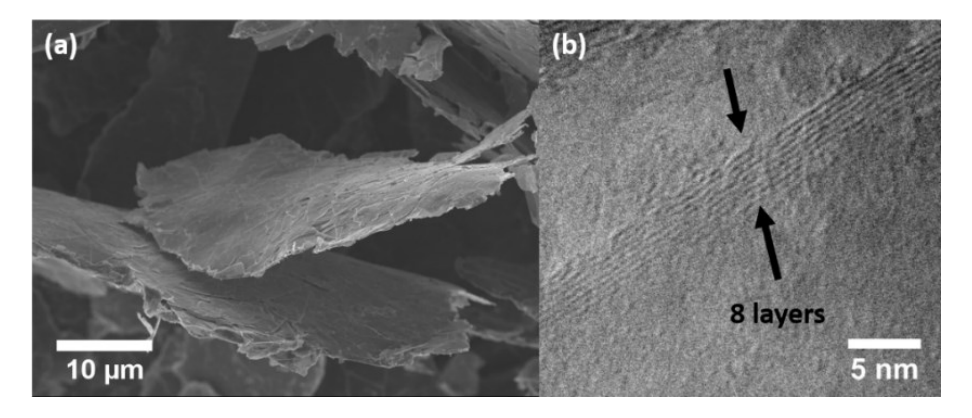


Figure 58. (a) FESEM and (b) HRTEM image of MLG particles.

The formation of MLG was further confirmed by analyzing XRD (Fig. 59) and Raman scattering (Fig. 60) results. The diffraction peaks in the XRD pattern of NGF are indexed to the characteristic (002) and (004) crystallographic planes in graphite (COD database file no. 96-901-1578) [62]. The d-spacing in NGF was calculated using the diffraction peak at 26.22 (0.339 nm), while the calculated crystallite size (La) using the Scherrer equation is 61.85 nm. In the case of MLG (i.e., the product exfoliated from NGF), the diffraction peak corresponding to (002) crystallographic plane is recorded at 26.66° (a higher diffraction angle in comparison to that in NGF) corresponding to a reduced d-spacing of 0.334 nm and La of 28.90 nm. Electron microscopic and XRD observations confirm that the MLG particles retained the graphitic nature but with only 8-12 graphene layers in each MLG particle.

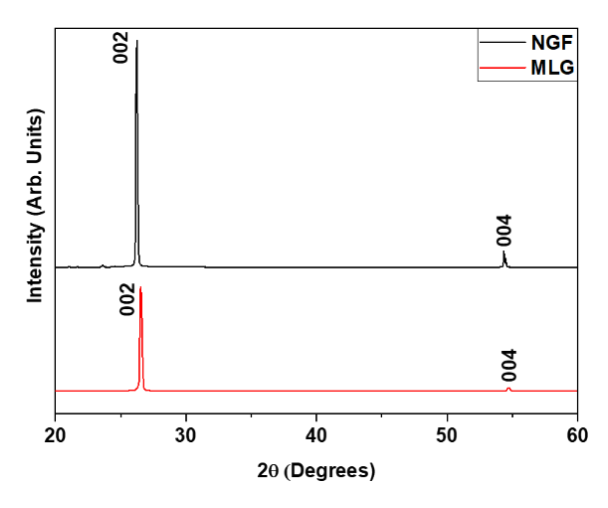


Figure 59. X-ray diffraction patterns of NGF and MLG.

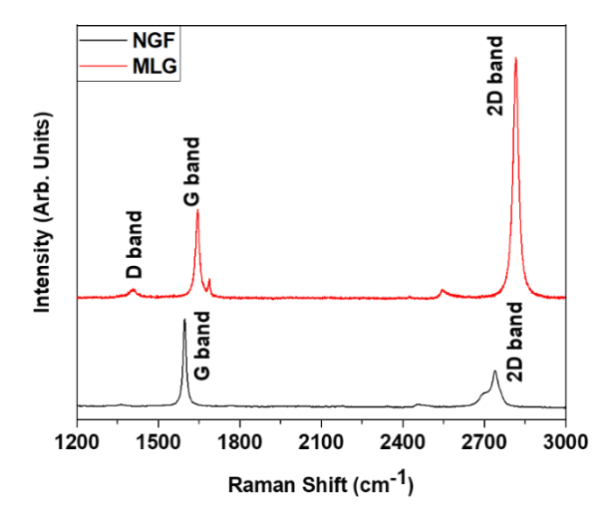


Figure 60. Raman spectra of NGF and MLG.

In Fig. 60, the Raman spectra of NGF and MLG are compared. The two prominent peaks in the spectrum of NGF are the G band at ~1585 cm⁻¹ and the 2D band at ~2700 cm⁻¹. In the case of MLG, the D and 2D bands are recorded at ~1352 cm⁻¹ and ~2703 cm⁻¹, respectively. The D band observed in the Raman spectrum of MLG is attributed to the defects induced during the intensive shearing and exfoliation. A distinctive difference is observed when the shape and the intensity of the 2D band (Figs. 61 and 62) in the case of NGF and MLG are compared. Typically, the 2D band of graphene is a single sharp peak, while that of graphite consists of two components, 2D₁ and 2D₂. The intensity of 2D₁ and 2D₂ is almost ½ and ½ th of that of the G band. The double structure of the 2D band in graphite is attributed to the intervalley double resonance (DR) mechanism that involves a transition between two inequivalent neighboring K points (K and K') of the hexagon of the first Brillouin zone of the graphite [63]. In the case of graphenaceous materials, the 2D band evolves with the number of layers present

and how the DR process links phonon wave vectors to the electronic band structure of graphenaceous materials [64-66]. The 2D band is observed at ~2739 and ~2703 cm⁻¹ for NGF and MLG, respectively. The observed 2D band's red shift in the case of MLG indicates that the exfoliation has led to the formation of MLG [64-66].

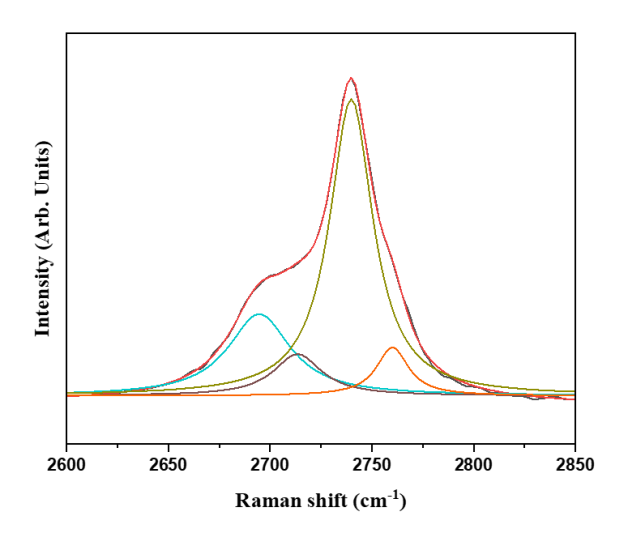


Figure 61. Peak fit of 2D Raman band in NGF.

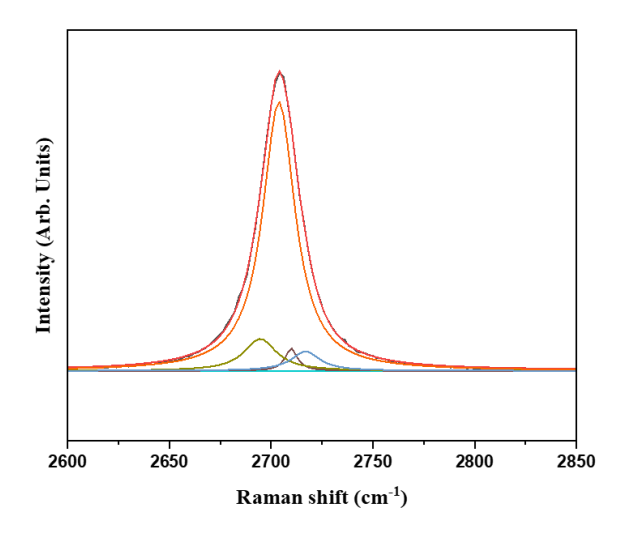


Figure 62. Peak fit of 2D Raman band in MLG.

The BO, CO, and respective MLG dispersed samples are subjected to a shear rate of 0 to $1000~\text{sec}^{-1}$ to observe the rheological behaviour of the samples. The apparent viscosity (η) and shear stress (τ) profiles of BO and BO-NL samples (BO-NL1, BO-NL2, and BO-NL3) are shown in Figs. 63 (a) and 63 (b), respectively. In the case of BO, η is ~150-155 cP, indicating a negligible shear thinning as the shear rate increased beyond 700 sec⁻¹, leading to a 6% reduction in the viscosity. BO-NL1 exhibits an overall increased viscosity of 173.7 cP, with

visible shear thinning leading to a loss of nearly 15% of the initial viscosity towards the end of the measurement. Dispersing different concentrations of MLG in BO induces uncertain rheological changes. In the case of BO-NL2, η is ~150.7 cP, surprisingly showing a non-Einstein-like reduction in viscosity with no noticeable shear thinning. A further increased concentration of MLG in BO, i.e., BO-NL3, again shows a leap in viscosity to 181.1 cP with no signs of shear thinning. While on the one hand, reports on the reduced viscosity of media upon the addition of various nanoparticles and related explanations are available, few articles mentioning an increase in viscosity after the addition of nanoparticles are also available [67-70]. The uncertainty on the changes in rheological properties upon the addition of nanoparticles requires in-situ studies on the fluid-particle interaction both physically and chemically to understand these anomalies better along with supporting information generated with tools like machine learning to design a nanolubricant effectively [71].

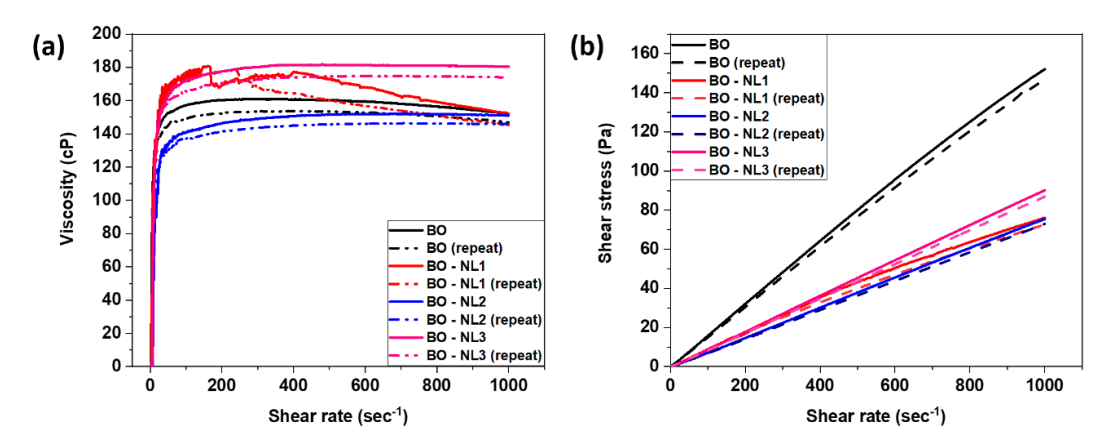


Figure 63. (a) Viscosity and (b) shear stress profiles of BO and BO-NL samples.

The BO and BO-NL samples' measured flow curves (shear stress versus shear rate) are shown in Fig. 63 (b). A linearly increasing trend is observed between the applied shear rate and shear stress for all the samples. It is evident from Fig. 63 (b) that all the samples start to flow as soon as the shear rate is applied and do not require the shear stress to reach a specific value to enable flow in the fluids (i.e., yield stress = 0). However, it is also observed that all the BO-NL samples exhibit lesser shear stress than the BO, which theoretically means they have lesser internal resistance to flow under an applied external force (shear rate) which doesn't correlate well with the corresponding viscosity profiles in Fig. 63 (a) The abrupt increase/decrease in viscosity due to the varying MLG concentration could be linked to several factors such as nanoparticle – fluid interaction, agglomeration of MLG or non-homogenous dispersion. Along with these factors, fluid dynamic aspects could also occur at molecular levels, leading to

unpredictable property changes. For instance, a turbulent flow in the BO-NL samples could occur during the rotational rheology measurements, causing the oil molecules and MLG nanoparticles to undergo random inter-layer movement, forming eddies/vortices and giving specious results. The measured viscosity values may be higher than the actual values due to pseudo-internal resistance among fluid layers being measured by the instrument. η and τ profiles of CO and CO-NL samples (CO-NL1, CO-NL2, and CO-NL3) are shown in Fig. 64 (a) and 64 (b), respectively.

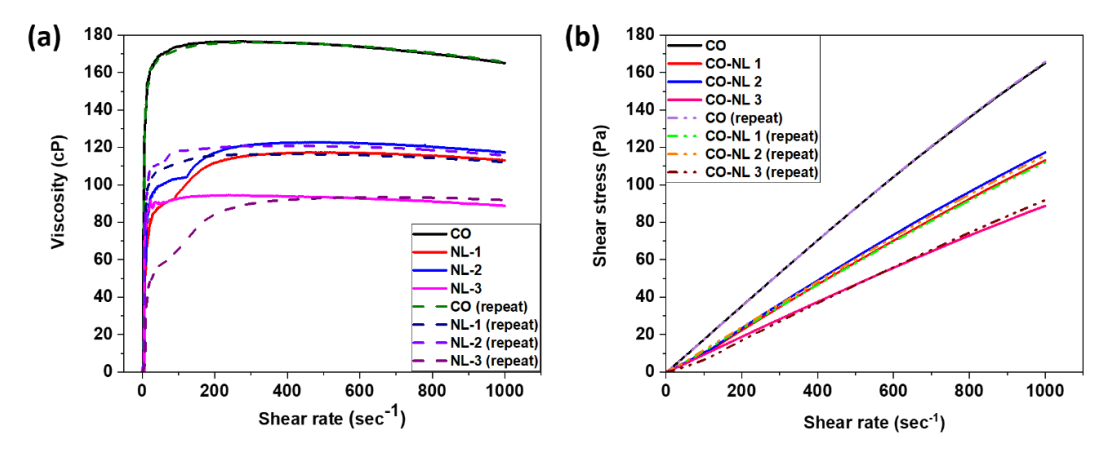


Figure 64. (a) Viscosity and (b) shear stress profiles of CO and CO-NL samples.

Adding MLG to CO reduces the viscosity of CO by 30% to 46%, depending on the MLG concentration. The CO and CO-NL samples show negligible shear thinning as the shear rate increased beyond 800 sec⁻¹. CO has an overall η 175.5 cP, which reduces as MLG is added. With regards to η , CO-NL1 and CO-NL2 remain close (112 cP and 117 cP, respectively) to that of CO, while CO-NL3 shows the highest reduction with η value as 91.9 cP. The measured flow curves (shear stress versus shear rate) of CO and CO-NL samples are shown in Fig. 62 (b). It is apparent from Fig. 63 and 64 adding fractional quantities of MLG to the BO and CO affects the rheological properties, primarily reducing the internal resistance between the fluid layers to flow. Although a lesser resistance to flow implies an improved flowability for the lubricants, excess reductions in the viscosity of oils can be detrimental as that would not allow the tribo-layer to withstand the contact stresses at the interface and will undergo continuous deformation, leading to high friction and wear. Therefore, the MLG concentration required for dispersion must be correlated with relevant tribological performance to improve the rheological and lubricating properties. Four ball wear tests at room temperature (RT) and as per ASTM-D 4172 were performed, and improvements in CoF and wear reduction were observed when BOand CO-supplemented with low concentrations of MLG were used as lubricants. Avg. CoF and

CoF profiles recorded in the case of BO and BO-NL samples are shown in Fig. 65. At RT, the avg. CoF of BO-NL1 (which is 0.055) is 16.66% less than the CoF of BO (which is 0.066). However, with further addition of MLG to BO, i.e., in the case of BO-NL2 and BO-NL3 samples, the average CoF shoots up to 0.07 (6% increase) and 0.095 (43.93% increase), respectively. This undesirable increase in CoF with MLG dispersion is attributed to a combined effect of abrupt changes in viscosity and agglomeration of MLG at higher concentrations. At 75 °C, the average CoF values follow a similar trend as those observed at RT.

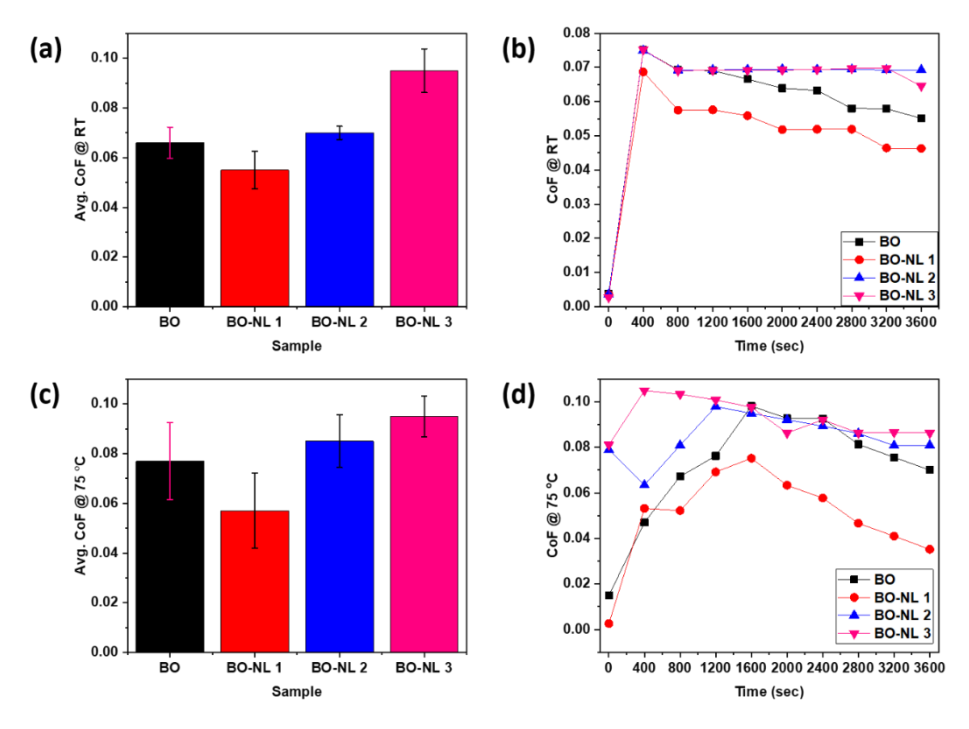


Figure 65. (a) Average CoF and (b) CoF profile of BO and BO-NL samples at RT; (c) average CoF and (d) CoF profile of BO and BO-NL samples 75 °C.

At 75 °C, the average CoF of BO-NL1 is the lowest (which is 0.057), which is 25.97% lower than the average CoF of BO (which is 0.077). The BO-NL2 and BO-NL3 were found to show an increased average CoF value of 0.085 and 0.095, which are 10.38% and 23.37% higher than the average CoF value of BO. The CoF profiles in Fig. 65 (d) clearly show that BO-NL2 and BO-NL3 exhibit a very high frictional behaviour throughout the test, while the BO-NL1 shows a reducing CoF after 1600 sec. Average CoF and CoF profiles recorded in the case of CO and CO-NL samples are shown in Fig. 66. At RT, after an initial CoF of ~0.08, the wear test specimens lubricated using CO become poorly lubricated (400 sec to 1200 sec), because of which there is a spike seen in the CoF to 0.15 which remains constant after 1200 sec till the end of the test. This shift in regime resulting in increased CoF can be attributed to the failure

of CO to form an effective tribo-layer and keep the CoF low. With the addition of MLG, it is observed that no such shift of regimes is visible, implying that the point of contacts being lubricated remains in the same regime throughout the test duration. The CO-NL1 sample shows a low CoF of ~0.065 throughout the test, with an average CoF of ~0.073 after multiple repetitions. The CO-NL2 shows a slight increase in the avg. CoF (0.078), while the CO-NL3 sample showed no improvement in the CoF. From Fig. 66 (a), CO-NL1 is most effective in CoF reduction. Adding 0.1wt.% of MLG to CO improves its CoF-reducing ability by 25.5%, while CO-NL2 showed a 20.4% CoF reduction when compared to CO. However, the avg. CoF of CO-NL3 shows an increase of 1% compared to CO.

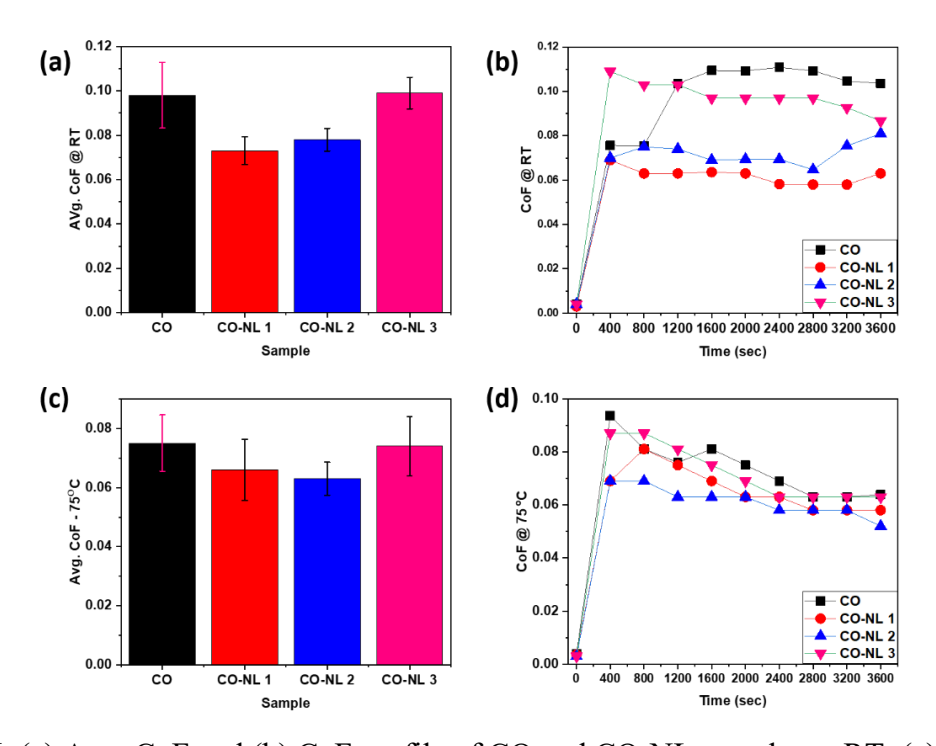


Figure 66. (a) Avg. CoF and (b) CoF profile of CO and CO-NL samples at RT; (c) avg. CoF and (d) CoF profile of CO and CO-NL samples 75 °C.

The poor friction characteristics of NL3 samples are speculated to be due to the drastic reduction of the rheological characteristics (Fig. 63 and 64) and undesired additives' agglomeration in the base fluids. In the case of CO-NL3, the drastically reduced viscosity and shear stress do not allow the oil to form a stable tribo-film on the contacting surfaces. In other words, the lubricant fails under the impact of high contact stress at the point of contact. The agglomerated MLG particles in the lubricant induce an adverse effect and resist the smooth sliding of the wear test specimens at the point of contact, resulting in an increased CoF at the interface. At 75 °C, the avg. CoF of CO (which is 0.075) was reduced by 12% and 16% when

CO-NL1 and CO-NL2 were used as lubricants, respectively. The avg. CoF of CO-NL3 was almost the same as that of CO. Fig. 64 (d) shows that CO and CO-NL samples have similar profiles from the start till the end of the test. Initially (at 400 sec), the CoF values are substantially higher for CO and CO-NL3 than CO-NL1 and CO-NL2. However, the values end up in the same range towards the end of the tests. The maximum and minimum CoF values resulting from using all the lubricants are presented in Table 7.

Table 7. Maximum and minimum CoF values when BO, CO, and respective MLG dispersed samples are tested as lubricants

Sample	Maximum CoF		Minimum CoF	
	at RT	at 75 °C	at RT	at 75 °C
ВО	0.0751	0.098	0.055	0.07
BO – NL1	0.0687	0.075	0.046	0.0352
BO – NL2	0.0751	0.097	0.069	0.080
BO – NL3	0.0751	0.104	0.064	0.0863
СО	0.110	0.093	0.075	0.063
CO – NL1	0.07	0.081	0.058	0.058
CO – NL2	0.07	0.069	0.064	0.052
CO – NL3	0.109	0.087	0.086	0.063

Wear scar depth (h) and the wear volume loss (V) directly indicate the material removed from the wear scar area. An increase or decrease in these values can be used to assess the wear resistance ability induced by the lubricants. Fig. 67 shows the wear-resistance characteristics (h in mm and V in mm³) when BO and BO-NL samples were used as the lubricants at RT and 75 °C. Adding MLG to BO reduced the avg. WSD at RT (Fig. 65 (a)). However, it is observed (Fig. 65 (a)) that the avg. WSD in the case of BO-NL samples increased as the concentration of MLG increased from 0.1wt.% to 0.5wt.%.

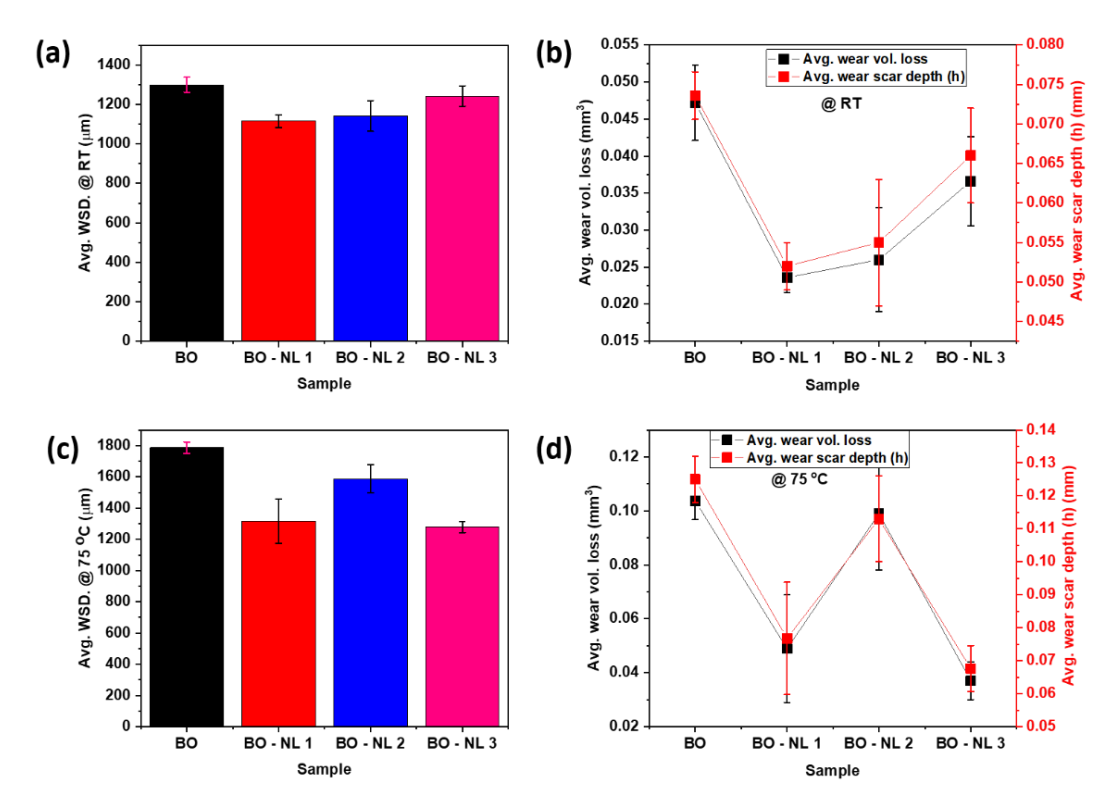


Fig. 67. (a) Avg. WSD and (b) wear volume loss and avg. wear scar depth of the test specimens at RT; (c) avg. WSD and (d) wear volume loss and avg. wear scar depth of the test specimens at 75 °C. Here, BO and BO-NL samples are used as the lubricants.

Using the BO-NL1 sample as the lubricant resulted in a 14.10% reduction in the WSD compared to BO. When BO-NL2 and BO-NL3 samples were used as lubricants, WSD was reduced by 12.18% and 4%, respectively. Fig. 67 (b) also shows that h and V were reduced when BO-NL samples were used as the lubricants. In the case of BO-NL1, the reduction is as high as 50% at RT. Similar trends in h and V were observed at 75 °C, as shown in Fig. 67 (c) and 67 (d). Even though overall improvement is observed when BO-NL samples (including that of BO-NL2 sample) were used as lubricants, the slightly anomalous observation in the BO-NL2 sample (among BO-NL samples) is unclear and needs further investigation.

Figure 68 shows the wear-resistance characteristics when CO and CO-NL samples were used as the lubricants at RT and 75 °C. Adding MLG to CO reduced the avg. WSD at RT (Fig. 68(a)). Fig. 68 (b) also shows that h and V were reduced when CO-NL samples (except for an anomaly in h when CO-NL3 was used as a lubricant) were used as the lubricants. A similar trend of wear-resistance characteristics was observed when the CO-NL samples were tested at 75 °C (Fig. 68 (c) and (d)). However, CO-NL2 as the lubricant gave the best results at 75 °C. It may be noted that with the testing temperature at 75 °C, the viscosity of CO will tend to

reduce considerably, thereby reducing the lubricity of the CO. From the observations shown in Fig. 68, both lower (i.e., CO-NL1) and higher (i.e., CO-NL3) concentration of MLG in CO fails to provide good wear resistance at 75 °C. In the case of CO-NL1, the concentration of MLG sheets is inadequate enough to minimize material wear at the interface. In contrast, in the case of CO-NL3, the concentration of MLG sheets is more than adequate, resulting in their agglomeration and failing to be appropriate wear preventive additive in lubricants.

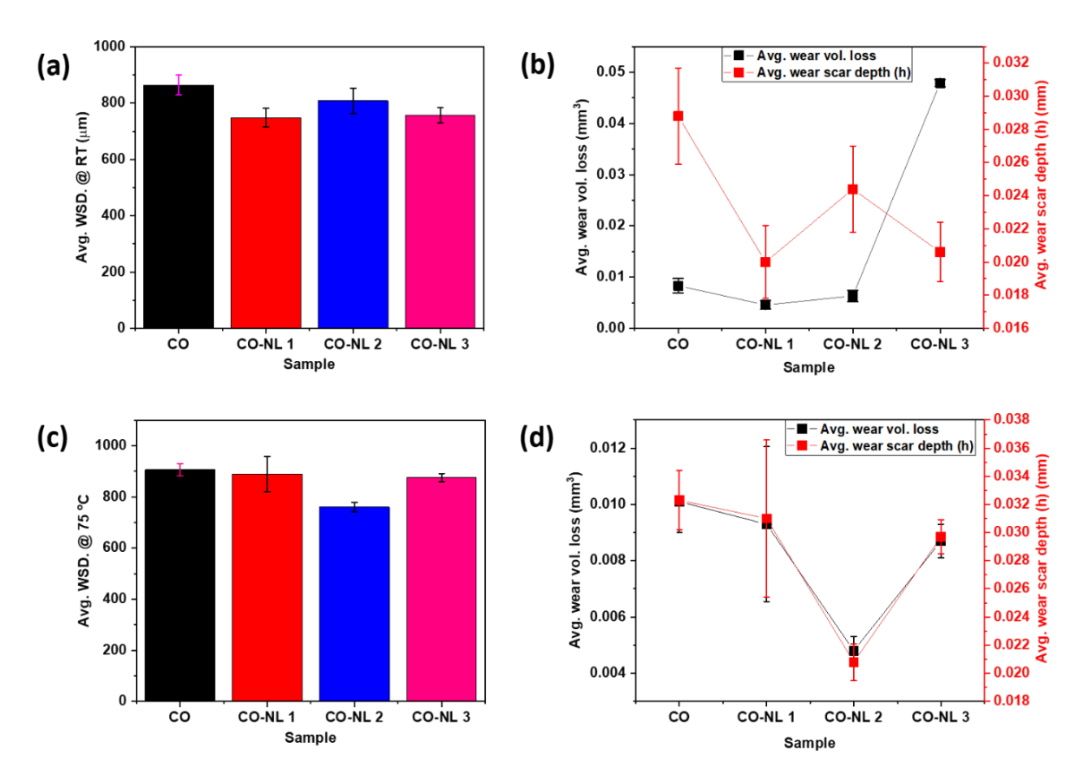


Figure 68. (a) Avg. WSD and (b) wear volume loss and avg. wear scar depth of the test specimens at RT; (c) avg. WSD and (d) wear volume loss and avg. wear scar depth of the test specimens at 75 °C. Here, CO and CO-NL samples are used as the lubricants.

The observations made from Figs. 67 and 68 suggest that depending on the operating conditions, the additives' concentration should be optimally chosen even when the additives have all the primary characteristics to be excellent lubricant additives. The optical micrographs of the wear scars (i.e., WSD) on the contacting surfaces after the wear tests using BO, CO, and respective MLG dispersed lubricants are shown in Fig. 69 and 70. The highest reductions in WSD are observed when BO-NL and CO-NL samples are used as lubricants. Along with the decrease in the WSD, the wear intensity within the scar also appears less severe in the optical micrograph corresponding to BO-NL1 (Fig. 69 (b)). At 75 °C, the role of MLG in BO becomes more crucial as the WSD on the tested specimen with BO shows a heavily worn-out scar, while the wear scars observed in the case of BO-NL samples are less intense.

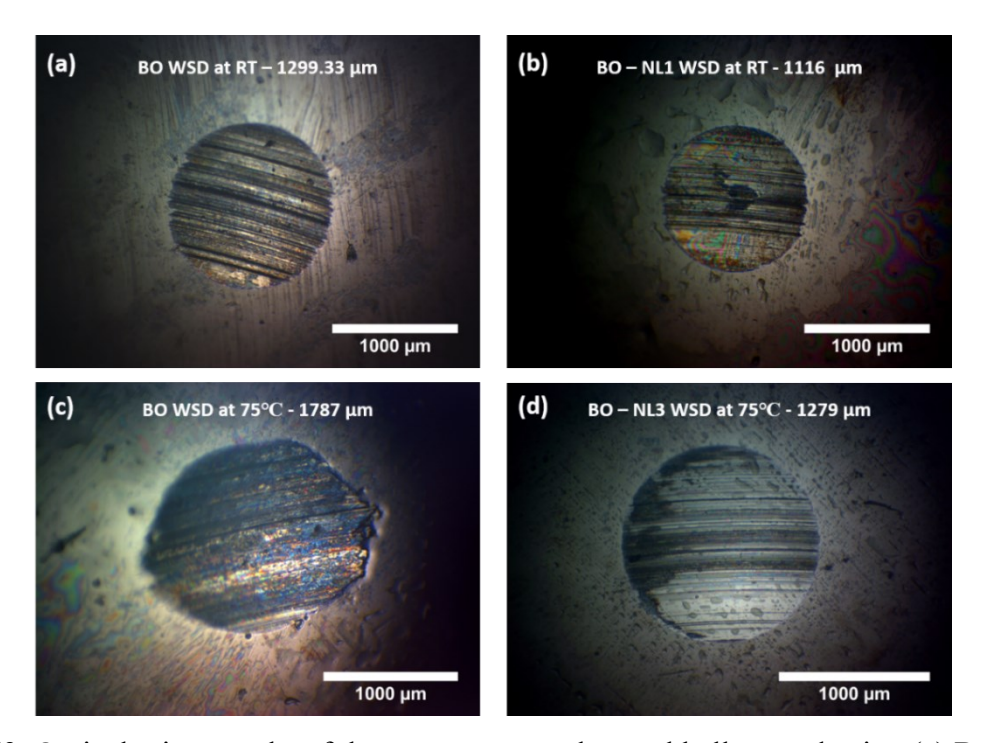


Figure 69. Optical micrographs of the wear scars on the steel balls tested using (a) BO at RT, (b) BO-NL1 at RT, and (c) BO at 75 °C and (d) BO-NL3 at 75 °C.

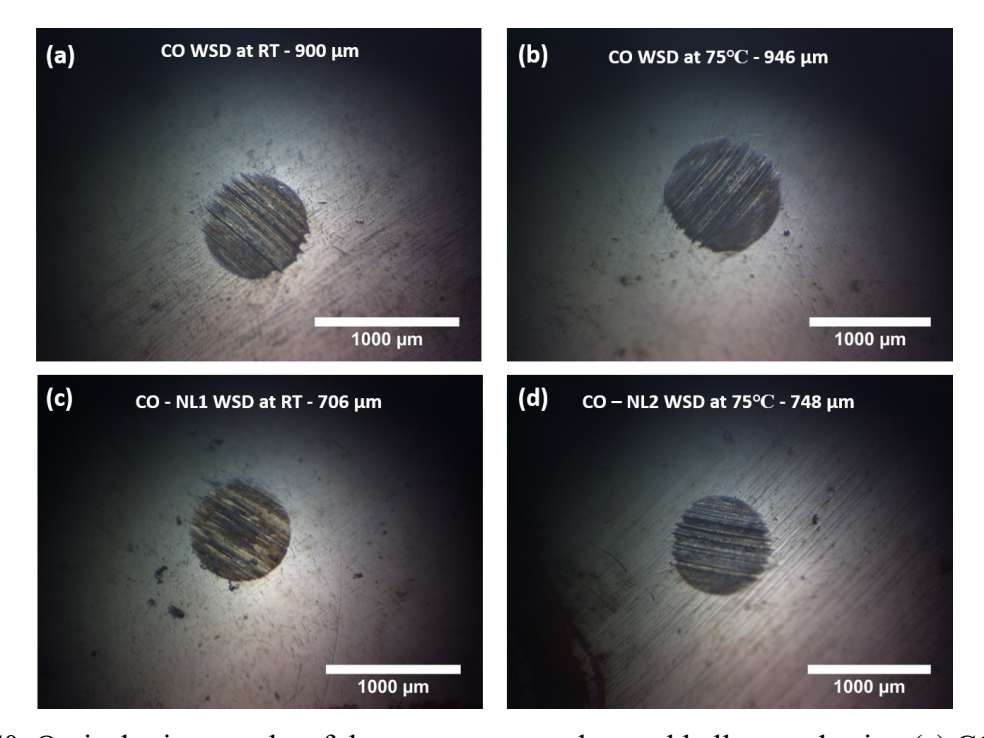


Figure 70. Optical micrographs of the wear scars on the steel balls tested using (a) CO at RT, (b) CO at 75 °C, (c) CO-NL1 at RT, and (d) CO-NL2 at 75 °C.

Although WSD values in the case of BO-NL1 and BO-NL3 are very much in close range, the highest WSD reduction was observed in the case of BO-NL3 as compared to that of BO, along with the substantial reduction in the wear severity. However, a cumulatively improved friction and wear reduction performance is observed in the case of BO-NL1. Adding MLG to the BO helps improve its lubricity as the MLG nanosheets form a tribo-layer at the point of contact, minimizing the direct metal-metal contact. A similar reduction in WSD was noticed in the case of CO-NL samples (Figs. 70 (a-d)). The MLG does not exhibit any antagonistic lubricating properties with the pre-dispersed additives present in the CO. Both at RT and 75 °C, a considerable reduction in the WSD was observed when CO-NL1 and CO-NL2 samples were used as lubricants. At RT, a very low concentration of MLG in CO (i.e., the case of CO-NL1) is sufficient to elevate its tribological characteristics. However, at 75 °C, when the oils tend to lose their viscosity drastically, CO-NL2 performed better. To keep the friction and wear low, the lubricant must have appropriate viscosity and an adequate quantity of additives to withstand the contact pressure at the interface and the test conditions. With increasing temperature, the loss of viscosity in lubricants is inevitable. At this point, the additives (here, MLG) play a crucial role in keeping friction and wear at a minimum. At 75 °C, due to the viscosity loss in CO, a higher concentration of MLG nanosheets is needed for adequate lubrication, as observed in the case of CO-NL2.

The underlying lubrication mechanism of MLG is shown in Fig. 71. When graphene is optimally added to the lubricants, it produces a firm, homogenous, and stable boundary layer on the contact surfaces. Graphene serves as a shield between the contacting surfaces, preventing direct metal-to-metal contact and minimizing friction. Graphene offers an incredibly smooth and low-shear sliding surface. This results in less surface wear and less energy loss due to friction. Its strength and load-bearing capability allow it to endure high loads while avoiding damage to the underlying surfaces. MLG comprises stacked graphene layers. Due to the weak interlayer forces, the layers in MLG can glide over one other with negligible friction, resulting in a slick surface. Although the carbon-carbon inter-layer bonds are strong, the forces keeping the layers together are weak. Under external pressures, the layers readily tear or glide past one other, minimizing friction. This is referred to as basal plane cleavage. Graphite has anisotropic friction qualities, meaning it has much less friction in the direction parallel to its basal planes than in the perpendicular direction. This anisotropy improves its self-lubricating properties even further. The MLG is derived from graphite to exhibit a similar phenomenon at the nanoscale. The protective boundary layer may be less robust and uniform

at lower MLG concentrations, resulting in higher metal-to-metal contact, causing less pronounced friction and wear reduction. This implies that using higher MLG concentrations in lubricants would give better lubrication but with diminishing returns if the MLG concentration used is beyond the optimal concentration. Excess MLG can create thicker, less stable boundary layers, which may increase friction due to the roughness of the layers and the possibility of agglomeration. Excess MLG also diminishes the overall viscosity of the lubricant, resulting in a lower load-bearing capacity. It should be noted that the appropriate MLG concentration varies based on the individual lubrication application. Therefore, the optimal concentration should be figured out through proper experimentation.

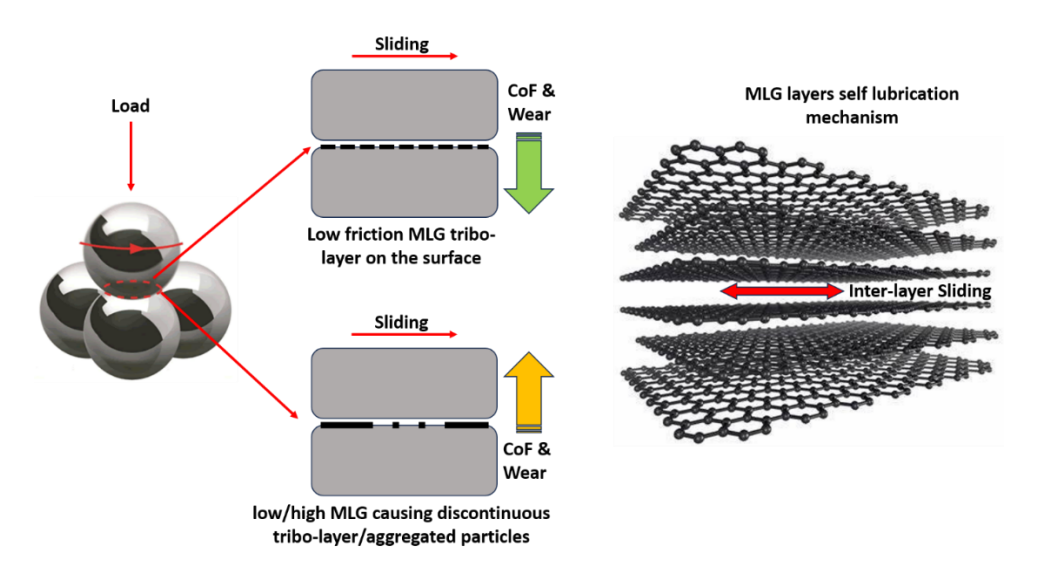


Figure 71. Underlying lubrication mechanism of MLG.

Raman data (Fig. 72) was collected from the representative wear scars to confirm MLG particles' friction and wear reduction participation. The wear scars of the specimens tested using the MLG containing BO and CO samples showed the presence of MLG (the presence of G-band and 2D-band in the corresponding Raman spectra). The MLG particles are found more prominently in the specimens of BO with MLG. The particles inside the wear scars indicated that their presence lowers the CoF and wear. The presence of α-Fe₂O₃ indicates oxidation of the wear scars. The concentration of the graphene, the number of layers of graphene nanosheets, the dispersion stability, and the lubrication conditions are the most critical elements that determine the lubricating characteristics of graphene-based nano lubricants [72-75].

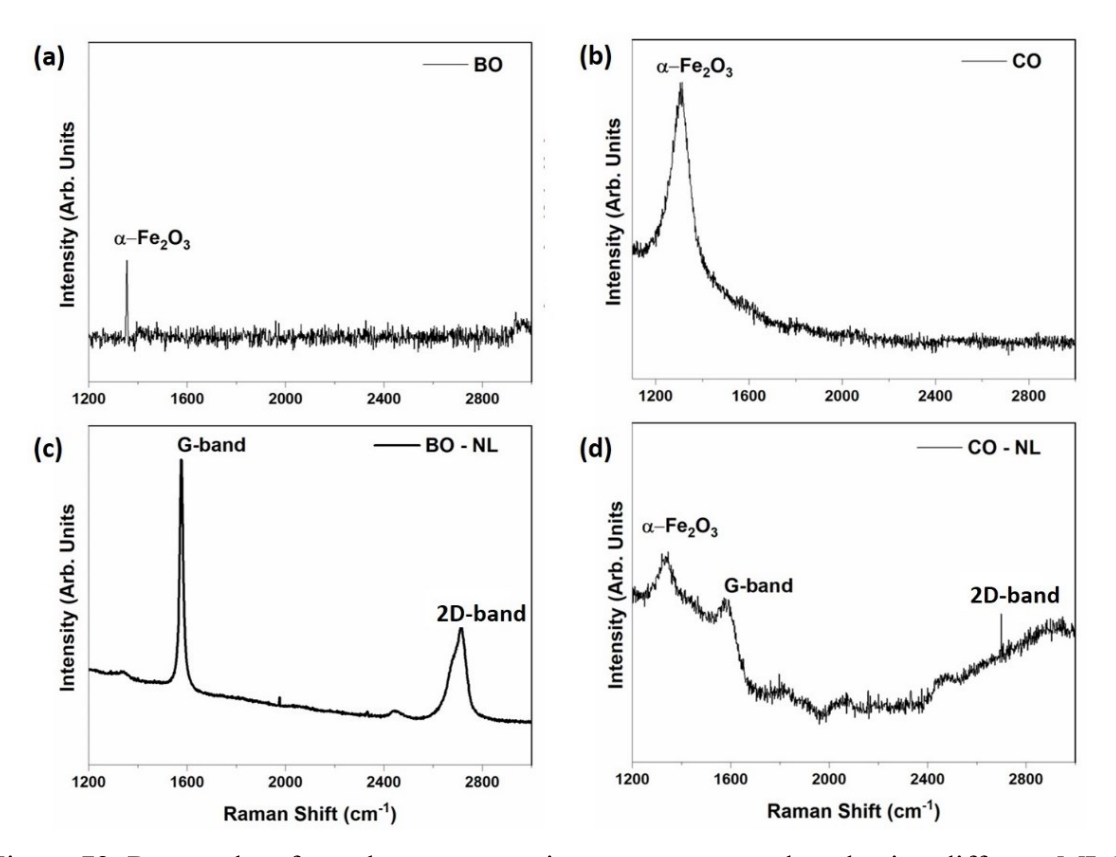


Figure 72. Raman data from the representative wear scars produced using different MLG dispersed BO and CO lubricant samples.

Graphene derived from top-down processes is more viable for application as lubricant additives, considering the aspects of yield and sustainability. A unique approach based on concentrated solar radiation was utilized to exfoliate graphite oxide, yielding ultrathin graphene. The frictional characteristics (FC), antiwear (AW), and extreme pressure (EP) qualities of graphene-based engine oil nanofluids have been studied. Compared to base oil, nanofluids enhance their FC, AW, and EP qualities by 80%, 33%, and 40%, respectively. The improvement was ascribed to graphene's nano-bearing mechanism in engine oil and graphene's ultimate mechanical strength [76]. However, this study's approach to producing graphene appears exotic but practically unsustainable. Electrochemically exfoliated graphene diffused consistently in polyethylene glycol 200 (PEG200) enhanced tribological properties, remarkably thinner and smaller modified graphene with decreased friction and wear (reduced by 16% and 25.9%, respectively). The modified graphene and as-formed protective layer on the mating contacts provide this important lubricating function. Furthermore, the interfacial contact changed the additive into an overlapping and ordered-sheet structure [77]. Experimental studies with 3-dimensional graphene nanosheets produced in an arc-discharge chemical vapor deposition as a lubricant additive showed tribological improvements. Under low and high loads (4.2 mm/s sliding speed and roughly 1.0 GPa contact pressure), the reduction in friction and wear were 29.1% and 55%, respectively, compared to the base oil. However, the material failed to lubricate effectively at higher loads owing to deteriorated structure [78]. Thermally reduced graphite oxide (Gr-O) was explored as a lubricant additive in a base oil. The base oil's varying CoF between 0.15 and 0.20 was significantly reduced by using 0.5wt.% Gr-O in the oil. At more significant concentrations (1.0 wt.%), the Gr-O particles were suspected to aggregate and block the sliding motion, resulting in a higher friction coefficient. Also, it was concluded that the structural flaws of fold and wrinkling in Gr-O nanosheets can reduce their lubricating properties [79]. In a study using commercially procured graphene nano additives in a 5W30 oil, CoF was decreased by 15%, and wear scar was reduced by 33%. The worn surfaces were characterized to understand the tribo-film formation of graphene nano additives [67]. The tribological behavior of lubricants (Pongamia oil and 15W40 engine oil) with and without the addition of commercial graphene nanoplatelets (GNPs) was studied. Worn surface analysis revealed the polishing impact of GNPs on the surfaces. The inclusion of 0.05 wt.% GNPs in lubricants reduce friction and wear by 17.5% and 12.24% (Pongamia oil), respectively, and by 11.96% and 5.14% (15W40 engine oil), respectively [70]. The MLG was processed sustainably at kg-scale, and the lubricating properties obtained are at par with most reports and, in some cases, better. As the MLG is derived from graphite, the excellent lubricating properties of the parent material are translated to the MLG nanoparticles. Two lubricating media, i.e., BO (mineral oil) and CO (synthetic oil) were used for the experimental studies. The improvement in the friction and wear properties of BO and CO when using MLG as an additive demonstrates its compatibility with different types of lubricating media, thus showcasing its wide range of usability. The Raman analysis of wear scars throws light on the presence of MLG particles in the wear scars, which is attributed to the lower friction and wear.

References

- [1] R. Kali, B. Padya, T. Rao, P. Jain, Solid waste-derived carbon as anode for high performance lithium-ion batteries, Diamond and Related Materials 98 (2019) 107517.
- [2] J. Wei, M. Cai, F. Zhou, W. Liu, Candle soot as particular lubricant additives, Tribology Letters 53 (2014) 521-531.
- [3] M.-f. Guo, Z.-b. Cai, Z.-c. Zhang, M.-h. Zhu, Characterization and lubrication performance of diesel soot nanoparticles as oil lubricant additives, RSC advances 5(123) (2015) 101965-101974.

- [4] C.L.D.Z.X. Hu, Effect of biodiesel soot on the tribological behavior of liquid paraffin, China Petroleum Processing & Petrochemical Technology 20(3) (2018) 106.
- [5] G. Huang, Q. Yu, Z. Ma, M. Cai, F. Zhou, W. Liu, Fluorinated candle soot as the lubricant additive of perfluoropolyether, Tribology Letters 65 (2017) 1-11.
- [6] E. Hu, X. Hu, T. Liu, Y. Liu, R. Song, Y. Chen, Investigation of morphology, structure and composition of biomass-oil soot particles, Applied Surface Science 270 (2013) 596-603.
- [7] C. Li, Q. He, J. Fu, P. Pu, H. Liu, Q. Cheng, H. Luo, Q. Zhao, X. Wang, Utilization of biodiesel soot particles as additives for improved aqueous lubrication, IOP Conference Series: Earth and Environmental Science, IOP Publishing, 2021, p. 012049.
- [8] A. Sadezky, H. Muckenhuber, H. Grothe, R. Niessner, U. Pöschl, Raman microspectroscopy of soot and related carbonaceous materials: Spectral analysis and structural information, Carbon 43(8) (2005) 1731-1742.
- [9] R. Panickar, C. Sobhan, S. Chakravorti, Investigations on tribological properties of non-catalytic CVD synthesized carbon spheres in lubricant, Diamond and Related Materials 106 (2020) 107834.
- [10] E.A. Taborda, C.A. Franco, M.A. Ruiz, V. Alvarado, F.B. Cortes, Experimental and theoretical study of viscosity reduction in heavy crude oils by addition of nanoparticles, Energy & Fuels 31(2) (2017) 1329-1338.
- [11] D.S. Udawattha, M. Narayana, U.P. Wijayarathne, Predicting the effective viscosity of nanofluids based on the rheology of suspensions of solid particles, Journal of King Saud University-Science 31(3) (2019) 412-426.
- [12] N. Masoumi, N. Sohrabi, A. Behzadmehr, A new model for calculating the effective viscosity of nanofluids, Journal of Physics D: Applied Physics 42(5) (2009) 055501.
- [13] M.E. Mackay, T.T. Dao, A. Tuteja, D.L. Ho, B. Van Horn, H.-C. Kim, C.J. Hawker, Nanoscale effects leading to non-Einstein-like decrease in viscosity, Nature materials 2(11) (2003) 762-766.
- [14] J. Buongiorno, Convective transport in nanofluids, (2006).
- [15] T. Li, B. Pan, C. Wang, S. Zhang, S. Huang, Effect of eco-friendly carbon microspheres on the tribological behavior of lithium lubricating grease, UPB Sci. Bull. Ser. B 81 (2019) 57-68.
- [16] C. Wu, C. Wei, X. Jin, R. Akhtar, W. Zhang, Carbon spheres as lubricant additives for improving tribological performance of polyetheretherketone, Journal of Materials Science 54(6) (2019) 5127-5135.

- [17] X. Lv, L. Cao, T. Yang, Y. Wan, J. Gao, Lubricating behavior of Submicrometer carbon spheres as lubricant additives, Particulate Science and Technology 38(5) (2020) 568-572.
- [18] J.-F. Peng, M.-X. Shen, Z.-B. Cai, Nano diesel soot particles reduce wear and friction performance using an oil additive on a laser textured surface, Coatings 8(3) (2018) 89.
- [19] A. Hirata, M. Igarashi, T. Kaito, Study on solid lubricant properties of carbon onions produced by heat treatment of diamond clusters or particles, Tribology International 37(11-12) (2004) 899-905.
- [20] A.A. Alazemi, A.D. Dysart, V.G. Pol, Experimental investigation of the mechanical and surface properties of sub-micron carbon spheres, Lubricants 8(7) (2020) 77.
- [21] R.L. Vander Wal, M.Y. Choi, Pulsed laser heating of soot: morphological changes, Carbon 37(2) (1999) 231-239.
- [22] K. Bogdanov, A. Fedorov, V. Osipov, T. Enoki, K. Takai, T. Hayashi, V. Ermakov, S. Moshkalev, A. Baranov, Annealing-induced structural changes of carbon onions: high-resolution transmission electron microscopy and Raman studies, Carbon 73 (2014) 78-86.
- [23] M. Szerencsi, G. Radnoczi, The mechanism of growth and decay of carbon nano-onions formed by ordering of amorphous particles, Vacuum 84(1) (2009) 197-201.
- [24] A.N. Uttaravalli, S. Dinda, V.R. Kakara, A.R. Rao, T. Daida, B.R. Gidla, Sustainable use of recycled soot (carbon black) for the cleaner production of value-added products: a compendium, Chemical Engineering Journal Advances 11 (2022) 100324.
- [25] C. He, N. Zhao, C. Shi, X. Du, J. Li, Effect of annealing on the structure of carbon onions and the annealed carbon coated Ni nanoparticles fabricated by chemical vapor deposition, Journal of alloys and compounds 472(1-2) (2009) 230-233.
- [26] C. Houska, B. Warren, X-Ray study of the graphitization of carbon black, Journal of Applied Physics 25(12) (1954) 1503-1509.
- [27] D.C. Pujals, O.A. de Fuentes, L.D. Garcia, E. Cazzanelli, L.S. Caputi, Raman spectroscopy of polyhedral carbon nano-onions, Appl. Phys. A 120(1339) (2015) e1345.
- [28] L.M. Malard, M.A. Pimenta, G. Dresselhaus, M.S. Dresselhaus, Raman spectroscopy in graphene, Physics reports 473(5-6) (2009) 51-87.
- [29] F. Zhang, K. Fan, J. Yu, F. Saba, J. Sun, Pulsed direct current field-induced thermal stability and phase transformation of nanodiamonds to carbon onions, RSC advances 9(25) (2019) 14360-14371.
- [30] R. Nowduru, B.R. Bodapati, P.K. Penumakala, S.R.K. Malladi, P.K. Jain, V.V.S.S. Srikanth, Carbon soot nanoparticles derived from wasted rubber: An additive in lubricating oil for efficient friction and wear reduction, Diamond and Related Materials 126 (2022) 109050.

- [31] L. Joly-Pottuz, B. Vacher, N. Ohmae, J. Martin, T. Epicier, Anti-wear and friction reducing mechanisms of carbon nano-onions as lubricant additives, Tribology Letters 30 (2008) 69-80.
- [32] L. Joly-Pottuz, N. Matsumoto, H. Kinoshita, B. Vacher, M. Belin, G. Montagnac, J. Martin, N. Ohmae, Diamond-derived carbon onions as lubricant additives, Tribology International 41(2) (2008) 69-78.
- [33] L. Joly-Pottuz, E. Bucholz, N. Matsumoto, S. Phillpot, S. Sinnott, N. Ohmae, J. Martin, Friction properties of carbon nano-onions from experiment and computer simulations, Tribology Letters 37 (2010) 75-81.
- [34] N. Luo, J.-X. Xiang, T. Shen, H.-L. Liang, S. Xin, One-step gas-liquid detonation synthesis of carbon nano-onions and their tribological performance as lubricant additives, Diamond and Related Materials 97 (2019) 107448.
- [35] E. Hu, X. Hu, T. Liu, L. Fang, K.D. Dearn, H. Xu, The role of soot particles in the tribological behavior of engine lubricating oils, Wear 304(1-2) (2013) 152-161.
- [36] A. Bos, The temperature at the wear scars of the four-ball apparatus, Wear 31(1) (1975) 17-27.
- [37] I. Feng, A new approach in interpreting the four-ball wear results, Wear 5(4) (1962) 275-288.
- [38] F. Yunusov, A. Breki, E. Vasilyeva, O. Tolochko, The influence of nano additives on tribological properties of lubricant oil, Materials today: proceedings 30 (2020) 632-634.
- [39] C. Li, M. Li, X. Wang, W. Feng, Q. Zhang, B. Wu, X. Hu, Novel carbon nanoparticles derived from biodiesel soot as lubricant additives, Nanomaterials 9(8) (2019) 1115.
- [40] E.W. Bucholz, S.R. Phillpot, S.B. Sinnott, Molecular dynamics investigation of the lubrication mechanism of carbon nano-onions, Computational materials science 54 (2012) 91-96.
- [41] Y. Jung, J. Hwang, C. Bae, Assessment of particulate matter in exhaust gas for biodiesel and diesel under conventional and low temperature combustion in a compression ignition engine, Fuel 165 (2016) 413-424.
- [42] N. Savic, M.M. Rahman, B. Miljevic, H. Saathoff, K.-H. Naumann, T. Leisner, J. Riches, B. Gupta, N. Motta, Z. Ristovski, Influence of biodiesel fuel composition on the morphology and microstructure of particles emitted from diesel engines, Carbon 104 (2016) 179-189.
- [43] D.J. Growney, O.O. Mykhaylyk, L. Middlemiss, L.A. Fielding, M.J. Derry, N. Aragrag, G.D. Lamb, S.P. Armes, Is carbon black a suitable model colloidal substrate for diesel soot?, Langmuir 31(38) (2015) 10358-10369.

- [44] A. Kontou, M. Southby, H. Spikes, Effect of steel hardness on soot wear, Wear 390 (2017) 236-245.
- [45] E. Hu, K. Dearn, B. Yang, R. Song, Y. Xu, X. Hu, Tribofilm formation and characterization of lubricating oils with biofuel soot and inorganic fluorides, Tribology International 107 (2017) 163-172.
- [46] A. Clague, J. Donnet, T. Wang, J. Peng, A comparison of diesel engine soot with carbon black, Carbon 37(10) (1999) 1553-1565.
- [47] G. Ferraro, E. Fratini, R. Rausa, P. Fiaschi, P. Baglioni, Multiscale characterization of some commercial carbon blacks and diesel engine soot, Energy & Fuels 30(11) (2016) 9859-9866.
- [48] A.L. Boehman, J. Song, M. Alam, Impact of biodiesel blending on diesel soot and the regeneration of particulate filters, Energy & Fuels 19(5) (2005) 1857-1864.
- [49] M. Terrones, Carbon nanotubes: synthesis and properties, electronic devices and other emerging applications, International materials reviews 49(6) (2004) 325-377.
- [50] Y. Su, Z. Tang, G. Wang, R. Wan, Influence of carbon nanotube on the tribological properties of vegetable-based oil, Advances in Mechanical Engineering 10(5) (2018) 1687814018778188.
- [51] N. Salah, M.S. Abdel-Wahab, A. Alshahrie, N.D. Alharbi, Z.H. Khan, Carbon nanotubes of oil fly ash as lubricant additives for different base oils and their tribology performance, RSC advances 7(64) (2017) 40295-40302.
- [52] N. Salah, M.S. Abdel-wahab, S.S. Habib, Z.H. Khan, Lubricant additives based on carbon nanotubes produced from carbon-rich fly ash, Tribology Transactions 60(1) (2017) 166-175.
- [53] B.M. Kamel, V. Tirth, A. Algahtani, M.S. Shiba, A. Mobasher, H.A. Hashish, S. Dabees, Optimization of the rheological properties and tribological performance of SAE 5w-30 base oil with added MWCNTs, Lubricants 9(9) (2021) 94.
- [54] D.K. Prasad, M. Amarnath, H. Chelladurai, Impact of Multi-walled Carbon Nanotubes as an Additive in Lithium Grease to Enhance the Tribological and Dynamic Performance of Roller Bearing, Tribology Letters 71(3) (2023) 88.
- [55] N.A.A. Mohamed Ariffin, C.T. Lee, M.B. Lee, I. Halid, S.H. Hamdan, M.I. Ismail, W.W.F. Chong, H. Zhang, Enhancing boundary friction and wear reduction through adsorption control in protic ionic liquid and carbon mixtures, Journal of Materials Science (2024) 1-16.
- [56] N. Kumar, P. Goyal, Experimental study of Carbon Nanotubes to enhance Tribological Characteristics of Lubricating Engine Oil SAE10W40, IOP Conference Series: Materials Science and Engineering, IOP Publishing, 2022, p. 012052.

- [57] K. Gong, X. Wu, G. Zhao, X. Wang, Tribological properties of polymeric aryl phosphates grafted onto multi-walled carbon nanotubes as high-performances lubricant additive, Tribology International 116 (2017) 172-179.
- [58] J. Kałużny, A. Merkisz-Guranowska, M. Giersig, K. Kempa, Lubricating performance of carbon nanotubes in internal combustion engines—engine test results for cnt enriched oil, International Journal of Automotive Technology 18 (2017) 1047-1059.
- [59] N. Jeyaprakash, S. Sivasankaran, G. Prabu, C.-H. Yang, A.S. Alaboodi, Enhancing the tribological properties of nodular cast iron using multi wall carbon nano-tubes (MWCNTs) as lubricant additives, Materials Research Express 6(4) (2019) 045038.
- [60] W. Khalil, A. Mohamed, M. Bayoumi, T. Osman, Tribological properties of dispersed carbon nanotubes in lubricant, Fullerenes, Nanotubes and Carbon Nanostructures 24(7) (2016) 479-485.
- [61] A. Elagouz, M.K.A. Ali, H. Xianjun, M.A. Abdelkareem, Thermophysical and tribological behaviors of multiwalled carbon nanotubes used as nanolubricant additives, Surface Topography: Metrology and Properties 9(4) (2021) 045002.
- [62] M.I. Kairi, S. Dayou, N.I. Kairi, S.A. Bakar, B. Vigolo, A.R. Mohamed, Toward high production of graphene flakes—a review on recent developments in their synthesis methods and scalability, Journal of Materials Chemistry A 6(31) (2018) 15010-15026.
- [63] L. Cançado, M. Pimenta, R. Saito, A. Jorio, L. Ladeira, A. Grueneis, A. Souza-Filho, G. Dresselhaus, M. Dresselhaus, Stokes and anti-Stokes double resonance Raman scattering in two-dimensional graphite, Physical Review B 66(3) (2002) 035415.
- [64] A.C. Ferrari, J.C. Meyer, V. Scardaci, C. Casiraghi, M. Lazzeri, F. Mauri, S. Piscanec, D. Jiang, K.S. Novoselov, S. Roth, Raman spectrum of graphene and graphene layers, Physical review letters 97(18) (2006) 187401.
- [65] D. Graf, F. Molitor, K. Ensslin, C. Stampfer, A. Jungen, C. Hierold, L. Wirtz, Spatially resolved Raman spectroscopy of single-and few-layer graphene, Nano letters 7(2) (2007) 238-242.
- [66] A. Merlen, J.G. Buijnsters, C. Pardanaud, A guide to and review of the use of multiwavelength Raman spectroscopy for characterizing defective aromatic carbon solids: From graphene to amorphous carbons, Coatings 7(10) (2017) 153.
- [67] B. Alqahtani, W. Hoziefa, H.M. Abdel Moneam, M. Hamoud, S. Salunkhe, A.B. Elshalakany, M. Abdel-Mottaleb, J.P. Davim, Tribological Performance and Rheological Properties of Engine Oil with Graphene Nano-Additives, Lubricants 10(7) (2022) 137.

- [68] S. Akl, S. Elsoudy, A.A. Abdel-Rehim, S. Salem, M. Ellis, Recent advances in preparation and testing methods of engine-based nanolubricants: a state-of-the-art review, Lubricants 9(9) (2021) 85.
- [69] Y. Pakharukov, F. Shabiev, R. Safargaliev, V. Mavrinskii, S. Vasiljev, B. Ezdin, B. Grigoriev, R. Salihov, The mechanism of oil viscosity reduction with the addition of graphene nanoparticles, Journal of Molecular Liquids 361 (2022) 119551.
- [70] Y.J.J. Jason, H.G. How, Y.H. Teoh, F. Sher, H.G. Chuah, J.S. Teh, Tribological behaviour of graphene nanoplatelets as additive in pongamia oil, Coatings 11(6) (2021) 732.
- [71] J. Kałużny, A. Świetlicka, Ł. Wojciechowski, S. Boncel, G. Kinal, T. Runka, M. Nowicki, O. Stepanenko, B. Gapiński, J. Leśniewicz, Machine Learning Approach for Application-Tailored Nanolubricants' Design, Nanomaterials 12(10) (2022) 1765.
- [72] G. Paul, H. Hirani, T. Kuila, N. Murmu, Nanolubricants dispersed with graphene and its derivatives: an assessment and review of the tribological performance, Nanoscale 11(8) (2019) 3458-3483.
- [73] L. Liu, M. Zhou, X. Li, L. Jin, G. Su, Y. Mo, L. Li, H. Zhu, Y. Tian, Research progress in application of 2D materials in liquid-phase lubrication system, Materials 11(8) (2018) 1314.
- [74] H. Zaharin, M. Ghazali, N. Thachnatharen, F. Ezzah, R. Walvekar, M. Khalid, Progress in 2D materials based Nanolubricants: A review, Flatchem (2023) 100485.
- [75] K. Suresh, P. Selvakumar, G. Kumaresan, M. Vijayakumar, M. Ravikumar, N.R. Jenita, A critical review on the effect of morphology, stability, and thermophysical properties of graphene nanoparticles in nanolubricants and nanofluids, Journal of Thermal Analysis and Calorimetry 148(2) (2023) 451-472.
- [76] V. Eswaraiah, V. Sankaranarayanan, S. Ramaprabhu, Graphene-based engine oil nanofluids for tribological applications, ACS applied materials & interfaces 3(11) (2011) 4221-4227.
- [77] Z. Han, C. Gan, X. Li, P. Feng, X. Ma, X. Fan, M. Zhu, Electrochemical preparation of modified-graphene additive towards lubrication requirement, Tribology International 161 (2021) 107057.
- [78] T. Ouyang, Y. Shen, W. Lei, X. Xu, L. Liang, H.S. Waqar, B. Lin, Z.Q. Tian, P.K. Shen, Reduced friction and wear enabled by arc-discharge method-prepared 3D graphene as oil additive under variable loads and speeds, Wear 462 (2020) 203495.
- [79] J. Zhao, Y. Li, J. Mao, Y. He, J. Luo, Synthesis of thermally reduced graphite oxide in sulfuric acid and its application as an efficient lubrication additive, Tribology International 116 (2017) 303-309.

Chapter 5 Conclusions and Future Scope

5.1 Conclusions

The current investigation is centered on the sustainable and large-scale processing of various nanocarbons (0D, 1D and 2D) and their utilization as lubricant additives. The study's nanocarbons have been kept devoid of compounds including sulphur, phosphorus, or any other metals found in commercial AF and AW lubricant additives. The use of carbon soot and carbon onions as lubricant additives is an exciting prospect for increasing lubrication in a variety of applications. Both materials have distinct features that can improve lubrication performance, but they each have their own set of benefits and drawbacks. Carbon soot and carbon onions have qualities that allow them to minimise friction between moving surfaces, leading in enhanced lubrication. Their presence in lubricants can result in smoother and more efficient machinery performance. Nanocarbons can form a protective boundary layer on surfaces, decreasing wear and increasing mechanical component lifespan. This might result in lower maintenance costs and longer equipment lifespan. Carbon soot and carbon onions are thermally stable compounds that can be used in high-temperature situations where typical lubricant additives may deteriorate. Carbon soot, a result of tyre pyrolysis, is copious and very inexpensive, making it an appealing alternative for lubricant compositions. Recycling carbon soot into carbon onions and utilising them as lubricant additives can help to reduce waste and make industrial operations more sustainable. Although the benefits appear to be encouraging, homogeneous dispersion of these nanocarbons in lubricants is difficult (but achievable). NP agglomeration can develop, resulting in uneven lubrication and decreased efficiency which was found prominent at higher concentrations of the developed 0D nanocarbons. The nanocarbons may interact with other lubricant additives or materials in ways that are not well understood, depending on their surface qualities. This work has produced large-scale, cost-effective processing, which is a significant bottleneck for nanocarbons. The potential for employing carbon soot and carbon onions as lubricant additives in the future is great, with benefits such as decreased friction, wear reduction, and thermal stability. Through experimental studies it is proved and established that using carbon soot produced by controlled combustion of waste tyre tubes in lubricating oil (group-2 N500 de-waxed oil) could reduce CoF and WSD by 48.93% and 28.12% respectively. The TPW and OLC (discussed in chapter 4) could reduce abrasive, WSD (12-20% by TPW & 17-30% by OLC) in low concentrations. However, addressing issues like dispersion, chemical reactivity, toxicity, control, and compatibility is critical for their

effective real-time use. The dispersion of the 0D nanocarbons studied shows good stability (visually) till 30 days in low concentrations (0.1wt.%). As the concentration of the RTS, TPW and OLC is increased the sedimentation is found to occur at a faster rate.

Using 1D MWCNTs as additives in lubricants has several advantages, but it also has certain drawbacks. MWCNTs generated in this study using a fluidized bed reactor were extremely effective as lubricant additives. They improved overall lubrication performance by reducing friction and wear between moving components. MWCNTs produced a protective layer on surfaces in various lubricating fluids, minimising wear. MWCNTs have exceptional thermal stability and can resist harsh temperatures and conditions. However, establishing steady dispersion of MWCNTs in lubricants proved difficult. They agglomerate, resulting in unequal hazy rheological characteristics that may contribute to decreased efficacy. MWCNTs may be expensive to make, which may limit their broad application as lubricant additives. This work proposes a more sustainable, cost-effective manufacturing approach. Compatibility with existing lubricant formulas and materials is crucial, and investigations conducted in this study demonstrate effective tribological improvements with both mineral and synthetic oil. The potential for employing MWCNTs as lubricant additives in the future is great, with benefits such as improved lubrication qualities and decreased wear. However, the dispersion of the MWCNTs in the BO and CO is very poor as compared to that of the 0D nanocarbon studied.

Exploring graphene as a lubricant additive offers immense promise, but it also comes with its own set of obstacles and complications. The sustainably generated MLG in this study improved the lubrication of the lubricating medium in which it was disseminated. Because of its outstanding surface smoothness and chemical stability, it provided reduced friction and great lubrication performance. The MLG developed a protective coating on the surfaces, decreasing wear and tear. MLG-based lubricants can contribute to environmental sustainability by lowering energy consumption, emissions, and the need for regular maintenance, resulting in less resources and materials needed. Furthermore, the MLG may be integrated into a broad number of lubricant formulations, including oils and greases, making it a versatile alternative for a variety of sectors. The planned MLG synthesis technique will make it less expensive. MLG particle agglomeration is more noticeable at greater concentrations, reducing their efficacy and causing uneven lubrication. Addition of MLG produced in this work in optimized quantities to base oil reduced CoF by 25% and wear was reduced by 50%. The addition of MLG to commercial oil improved the CoF and wear resistance by 16% and 50% respectively. While laboratory-scale investigations have yielded encouraging results, scaling up production of graphene-based lubricants to satisfy industrial demands remains a substantial problem that

will necessitate a coordinated approach between lubricant formulators and their end users. The future potential of employing graphene as a lubricant additive is intriguing, with benefits such as increased lubricating qualities, decreased wear and tear, and improved thermal conductivity. Figure 73 shows the average CoF values (as per ASTM D4172) obtained in different lubricating media using the various nanocarbons along with the respective dispersion quality. It can be conclusively said after all the experimental studies and data analysis that the studied nano carbons i.e., carbon soot, tyre pyrolysis waste carbon, onion like carbon, multi-walled carbon nanotubes and multi-layer graphene have the potential to serve as excellent anti-wear and anti-friction additives in lubricating media.

Base oil				Commercial oil			
Samples	0.1 wt.%	0.3 wt.%	0.5 wt.%	Samples	0.1 wt.%	0.3 wt.%	0.5 wt.%
				4711140 11			
G2 Base oil		0.094		15W40 oil	0.075 (0.00952)		
MLG	0.057	0.085	0.095	MLG	0.066	0.063	0.074
TPW	0.057	0.045	0.104	TPW	0.063	0.076	0.097
OLC	0.058	0.084	0.075	OLC	0.062	0.081	0.086
CNT	0.027	0.053	0.046	CNT	0.039	0.047	0.07
	table dispersion (r more) and low (Moderate dispersion (3 to 7 days) and low CoF Poor dispersion (nearly 24 hours) and high CoF			•

Figure 73. Average CoF values and dispersion stability of the studies carried out with MLG, TPW, OLC and MWCNTs (printed as CNT here) in BO and CO.

The desired properties are effectively improved when these NPs are used in low concentration (0.1wt.% to 0.3wt.%) beyond which the challenges like faster agglomeration, associated sedimentation and property deterioration get aggravated. Also, the dispersion of the nanocarbons in the lubricating media (oils) induces certain changes in the rheological properties which are clearly anomalous in nature. Non-Einstein like reduction in viscosity is observed in most cases which needs further investigation through in-situ studies which could throw light on the particle fluid interactions and could help to decipher fluid mechanics at nanoscale. Apart from the lubricating media studied in this work (oils) the developed nanocarbons could be highly effective in other lubricating media like greases in which sedimentation and agglomeration is not a primary concern. As the nanocarbons exhibit excellent thermal stability at high temperatures (above 400-500°C) they could be able to withstand harsher operating conditions as compared to the conventional lubricating additives

(ZDDP, a common lubricant additive degrades around 150-200 °C). The factor of sustainability has been kept in mind while developing the processing methods in these studies along with inclination to meet the possible stringent regulations related to lubricant additives.

5.2 Future Scope

This study has been focused on the sustainable production of various carbon materials and exploring their potential as anti-wear and anti-friction additives in lubricants. Aspects like material characterization impact the concentration of developed materials in lubricants on properties like viscosity, shear stress, and tribological performance, which are evaluated. It can be affirmatively said that the material processing techniques developed in this work and the material properties evaluated are at TRL-4 (technology readiness level). The developed CNMs can be explored as additives in various liquid and semi-solid (greases) lubricating media, considering their excellent thermal stability at high temperatures and their tribological properties. Using the discovered carbonaceous materials might increase the tribological characteristics of the lubricants and make them more effective against friction and wear, resulting in extended component life. The functionalization of the produced materials and their influence on qualities such as dispersion stability and lubricity can also be investigated. The use of 0D (zero-dimensional), 1D (one-dimensional), and 2D (two-dimensional) carbon nanomaterials as engine oil additives has excellent potential for enhancing engine performance, efficiency, and environmental sustainability in the future. When employed as additives in engine fluids, each type of carbon nanostructure has distinct benefits and problems. Reduced friction can lead to increased fuel economy and lower emissions, which can be investigated further to correlate laboratory results with real-world outcomes.

Further research using the produced nanocarbons can be conducted utilizing semi-solid lubricating media. Extensive research may be conducted to determine how changing the size, shape, and surface characteristics of carbon nanostructures affect their effectiveness as lubricant additives. The effect of functionalization and surface treatments on their behavior might also be investigated. Another ignored but critical factor is the environmental and health ramifications of using carbon nanostructures as lubricant additives. Their biocompatibility and long-term ecological consequences can be studied to assure safety and sustainability. Similar research might be conducted to investigate the application-specific advantages of carbon nanostructure additions. Examine its efficacy in decreasing friction and wear in automobile engines, industrial machinery, aeronautical applications, and other related applications. The fundamental tribological mechanisms responsible for the better lubricating qualities of carbon

nanostructures might be revealed by utilizing in-situ approaches, shedding information on how they affect friction and wear behaviour at the nanoscale. Contributions can be made to creating standardized testing methods for evaluating the performance of carbon nanostructure-based lubricant additives and establishing a benchmark criterion for their practical deployment. To show how these additions assist in minimizing waste and environmental effects, a focus on the function of carbon nanostructures in promoting sustainability and green efforts in the lubricant sector must be gathered.

The future potential of new and sustainable nanocarbon preparation as additives for increased lubrication offers enormous promise for revolutionizing different sectors that rely on effective lubrication systems. As worldwide concerns about environmental sustainability grow, the need for eco-friendly lubricants with great performance qualities grows more critical. Nanocarbons have exceptional lubricating attributes because of their distinct structural characteristics and surface chemistry. The use of these nanoparticles as lubricant additives has demonstrated tremendous potential for lowering friction, wear, and energy consumption while increasing machinery lifespan. Various research areas may be pursued to develop further and apply nanocarbon-based lubricants.

Furthermore, fundamental research into the tribological mechanics underpinning the lubricating process at the nanoscale is critical for optimizing additive formulations. Advanced characterization methods, including atomic force microscopy (AFM) and molecular dynamics simulations, could provide helpful information about interfacial interactions, lubricant layer development, and tribo-chemical reactions. Understanding these sophisticated dynamics could make it easier to create nanocarbon compounds with specialized qualities for specific applications, such as automobile engines and aerospace components. Combining artificial intelligence (AI) and machine learning (ML) approaches is a transformational strategy to expedite research and development in this sector. AI algorithms can find correlations, patterns, and structure-property links by analysing large datasets containing experimental results, computer simulations, and material characteristics. ML models trained on varied datasets may predict optimal synthesis conditions, identify suitable additives, and optimize lubricant compositions for improved performance and sustainability metrics. Furthermore, AI-powered virtual screening approaches enable the quick identification of interesting nanocarbon structures with desirable tribological characteristics, which speeds up the discovery process. To improve knowledge of the intricate interactions between carbon nanostructures and

To improve knowledge of the intricate interactions between carbon nanostructures and lubricants, advanced data analysis techniques such as AI and machine learning may be used to enhance the quality of study and bring in the newest tools and methodology. In addition to

material processing and characterization, AI/ML approaches provide real-time monitoring and predictive maintenance of lubricating systems. Sensor data combined with AI algorithms may detect abnormalities, anticipate equipment failures, and optimize lubricant replenishment schedules, reducing downtime and increasing operational efficiency. Furthermore, AI-enabled digital twins replicate the dynamic behaviour of lubricated components under various operating circumstances, allowing for predictive modelling of wear processes and performance deterioration over time.

Collaborative multidisciplinary research efforts combining materials scientists, chemists, mechanical engineers, and data scientists are required to fully realize the promise of nanocarbon-based lubricants. Multiscale modelling methodologies that combine experimental validation and computer simulations offer thorough knowledge and optimization of lubrication processes. Furthermore, collaborative relationships across academia, business, and government agencies promote innovation and technology transfer, propelling research discoveries into practical applications and commercial goods. To summarise, the future prognosis for innovative and sustainable nanocarbon preparation as additives for improved lubrication is marked by revolutionary potential and difficulties. Researchers may produce next-generation lubricants with higher performance, durability, and environmental sustainability by using a synergistic mix of sophisticated synthesis techniques, basic knowledge of tribological principles, and AI/ML-based methodologies. This multidisciplinary endeavour has the potential to revolutionize various industries, from transportation and manufacturing to renewable energy, paving the way for a greener and more efficient future.

Novel and Sustainable Production, Characterization, and Testing of Various Nanocarbons as Excellent Additives in Lubricants

by Ravikiran Nowduru

Librarian

Indira Gandhi Memorial Library UNIVERSITY OF HYDERABAD Central University P.O. HYDERABAD-500 046.

Submission date: 26-Apr-2024 11:21AM (UTC+0530)

Submission ID: 2362341619

File name: Ravikiran_Nowduru.pdf (7.87M)

Word count: 40428

Character count: 215340

Novel and Sustainable Production, Characterization, and Testing of Various Nanocarbons as Excellent Additives in Lubricants

ORIGINALITY REPORT

SIMILARITY INDEX

INTERNET SOURCES

PUBLICATIONS

STUDENT PAPERS

PRIMARY SOURCES

Ravikiran Nowduru, Harita Pant, Balaji Padya, Pawan Kumar Jain, Vadali Venkata Satya Siva Srikanth. "Novel top-down kg-scale processing of 2D multi-layered graphene powder and its application as excellent

lubricating additives in commercial engine oils", Diamond and Related Materials, 2024

Publication

Ravikiran Nowduru, Bolla Reddy Bodapati, Pavan Kumar Penumakala, Sai Ram Krishna Malladi et al. "Carbon soot nanoparticles derived from wasted rubber: An additive in lubricating oil for efficient friction and wear reduction", Diamond and Related Materials, 2022

Publication

"Advanced Nanomaterials", Springer Science and Business Media LLC, 2022

Publication

School of Eugineering Sciences & Technology Elmientity of H. derabad Tyderadad-200 046.

- Ravikiran Nowduru, Harita Pant, Pawan Kumar Jain, Vadali Venkata Satya Siva Srikanth. "Dispersion of novel 0D carbons in 15W40 engine oil using ultrasonication for enhanced lubrication", Chemical Engineering and Processing Process Intensification, 2024

 Nowduru Ravikiran, Balaji Padya, Syed Junaid,
- Nowduru Ravikiran, Balaji Padya, Syed Junaid, Pawan Kumar Jain, Vadali V. S. S. Srikanth.

 "Sustainable Kilogram-Scale Conversion of Tire Pyrolysis Waste into Nanosized Onion-like Carbons with Extraordinary Lubricant-sasrikanth Additive Properties", ACS Sustainable Chemistry & Engineering, 2023

 Publication

 Nowduru Ravikiran, Balaji Padya, Syed Junaid, 500

 Sustainable From Strain Strikanth Additive Properties ACS Sustainable Chemistry & Engineering, 2023
- Submitted to Visvesvaraya Technological
 University
 Student Paper

 Submitted to Visvesvaraya Technological

 Visvesvaraya Technological
- Jun Zhao, Tong Gao, Yingru Li, Yongyong He,
 Yijun Shi. "Two-dimensional (2D) graphene
 nanosheets as advanced lubricant additives: A
 critical review and prospect", Materials Today
 Communications, 2021
 Publication

<1%

Ahmed Elagouz, Mohamed Kamal Ahmed Ali, Hou Xianjun, Mohamed A.A. Abdelkareem. "Thermophysical and tribological behaviors of multiwalled carbon nanotubes used as

nanolubricant additives", Surface Topography: Metrology and Properties, 2021

Publication

9	Éncyclopedia of Tribology, 2013. Publication	<1%
10	www.researchgate.net Internet Source	<1%
11	Submitted to University College London Student Paper	<1%
12	Lijesh K. P., Deepak Kumar, Muzakkir S. M., Harish Hirani. "Thermal and frictional performance evaluation of nano lubricant with multi wall carbon nano tubes (MWCNTs) as nano-additive", AIP Publishing, 2018 Publication	<1%
13	Ravi Kali, Balaji Padya, T.N. Rao, P.K. Jain. "Solid waste-derived carbon as anode for high performance lithium-ion batteries", Diamond and Related Materials, 2019 Publication	<1%
14	Submitted to University of Hyderabad, Hyderabad Student Paper	<1%
15	minerva.usc.es Internet Source	<1%

16	Submitted to Indian Institute of Technology, Madras Student Paper	<1%
17	Numan Salah, M. Sh. Abdel-wahab, Sami S. Habib, Zishan H. Khan. "Lubricant Additives Based on Carbon Nanotubes Produced from Carbon-Rich Fly Ash", Tribology Transactions, 2016	<1%
18	Homender Kumar, A. P. Harsha. "Influence of oleic acid-treated LaF nanoparticles as an additive on extreme pressure properties of various grades of polyalphaolefins ", Tribology Transactions, 2021	<1%
19	riunet.upv.es Internet Source	<1%
20	aaltodoc.aalto.fi Internet Source	<1%
21	projects.ncsu.edu Internet Source	<1%
22	www.mdpi.com Internet Source	<1%
23	mafiadoc.com Internet Source	<1%

24	S. P. Srivastava. "Developments in Lubricant Technology", Wiley, 2014 Publication	<1%
25	Sudesh Singh, Xinchun Chen, Chenhui Zhang, Rajnesh Tyagi, Jianbin Luo. "Investigation on the lubrication potential of graphene oxide aqueous dispersion for self-mated stainless steel tribo-pair", Vacuum, 2019	<1%
26	etheses.bham.ac.uk Internet Source	<1%
27	Talaeemashhadi, Sadaf, Maurizio Sansotera, Cristian Gambarotti, Antonino Famulari, Claudia L. Bianchi, P. Antonio Guarda, and Walter Navarrini. "Functionalization of multiwalled carbon nanotubes with perfluoropolyether peroxide to produce superhydrophobic properties", Carbon, 2013. Publication	<1%
28	Submitted to Texas A&M University, College Station Student Paper	<1%
29	public.thinkonweb.com Internet Source	<1%
30	spectrum.library.concordia.ca Internet Source	<1%

Exclude quotes

On

Exclude matches

< 14 words

Exclude bibliography On